OBSERVATIONS AND MODELLING OF TRANSPARENT EXOPOLYMER PARTICLES (TEP) AND THEIR ROLE IN CARBON CYCLING IN SHELF SEAS

Gianfranco Anastasi

Thesis submitted in fulfilment of the requirements
For the degree of Doctor of Philosophy

School of Environmental Sciences
University of East Anglia
April 2018

ABSTRACT

A key requirement for the quantitative assessment of the global marine carbon cycle is to improve understanding of the regulation of dissolved organic carbon (DOC) concentrations. Continental shelf seas make an important contribution to sequestration of CO_2 from the atmosphere, through physical and biological processes, i.e. the Continental Shelf Pump (CSP). However, the role of organic matter dynamics in the CSP is poorly understood. Decoupling the carbon to nitrogen stoichiometry of organic matter production from that of the primary producers can lead to excess uptake of dissolved carbon relative to nitrogen, allowing for 'overconsumption' of carbon and increased biological pump efficiency. This process could be particularly effective if carbon-rich material such as gel-like Transparent Exopolymer particles (TEP) are formed, as these can sink out of the surface layer. This research investigated the role played by TEP in carbon cycling in NW European shelf seas by using a combination of field observations and modelling approaches. Results show that shelf sea systems with higher primary production (PP) lead to a higher TEP concentrations. In shelf seas TEP can be produced as a by-product of primary production, in coastal areas or during periods of nutrient limitation via overflow production of carbon-rich TEP precursors in seasonally stratified areas. A clear relationship between TEP and chlorophyll *a* observed in this study reinforces the evidence that phytoplankton is the main driver of TEP production. Results from the modelling work indicate that TEP can change the partitioning of the exported carbon, leading to an increase of the benthic respiration of ~ 30 %. This result improves our understanding of TEP dynamics and demonstrates that TEP can play a potentially significant role in carbon cycling and export in shelf seas, where its concentration is disproportionately high relative to the open ocean.

ACKNOWLEDGEMENTS

This Ph.D. would not have been possible without the scientific support and constant encouragement from my supervisory team. I would like to thank my primary supervisor Dr. Martin Johnson for giving me the opportunity to start this amazing adventure, but also for his support guidance and encouragement. I would like to thank my co-supervisors Dr. Gill Malin, Dr. Naomi Greenwood, Dr. Dorothee Bakker and Dr. Luca Polimene for giving me valuable systematic criticisms, advice and comments on this research. This research would not have been possible without the financial support from the Centre for Environment, Fisheries and Aquaculture Science (Cefas). I also would like to thank people external to UEA who have helped me to achieve my goals, starting with the modelling group at Plymouth Marine Laboratory (PML). In particular I would like to thank Dr. Luca Polimene, who with his advice and guidance has helped me to achieve my objectives and develop further my modelling skills. Dr. Yuri Artioli and Dr. Momme Butenschön I thank for their technical support with the modelling part of my Ph.D.. A special thanks is for the Cefas SmartBuoy team, in particular Dave Sivyer, Tom Hull, the Capitan and crew of the RV Cefas Endeavour for the great and enjoyable time I had during the fieldwork. I also would like to thank Dr. Elisa Capuzzo for helping me during my first adventure at sea and John Aldridge for sharing pieces of ERSEM code with me. A special thanks goes to Dr. Isabel Seguro Requejo (Chata), who has contributed to this research with the collection of TEP samples during the Shelf Sea Biogeochemistry Programme (SSB). A big thanks also to Martha for all her time and effort in proof reading this thesis for me.

A special and profound thanks goes to my family for supporting and encouraging me in all my decisions. The last but not the least thanks goes to my lovely girlfriend Ann for supporting and encouraging me during this important moment of my life.

LIST OF CONTENTS

ABSTRACT 1

ACKNOWLEDGEMENTS 2

LIST OF CONTENTS 3

LIST OF FIGURES 7

LIST OF TABLES 20

Chapter 1 Introduction 25

1.1 Ocean carbon cycling 25

1.2 Biological pump, solubility pump and microbial carbon pump 25

1.2.1 Continental shelf pump (CSP) 26

1.3 Continental shelf seas 28

1.3.1 Northwestern European shelf seas 28

1.3.1.1 Celtic Sea 28

1.3.1.2 North Sea 30

1.4 Organic carbon in shelf seas 32

1.4.1 The organic carbon pump 32

1.4.2 Carbon export 33

1.5 Carbon overconsumption 33

1.6 Transparent Exopolymer Particles (TEP) 36

1.7 Ecological and biogeochemical relevance of TEP in the marine ecosystem 37

1.7.1 Abundance and distribution of TEP 37

1.7.2 Role of TEP in the formation of marine aggregates 38

1.7.3 Accumulation of TEP in surface waters: production and consumption 42

1.7.4 Contribution of TEP to carbon cycling 44

1.8 Representation of TEP in marine ecosystem models 45

1.9 Project rationale 46

1.9.1 Motivation 46

1.9.2 Aim 47

1.9.3 Hypotheses and Objectives 47

Chapter 2 Analytical methods 50

2.1 Introduction 50

2.2 TEP analytical method 50

2.3 Alcian Blue solution preparation and testing 52

2.4 Gum Xanthan standard solution preparation and testing 53
2.5 Calibration of the standard solution 54
2.6 TEP concentration determination 56
2.7 First Alcian Blue calibration curve 57
2.8 Second Alcian Blue calibration curve 58
2.9 Photographic method for TEP detection 60
2.9.1 Introduction 60
2.9.2 Material and method 61
2.9.3 Results 62
2.9.4 Standard spectrophotometric method versus photographic method 63
2.9.5 Conclusion and future work 64
2.10 TEP storage experiment 64
2.10.1 Introduction 64
2.10.2 Testing various preservatives 64
2.10.3 Results 66
2.10.4 Conclusion 67
2.10.5 Testing unbuffered formalin and saturated mercuric chloride 68
2.10.6 Results 68
2.10.7 Conclusion 73
2.11 Analysis of Particulate Organic Matter (POM) 73
2.12 Analysis of chlorophyll *a* 74
Chapter 3 Modelling the effect of TEP on particle aggregation and export 76
3.1 Introduction 76
3.2 The model 77
3.2.1 The European Regional Seas Ecosystem Model (ERSEM) 77
3.2.3 Model set up 78
3.3 Model development 79
3.3.1 New parameterization of TEP and aggregates containing TEP 79
3.3.1.1 Preliminary version of the TEP aggregation process in ERSEM 81
3.3.2 Aggregation process 82
Chapter 4 Vertical distribution of TEP at Celtic Sea sites during spring and summer 2015 92
4.1 Introduction 92
4.2 Observations 93
4.2.1 Method: TEP sample collection and processing 93

4.2.2 Results 95
4.3 Box model: Estimation of the production and fate of TEP 105
4.3.1 Description and method 105
4.3.2 Results 108
4.4 TEP in the aggregation model 112
4.4.1 Description 112
4.4.2 Method 112
4.4.3 Results 119
4.5 Modelling the effect of TEP on particle aggregation and export 123
4.5.1 Method 123
4.5.2 Model assessment: test case Celtic Sea (Station A) 123
4.5.3 Model assessment: test case Western English Channel (Station L4) 126
4.5.4 Results simulation at Station A 131
4.5.4.1 TEP configuration versus observation and reference 131
4.5.4.2 CO_2 air-sea flux, DIC and NO_3 135
4.5.4.3 TEP and POC fluxes and sinking POC molar ratio 137
4.5.4.4 Carbon budget 139
Chapter 5 Distribution of TEP in the North Sea in summer 151
5.1 Introduction 151
5.2 Materials and methods 152
5.2.1 Data collection 152
5.2.2 Cluster analysis 154
5.2.3 Box model 156
5.2.4 Statistical analyses 157
5.4 Results: distribution of TEP in summer 2014 158
5.4.1 Characterisation of environmental conditions 158
5.4.2 TEP observations in 2014 160
5.4.3 Cluster analysis for 2014 162
5.4.4 Box model for 2014 168
5.5 Results: distribution of TEP in summer 2015 171
5.5.1 Characterisation of environmental conditions 171
5.5.2 TEP observations in 2015 173
5.5.3 Cluster analysis for 2015 174
5.5.4 Box model 2015 181
5.6 TEP incubation experiments 183

5.6.1 Method 183
5.6.2 Results 184
5.7 Seasonal cycle of TEP 187
5.7.1 Method: TEP sample collection and analysis 187
5.7.2 Results 188
5.7.2.1 SmartBuoy bag testing 191
5.7.2.2 Method and results 191
5.8 Discussion 192
5.9 Conclusions 198
Chapter 6 Discussion and synthesis 200
6.1 Introduction 200
6.2 TEP in the NW European shelf seas: evaluation of the hypotheses 200
6.3 The role of other factors in controlling TEP dynamics 206
6.4 Further research 208
6.5 Conclusions 210
References 212
Appendix 4 231

LIST OF FIGURES

Figure 1.1 Schematic representation of the global carbon cycle (Ciais *et al.*, 2013). 25

Figure 1.2 Air-sea CO_2 fluxes (mmol C m^{-2} y^{-1}) on a global scale (Gruber, 2015). Air-sea CO_2 fluxes are high in coastal areas..... 27

Figure 1.3 The Celtic Sea with its circulation and carbon transport pathway adapted from de Haas *et al.* (2002). → indicates main oceanographic currents; ➸ indicates main carbon tranport. The white colour indicates depth of less than 100 m, the light grey of 100-200 m and the medium grey of more than 200 m. 29

Figure 1.4 The North Sea with its circulation pattern and carbon transport pathway adapted from de Haas *et al.* (2002). → indicates the main oceanographic currents; ➸ indicates the main carbon tranport. The dashed red line indicates the approximate boundary between the two biogeochemical regions (northern and southern). 31

Figure 1.5 Formation of TEP from dissolved organic matter proposed by Passow (2002) from Meng *et al.* (2013). 37

Figure 2.1 Molecular structures of Alcian Blue and Gum Xanthan. Red circles indicate the formation of the Alcian Blue-Gum Xanthan complex. 51

Figure 2.2 Diagram illustrating TEP analysis step by step. a) Determination of TEP or standard solution absorbance, b) determination of the weight of the standard solution on the dry filter. 52

Figure 2.3 Sample spectrum measurement with the UV-Vis spectrophotometer LAMBDA 35 (Absorbance versus wavelength in nm)..... 53

Figure 2.4 Relationship between the volume of the standard solution of Gum Xanthan filtered and the time taken to filter the sample..... 54

Figure 2.5 Calibration curve, linear regression and residuals of the standard Gum Xanthan. 57

Figure 2.6 Calibration curve, linear regression and residuals of the standard Gum Xanthan. 59

Figure 2.7 Example of standard Gum Xanthan solution on a filter, stained with Alcian Blue during the image processing analysis. The red square indicates the area

of the filter analysed by the software to get the RGB (Red, Green and Blue) colour. 61

Figure 2.8 Photographic method: Calibration curve, linear regression and residuals of the standard Gum Xanthan. 62

Figure 2.9 The photographic method versus spectrophotometric method. 63

Figure 2.10 Results of TEP concentration detected for each storage experiment at five different time steps; (dashed line) reference threshold. Reference (frozen sample 108.75 ± 0.02 μg Xeq. l^{-1}). The results from experiment four are not shown. 66

Figure 2.11 Variability of TEP sample concentration collected during Cend 8/15 (ST 1 51.9946° N, 2.1066°E) in May 2015 using different preservation methods for up to six months after collection. The dashed line indicates reference threshold. 69

Figure 2.12 Variability of TEP sample concentration collected during Cend 8/15 (ST 6 53.5279° N, 1.0704° E) in May 2015 using different preservation methods for up to six months after collection. The dashed line indicates the reference threshold. 70

Figure 2.13 Variability of TEP sample concentration collected during Cend 24/15 (ST 8 53.5347° N, 3.3831° E) in November 2015 using different preservation methods for up to six months after collection. The dashed line indicates the reference threshold. 71

Figure 2.14 Variability of TEP sample concentration collected during Cend 24/15 (ST 21 51.9789° N, 2.0882 E°) in November 2015 using different preservation methods for up to six months after collection. The dashed line indicates the reference threshold. 72

Figure 2.15 The chlorophyll *a* versus fluorescence linear regression analysis used to determine surface chlorophyll *a* concentrations in the year 2014. 75

Figure 2.16 The chlorophyll versus fluorescence linear regression analysis used to determine bottom chlorophyll *a* concentrations in the year 2014. 75

Figure 3.1 The pelagic ecosystem model flow diagram in ERSEM indicating the carbon and nutrient pathways between functional groups (Blackford *et al.*, 2004). 78

Figure 3.2 The European Regional Seas Ecosystem Model (Butenschön *et al.*, 2016). 79

Figure 3.3 Modified version of the European Regional Seas Ecosystem Model (Butenschön et al., 2016) showing the TEP scheme. Pathway a) shows the production of TEP by the phytoplankton community during nutrient limitation in the form of dissolved organic matter (DOM). Pathway b) shows the interaction of TEP in the water column with bacterial food web. Pathway c) shows the fate of TEP when ballasted with solid particles which promote sinking of POC and TEP in form of an aggregate to the seafloor. 80

Figure 3.4 Schematic conceptual diagram representing TEP aggregation process. Dashed lines represent processes, solid lines represent fluxes. Stickiness coefficient (α), aggregation threshold ($\boldsymbol{\alpha aggr}$), aggregate density ($\boldsymbol{Aggrdensity}$) and density of seawater ($\boldsymbol{\rho w}$). 81

Figure 3.5 Phytoplankton functional types (Diatoms, Nanophytoplankton, Picophytoplankton and Microphytoplankton) in ERSEM for the year 2015 at station L4 in surface waters for a) a reference run without TEP b) a preliminary TEP model with density process only and c) a TEP model with density and stickiness processes. 82

Figure 4.1 Sampling area: Celtic Deep (A); Candyfloss (CCS); Shelf Edge (CS2). 93

Figure 4.2 Vertical distribution of TEP_c content (µmol l^{-1}), chlorophyll *a* (µg l^{-1}), temperature (°C), salinity, density (kg m^{-3}), TOxN (µM), NO_2 (µM), PO_4 (µM) and SiO_4 (µM), in a) spring and b) summer 2015 at Station Celtic Deep (A). TEP values are based on a single measurement at each depth. The dashed line indicates the Surface Mixed Layer Depth (SMLD). 97

Figure 4.3 Vertical distribution of TEP_c content (µmol l^{-1}), chlorophyll *a* (µg l^{-1}), temperature (°C), salinity, density (kg m^{-3}), TOxN (µM), NO_2 (µM), PO_4 (µM) and SiO_4 (µM), in a) spring and b) summer 2015 at Station Candy Floss (CCS). TEP values are based on a single measurement at each depth. The dashed line indicates the Surface Mixed Layer Depth (SMLD). 98

Figure 4.4 Vertical distribution of TEP_c content (µmol l^{-1}), chlorophyll *a* (µg l^{-1}), temperature (°C), salinity, density (kg m^{-3}), TOxN (µM), NO_2 (µM), PO_4 (µM) and SiO_4 (µM), in summer 2015 at Station Shelf Edge (CS2). TEP values are based on a single measurement at each depth. The dashed line indicates the Surface Mixed Layer Depth (SMLD). 99

Figure 4.5 TEP_c (µmol l^{-1}) versus chlorophyll *a* (µg l^{-1}) at station CS2 in summer (whole water column, ■ red squares indicate samples in the SML; ● blue circles indicate samples in the BML). 100

Figure 4.6 Relationship between TEP_c (µmol l^{-1}) and salinity along the transect from coast to shelf edge for the SML and the BML in a) spring and b) summer. 101

Figure 4.7 Box model describing the fate of the TEP_c and fluxes. The white arrow indicates TEP_c production, the black arrow indicates export of TEP_c from the SML, white dashed arrow indicates the fraction of TEP_c removed due to potential bacterial remineralization. $\boldsymbol{TEPcSML}$ - average TEP_c concentration in the SML (µmol l^{-1}), $\boldsymbol{TEPc\ form}$ - TEP_c formation rate in the SML (µmol l^{-1} d^{-1}), $\boldsymbol{TEPc\ exp}$ - TEP_c export flux (mmol m^{-2} d^{-1}), $\boldsymbol{sinkSML}$ - TEP_c sinking rate at the SML (m d^{-1}), $\boldsymbol{TEPcBML}$ - average TEP_c concentration in the BML (µmol l^{-1}), $\boldsymbol{TEPc\ acc}$ - potential accumulation rate of TEP_c in the BML (µmol l^{-1} d^{-1}) without bacterial uptake, $\boldsymbol{TEPc\ res}$ - TEP_c residence time (days), $\boldsymbol{TEPc\ uptb}$ - TEP_c loss due to bacterial uptake (mmol m^{-2} d^{-1}), $\boldsymbol{sinkbott}$ - potential TEP_c sinking rate without bacterial uptake (m d^{-1}), $\boldsymbol{sinkbottb}$ - potential TEP_c sinking rate with bacterial uptake (m d^{-1}) , $\boldsymbol{SMLD}$ - Surface Mixed Layer Depth (m), $\boldsymbol{Wdepth}$ - total depth of the water column (m). 105

Figure 4.8 Relationship between TEP_c (µmol l^{-1}) concentration and TEP_c formation rate (µmol l^{-1} d^{-1}) extrapolated from data published in Wurl *et al.* (2011). 106

Figure 4.9 Schematic representation showing the results from the box model describing the fate of TEP_c and fluxes at three stations in the Celtic Sea in spring and summer 2015. 110

Figure 4.10 Example of aggregate composition, aggregate density, aggregate velocity and fluxes of TEP_c and POC estimated in summer 2015 at Station A (Celtic Deep), in three different scenarios: a) aggregate composed of TEP and POM and particle size range from 40 to 160 µm, b) aggregate composed of TEP, POM and mineral with turbidity calibration factor range from 1 to 3 and particle size range from 40 to 160 µm, c) aggregate composed of TEP, POM and mineral with turbidity calibration factor range from 1 to 20 and particle size range from 40 to 160 µm. The horizontal line indicates standard deviation (SD). 122

Figure 4.11 Sensitivity analysis conducted at Station A in the Celtic Sea on the 26th July 2015 for the following parameters: a) daily fraction of POC and Phytoplankton aggregate going to the aggregate per day (***aggr***), b) aggregation threshold (***αaggr***) and c) daily fraction of floating aggregate going to the sinking aggregate per day (ß). Each line indicates a TEP_c profile from the TEP model run with the different parameters setting used against the TEPc observations (obs.). The yellow dashed line in a), b) and c) represents the TEP_c profile closest to the TEP observations from which ***aggr***, ***αaggr*** and ß values are used in the TEP model to simulate TEP dynamics and results are presented in this chapter. The black dashed line indicates observed Surface Mixed Layer Depth (SMLD). 125

Figure 4.12 Western English Channel, Station L4 (Wyatt *et al.*, 2010)..... 127

Figure 4.13 Mass balance for a) carbon, b) nitrogen, c) phosphorus and d) silicium at Station L4 in the Western English Channel from the 2006 to the 2015 for the reference (standard ERSEM) and the TEP model. Note the low scale of the y axis. 128

Figure 4.14 Surface: a) chlorophyll *a*, b) particulate organic carbon, c) nitrate, d) ammonium, e) phosphate and f) silicate concentrations at Station L4 from 2005 to 2015 from fieldwork observations, reference and TEP model. For comparison with POC from observations the modelled POC from the reference and TEP model includes: particulate carbon from phytoplankton (diatoms, nano-, pico- and micro-phytoplankton), zooplankton (micro-zooplankton and nano-flagellates), bacteria and particulate organic matter (small-, medium- and large size). Plus particulate carbon from sinking and floating aggregates (only for TEP model)..... 129

Figure 4.15 Statistical analysis: a) Pearson correlation, b) root mean square error (RMSE) of surface chlorophyll *a*, particulate organic carbon and nutrients at Station L4 from 2005 to 2015 of fieldwork observations against reference and TEP model..... 129

Figure 4.16 Surface: a) chlorophyll *a*, b) particulate organic carbon (POC), c) nitrate, d) ammonium, e) phosphate and f) silicate concentrations at Station L4 for the year 2015 from fieldwork observations, reference and TEP model. The red

error bar indicates the SD of the monthly averaged values. See Figure 4.14 for information on modelled POC. 130

Figure 4.17 Surface chlorophyll *a* (1 m depth) observed (Celtic Deep 2 SmartBuoy) at Station A in the Celtic Sea, compared with the reference and TEP model. 131

Figure 4.18 Vertical profiles of a) TEP_c, b) chlorophyll and c) POC from fieldwork observations and model (reference and TEP model) at Station A in the Celtic Sea on the 26th July 2015. TEP_c profiles show: the concentration of TEP_c in sinking and floating aggregates, the concentration of the "free" TEP_c (non-associated to other particles) and the sum of the sinking and floating TEP_c. The latter was used to compare the TEP_c model output with the observations. The black dashed line indicates observed Surface Mixed Layer Depth (SMLD). See Figure 4.14 for information on modelled POC. 132

Figure 4.19 Simulation results from the TEP model of a) TEP_c and b) chlorophyll *a* in July 2105 at Station A in the Celtic Sea. 133

Figure 4.20 Vertical profiles of a) TEP_c, b) chlorophyll and c) POC from fieldwork observations and model (reference and TEP model) at Station A in the Celtic Sea on the 13th April 2015. TEP_c profiles show: the concentration of TEP_c in sinking and floating aggregates, the concentration of the "free" TEP_c (non-associated to other particles) and the sum of the sinking and floating TEP_c. The latter was used to compare the TEP_c model output with the observations. The black dashed line indicates the observed Surface Mixed Layer Depth (SMLD). See Figure 4.14 for information on modelled POC. 134

Figure 4.21 Simulation results from the TEP model of a) TEP_c and b) chlorophyll *a* in April 2105 at Station A in the Celtic Sea. 134

Figure 4.22 Simulation results from the TEP model and the reference of a) CO_2 air-sea flux, b) variation in percentage of the CO_2 air-sea flux (TEP model and reference) and CO_2 air-sea flux difference between the TEP model and the reference at Station A in the Celtic Sea for the year 2015. 135

Figure 4.23 Simulation results from the TEP model and the reference of surface water a) Dissolved Inorganic Carbon (DIC), b) nitrate (NO_3) and TEP_c at Station A in the Celtic Sea for the year 2015. 136

Figure 4.24 Simulation results of nitrate (NO_3) for a) the reference and b) the TEP model at the Station A in the Celtic Sea for the year 2015. 137

Figure 4.25 Simulation results from the TEP model and the reference of fluxes of a) TEP_c and b) Particulate organic carbon and the flux of POC minus TEP_c). The cyclic pattern of TEP and POC export in both the TEP model and the reference may be determined by the fact that the exported primary production is consumed by microorganisms (i.e. zooplankton and bacteria). 138

Figure 4.26 Simulation results of the molar ratio of particulate organic carbon : particulate nitrogen (C : N) for a) the reference and b) the TEP model. 138

Figure 4.27 Simulation results of the carbon budget for the reference and the TEP model at Station A in the Celtic Sea for the year 2015. 139

Figure 5.1 Map of the 76 sampling stations within the North Sea. 153

Figure 5.2 MODIS weekly median composite map of chlorophyll *a* (µg l^{-1}) from 29th August to 04th September 2014 (Plymouth Marine Laboratory – Remote Sensing Group). The frame highlights the beginning of an algal bloom. .. 154

Figure 5.3 Cluster analysis describing the five different regions of the North Sea: Southern Coastal (SC), Southern Mixed (SM), Transitional (T), Northern Stratified (NS) and Northern Coastal (NC) in the year a) 2014 and b) 2015. 155

Figure 5.4 Box-whisker plot of the cluster analysis describing the five different regions of the North Sea: Southern Coastal (SC), Southern Mixed (SM), Transitional (T), Northern Stratified (NS) and Northern Coastal (NC) in the year a) 2014 and b) 2015. The box indicates the lower and the upper quartile. The horizontal line within the box represents the median. The whiskers indicate the lower and higher data points. The red crosses indicate outliers. The outliers were classified as two times the interquartile range from the median. 156

Figure 5.5 Box model describing the fate of TEP_c and fluxes in a) stratified region and a b) mixed region of the North Sea. White arrow indicates TEP_c input, the black arrow indicates export of TEP_c from the SML, the white dashed arrow indicates the fraction of TEP_c removed due to potential bacterial remineralization. $\boldsymbol{TEPcSML}$ - average TEP_c concentration in the SML (µmol l^{-1}), $\boldsymbol{TEPc\ form}$ - TEP_c formation rate in the SML (µmol l^{-1} d^{-}

^{1}), $\boldsymbol{TEPc\ exp}$ - TEP_c export flux (mmol m^{-2} d^{-1}), $\boldsymbol{sinkSML}$ - TEP_c sinking rate at the SML (m d^{-1}), $\boldsymbol{TEPcBML}$ - average TEP_c concentration in the BML (µmol l^{-1}), $\boldsymbol{TEPc\ acc}$ - potential accumulation rate of TEP_c in the BML (µmol l^{-1} d^{-1}) without bacterial uptake, $\boldsymbol{TEPc\ res}$ - TEP_c residence time (d), $\boldsymbol{TEPc\ uptb}$ - TEP_c loss due to bacterial uptake (mmol m^{-2} d^{-1}), $\boldsymbol{sinkbott}$ - potential TEP_c sinking rate without bacterial uptake (m d^{-1}), $\boldsymbol{sinkbottb}$ - potential TEP_c sinking rate with bacterial uptake (m d^{-1}) , $\boldsymbol{SMLD}$ - Surface Mixed Layer (m), $\boldsymbol{Wdepth}$ - total depth of the water column (m). 157

Figure 5.6 Environmental condition of the North Sea in summer 2014. a-b) temperature (°C) in surface and bottom waters, c-d) salinity in surface and bottom waters, e) nitrate plus nitrite in surface waters (µmol l^{-1}), f) phosphate in surface waters (µmol l^{-1}), g) silicate in surface waters (µmol l^{-1}). 159

Figure 5.7 Spatial distribution of TEP_c content (µmol l^{-1}) for a) surface (4 meters depth) and b) bottom waters; c) chlorophyll (µg l^{-1}) surface and d) bottom waters during summer 2014 in the North Sea. The frame highlights an algal bloom (55.8°N, 1°E) of *Karenia mikimotoi*. 161

Figure 5.8 TEP_c concentration (µmol l^{-1}) differences between surface and bottom waters during summer 2014 in the North Sea. 162

Figure 5.9 Box-whisker plots of TEP_c (µmol l^{-1}) concentrations in a) surface and b) bottom waters during summer 2014 in the five different regions of the North Sea: Southern Coastal (SC), Southern Mixed (SM), Transitional (T), Northern Stratified (NS) and Northern Coastal (NC). See Figure 5.4 for an explanation of box and whisker plots. 163

Figure 5.10 Plots of TEP_c (µmol l^{-1}) versus chlorophyll *a* (µg l^{-1}) concentrations in a) surface and b) bottom waters during summer 2014 in the five different regions of the North Sea: Southern Coastal (SC), Southern Mixed (SM), Transitional (T), Northern Stratified (NS) and Northern Coastal (NC). The black line represents the linear regression curve for all the data points. 164

Figure 5.11 Plots of TEP_c concentration (µmol l^{-1}) versus temperature (ºC) and salinity in a-c) surface and b-d) bottom waters during summer 2014 in the five different regions of the North Sea: Southern Coastal (SC), Southern Mixed (SM), Transitional (T), Northern Stratified (NS) and Northern Coastal (NC).

The black line represents the linear regression curve for all the data points. 165

Figure 5.12 Plots of TEP_c (µmol l^{-1}) versus nutrient concentrations a) TOxN, b) NH_4, c) PO_4, d) SiO_4 in surface waters during summer 2014 in the five different regions of the North Sea: Southern Coastal (SC), Southern Mixed (SM), Transitional (T), Northern Stratified (NS) and Northern Coastal (NC). The black line represents the linear regression curve for all the data points. ... 166

Figure 5.13 Plots of TEP_c (µmol l^{-1}) versus nutrient (µmol l^{-1}) concentrations a) TOxN, b) PO_4, c) SiO_4 in bottom waters during summer 2014 in the five different regions of the North Sea: Southern Coastal (SC), Southern Mixed (SM), Transitional (T), Northern Stratified (NS) and Northern Coastal (NC). The black line represents the linear regression curve for all the data points. ... 167

Figure 5.14 Principal coordinates plot (PCO) showing relationships between variables in the five different regions of the North Sea: Southern Coastal (SC), Southern Mixed (SM), Transitional (T), Northern Stratified (NS) and Northern Coastal (NC); in surface waters in the year 2014. 168

Figure 5.15 Environmental condition of the North Sea in summer 2015. a-b) temperature (°C) in surface and bottom waters, c-d) salinity in surface and bottom waters, e) nitrate + nitrite in surface waters (µmol l^{-1}), f) phosphate in surface waters (µmol l^{-1}), g) silicate in surface waters (µmol l^{-1}). 172

Figure 5.16 Spatial distribution of TEP_c content (µmol l^{-1}) for a) surface (4 meters depth) and b) bottom waters; c) chlorophyll *a* (µg l^{-1}) surface and d) bottom waters during summer 2015 in the North Sea. 173

Figure 5.17 TEP_c concentration (µmol l^{-1}) differences between surface and bottom waters during summer 2015 in the North Sea. 174

Figure 5.18 Box-whisker plots of TEP_c (µmol l^{-1}) concentrations in a) surface and b) bottom waters during summer 2015 in the five different regions of the North Sea: Southern Coastal (SC), Southern Mixed (SM), Transitional (T), Northern Stratified (NS) and Northern Coastal (NC). See Figure 5.4 for an explanation of box and whisker plots. 175

Figure 5.19 Plots of TEP_c (µmol l^{-1}) versus chlorophyll *a* (µg l^{-1}) concentrations in a) surface and b) bottom waters during summer 2015 in the five different regions of the North Sea: Southern Coastal (SC), Southern Mixed (SM), Transitional

(T), Northern Stratified (NS) and Northern Coastal (NC). The black line represents the linear regression curve for all the data points. 176

Figure 5.20 Plots of TEP_c (µmol l^{-1}) versus temperature (ºC) and salinity concentrations in a-c) surface and b-d) bottom during summer 2015 in the five different regions of the North Sea: Southern Coastal (SC), Southern Mixed (SM), Transitional (T), Northern Stratified (NS) and Northern Coastal (NC). Black line represents linear regression curve for all the data points. 177

Figure 5.21 Plots of TEP_c (µmol l^{-1}) versus nutrients concentrations a) TOxN, b) PO_4, c) SiO_4 in surface during summer 2015 in the five different regions of the North Sea: Southern Coastal (SC), Southern Mixed (SM), Transitional (T), Northern Stratified (NS) and Northern Coastal (NC). The black line represents the linear regression curve for all the data points. 178

Figure 5.22 Plots of TEP_c (µmol l^{-1}) versus nutrient (µmol l^{-1}) concentrations a) TOxN, b) PO_4, c) SiO_4 in bottom waters during summer 2015 in the five different regions of the North Sea: Southern Coastal (SC), Southern Mixed (SM), Transitional (T), Northern Stratified (NS) and Northern Coastal (NC). The black line represents the linear regression curve for all the data points. ... 179

Figure 5.23 Plots of TEP_c (µmol l^{-1}) versus POC (µmol l^{-1}) and PON (µmol l^{-1}) concentrations in a-c) surface and b-d) bottom waters during summer 2015 in the five different regions of the North Sea: Southern Coastal (SC), Southern Mixed (SM), Transitional (T), Northern Stratified (NS) and Northern Coastal (NC). The black line represents the linear regression curve for all the data points. 180

Figure 5.24 Principal coordinates plot (PCO) showing relationships between variables in the five different regions of the North Sea: Southern Coastal (SC), Southern Mixed (SM), Transitional (T), Northern Stratified (NS) and Northern Coastal (NC); in a) surface and b) bottom waters in the year 2015. 181

Figure 5.25 Scheme of the on-deck incubation experiment conducted in the North Sea in the year 2015. Three different treatments were used: (N + P + Si) comprised of nitrogen, phosphorus and silica, (P + Si) comprised of phosphorus and silica and (N) comprised of only nitrogen. 184

Figure 5.26 Plots of TEP_c (µmol l^{-1}) concentrations in the four experiments (a, b, c and d) at starting point control 0 h and after 48 h for the control and the three

different treatments: (N + P + Si) comprised of nitrogen, phosphorus and silica, (P + Si) comprised of phosphorus and silica and (N) comprised of only nitrogen. 185

Figure 5.27 Map showing the location of the SmartBuoy sites: West Gabbard, Warp and Dowsing along the UK coast (Cefas, 2018). 187

Figure 5.28 Seasonal cycle of TEP_c concentration (µmol l^{-1}) collected with Niskin bottle (4 m depth) at three different Smartbuoy sites, a) West Gabbard, b) Warp and c) Dowsing in surface and bottom waters in the year 2015. 189

Figure 5.29 Seasonal cycle of TEP_c concentration (µmol l^{-1}) at the SmartBuoy sites, a) West Gabbard, b) Warp and in surface waters in the year 2015. Comparison between samples of TEP_c collected with the Niskin bottle (4 m depth) and from the SmartBouy (~ 1 m depth). 190

Figure 5.30 Seasonal cycle of TEP_c (µmol l^{-1}) and chlorophyll *a* (µg l^{-1}) concentrations at the SmartBuoy site West Gabbard in surface waters in the year 2015. Comparison between samples of TEP_c (collected with the Niskin bottle and from the SmartBuoy) with chlorophyll *a*. 190

Figure 5.31 TEP_c concentrations (µmol l^{-1}) during the SmartBuoy bag testing experiments. Three experiments: a) experiment 1 reference and sample treated with $HgCl_2$ placed in a horizontal shaker and agitated from 0 h to 168 h at 100 RPM (Revolutions Per Minute); b) experiment 2 reference and sample treated with $HgCl_2$ placed in a vertical shaker and agitated from 0 h to 24 h at 50 RPM; c) experiment 3 reference and sample treated with $HgCl_2$ placed in a rotation shaker and agitated from 0 h to 48 h at 5 and 10 RPM and up to a month at 10 RPM. 192

Figure 5.32 Spatial distribution of TEP_c concentration (µmol l^{-1}) differences in a) surface and b) bottom waters in the North Sea between summer 2015 and 2014.. 194

Figure 6.1 Box and whisker plots of TEP_c (µmol l^{-1}) concentrations in a) surface and b) bottom waters in the Celtic Sea and the North Sea. Celtic Sea three stations: Station A in spring (A SP) and summer (A SU), Station CCS in spring (CCS SP) and summer (CCS SU), Station CS2 in summer (CS2 SU) in the year 2015. For the North Sea five different regions are shown: Southern Coastal (SC), Southern Mixed (SM), Transitional (T), Northern Stratified (NS) and Northern Coastal (NC) in the year 2014 and 2015. The box indicates the lower

to the upper quartile. The horizontal line within the box represents the median. The whiskers indicate the lower and higher data points. The red crosses indicate outliers. The outliers were classified as two times the interquartile range from the median. 201

Figure 1a Relationship between TEP_c (µmol l^{-1}) and biological and physicochemical variables [temperature (°C), salinity, density (kg m^{-3}), chlorophyll *a* (µg l^{-1}), nitrate + nitrite (µM), nitrite (µM), ammonium (µM), phosphate (µM) and silicate (µM)] at Station Celtic Deep (A) in spring 2015 (whole water column ■ the red square indicates samples in the SML; ● the blue circle indicates samples in the BML). 231

Figure 1b Relationship between TEP_c (µmol l^{-1}) and biological and physicochemical variables [temperature (°C), salinity, density (kg m-3), chlorophyll a (µg l^{-1}), nitrate + nitrite (µM), nitrite (µM), ammonium (µM), phosphate (µM) and silicate (µM)] at Station Celtic Deep (A) in summer 2015 (whole water column ■ the red square indicates samples in the SML; ● the blue circle indicates samples in the BML). 232

Figure 2a Relationship between TEP_c (µmol l^{-1}) and biological and physicochemical variables [temperature (°C), salinity, density (kg m^{-3}), chlorophyll *a* (µg l^{-1}), nitrate + nitrite (µM), nitrite (µM), ammonium (µM), phosphate (µM) and silicate (µM)] at Station Candy Floss (CCS) in spring 2015 (whole water column ■ the red square indicates samples in the SML; ● the blue circle indicates samples in the BML). 233

Figure 2b Relationship between TEP_c (µmol l^{-1}) and biological and physicochemical variables [temperature (°C), salinity, density (kg m^{-3}), chlorophyll *a* (µg l^{-1}), nitrate + nitrite (µM), nitrite (µM), ammonium (µM), phosphate (µM) and silicate (µM)] at Station Candy Floss (CCS) in summer 2015 (whole water column ■ the red square indicates samples in the SML; ● the blue circle indicates samples in the BML). 234

Figure 3 Relationship between TEP_c (µmol l^{-1}) and biological and physicochemical variables [temperature (°C), salinity, density (kg m^{-3}), chlorophyll *a* (µg l^{-1}), nitrate + nitrite (µM), nitrite (µM), ammonium (µM), phosphate (µM) and silicate (µM)] at Station Shelf Edge (CS2) in summer 2015 (whole water

column ■ the red square indicates samples in the SML; ● the blue circle indicates samples in the BML). 235

LIST OF TABLES

Table 1.1 Average concentrations (minimum – maximum) of TEP (µg Xeq. l^{-1}) for different locations, seasons and depths. TEP concentrations are expressed in micrograms of Gum Xanthan equivalent per litre (µg Xeq. l^{-1}). 38

Table 2.1 Regression statistic and ANOVA of the calibration curve..... 58

Table 2.2 Regression statistic and ANOVA of the calibration curve..... 60

Table 2.3 The specific settings of the camera. 61

Table 2.4 Photographic method: regression statistic and ANOVA of the curve..... 63

Table 2.5 TEP concentration (µg Xeq. l^{-1}) for each storage experiment at five different time steps and the reference. 66

Table 2.6 Mean concentrations of TEP (µg Xeq. l^{-1}), standard deviation and percentage of increase/decrease of TEP concentrations respect to the reference for each storage experiment. 67

Table 2.7 TEP concentration (µg Xeq. l^{-1}) in each storage experiment at five different time steps and the reference for Cend 8/15 Station 1. 69

Table 2.8 Mean concentrations of TEP (µg Xeq. l^{-1}), standard deviation and percentage of increase/decrease of TEP concentrations with respect to the reference for each storage experiment. 69

Table 2.9 TEP concentration (µg Xeq. l^{-1}) in each storage experiment at five different time steps and the reference for Cend 8/15 Station 6. 70

Table 2.10 Mean concentrations of TEP (µg Xeq. l^{-1}), standard deviation and percentage of increase/decrease of TEP concentrations with respect to the reference for each storage experiment. 70

Table 2.11 TEP concentration (µg Xeq. l^{-1}) in each storage experiment at five different time steps and the reference for Cend 24/15 Station 8. 71

Table 2.12 Mean concentrations of TEP (µg Xeq. l^{-1}), standard deviation and percentage of increase/decrease of TEP concentrations with respect to the reference for each storage experiment. 71

Table 2.13 TEP concentration (µg Xeq. l^{-1}) in each storage experiment at five different time steps and the reference for Cend 24/15 Station 21. 72

Table 2.14 Mean concentrations of TEP (µg Xeq. l^{-1}), standard deviation and percentage of increase/decrease of TEP concentrations with respect to the reference for each storage experiment. 72

Table 3.1 Summary of the specific parameters (symbol, description and unit) used to represent TEP in ERSEM. 91

Table 4.1 Results of TEP (µg Xeq. l^{-1}), TEP_c (µmol l^{-1}), chlorophyll *a* (µg l^{-1}), Particulate Organic Carbon (POC) (µmol l^{-1}), Particulate Organic Nitrogen (PON) (µmol l^{-1}), % of TEP_c in the pool of POC, TEP:Chl ratio (µg Xeq. µg Chl *a* $^{-1}$), Stickiness (α), Salinity and Temperature (°C) (minimum, maximum and average) for each station during spring and summer, in the SML and in the BML. 102

Table 4.2 Table summarising the results from the box model describing the fate of TEP_c and fluxes at three stations in the Celtic Sea. $\boldsymbol{TEPcSML}$ - average TEP_c concentration in the SML (µmol l^{-1}), $\boldsymbol{TEPc\ form}$ - TEP_c formation rate in the SML (µmol l^{-1} d^{-1}), $\boldsymbol{TEPc\ exp}$ - TEP_c export flux (mmol m^{-2} d^{-1}), $\boldsymbol{sinkSML}$ - TEP_c sinking rate at the SML (m d^{-1}), $\boldsymbol{TEPcBML}$ - average TEP_c concentration in the BML (µmol l^{-1}), $\boldsymbol{TEPc\ acc}$ - potential accumulation rate of TEP_c in the BML (µmol l^{-1} d^{-1}) without bacterial uptake, $\boldsymbol{TEPc\ res}$ - TEP_c residence time (days), $\boldsymbol{TEPc\ uptb}$ - TEP_c loss due to bacterial uptake (mmol m^{-2} d^{-1}), $\boldsymbol{sinkbott}$ - potential TEP_c sinking rate without bacterial uptake (m d^{-1}), $\boldsymbol{sinkbottb}$ - potential TEP_c sinking rate with bacterial uptake (m d^{-1}) 111

Table 4.3 Equation symbols, description and units. 116

Table 4.4 Parameter symbols, description, range and unit. 117

Table 4.5 Porosity and particle size values from different aggregate types, from different studies at different locations. 118

Table 4.6 Comparison of aggregate velocity (m d^{-1}) results from the TEP in the aggregation model and the box model at the Stations A, CCS and CS2 in spring and summer. Three possible ranges of particle size 4 - 10, 10 - 40 and 40 - 60 µm in diameter were investigated. Aggregates were composed of Transparent Exopolymer Particle (TEP), Particular Organic Matter (POM) and mineral (min). 121

Table 4.7 Parameter symbols, description, value and unit used in the TEP model. 124

Table 4.8 Comparison of TEP concentration (µg Xeq. l^{-1}), TEP : Chlorophyll *a* ratio (µg Xeq. µg Chl a $^{-1}$), TEP (log_{10} µg Xeq. l^{-1}) versus chlorophyll *a* (log_{10} µg l^{-1}) equation between different studies with comparable water column depth. For TEP concentration these values are indicated: average (minimum – maximum). The TEP to chlorophyll fits are for logarithms to base 10. 141

Table 4.9 Comparison of the three different modelling approaches (box model, TEP in the aggregation model and TEP model in ERSEM). 147

Table 4.10 Summary of the different approaches (box model and TEP model in ERSEM) used at the Station A in the Celtic Sea in spring and summer to discover the role played by TEP in carbon cycling..... 149

Table 5.1 Regression analysis of TEP_c (µmol l^{-1}) versus chlorophyll *a* (µg l^{-1}) concentrations in surface and bottom waters during summer 2014 in the five different regions of the North Sea: Southern Coastal (SC), Southern Mixed (SM), Transitional (T), Northern Stratified (NS) and Northern Coastal (NC). 165

Table 5.2 Regression analysis of TEP_c concentration (µmol l^{-1}) versus temperature (ºC) and salinity in surface and bottom waters during summer 2014 in the five different regions of the North Sea: Southern Coastal (SC), Southern Mixed (SM), Transitional (T), Northern Stratified (NS) and Northern Coastal (NC). 166

Table 5.3 Regression analysis of TEP_c (µmol l^{-1}) versus nutrient (µmol l^{-1}) concentrations in surface and bottom waters during summer 2014 in the five different regions of the North Sea: Southern Coastal (SC), Southern Mixed (SM), Transitional (T), Northern Stratified (NS) and Northern Coastal (NC). 167

Table 5.4 Table summarising the results from the box model describing the fate of TEP_c and fluxes in the North Sea in stratified and mixed waters for the year 2014 in the five regions of the North Sea: Southern Coastal (SC), Southern Mixed (SM), Transitional (T), Northern Stratified (NS) and Northern Coastal (NC). $\boldsymbol{TEPcSML}$ - TEP_c concentration in the SML (µmol l^{-1}), $\boldsymbol{TEPc\ form}$ - TEP_c formation rate in the SML (µmol l^{-1} d^{-1}), $\boldsymbol{TEPc\ exp}$ – TEP_c export flux (mmol m^{-2} d^{-1}), $\boldsymbol{sinkSML}$ – TEP_c sinking rate at the SML (m d^{-1}), $\boldsymbol{TEPcBML}$ - TEP_c concentration in the BML (µmol l^{-1}), $\boldsymbol{TEPc\ acc}$ – potential accumulation rate of TEP_c in the BML (µmol l^{-1} d^{-1}) without

bacterial uptake, $\boldsymbol{TEPc\ res}$ - TEP_c residence time (d), $\boldsymbol{TEPc\ uptb}$ – TEP_c loss due to bacterial uptake (mmol m^{-2} d^{-1}), $\boldsymbol{sinkbott}$ – potential TEP_c sinking rate without bacterial uptake (m d^{-1}), $\boldsymbol{sinkbottb}$ – potential TEP_c sinking rate with bacterial uptake (m d^{-1}). 170

Table 5.5 Regression analysis of TEP_c (µmol l^{-1}) versus chlorophyll *a* (µg l^{-1}) concentrations in surface and bottom waters during summer 2015 in the five different regions of the North Sea: Southern Coastal (SC), Southern Mixed (SM), Transitional (T), Northern Stratified (NS) and Northern Coastal (NC). 177

Table 5.6 Regression analysis of TEP_c concentration (µmol l^{-1}) versus temperature (ºC) and salinity in surface and bottom waters during summer 2015 in the five different regions of the North Sea: Southern Coastal (SC), Southern Mixed (SM), Transitional (T), Northern Stratified (NS) and Northern Coastal (NC). 178

Table 5.7 Regression analysis of TEP_c (µmol l^{-1}) versus nutrient (µmol l^{-1}) concentrations in surface and bottom waters during summer 2015 in the five different regions of the North Sea: Southern Coastal (SC), Southern Mixed (SM), Transitional (T), Northern Stratified (NS) and Northern Coastal (NC). 179

Table 5.8 Regression analysis of TEP_c (µmol l^{-1}) versus POC (µmol l^{-1}) and PON (µmol l^{-1}) concentrations in surface and bottom waters during summer 2015 in the five different regions of the North Sea: Southern Coastal (SC), Southern Mixed (SM), Transitional (T), Northern Stratified (NS) and Northern Coastal (NC). 180

Table 5.9 Table summarising the results from the box model describing the fate of TEP_c and fluxes in the North Sea in stratified and mixed waters for the year 2015 in the five regions of the North Sea: Southern Coastal (SC), Southern Mixed (SM), Transitional (T), Northern Stratified (NS) and Northern Coastal (NC). $\boldsymbol{TEPcSML}$ - TEP_c concentration in the SML (µmol l^{-1}), $\boldsymbol{TEPc\ form}$ - TEP_c formation rate in the SML (µmol l^{-1} d^{-1}), $\boldsymbol{TEPc\ exp}$ - TEP_c export flux (mmol m^{-2} d^{-1}), $\boldsymbol{sinkSML}$ - TEP_c sinking rate at the SML (m d^{-1}), $\boldsymbol{TEPcBML}$ -TEP_c concentration in the BML (µmol l^{-1}), $\boldsymbol{TEPc\ acc}$ - potential accumulation rate of TEP_c in the BML (µmol l^{-1} d^{-1}) without bacterial uptake, $\boldsymbol{TEPc\ res}$ - TEP_c residence time (d), $\boldsymbol{TEPc\ uptb}$ - TEP_c loss due to bacterial uptake (mmol m^{-}

^{2} d^{-1}), ***sinkbott*** - potential TEP_c sinking rate without bacterial uptake (m d^{-1}), ***sinkbottb*** - potential TEP_c sinking rate with bacterial uptake (m d^{-1}). 182

Table 5.10 Table summarising the results of the four different incubation experiments in the North Sea in year 2015. Location of the sample (latitude and longitude), temperature (ºC), salinity, chlorophyll *a* (µg l^{-1}), nitrate (NO_3), phosphate (PO_4), silicate (SiO_4) and TEP_c (µmol l^{-1}) at starting point 0 h. TEP_c concentrations after 48 h for control and the three different treatments: (N +P + Si) comprised of nitrogen, phosphorus and silica, (P + Si) comprised of phosphorus and silica and (N) comprised of only nitrogen. 186

Chapter 1 Introduction

1.1 Ocean carbon cycling

The ocean plays an important role in the carbon cycle by storing large amounts of carbon, particularly in the deep ocean. Figure 1.1 of the global carbon cycle shows that the ocean stores many more times the carbon than that which is in the atmosphere. This storage is mediated by the export of organic matter from the surface ocean, which is biological in origin. Whilst a small amount of carbon globally comes from terrestrial environment via rivers, this may be more significant in shelf seas (Hansell, 2013; Barrón and Duarte, 2015).

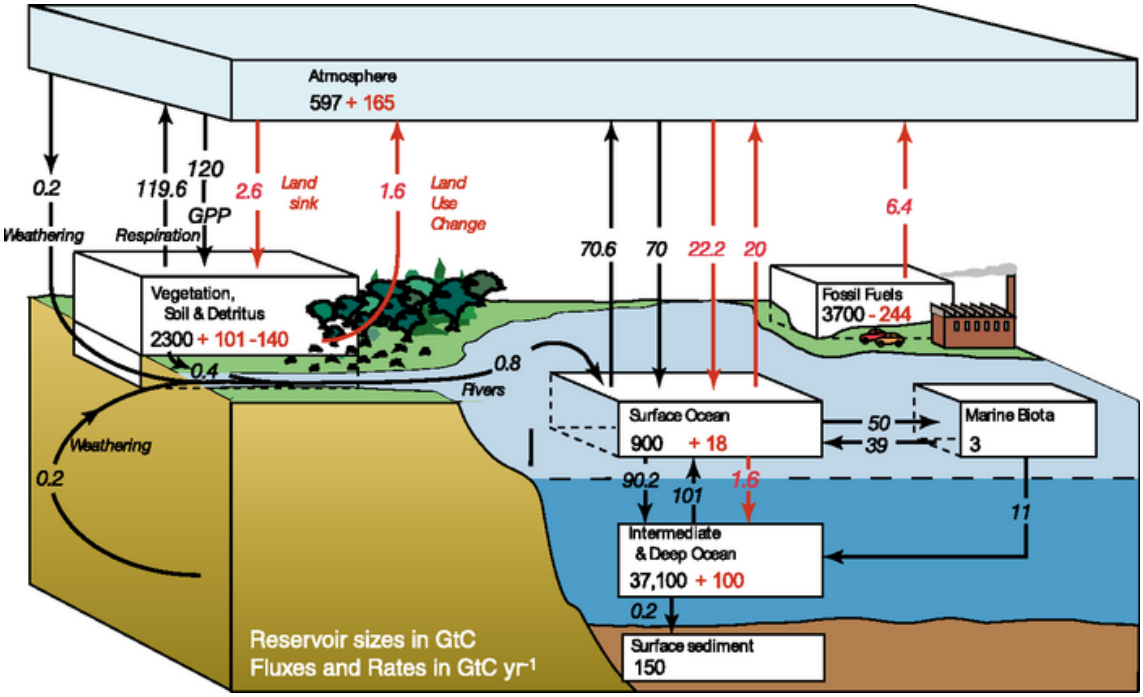

Figure 1.1 Schematic representation of the global carbon cycle (Ciais *et al.*, 2013).

1.2 Biological pump, solubility pump and microbial carbon pump

Two mechanisms are responsible for the regulation of the atmospheric carbon dioxide (CO_2) by the oceans. The first mechanism is the cycling of the inorganic carbon and involves CO_2 air-sea exchange (Liss and Merlivat, 1986; Nightingale *et al.*, 2000) and the dissociation of the carbonic acid (Dickson *et al.*, 2007). The second mechanism is biotic and it is linked to the biological activity and cycling of inorganic or organic carbon (Heinze *et al.*, 2015).

In the solubility pump, the ocean equilibrates with the atmosphere via ocean-atmosphere gas exchange. Given a steady atmospheric concentration of CO_2, the surface ocean would be in long-term equilibrium with the atmosphere, or at least at steady state and no biological activity. However, as we are pumping CO_2 into the atmosphere by human activity the ocean is responding by taking up more inorganic carbon (Sabine *et al.*, 2004; Le Quéré *et al.*, 2016). In the biological pump the surface ocean is under-saturated with respect to CO_2 in spring and summer in many parts of the ocean following biological uptake, which leads to a solubility-driven response in air-sea CO_2 flux. The deep ocean is supersaturated in dissolved inorganic carbon (DIC) due to the subsequent sinking and remineralization of this organic carbon produced in the surface. For most organic matter the remineralistion is kinetically limited, so the faster the sinking rate the more efficient the carbon export (Ducklow *et al.*, 2001). The biological pump efficiency has generally been estimated using sediment trap data from the mesopelagic (Ducklow *et al.*, 2001) and relies on the assumption that particles sink fast enough for the system to be assumed to be at steady state. However, Giering *et al.* (2017) recently observed that particle sinking velocities in the N. Atlantic of < 40 m d^{-1} were too slow for the steady state assumption to hold. This means that the sinking rates and strength of the biological pump are not fully understood. In the microbial carbon pump, refractory organic matter from the terrestrial environment (Ward *et al.*, 2017) or produced in the ocean that cannot be remineralized or broken down, forms a significant pool of carbon in the deep ocean which has a lifetime of tens of thousands of years (Hansell, 2013). This refractory pool has a high C : N ratio as more bioavailable, relatively N-rich organic compounds tend to be remineralised (Jiao *et al.*, 2014).

1.2.1 Continental shelf pump (CSP)

Shelf seas play an important role in the ocean carbon cycle due to their high productivity and differential cooling relative to the adjacent open ocean (Tsunogai *et al.*, 1999; Yool and Fasham, 2001) and physical processes at the shelf edge favoring export of water off-shelf to depth (Huthnance, 1995; Simpson and McCandliss, 2013). Whilst still poorly understood, there is an increasing body of evidence from both measurements and models that continental shelves are a source of DIC (Bozec *et al.*, 2005; Thomas *et al.*, 2005; Chen and Borges, 2009; Wakelin *et al.*, 2012) dissolved organic carbon (DOC) (Barrón and Duarte, 2015; Mannino *et al.*, 2016; Chaichana, 2017) and particulate organic carbon

(POC) (Thomsen *et al.*, 2017) to the open ocean. In recent synthesis papers the continental margins are found to be significant sinks for atmospheric CO_2 in spite of the terrestrial organic matter loading from rivers (Bauer *et al.*, 2013). During pre-industrial times the continental shelf appeared to be heterotrophic. However, in a future scenario the interaction of multiple factors such as acidification and eutrophication would increase the complexity of the system leading to a weaker prediction of the magnitude of organic and inorganic carbon and CO_2 fluxes (Bauer *et al.*, 2013).

The link between air-sea CO_2 uptake in a shelf sea and the export of carbon to the open ocean is complex (Gruber, 2015), and depends on the CO_2 concentration of water coming on to the shelf, seasonal cycles of temperature and stratification and the amount of organic and inorganic carbon travelling down rivers. However, all else being equal, increased sinking of particulate carbon, and production of carbon-rich organics in a shelf sea greatly act to enhance carbon export. The Figure 1.2 from Gruber (2015) shows the global ocean of sinks and sources of carbon dioxide. The map highlights that temperate and high latitude coastal regions are sinks for atmospheric CO_2 (e.g. the North Sea and the Celtic Sea).

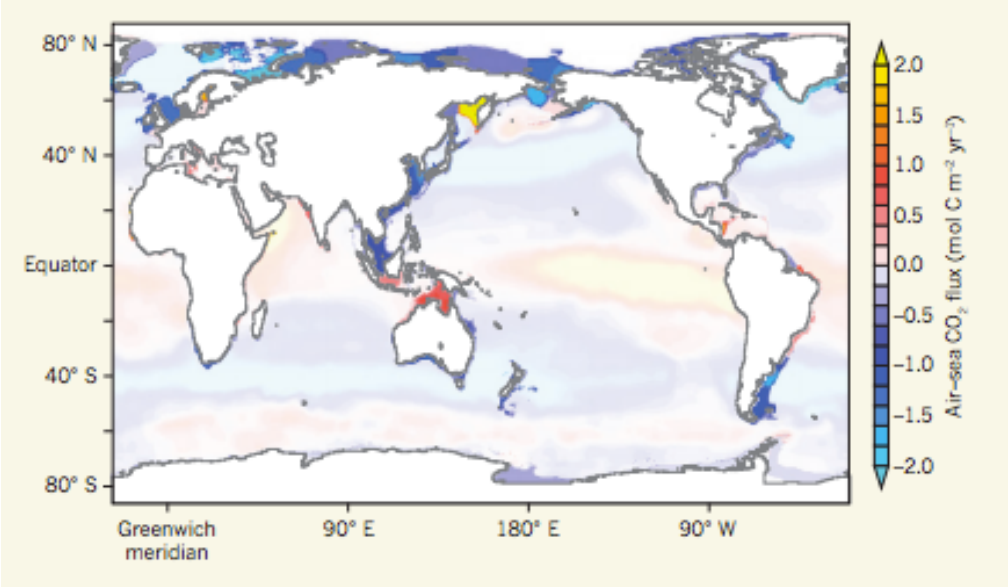

Figure 1.2 Air-sea CO_2 fluxes (mmol C m^{-2} y^{-1}) on a global scale (Gruber, 2015). Air-sea CO_2 fluxes are high in coastal areas.

1.3 Continental shelf seas

Shelf seas cover 7% of the global ocean surface area. Despite this, shelf seas account for 10-30% of the global marine primary production (Gattuso *et al.*, 1998) and they play a key role in the global carbon cycle (Walsh, 1991; Mackenzie *et al.*, 2004). Shelf seas have strong biological activity and represent a link between the terrestrial, oceanic and atmospheric carbon reservoirs (Gattuso *et al.*, 1998). Continental shelf seas, such as the North Sea, make an important contribution to uptake of CO_2 from the atmosphere, through physical and biological processes, i.e. the Continental Shelf Pump (CSP) (Tsunogai *et al.*, 1999; Thomas *et al.*, 2004; Borges *et al.*, 2005). Nevertheless, the mechanisms and seasonality of this continental shelf pump are not fully understood (Prowe *et al.*, 2009). The North Sea for instance, has a shallow, permanently mixed southern region and a northern, seasonally stratified region. The North Sea has been recognised as a system with a strong sink for atmospheric CO_2 of 1.4 mol C m^{-2} yr^{-1} (Thomas *et al.*, 2004; Thomas *et al.*, 2005). Ninety percent of this CO_2 uptake from the atmosphere by the North Sea is exported to the North Atlantic Ocean, making the North Sea a very efficient CSP (Thomas *et al.*, 2005).

1.3.1 Northwestern European shelf seas

1.3.1.1 Celtic Sea

The Celtic Sea (Figure 1.3) is a temperate shelf sea on the northwestern European continental margin, covering an area from Brittany (France), to the south of Ireland, St. Georges Channel and Cornwall (UK). The continental shelf has a total surface area of 130,000 km^2. It represents a transition zone which separates Atlantic waters on the margins of the European continental shelf from the coastal waters of the Bristol Channel and the Irish Sea (Brown *et al.*, 2003).

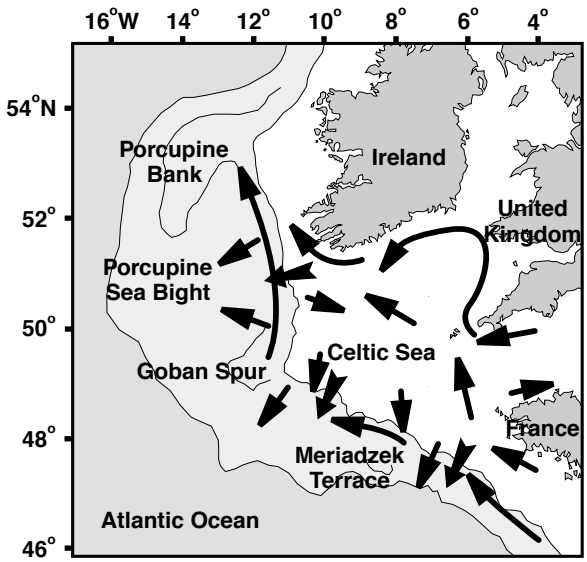

Figure 1.3 The Celtic Sea with its circulation and carbon transport pathway adapted from de Haas *et al.* (2002). → indicates main oceanographic currents; ➤ indicates main carbon tranport. The white colour indicates depth of less than 100 m, the light grey of 100-200 m and the medium grey of more than 200 m.

The water column structure of the Celtic Sea is determined by the combination of two processes: buoyancy input by surface heating and turbulent mixing induced by shear stresses due to barotropic tides (Simpson and Hunter, 1974; Simpson and Bowers, 1981). The water column is mixed from late December to early May due to wind forcing (Brown, 1991; Knight and Howarth, 1999; Young *et al.*, 2001; Brown *et al.*, 2003). During winter/spring the Celtic Sea is influenced by water masses from the Atlantic Ocean with high salinity along the Cornish coast (Pingree 1980) and by water from the River Severn. In the Celtic Sea the shelf edge at 200 m depth represents the boundary between the shallow shelf sea and the deep ocean (Huthnance, 1995). It has a distinct biological activity (Fernández *et al.*, 1993) and plays an important role in mediating the exchange of water, nutrient and carbon fluxes with the open ocean (Liu *et al.*, 2000). The shelf edge is an area where turbulence and mixing are able to re-suspend sediment (Heathershaw *et al.*, 1987; Puig *et al.*, 2004) and nutrients (Holligan *et al.*, 1985; Brickman and Loder, 1993; Sharples *et al.*, 2001).

Primary production (PP) at the shelf edge in the Celtic Sea at the beginning of spring bloom is estimated to be ~ 70 mmol C m^{-2} d^{-1}, reaching 120 mmol C m^{-2} d^{-1} during the later stages of the spring bloom (Rees *et al.*, 1999). The PP in the seasonal thermocline (summer) in the Celtic Sea ranges from 16 to 32 mmol C m^{-2} d^{-1} (Hickman *et al.*, 2012). On an annual scale the Celtic Sea has a primary production of 102 g C m^{-2} y^{-1} (Joint *et al.*, 1986). By including dissolved organic matter, total primary production reaches ~15

x 10^6 ton C y^{-1}. The Celtic slope is a very productive area of the Celtic Sea where the primary production reaches 162 g C m^{-2} y^{-1} (de Haas *et al.*, 2002). The Celtic Sea is characterized by fine and coarse sandy, gravelly or muddy sediments (grain diameter <63 μm) (Belderson and Stride, 1966; Pantin and Evans, 1984; Heathershaw and Codd, 1986). The majority of the organic carbon produced in the Celtic Sea is exported off the shelf to the continental slope where it is stored long-term (de Haas *et al.*, 2002). Only a small area of the Celtic Sea with a weak current allows deposition of the organic carbon in shelf sediments (McCave, 1971).

1.3.1.2 North Sea

The North Sea (Figure 1.4) is a marginal, shallow sea (area of around 750,000 km^2) on the European continental shelf with an open northern boundary to the North Atlantic Ocean. In the west and south it is surrounded by the British Isles, and the European continent (France, Belgium, Netherlands, Germany and Denmark), while Norway is on its north-eastern and eastern side. The North Sea has a shallow southeastern region (< 50 m), separated by the Dogger Bank from a deeper central region (50 – 100 m), which extends along the north British coast. The central northern region of the shelf gradually deepens to 200 m before reaching the shelf edge (Howarth, 2001). The main circulation in the North Sea is an anti-clockwise rotation along its edges. The main inflow of water is from the North Atlantic Ocean via the Shetland Channel and the Fair Island Channel, with the outflow leaving along the Norwegian Trench on the eastern boundary (Lenhart and Pohlmann, 1997). A small proportion of the North Atlantic inflow reaches the region south of the Dogger Bank (55° N, 3° E), which is otherwise dominated by an inflow of water from the English Channel (Thomas *et al.*, 2005). Furthermore, there is a high variability in the source and volume of water entering into the system between seasons and years, that is correlated to climatic conditions. The average water temperature ranges from 17 °C in summer to 6 °C in winter. The salinity averages ranges from 34 to 35. Based on water column stratification, the North Sea can be separated into two different biogeochemical regions: a shallow, southern region and a seasonally stratified, northern region (Thomas *et al.*, 2004). The boundary between the two biogeochemical regions is at approximately 54° N in the west and at 57° N in the east (Figure 1.4), corresponding to the northern part of the Dogger Bank (Ducrotoy *et al.*, 2000; Emeis *et al.*, 2015).

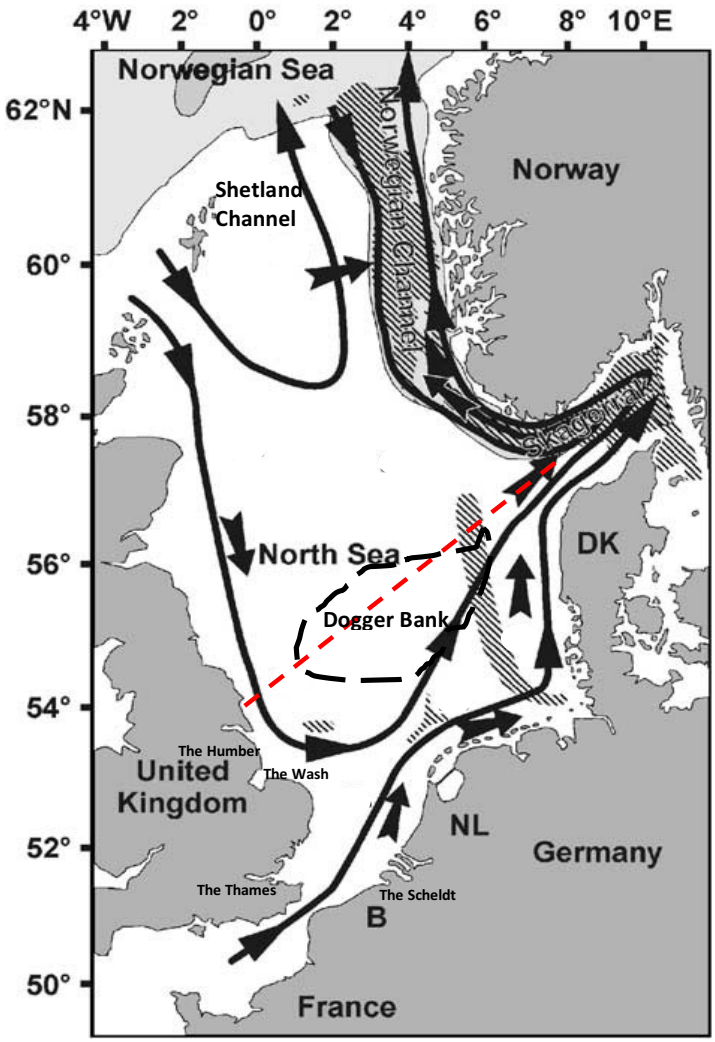

Figure 1.4 The North Sea with its circulation pattern and carbon transport pathway adapted from de Haas *et al.* (2002). → indicates the main oceanographic currents; ➟ indicates the main carbon tranport. The dashed red line indicates the approximate boundary between the two biogeochemical regions (northern and southern).

The shallow southern region with high primary productivity (300 - 350 g C m^{-2} y^{-1}) (Emeis *et al.*, 2015) is affected by terrestrial and anthropogenic nutrient inputs and is characterized by a permanently mixed water column throughout the year. After an initial uptake of dissolved inorganic carbon (DIC) during the spring bloom, DIC remains at intermediate levels throughout the water column (Prowe *et al.*, 2009). The northern region is characterized by lower primary productivity (50 - 100 g C m^{-2} y^{-1}) as a result of seasonal stratification and the influence of the Atlantic waters (Emeis *et al.*, 2015) and a net export of particulate organic matter (POM) and nutrients to the deeper layers (Thomas *et al.*, 2004). The southern region has very low annual net air–sea CO_2 fluxes when compared with the northern region, where a strong uptake of atmospheric CO_2 is recorded (Thomas *et al.*, 2004).

Marine suspended sediments are supplied to the North Sea from the Norwegian Sea, the English Channel and the Baltic Sea. Riverine input reaches the North Sea by the Elbe, Ems (German coast), Rhine, Meuse, Scheldt (Dutch and Belgium coasts), Thames, Wash and Humber (UK coast), suppling ~ 4.0 x 10^6 ton C y^{-1} (Brockmann *et al.*, 1990). Due to riverine influences the shallow southern region of the North Sea is characterized by a high suspended particulate matter load, especially during the winter time from the Thames plume (Eleveld *et al.*, 2008; Weston *et al.*, 2008; Chaichana, 2017). Sediments of fine grain which are rich in organic matter are prevalent in the North Sea. A large part of those sediments is transported by the anti-clockwise residual circulation and accumulates in the Skagerrak. A small part is transported into the Norwegian Channel (de Haas *et al.*, 1997; de Haas and van Weering, 1997).

1.4 Organic carbon in shelf seas

1.4.1 The organic carbon pump

The ocean is one of the largest reservoirs of carbon in the world (Figure 1.1). Dissolved organic carbon (DOC) is the second largest carbon pool in the oceans (Hansell and Carlson, 2001). Therefore, a key aim for the quantitative assessment of the ocean carbon cycle is comprehending the processes regulating DOC production and consumption (Polimene *et al.*, 2006). In the past decade the role of coastal shelf seas in the uptake of atmospheric CO_2 has been investigated (Borges *et al.*, 2005) and several studies have shown the significant contribution of shelf seas in global ocean carbon uptake (Takahashi *et al.*, 2009). Continental shelf seas play a key role in the cycling of biogeochemical elements through physical and biological mechanisms (Thomas *et al.*, 2004; Borges *et al.*, 2005). Through the 'organic carbon pump', one of the biological pumps (Heinze *et al.*, 1991), shelf seas capture carbon from the atmosphere via primary production and export it to the deep sea. In the organic carbon pump most of the biomass produced in surface waters during primary production by phytoplankton is turned over and respired within the euphotic zone. Only a small portion of this biomass sinks as POC which reach deeper waters. An even smaller fraction of this biomass reaches the seafloor where is buried in sediments (Boyd and Trull, 2007). The greatest part of the sinking particles are remineralised by heterotrophic organisms and CO_2 produced from this process is returned to the atmosphere. The efficiency of this biological pump in removing CO_2 from the atmosphere is affected by the capability of the marine ecosystem to "export" the particulate organic carbon and dissolved organic carbon, produced by biological activity,

from the surface layer to the deep ocean, where it can be stored "long-term". However, the mechanisms of how the CO_2 can be sequestered by shelf seas and the seasonality are not well understood (Prowe *et al.*, 2009).

1.4.2 Carbon export

Coastal seas are important for the marine carbon cycling (Walsh, 1991). However, the mechanism of how the carbon cycles within the coastal areas and its export to the open ocean is not fully understood (Bauer *et al.*, 2001; Vlahos *et al.*, 2002). In coastal seas, the main input of organic carbon comes from rivers (Cauwet, 2002) and discharges of water from land (Burnett *et al.*, 2003). A small fraction is due to atmospheric inputs (Willey *et al.*, 2000). Riverine input of organic carbon in coastal areas is estimated to be ~ 426 Tg C yr^{-1}, of which ~ 250 Tg C yr^{-1} is in form of DOC and ~ 176 Tg C yr^{-1} is in form of POC (Cauwet, 2002).

Diesing *et al.* (2017) found that coastal sediments are important for POC sequestration and storage on the NW European continental shelf. The coastal seas are areas of high productivity where the organic carbon produced exceed rates of respiration (Duarte and Cebrian, 1996; Gattuso *et al.*, 1998). The remaining organic carbon is buried in the sediments or exported to the open ocean (Duarte *et al.*, 2004). The exported carbon can be in the form of particulate organic carbon or dissolved organic carbon . The DOC concentration is usually twice the concentration of POC in surface waters (Druffel *et al.*, 1992; Bauer and Druffel, 1998). The retention time of POC in the ocean (< 1 month) (Lande and Wood, 1987) is shorter than that in the coastal areas (~ 4 months) (Huthnance, 1995). This might indicate that POC is produced and retained in coastal areas (Huthnance, 1995). Furthermore, regional studies showed that 80 % of the organic carbon exported from coastal areas to the open ocean is in form of DOC (Bauer *et al.*, 2001; Vlahos *et al.*, 2002).

1.5 Carbon overconsumption

Biological, chemical and physical mechanisms control the chemical composition of seawater. The average molar C : N : P ratio of oceanic particulate organic matter has been found to be close to 106 : 16 : 1 (Redfield, 1963). This C : N : P stoichiometry refers to the relationships between the organisms and the ecosystem structure, as well as the function with environment and stoichiometry of the organisms (Sterner and Hessen, 1994;

Elser *et al.*, 1996; Elser *et al.*, 2000). However, the C : N : P stoichiometry is not fixed and modifications to its value and range have been reported (Anderson and Sarmiento, 1994; Arrigo, 2005; Moore *et al.*, 2013). Its deviation from the Redfield ratio provides information on nutrient limitation, on primary production (Moore *et al.*, 2013), phytoplankton physiology (Quigg *et al.*, 2003) and the capability of the ocean to sequester carbon (Sigman and Boyle, 2000).

In the marine environment phytoplankton plays an important role in the regulation of atmospheric CO_2, through the fixation of CO_2 by photosynthesis, followed by the export of the organic carbon to the deep ocean (Engel, 2004). The capability of the ocean to take up carbon is related to the availability of nutrients in the surface ocean. Nitrate uptake, along with a carbon to nitrogen (C : N) ratio of 106 : 16 is often used to estimate the new production in the open ocean (Dugdale and Goering, 1967). This is usually done by using a nutrient-based carbon assimilation of the nitrate consumption multiplied by the C : N ratio of 6.6. The new production calculated with this method determines a link between nitrate uptake and the sequestration of carbon by the biological pump (Eppley and Peterson, 1979). However, the Redfield stoichiometry of 6.6 often disagrees with observations, particularly during short periods of time and at specific locations. This indicates a decoupling between the turnover of nitrogen and carbon (Banse, 1974). Sambrotto *et al.* (1993) have found that in coastal areas, shelf seas and the open ocean the ratio of carbon to nitrate uptake in surface waters exceeds the Redfield ratio. This was observed particularly during phytoplankton blooms, where C : N ratios of 8 - 14 were reported (Sambrotto *et al.*, 1993). This phenomenon, where the dissolved inorganic carbon uptake exceeds the amount deduced from the observed nitrate uptake and Redfield stoichiometry (Körtzinger *et al.*, 2001) is known as "carbon overconsumption" (Toggweiler, 1993). The following explanations have been put forward for carbon overconsumption: enzymatic conversion of dinitrogen gas (N_2) to other forms of nitrogen (e.g. ammonia) by microorganisms (Hood *et al.*, 2001), and the formation of extra-cellular Transparent Exopolymer Particles (TEP) rich in carbon exuded by phytoplankton and bacteria (Passow, 2002). In the ocean a dissolved organic matter (DOM) production with high C : N ratios (low-N DOM) has been observed and has been associated with carbon overconsumption (Kähler and Koeve, 2001). In a future scenario (increase in atmospheric CO_2, climate change and eutrophication) the increase of the C : N ratios of DOM from the standard Redfield ratio may affect nutrient cycling, by changing DOM composition from nutrient-rich to nutrient-poor (Sardans *et al.*, 2012) .

Taucher *et al.* (2012) provided a piece of evidence for the possible link between the increase of the C : N ratios under a future scenario of higher atmospheric CO_2 and seawater temperature. They conducted a mesocosm experiment with a natural plankton community collected from the Baltic Sea in summer to investigate how the increase in atmospheric carbon dioxide concentrations and the consequent increase in sea surface temperatures may enhance carbon overconsumption. They carried out a one month experiment where the growth rate of the phytoplankton community was stimulated with the addition of nutrient. Furthermore, the experiment was produced under altered growth temperature conditions from the ambient temperature of ± 4 °C. The increased temperature produced an increase in the uptake of DIC and in the production of DOC and POC. Furthermore, the authors reported an increase of the elemental ratios of carbon and nitrogen (C : N) in dissolved organic matter and particulate organic matter, with C : N ratios of more than 30. They suggest that high temperatures produce an increase in the fixation of carbon. However, their results are opposite to similar experiments conducted in spring. They concluded that mesocosm experiments in different seasons are dominated by different phytoplankton species. Therefore, the phytoplankton community might play a role in the response of the biogeochemical cycling to the increase in seawater temperatures.

Prowe *et al.* (2009) investigated the mechanisms that control the air-sea CO_2 flux in the North Sea by using a three-dimensional ecosystem model. They ran the model in the northern and southern region of the North Sea for the year 2001 and validated the model output against fieldworks observations. Two runs were performed at each location. The first run using a model with fixed Redfield ratio and the second run using a model with a non-fixed Redfield ratio. Their results indicated that the air-sea CO_2 flux in the two regions were strongly affected by water column stratification. For instance, in the southern North Sea the continuum recycling of nutrients did not allow the fixation of carbon. Both models and observations showed no significant differences in the uptake of DIC. On the contrary in the northern North Sea, the stratification of the water column in summer produced nutrient limitation, which facilitated the fixation of carbon and produced a net difference in DIC uptake between the two models and the observations. In particular, the model with a non-fixed Redfield ratio was in a good agreement with the observations, indicating a carbon overconsumption of DIC of 40 μmol kg^{-1} in respect to the model with a fixed Redfield ratio in summer. They argued that this carbon overconsumption may be in part associated with the production of TEP in surface water

in the northern North Sea region in summer. The authors concluded that during productive season carbon overconsumption and the formation of dissolved organic carbon, (e.g. TEP) by primary production is important for driving CO_2 fluxes in the northern North Sea.

Another modelling study conducted by Schartau *et al.* (2007) simulated the phenomenon of carbon overconsumption in conjunction to the formation of TEP. Their modelling approach was used to reproduce a mesocosm experiment, which was performed in a tank under controlled experimental conditions with seawater collected from the Santa Barbara Channel. The authors assessed the ability of the model to reproduce a combination of processes such as phytoplankton acclimation to nitrogen stress, carbon overconsumption, exudation and coagulation of DOC to form TEP. The model reproduced two pathways that involve the overconsumption of carbon. In the first pathway DOC is exuded during phytoplankton growth. In the second pathway POC is produced by phytoplankton under nutrient limited conditions. The results from the modelling work were consistent with the observations from the mesocosm experiment. The authors reported that the predicted and observed increase in POC of 30% found in their study was associated with the formation of TEP.

1.6 Transparent Exopolymer Particles (TEP)

Alldredge *et al.* (1993) describe transparent exopolymer particles as transparent gel particles formed from extracellular polymeric substances (EPS) exuded by microorganisms. TEP are abundant in open oceans and coastal waters with sizes ranging from <1 μm to 200 μm. Due to their high carbon content and low nitrogen content (Mari *et al.*, 2001), and their high capability to aggregate solid particles, TEP may provide a mechanism by which DOM, originating from excess carbon uptake in the euphotic zone, can contribute to particle export by interaction with sinking particles (Engel and Passow, 2001). Passow (2002) proposed two different mechanisms of TEP formation from dissolved organic matter in the marine environment (Figure 1.5).

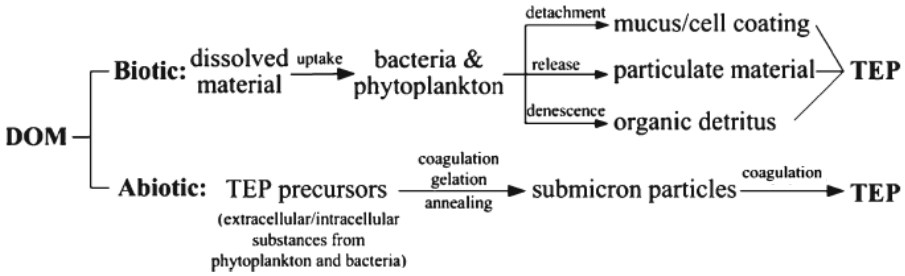

Figure 1.5 Formation of TEP from dissolved organic matter proposed by Passow (2002) from Meng *et al.* (2013).

In the first pathway, TEP is generated by bacteria and phytoplankton from particulate material, mucus, organic detritus and cell-coating surfaces. In the second pathway, precursor substances form TEP under specific environmental conditions such as turbulence and presence of inorganic colloids. The latter pathway could be the primary source of TEP in marine environments (Passow, 2002). The precursor substances, for example polysaccharide fibrils, are produced by cell breakage or lysis or are secreted by microorganisms (Leppard *et al.*, 1977). Submicron gel-like substances are then produced from these polysaccharide fibrils through three different processes: 1) coagulation, the formation of a gel particle by the collision and subsequent sticking of two smaller polymers (Wells and Goldberg, 1993), 2) gelation where the formation of a gel from linking between chains of branched polymers leads to the formation of a progressively larger polymer, or 3) annealation where the polymers from one gel diffuse and interpenetrate with other gels forming a larger polymer (Chin *et al.*, 1998).

1.7 Ecological and biogeochemical relevance of TEP in the marine ecosystem

1.7.1 Abundance and distribution of TEP

Transparent exopolymer particles have been found in fresh water and in marine waters (Passow, 2002). High TEP concentrations have been associated with phytoplankton blooms (Passow and Alldredge, 1994; Passow *et al.*, 1995; Mari and Kiørboe, 1996; Passow *et al.*, 2001). Due to its link with primary production TEP is predominantly found in the euphotic zone and has higher concentrations in coastal seas than in the open ocean (Passow and Alldredge, 1994; Engel and Passow, 2001). The distribution and concentrations of TEP reported for the marine environment are presented in Table 1.1 and expressed as micrograms of Gum Xanthan equivalent per litre (µg Xeq. l^{-1}). The maximum concentration of TEP (14800 µg Xeq. l^{-1}) in marine waters was reported for the Adriatic Sea, which was associated with the production of large amount of mucus

(Radić *et al.*, 2005). Generally, peak concentrations of TEP during phytoplankton blooms are 1000 µg Xeq. l^{-1}, while TEP concentrations in sea ice range from 790 to 7710 µg Xeq. l^{-1} (Krembs *et al.*, 2002). TEP concentrations in the open ocean are two orders of magnitude lower than in coastal areas (Passow, 2002).

Table 1.1 Average concentrations (minimum – maximum) of TEP (µg Xeq. l^{-1}) for different locations, seasons and depths. TEP concentrations are expressed in micrograms of Gum Xanthan equivalent per litre (µg Xeq. l^{-1}).

Location	Season	Depth (m)	TEP (µg Xeq. l^{-1})	References
Santa Barbara mooring, station 2, USA	year-round	20	213 (max = 1042)	Passow *et al.*, 2001
Santa Barbara Channel, USA	summer	20	(80-310)	Passow and Alldredge, 1995
Santa Barbara Channel, USA	summer	10	72 (max = 74)	Passow, 2000
Santa Barbara Channel, USA	winter, summer	0-75	- (29-252)	Passow and Alldredge, 1995
Monterey Bay, USA	summer	10	(50-310)	Passow and Alldredge, 1995
Great Barrier Reef, Australia	winter	5	(23-791)	Wild, 2000
North Adriatic	summer	up to 37	570 (4-14800)	Radić *et al.*, 2005
Mediterranean Sea	-	0-200	21 (5-94)	Ortega-Retuerta *et al*., 2010
Gulf of Cadiz	summer	0-100	118 (25-609)	Garcia *et al.,* 2002
Gulf of Cadiz / Strait of Gibraltar	-	0- 200	- (25-205)	Prieto *et al.,* 2006
NE Atlantic, 47° N	summer	surface	53 (27-294)	Engel *et al.*, 1997
NE Atlantic, 47° N	winter	surface	36	Engel and Passow, 2001
Norwegian fjords	spring	36	193 (max = 258)	Riebesell *et al.*, 1995
Baltic Sea	spring	-	1300	Engel, 2000
Baltic Sea	summer	-	241	Engel and Passow, 2001
Central Baltic Sea	summer	-	(145-322)	Passow, 2002
Chukchi Sea, sea ice, Alaska	spring	-	(790-7710)	Krembs *et al.*, 2002
Otsuchi Bay	spring	-	1344 (24-2321)	Ramaiah *et al.*, 2001
Ross Sea	spring	-	308 (max = 2800)	Hong *et al.*, 1997
Gerlache Strait	-	0-100	- (0-283)	Corzo *et al.*, 2005
Antarctic Peninsula	-	0- 200	15.4 (0-48.9)	Ortega-Retuerta *et al*., 2009

1.7.2 Role of TEP in the formation of marine aggregates

Several studies have reported the crucial role of TEP for the aggregation and potential sinking of particles (Dam and Drapeau, 1995; Logan *et al.*, 1995; Engel, 2000a; Fabricius *et al.*, 2003; Engel *et al.*, 2004; Engel, 2004). Due to its stickiness TEP can act as a glue (Passow, 2002) and can be responsible for the formation of fast sinking aggregates (Mari *et al.*, 2017). TEP itself cannot sink because its density is lower than that of seawater (from 700 to 840 kg m^{-3}) (Azetsu-Scott and Passow, 2004a). This indicates that TEP

represents a pool of carbon-rich POC in surface waters that does not readily sink (Mari *et al.*, 2017). However, TEP is able to promote the aggregation of particles and the consequent formation of marine aggregates. The buoyancy/sinking of these aggregates has been proposed to be sensitive to the ratio of TEP to other particles (of different density) in the aggregate (Mari *et al.*, 2017). A study reports that the fraction of TEP collected at 500 m from sediment traps was lower than the standing stock of TEP (Passow *et al.*, 2001). This may indicate that the buoyancy/sinking mechanism could extend the residence time of aggregates containing TEP in surface waters (Azetsu-Scott and Passow, 2004a) and delay its sinking.

Generally marine snow (aggregates > 0.5 mm (Engel *et al.*, 2002)) has a sinking rate from 20 to 200 m d^{-1} (Armstrong *et al.*, 2009; McDonnell and Buesseler, 2010). In contrast, the sinking velocity of a single diatom cell varies from 0.1 to 1 m d^{-1} (Culver and Smith, 1989). Aggregates containing TEP show a large and variable range of sinking rates not very well estimated, which depends on the size of the aggregate, packaging, porosity (Iversen and Ploug, 2010) and density (Christina and Passow, 2007). The buoyancy/sinking of these aggregates depends on their density which seems to be sensitive to the ratio of TEP to other particles (of different density) in the aggregate (Engel and Schartau, 1999; Azetsu-Scott and Passow, 2004a). Therefore, an increase in the production of TEP might determine a decrease in the downward flux or in the case of very high TEP production may lead to an upward flux that extend the residence time of aggregates containing TEP in surface waters (Azetsu-Scott and Passow, 2004a) and delays their sinking (Mari *et al.*, 2017).

A study conducted by Alonso-González *et al.* (2010) in the south of the Canary Islands reported that more than 60% of the sinking POM collected at 260 m depth in summer/autumn was sinking at a velocity of less than 11 m d^{-1}. They also found that 53% of POM in winter/spring was sinking at a higher velocity of more than 326 m d^{-1}. Their finding may indicate that the lower sinking velocity of the POM found in summer/autumn may be due to the higher presence of TEP in the POM (Mari *et al.*, 2017). TEP is generally produced and accumulated in surface waters during summer (Mari and Burd, 1998).

The North Adriatic Sea is a eutrophic coastal area characterized by the formation of mucilage associate with blooms of diatoms which accumulate in the surface waters. This accumulation has been hypothesized to have occurred due to the strong vertical density

gradient observed in the area (MacIntyre *et al.*, 1995) or the formation of gas bubbles due to the metabolic activity of attached microbes (Riebesell, 1992). However, several studies have reported a high production of TEP in the Adriatic Sea (Schuster and Herndl, 1995; Radić *et al.*, 2005a). Due to their low density and abundance TEP may significantly contribute to the accumulation of mucilage in the surface waters (Mari *et al.*, 2017). Moreover, the potential contribution of TEP in the accumulation of these aggregates in surface waters can be supported by their high C : N molar ratio, typically of TEP (Müller-Niklas *et al.*, 1994).

Another piece of evidence that shows the potential role of TEP in reducing the export of POM comes from a study conducted by Mari *et al.* (2017) in two different systems: the Kattegat and the Mediterranean Sea. They estimated the density of an hypothetical aggregate composed of TEP and phytoplankton cells (diatoms). In this study the density of the aggregate containing TEP was computed by using an approximate density of diatom cells of 1120 kg m^{-3} (Van Ierland and Peperzak, 1984) and the highest TEP density of 840 kg m^{-3} (Azetsu-Scott and Passow, 2004a). They also assumed that the aggregate containing TEP had a porosity of 90% (Ploug and Passow, 2007). The study concluded that the export of POC was influenced by the aggregate containing TEP density and that this mechanism led to the accumulation of a carbon-rich pool (i.e. TEP) in surface waters, with a temporary reduction of the downward export of POM. The accumulation in surface waters of this carbon-rich pool determines its direct exposure to the sunlight, which may lead to an increase of its biological remineralization and photochemical degradation (Mari *et al.*, 2017). Mari *et al.* (2017) concluded that an aggregate composed of TEP and diatoms might sink only if the carbon content of TEP is less than 5% of the total aggregate composition.

In the deep ocean a concept called ballast effect has been reported and used to explain the strong correlation between downward fluxes of POC and their mineral content (Klaas and Archer, 2002; Armstrong *et al.*, 2009). However, such a relationship is not so evident in surface waters (Sanders *et al.*, 2010). Nevertheless, the ballast effect seems to be the mechanism capable to cause the export of TEP from the surface waters (Mari *et al.*, 2017). TEP because of its low density to sink needs to be ballasted with dense particles, which are heavy enough to counteract the low density of TEP. Those particles may be heavy minerals such as carbonate from coccolithophores and foraminifera or siliceous compounds called opal from diatoms (Mari *et al.*, 2017).

To investigate the role of heavy particles on ballasting aggregates containing TEP Mari *et al.* (2017), conducted a study in the northwestern Mediterranean Sea. The study aimed to estimate the density of TEP-mineral aggegrates during winter and summer. As a heavy mineral fraction was used the mineral dust deposition events happened between 2003 and 2007 in the Mediterranean Sea (Ternon *et al.*, 2010). The density of the dust was extrapolated from literature as an average value of 2300 kg m^{-3} (Chou *et al.*, 2011) and the TEP density was supposed to be 840 kg m^{-3} (Azetsu-Scott and Passow, 2004a). The result revealed that even the strongest dust deposition event was not able to cause a downward flux of the TEP-mineral aggregates in summer. In contrast, during winter due to lower concentrations of TEP in surface waters a downward flux of TEP-mineral aggregates was predicted (Mari *et al.*, 2017). This result indicates the complexity of TEP dynamics and the relative contribution of TEP and other ballasting particles in determining the upward or downward flux of aggregates containing TEP (Azetsu-Scott and Passow, 2004a).

In the TEP aggregation process the presence of heavy particles alone does not lead to the formation of sinking aggregate. This is because the aggregation process is a function of other factors such as particle size, rate of collision and particle stickiness (Jackson, 1990; Jackson and Burd, 1998). The formation of aggregates containing TEP is linked to the abundance, size of particles and TEP stickiness, which can define the probability that two different particles stick together. It is clear that TEP stickiness is the main driver of particle aggregation (Engel, *et al.*, 2004). Therefore, any change in TEP stickiness will lead to a change in the formation of aggregates containing TEP, with a consequent potential negative effect on the export of carbon. For instance, it has been reported that low TEP stickiness increases the retention time of particles in surface water, resulting in a lower flux of POC (Kiørboe *et al.*, 1998; Mari *et al.*, 2012). The stickiness varies in relation to the source of TEP, its age and degradation stage. Common values of TEP stickiness ranges from 0.1 to 0.8 and it is linked to the physiological state of the phytoplankton (Kiørboe *et al.*, 1994). Furthermore, an increase of the age of an aggregate produces a decrease in the fraction of TEP (e.g. due to bacterial uptake) which promotes sinking (Ploug *et al.*, 2008). With increasing water column depth, nutrients are not limiting to bacteria which enables an increase of the bacterial remineralization of TEP and a further increase in sinking velocity of the aggregates (Mari *et al.*, 2017).

1.7.3 Accumulation of TEP in surface waters: production and consumption

The accumulation of TEP is result of the balance between the rate of its production and its consumption in surface waters. The factors that affect the production of TEP by phytoplankton include: the light regime (Hong *et al.*, 1997), nutrient limitation (Obernosterer and Herndl, 1995), the physiological state of the phytoplankton (Passow, 2002), the carbon dioxide concentration (Engel, 2002) and phytoplankton growth rate (Waite *et al.*, 1995). Moreover, turbulence can impact on the formation of TEP from exuded DOM (Schuster and Herndl, 1995; Stoderegger and Herndl, 1999; Passow, 2000). Conversely the mechanisms that remove TEP from the surface waters include bacterial remineralization, filter feeders and photodegradation (Mari *et al.*, 2017).

Several studies have linked elevated seawater temperature with the release of extracellular material by phytoplankton, which might lead to an increase in TEP production (Claquin *et al.*, 2008; Piontek *et al.*, 2009; Wohlers *et al.*, 2009; Engel *et al.*, 2010; Fukao *et al.*, 2012; Taucher *et al.*, 2012; Biermann *et al.*, 2014; Seebah *et al.*, 2014a). Morán *et al.* (2006) estimated that an increase of 2 °C of seawater can lead to an extracellular release of TEP precursors by up to 54%.

Nutrient limitation is another factor that may be responsible for an increase in TEP production. It seems that when phytoplankton are nutrient limited there is a consequent increase in the release of extracellular polysaccharides (i.e. TEP precursors) (Myklestad, 1995). Limiting levels of nutrients may lead to the phenomenon called carbon overconsumption, which determines the exudation of carbon-rich DOM from phytoplankton (i.e. precursor of TEP) (Engel, 2002).

Furthermore, ocean acidification seems to have a role in TEP production. Experiments using high partial pressure of carbon dioxide (pCO_2) have shown that ocean acidification may lead to an increase in TEP production (Engel, 2002; Riebesell *et al.*, 2007; MacGilchrist *et al.*, 2014; Song *et al.*, 2014). However, the effect of high pCO_2 on TEP production is questionable (Egge *et al.*, 2007; Passow *et al.*, 2014).

Not very well studied and documented is the role played by bacterial activity in the production of TEP. Bacteria produce extracellular polymeric substances (EPS) (Decho,

1990), which might contribute to the total TEP production (Schuster and Herndl, 1995; Stoderegger and Herndl, 1999; Passow, 2002b; Sugimoto *et al.*, 2007; Koch *et al.*, 2014).

Another mechanism that promotes the formation of TEP is the injection of air bubbles in surface waters due to wind speed (Zhou *et al.*, 1998). This mechanism has also been used in laboratory experiments to generate TEP from seawater rich in DOM (Mopper *et al.*, 1995; Mari and Kiørboe, 1996; Mari, 1999) and investigated by Wurl *et al.* (2011) in their conceptual model of TEP production. Intense wind speed leads to the coagulation of TEP precursors with a consequent increase in the concentration of TEP in surface waters. However, at the same time the introduction of bubbles may increase the buoyancy of TEP and extend its retention time in surface waters (Mari *et al.*, 2017). Still, it has been shown that this mechanism can increase the microbial respiration of DOC (Kepkay and Johnson, 1989) and that it can stimulate the remineralization of TEP by bacteria (Mari *et al.*, 2017).

In addition to removal by sinking of aggregates, TEP can also be removed from the surface waters due to its exposure to strong UV-B radiation especially in the Surface Microlayer (SML) (Mari *et al.*, 2017). The degradation of TEP due to strong UV-B exposure has been predicted in photodegradation experiments conducted by Ortega-Retuerta *et al.* (2009). They observed an average photodegradation rate of ~ 0.3 d^{-1}, which is consistent with the laboratory experiments conducted by Kovac *et al.* (1998) in the northern Adriatic Sea with mucilage.

Another way that TEP can be removed from surface waters is due to bacterial remineralization. Several studies have reported the capability of bacteria to colonise TEP (Alldredge *et al.*, 1993; Passow and Alldredge, 1994; Schuster and Herndl, 1995; Mari and Kiørboe, 1996) and a linear positive relationship between TEP and the alpha/beta glucosidase activity of bacteria was observed (Smith *et al.*, 1995). However, the specific degradation rate of TEP is still unknown due to the practical difficulty in separating processes of formation, degradation and transformation of TEP by bacteria (Mari *et al.*, 2017). The only information available is from a study conducted on extracellular particulate carbohydrates (in part TEP) released by phytoplankton which has shown a degradation rate due to bacterial remineralization of 0.53 d^{-1}. This is much higher than that of POC (0.25 d^{-1}) (Harvey *et al.*, 1995; Mari *et al.*, 2017).

Bacterial degradation can be inhibited during conditions of nutrient limitation in summer in stratified waters. This is determined by the fact that the availability of nitrogen and phosphorus controls the bacterial remineralization rate and bacterial cell division (Zweifel *et al.*, 1993). Moreover, during nutrient limitation phytoplankton releases large amounts of dissolved carbohydrates, which might inhibit the enzymatic activity of bacteria (Obernosterer and Herndl, 1995; Thingstad *et al.*, 1997).

1.7.4 Contribution of TEP to carbon cycling

The formation and export of organic carbon from the surface waters to the seafloor plays a central role in carbon cycling (Mari *et al.*, 2017). TEP, due to its high capability to aggregate solid particles and its high C : N ratio (more than 20; Mari *et al.*, 2017) can promote the export of carbon-rich aggregates. This selective export of carbon by TEP (e.g. high C : N ratio) could produce a decoupling between the export of carbon and nitrogen (Passow, 2002). However, the density of TEP is lower than that of seawater. Therefore the buoyancy/sinking of these aggregates is sensitive to the ratio of TEP to other particles (e.g. phytoplankton cells, POC and detritus) in the aggregate (Mari *et al.*, 2017). Mari *et al.* (2017) estimated that an aggregate formed of TEP and diatoms should sink out only when TEP is less than 5 % of the total aggregate composition. Their modelling experiment showed that the initial concentration of TEP in the aggregate plays a crucial role in the export of organic carbon produced during primary production. As a consequence this may impact on the efficiency of the biological carbon pump in exporting organic carbon from the surface waters to the seafloor. They also postulated that an increase in the fraction of TEP in the aggregate from 5 to 10 % may increase the remineralisation of the fraction of POC from 23 to 48 % in the aggregate in surface waters. The doubling of the fraction of POC remineralised in the surface waters would determine a significant reduction of the efficiency of the carbon pump. This indicates that small changes in the production or degradation of TEP in respect to the other fractions in the aggregate can alter the efficiency of the carbon pump.

The contribution of TEP to carbon cycling in a future scenario (global warming and ocean acidification) is controversial. Some authors reported that an increase in the production of TEP may enhance the flux of POC (Riebesell *et al.*, 2007; Arrigo, 2007). Other authors postulated that this increase in the production of TEP would reduce the biological carbon pump efficiency, by extending the retention time of POC in surface waters (Mari *et al.*,

2017). One phenomenon that in the future will affect the production of TEP would be the increase of the surface temperature of the ocean. There is evidence in literature supporting the hypothesis that global warming will increase the production of TEP in surface waters (Ramaiah *et al.*, 2001; Claquin *et al.*, 2008; Piontek *et al.*, 2009; Wohlers *et al.*, 2009; Fukao *et al.*, 2012; Seebah *et al.*, 2014b). Another future phenomenon related to the increase of the surface temperature in the ocean is the increase of the vertical stratification of the upper ocean (Behrenfeld *et al.*, 2006) and the consequent reduction of the mixed layer depth (Boyd *et al.*, 2007; Rost *et al.*, 2008; Bijma *et al.*, 2013; Reusch and Boyd, 2013). As a consequence in the future the shallower mixed layer and increased vertical stratification will reduce the availability of nutrients in surface waters (Rost *et al.*, 2008; Steinacher *et al.*, 2010) and will extend the period of nutrient limitation. Nutrient limitation is one of the factors that cause the increase of TEP production in surface waters and at the same time it reduces the capability of bacteria to consume TEP (Mari *et al.*, 2017). Ocean acidification is another phenomenon that leads to the production of TEP and TEP precursors (e.g. carbohydrates) (Engel, 2002; Riebesell *et al.*, 2007; Thornton, 2009; Engel *et al.*, 2014; Taucher *et al.*, 2015). The effect of ocean acidification and an increase in the temperature of surface seawaters, in relation to TEP production was investigated for the diatom *Thalassiosira weissflogii* (Seebah *et al.*, 2014a). This study reported that a reduction in the pH, combined with high seawater temperature produced an increase in the production of TEP. The authors observed a reduction in TEP aggregation and a decrease of the sinking velocity of aggregates containing TEP. The role of TEP in the aggregation of particles is well documented in literature. However, there is a lack of information on how TEP is able to mediate this process, the retention time of aggregates containing TEP in surface waters and their sinking velocities. In order to better estimate the contribution of TEP to carbon cycling under future climate change it is important to understand how these changes affect the production of TEP and its physical-chemical properties (e.g. TEP stickiness) (Mari *et al.*, 2017).

1.8 Representation of TEP in marine ecosystem models

TEP is not very often considered in models. However, some efforts have been made to incorporate TEP processes in biogeochemical models (e.g. Kriest, 2002; Schartau *et al.*, 2007; Oguz, 2017b). TEP is usually not included in ecosystem models because it is thought to belong to the refractory dissolved organic matter pool, despite the evidence of its role in particle aggregation processes and sinking of organic matter (Verdugo *et al.*,

2004). From the best of my knowledge there are no studies that have mechanistically investigated the role of TEP in particle aggregation and carbon export by means of a biogeochemical model. Only one recent study used a 1-dimensional approach to model particle aggregation dynamics and the interaction of TEP with the pelagic food webs (Oguz, 2017b). Modelling studies of TEP have investigated TEP processes (e.g. TEP formation, sedimentation) in conceptual models, which were parameterized with the use of experimental cultures of phytoplankton and/or field observations (e.g. Wurl *et al.*, 2011).

1.9 Project rationale

1.9.1 Motivation

There has been growing interest in the role and importance of polymer gel particles (i.e. TEP) in the microbial loop, sedimentation processes, biogeochemical cycling, marine carbohydrate chemistry and particle dynamics in the ocean (Verdugo *et al.*, 2004). At present the role played by TEP in continental shelf seas for the uptake, export and storage of organic carbon is not well understood. What is well known is that TEP is exuded by phytoplankton as a carbon-rich compound (Mari *et al.*, 2017). Its production is thought to be associated with carbon overconsumption which occurs in summer when the phytoplankton community is nutrient limited (Mari *et al.*, 2017). TEP due to its stickiness and low density (Azetsu-Scott and Passow, 2004a) can act as a glue by promoting the formation of large aggregates, which when ballasted with negatively buoyant particles may sink out exporting POC and TEP to the seafloor (Passow *et al.*, 2001; Burd and Jackson, 2009; Mari *et al.*, 2017).

A study suggests that the North Sea in summer is characterized by an excess of dissolved inorganic carbon uptake (~ 40 μmol kg^{-1}) without a corresponding nitrate uptake (Prowe *et al.*, 2009), which may involve a non-Redfield pathway for carbon fixation (carbon overconsumption) (Toggweiler, 1993; Thomas *et al.*, 1999; Koeve, 2005). This process could be particularly effective if carbon-rich material, such as gel-like particles (i.e. TEP), is formed as these sink out of the surface layer in form of aggregates. This mechanism could increase efficiency of the continental shelf pump. Moreover, TEP dynamics are poorly understood and not represented in marine ecosystem models.

The main knowledge gaps are the following:

- Lack of information on the vertical and spatial distribution, as well as the seasonality of TEP in NW European shelf seas (North Sea and Celtic Sea).
- Knowledge gaps on linking TEP production to carbon overconsumption in summer (i.e. North Sea).
- Little information on the importance and the role of TEP in the continental shelf pump for CO_2 uptake and carbon export.
- No representation of TEP dynamics in marine ecosystem models.

1.9.2 Aim

The main aim of this research is to investigate the role played by TEP in carbon cycling in NW European shelf seas. For this purpose, two different approaches have been used:

✓ Observations:

1. To discover the spatial distribution and the seasonality of TEP in the North Sea and the vertical distribution of TEP in the Celtic Sea.
2. To investigate the formation and accumulation of TEP in the euphotic zone and how these are related to water column stratification, primary production and sea surface conditions in the context of carbon cycling in NW European shelf seas.

✓ Experimental-modelling approach:

1. To develop a new formulation describing TEP dynamics in marine ecosystem models.
2. To investigate the vertical distribution of TEP and the associated carbon export.

1.9.3 Hypotheses and Objectives

The specific Hypotheses and Objectives of this research are:

Hypothesis 1:

Transparent exopolymer particles are produced *in situ* in shelf seas as a by-product of phytoplankton productivity and will therefore have similar spatial and temporal patterns as primary productivity and related variables, e.g. chlorophyll.

Objective 1:

- To use *in situ* observations of TEP to investigate the vertical distribution of TEP in the Celtic Sea (Chapter 4), as well as the spatial distribution and the seasonality of TEP in the North Sea (Chapter 5).

- To determine the key processes controlling the vertical and spatial dynamics of TEP by means of linear regression analyses of TEP versus chlorophyll and other variables (Chapters 4 and 5).

- To investigate whether the TEP to chlorophyll relationship and the TEP to chlorophyll ratio are reliable indicators of TEP production (Chapter 4).

- To use the European Regional Seas Ecosystem Model (ERSEM), along with *in situ* data to model TEP concentrations (Chapter 4).

Hypothesis 2:

Transparent exopolymer particles aggregate into large particles that sink out, leading to export of carbon-rich POC. Aggregates containing TEP composition and size can substantially affect the quality, quantity, degradation and sinking of the exported carbon.

Objective 2:

- To use a simple box model to estimate TEP formation, accumulation rate, turnover, sinking rate, carbon export and bacterial remineralization (Chapters 4 and 5).

- To use a modeling approach to understand how aggregates containing TEP composition can affect particle aggregation, sinking and carbon export (Chapter 4).

- To model the effect of TEP on particle aggregation and sinking in ERSEM (Chapter 4).

Hypothesis 3:

TEP production and associated carbon overconsumption occurs in summer when the phytoplankton community is nutrient limited. The effect increases the quantity of sinking carbon and therefore increases the efficiency of the continental shelf pump. By consequence, TEP should play a substantial role in controlling air-sea CO_2 flux in shelf seas.

Objective 3:

- To use ERSEM to investigate the fate of carbon exported due to TEP and the potential effect of TEP on CO_2 uptake, carbon sequestration and C : N stoichiometry of organic matter (Chapters 4 and 5).

Chapter 2 Analytical methods

2.1 Introduction

This chapter describes the general analytical methodology used within this research project. The analytical methods described have been developed to quantify transparent exopolymer particles (TEP), Particulate Organic Matter (POM) and chlorophyll *a* in sea water samples taken from the European continental shelf. TEP concentration was determined by using the semi-quantitative colorimetric approach developed by Passow and Alldredge (1995).

Particulate Organic Carbon (POC) and Nitrogen (PON) concentration in sea water were quantified with the CHN Elemental Analyser, which separates H, CO_2, and N_2 through a gas chromatographic column. Concentrations were detected with a thermal conductivity detector (Ehrhardt and Koeve, 1999). Samples of chlorophyll *a* were analyzed by high performance liquid chromatography (HPLC) and fluorometry. Furthermore, a new method for TEP detection was developed and storage experiments for TEP preservation were conducted.

2.2 TEP analytical method

TEP are defined as polysaccharide particles containing acidic sugars (Wurl, 2009), that are retained on a 0.4 μm polycarbonate filter, under low vacuum (150 mm Hg) and stained with Alcian Blue (8GX) at pH 2.5 (Alldredge *et al.*, 1993). The Alcian Blue molecule is a cation copper phthalocyanine dye (Decho, 1990; Alldredge *et al.*, 1993) that in aqueous solutions binds with anionic carboxyl, phosphate and half-ester sulphate groups of acidic polysaccharides (Parker and Diboll, 1966; Ramus, 1977) such as TEP. Passow and Alldredge (1995) tested ten different compounds (Agarose, Amylose, Chitin, Laminarin, Alginic Acid, Gum Xanthan, D-Glucuronic Acid, Carrageenin, Bovine Serum Albumen, Carboxylase) for their suitability as standards for TEP determination. They found that the two most appropriate standards were Alginic Acid and Gum Xanthan for the higher capacity of Alcian Blue to stain the TEP-like particles created by these compounds. However, Gum Xanthan was chosen as the most appropriate standard to quantify TEP, due to the higher replicability of the method. The molecular structure of the Alcian Blue, Gum Xanthan and the Alcian Blue-Gum Xanthan complex are shown in Figure 2.1.

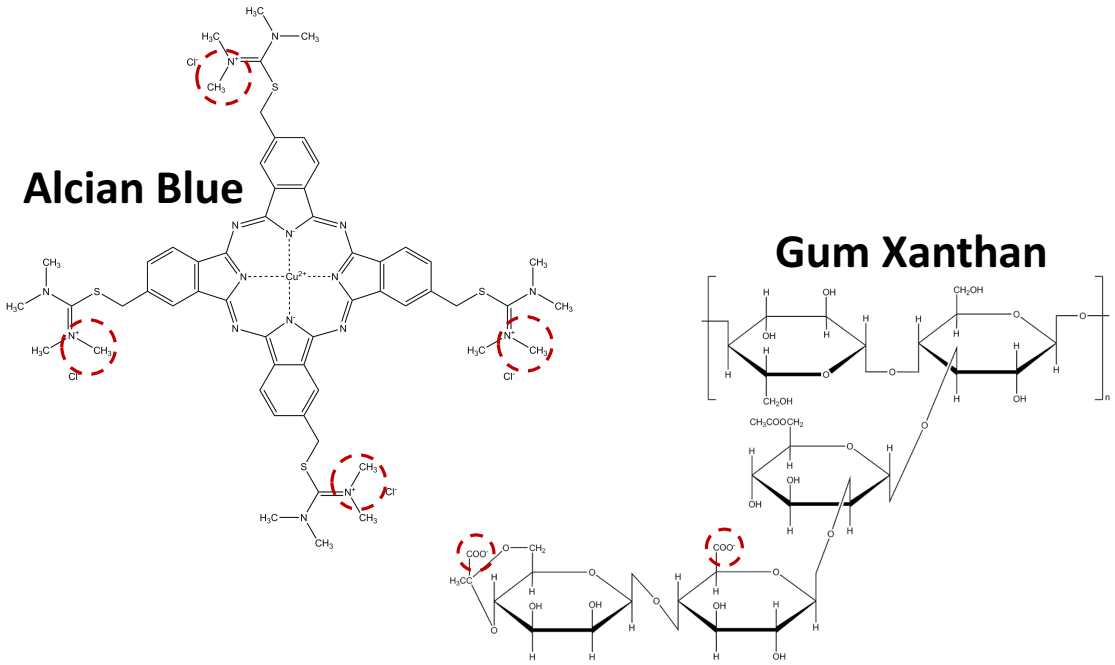

Figure 2.1 Molecular structures of Alcian Blue and Gum Xanthan. Red circles indicate the formation of the Alcian Blue-Gum Xanthan complex.

All steps of TEP analysis are illustrated in Figure 2.2. The method uses a range of volumes of sea water (100 ml – 1 litre), filtered under 150 mm of Hg vacuum through a polycarbonate filter, with a 0.4 µm pore-size and 47 mm diameter (Nuclepore, Whatman). Wherever possible, TEP samples and blanks were collected in triplicate. TEP concentration was determined colorimetrically following the approach of Passow and Alldredge (1995). After filtration, 1 ml of an aqueous operating solution (section 2.3) of 0.02% Alcian Blue (8GX) in 0.06% of acetic acid, with a pH of 2.5 was added to the filter. After a few seconds, the filter was rinsed with 10 ml of Milli-Q water in order to remove any excess dye. Afterwards, the stained filter was stored frozen at -20°C for up to 6 months according to Passow and Alldredge (1995) for later analysis.

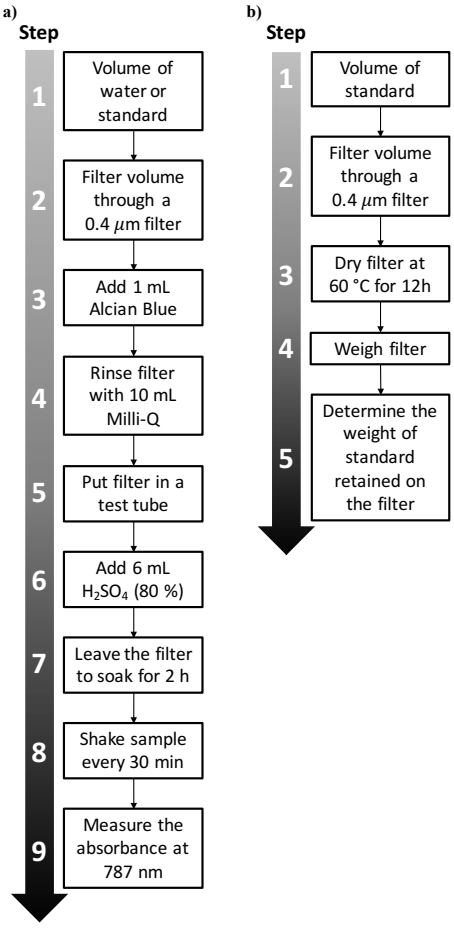

Figure 2.2 Diagram illustrating TEP analysis step by step. a) Determination of TEP or standard solution absorbance, b) determination of the weight of the standard solution on the dry filter.

2.3 Alcian Blue solution preparation and testing

A concentrated aqueous solution of Alcian Blue was prepared as follows (Wurl, 2009) :

97 ml Milli-Q water

3 ml Glacial Acetic acid

1 g Alcian Blue (8GX)

Subsequently, an aliquot of the solution was diluted in a ratio of 1 : 50 with Milli-Q in order to obtain the Alcian Blue aqueous operating solution (Wurl, 2009). Prior to being used the Alcian Blue operating solution was filtered through a 0.2 µm syringe filter membrane in order to remove any possible dye particles that might have formed spontaneously (Passow and Alldredge, 1995; Wurl, 2009).

In order to verify if the Alcian Blue operating solution was suitable for staining a sample was stained as described in section 2.2, and the continuous absorbance spectrum of Alcian

Blue in 80% of sulfuric acid was determined with the UV-Vis spectrophotometer LAMBDA 35 (Figure 2.3). The maximum absorbance of Alcian Blue in 80% sulfuric acid occurs at a wavelength of 787 nm (Figure 2.3) (Passow and Alldredge, 1995).

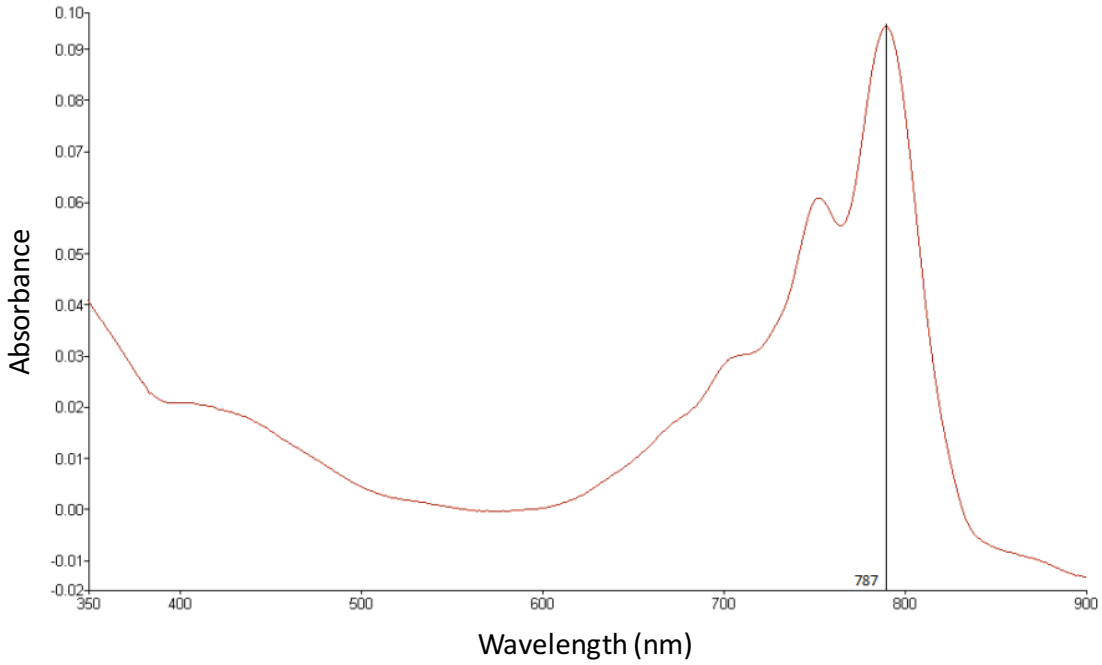

Figure 2.3 Sample spectrum measurement with the UV-Vis spectrophotometer LAMBDA 35 (Absorbance versus wavelength in nm).

2.4 Gum Xanthan standard solution preparation and testing

The standard solution for calibration was prepared by mixing 30 mg of Gum Xanthan (Sigma G-1253) into 200 ml of Milli-Q water, permitting the polysaccharide to swell for 30 minutes. Subsequently 30 ml of the solution was processed with a tissue grinder, where a pistil was lowered and raised two times to break up big particles (Wurl, 2009). The whole solution (200 ml) was treated as described above to break up the big particles and obtain an homogeneous solution similar in size to TEP.

To determine whether the solution was suitable as standard for calibration a clogging test was performed. For this one litre of standard solution of Gum Xanthan (150 mg L^{-1}) was prepared as described above. Increasing volumes of the Gum Xanthan solution (1 to 30 ml) were filtered under 150 mm of Hg pressure through polycarbonate filters with 47 mm diameter and a pore size of 0.4 µm (Nuclepore, Whatman). The time taken for each sample to filter was measured to investigate a linear response, as well as how much sample the filter could take before clogging. Figure 2.4 shows the relationship between

volume filtered and time to filter. A linear relationship was found below 15 ml. Above this volume the filter starts to clog and there is a non-linear increase in filter time.

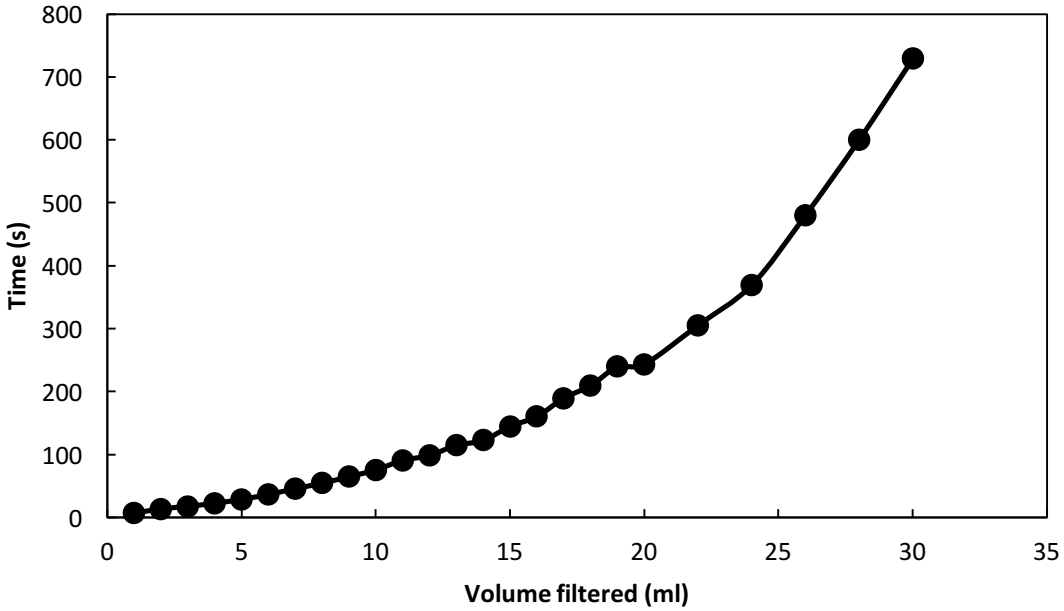

Figure 2.4 Relationship between the volume of the standard solution of Gum Xanthan filtered and the time taken to filter the sample.

2.5 Calibration of the standard solution

Six different volumes up to 30 ml of the Gum Xanthan solution used during the clogging test (section 2.4) were tested to perform the calibration curve. The result showed that volumes up to 25 ml of the Gum Xanthan solution provided the best regression fit with the highest coefficient of determination. Therefore a five-point calibration was carried out by using volumes of 6 ml, 8 ml, 10 ml, 15 ml and 25 ml of the standard solution of the Gum Xanthan (150 mg L^{-1}). The capability of the Alcian Blue to stain particles was measured by filtering the five different volumes of the Gum Xanthan standard solution, while following the protocol for TEP sample analysis (section 2.2). Each volume was filtered in triplicate and three filters were used as a blank to determine the absorbance of the empty filter. Next the filters were stained with Alcian Blue, as described in section 2.2. The absorbance of these filters was measured following the protocol in section 2.6.

A second set of filters were used to determine the mass of the Gum Xanthan retained on the filter for each volume of the standard solution. First empty filters were dried at 60°C for 12 hours and subsequently weighed five times to ensure accuracy. Following this each

volume of the standard solution was filtered five times across the pre-weighed filters, while 10 ml of Milli-Q was filtered across another five filters for determination of the blank. Upon filtration the filters were dried at 60°C for 12 hours and weighed five times. The average and standard deviation of mass of Gum Xanthan were calculated for each volume filtered from the five replicates.

All filters were electrically neutralized with a high voltage ionizer (Wurl, 2009) prior to being weighed with the electronic ultra-microbalance Sartorius SE2. Furthermore, the filters were stored individually in combusted glass petri dishes (450°C for 4 hours) to avoid possible contamination (Wurl, 2009). The petri dishes were kept in a closed plastic box with silica gel to absorb the humidity of the surrounding environment.

The weight of the standard solution retained on the filter for each volume filtered $\boldsymbol{W_{Xanthan\,(\mu g)}}$ was determined using Eq. (2.1) (Wurl, 2009).

$$\boldsymbol{W_{Xanthan\,(\mu g)} = \left(W_{standard} - W_{empty}\right) - \left(W_{blk2} - W_{blk1}\right)} \qquad \boldsymbol{(2.1)}$$

where:

$\boldsymbol{W_{standard}}$ is the average weight of the dry filters with the standard solution for each volume

$\boldsymbol{W_{empty}}$ is the average weight of the empty filters for each volume

$\boldsymbol{W_{blk1}}$ is the average weight of the empty blank filters

$\boldsymbol{W_{blk2}}$ is the average weight of the blank filters rinsed with 10 ml of Milli-Q water

The $\boldsymbol{(W_{blk2} - W_{blk1})}$ is a correction for possible changes that can occur in the weight of the blank filters due to the use of Milli-Q water (Wurl, 2009).

Two Alcian Blue calibration curves were determined and applied to the two different years of TEP sampling (2014 and 2015). A calibration curve needs to be made every time a new solution of Alcian Blue is made to relate blueness to Gum Xanthan equivalents. As part of this research two solutions of Alcian Blue were prepared and calibrated just before each cruise in the year 2014 and 2015. Furthermore, Alcian Blue solution was tested after about six months to check its stability. The weight of the standard solution retained on the filters for the five volumes was determined in a laboratory calibration made in the

year 2014. In the year 2015 the weight of the standard solution on the filters was assumed to be the same as in the year 2014. Both calibration curves are shown in sections 2.7 and 2.8.

2.6 TEP concentration determination

To determine the concentration of the standard solution of Gum Xanthan or of TEP in samples, the stained filter was transferred into a glass tube and 6 ml of sulphuric acid (80%) was added. Afterwards, the tube was incubated for two hours, while being agitated several times during this period. After incubation the sample absorbance was determined at 787 nm against Milli-Q water with a UV-Vis spectrophotometer LAMBDA 35. TEP concentration was expressed in µg l^{-1} of Xanthan equivalent and calculated using Eq. (2.2) (Passow and Alldredge, 1995; Wurl, 2009).

$$\boldsymbol{TEP\ (\mu g\ Xeq.\ l^{-1}) = \frac{[(Sample_{787} - Blk_{787}) - b]}{V \cdot m}} \qquad (\mathbf{2.2})$$

where:

$\boldsymbol{Sample_{787}}$ is the absorbance of the sample at 787 nm

$\boldsymbol{Blk_{787}}$ is the absorbance of the blank at 787 nm

V is the volume of sample filtered, expressed in litres

$\boldsymbol{m}$ is the slope of the linear regression curve

$\boldsymbol{b}$ is the y-intercept of the linear regression curve

The limit of detection (LOD) for TEP analysis was 11.3 µg Xeq. l^{-1}. It was calculated based on the analyte concentration that gave a signal equal to the blank signal, plus three times the standard deviation of the blank (Miller and Miller, 2010). The precision of TEP analysis was ± 15%. It was determined by using all TEP measurements. Firstly, TEP measurements were normalised into a range of zero to one by dividing the individual concentrations by the mean concentration of each sample. Secondly the standard deviation of all the normalised values was calculated and multiplied by two to get the precision of TEP measurement at 95% confidence interval. Each time TEP samples were run a sample of the Gum Xantham in triplicate was used as check standards. The variability in repeated measurements of this standard demonstrated a precision of about 13 %.

The TEP concentration was converted to the carbon content of TEP (TEP_c) by applying the empirical conversion factor of 0.63 ± 0.03 shown in Eq. (2.3) (Wurl, 2009). This was done to enable a comparison with TEP carbon (TEP_c) measurements from the literature. To compare TEP to particulate organic carbon measurements, TEP_c in µg l^{-1} was converted to µmol l^{-1} by diving TEP_c (µg l^{-1}) by twelve (molar mass of carbon).

$$\boldsymbol{TEP_c(\mu g\, l^{-1}) = 0.63\, TEP(\mu g\, Xeq.\, l^{-1})} \qquad \textbf{(2.3)}$$

2.7 First Alcian Blue calibration curve

The calibration curve shown in Figure 2.5 was obtained from the absorbance at 787 nm versus the weight of the standard Gum Xanthan. The first calibration curve was used to determine the concentration of TEP samples collected in the year 2014.

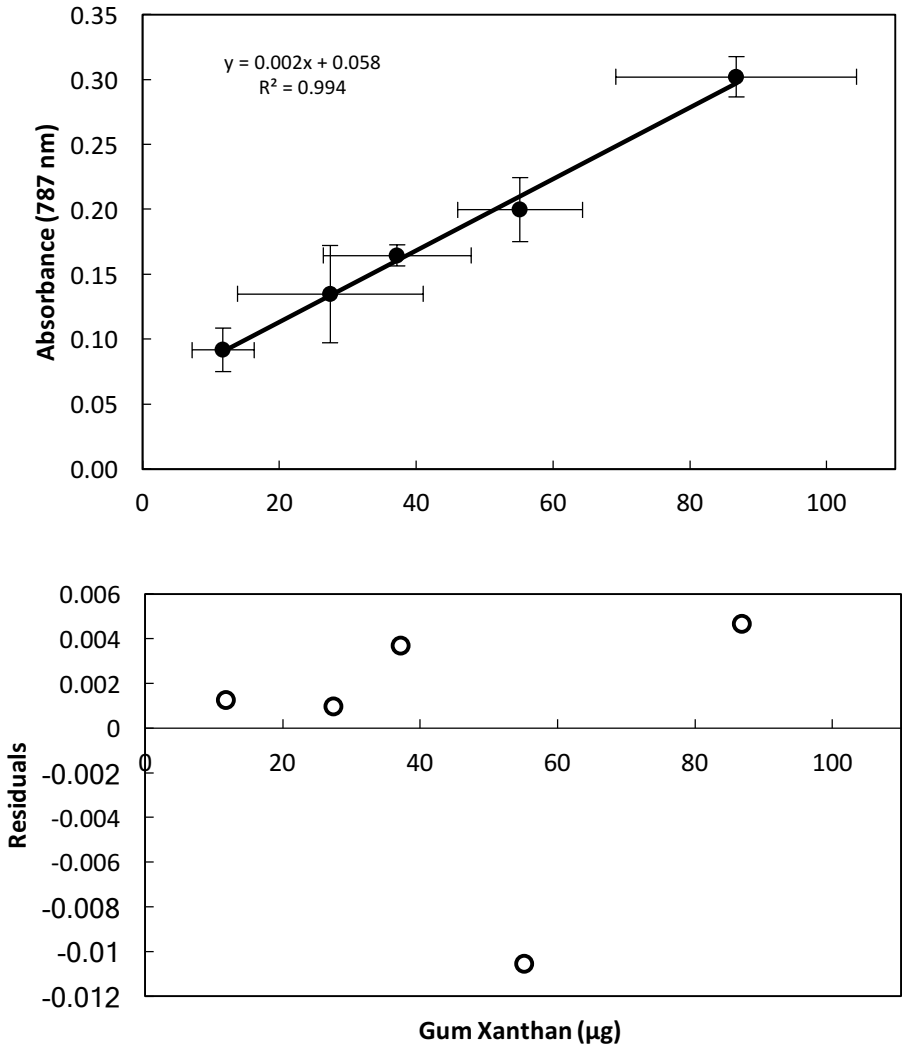

Figure 2.5 Calibration curve, linear regression and residuals of the standard Gum Xanthan.

The semi-quantitative method for TEP analysis uses the relationship between the staining capability of the Alcian Blue and the weight of the polysaccharide Gum Xanthan. The large error bars (Figure 2.5) are due to the difficulty of quantifying the dry weight of the standard. The amount of the Gum Xanthan on the filter is quite low, therefore it requires a balance with high resolution. Also the weighing process is affected by the nature of the filter (polycarbonate), which has an electrostatic charge and by the humidity of the surrounding working environment.

To evaluate the quality of the first calibration curve, statistical analyses (regression statistics and ANOVA) were performed. The results reported in Table 2.1 and Figure 2.5 showed a coefficient of determination of 0.994 and a p-value less than 0.01.

Table 2.1 Regression statistic and ANOVA of the calibration curve.

Regression Statistics	
Multiple R	0.997
R Square	0.994
Adjusted R Square	0.992
Standard Error	0.0070
Observations	5

ANOVA

	df	***SS***	***MS***	***F***	***Significance F***
Regression	1	0.025	0.025	509.0565	0.00019
Residual	3	0.0001	4.95E-05		
Total	4	0.025			

	Coefficients	***Standard Error***	***t Stat***	***p-value***
Intercept	0.058	0.006	9.365	0.002
Slope	0.002	0.0001	22.562	0.00019

2.8 Second Alcian Blue calibration curve

In 2015 a new Alcian Blue solution was used. This new Alcian Blue solution was calibrated by determining the absorbance of five volumes of Gum Xanthan standard solution, as described in section 2.5. Due to the operational difficulty of quantifying the weight of the Gum Xanthan on the filters, the weight of the standard solution retained on

the filters of the five volumes measured in the first calibration curve was used (section 2.7). The calibration curve in Figure 2.6 shows the absorbance measurements versus the weight of the standard Gum Xanthan. This second calibration curve was used to determine the concentration of TEP samples collected in the year 2015.

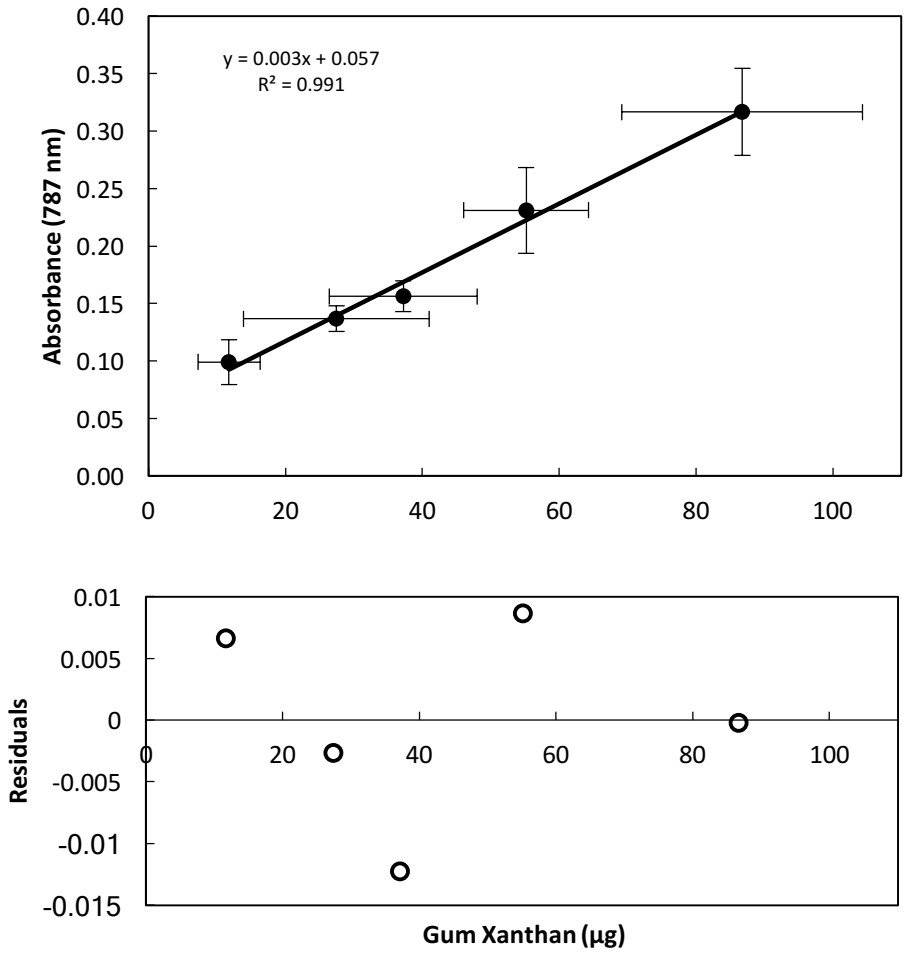

Figure 2.6 Calibration curve, linear regression and residuals of the standard Gum Xanthan.

The statistical analyses of the standard curve (regression statistics and ANOVA) were performed. The results reported in Table 2.2 and Figure 2.6 showed a coefficient of determination of 0.990 and a p-value < of 0.01.

Table 2.2 Regression statistic and ANOVA of the calibration curve.

Regression Statistics	
Multiple R	0.995
R Square	0.991
Adjusted R Square	0.987
Standard Error	0.009
Observations	5

ANOVA

	df	*SS*	*MS*	*F*	*Significance F*
Regression	1	0.029	0.029	322.5213	0.0003
Residual	3	0.0002	9.2E-05		
Total	4	0.029			

	Coefficients	*Standard Error*	*t Stat*	*p-value*
Intercept	0.057	0.008	6.777	0.006
Slope	0.0029	0.0001	17.958	0.0003

2.9 Photographic method for TEP detection

2.9.1 Introduction

The spectrophotometric method for the determination of TEP (Passow and Alldredge, 1995) described in the previous sections of this Chapter, involves several critical steps, is time consuming and requires working with a hazardous chemical. In this work a simple, reliable, accurate and rapid photographic method was developed to determine the TEP concentration in seawater samples based on the same relationship between TEP and Alcian Blue. The photographic method is easy to put in place and does not require working with sulfuric acid. Furthermore, the TEP concentration on the filter can be determined quickly and easily with the use of image processing and analysis software such as ImageJ. The method's approach is based on the linear positive relationship found between the intensity of the blue colour of the filter and the amount of the standard Gum Xanthan on the filter.

2.9.2 Material and method

The standard solution (Gum Xanthan) was prepared as described in section 2.4. Afterwards, a five-point calibration curve was determined by filtering five different volumes of the Gum Xanthan standard solution (section 2.5). Next the filters were stained with Alcian Blue, following the protocol in section 2.2. Each volume was filtered in triplicate and three filters were used as a blank to determine the absorbance of the empty filter. The stained filters were placed in clean petri dishes and placed under a camera (Canon EOS 1200D) (Figure 2.7). The camera was set with the parameters reported in Table 2.3. Images of each filter were then taken and processed with the image processing and analysis software ImageJ.

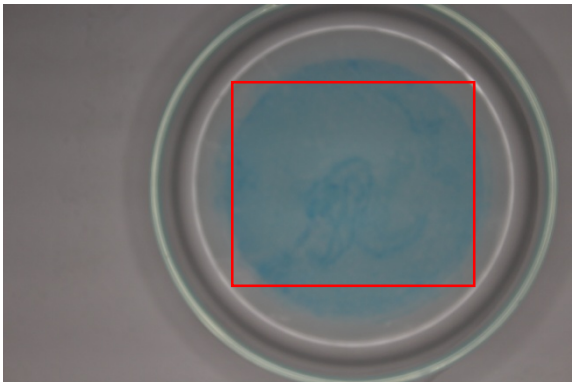

Figure 2.7 Example of standard Gum Xanthan solution on a filter, stained with Alcian Blue during the image processing analysis. The red square indicates the area of the filter analysed by the software to get the RGB (Red, Green and Blue) colour.

Table 2.3 The specific settings of the camera.

Camera setting	
Flash	Lowest power (-1.5)
Shutter	F 5.6
ISO	200
Auto white balance	On

An area of the filter (Figure 2.7) was sampled and analysed with ImageJ, which splits the composite RGB (Red, Green and Blue colour) picture into the individual red, green, and blue channels. Subsequently, the intensity of the colour (***Colour int.***) of the filter was calculated with Eq. (2.4) (Tariq, 2015). All the samples were blank corrected.

$$\boldsymbol{Colour\ int.} = \frac{(\boldsymbol{R} - \boldsymbol{B})}{\boldsymbol{G}} \qquad (\mathbf{2.4})$$

where:

R = red

B = blue

G = green

2.9.3 Results

The calibration curve in Figure 2.8 shows the absolute values of intensity of the blue colour detected from the filter image analysis versus the weight of the standard Gum Xanthan. This calibration curve uses the weight of the Gum Xanthan determined for the first calibration curve (section 2.7).

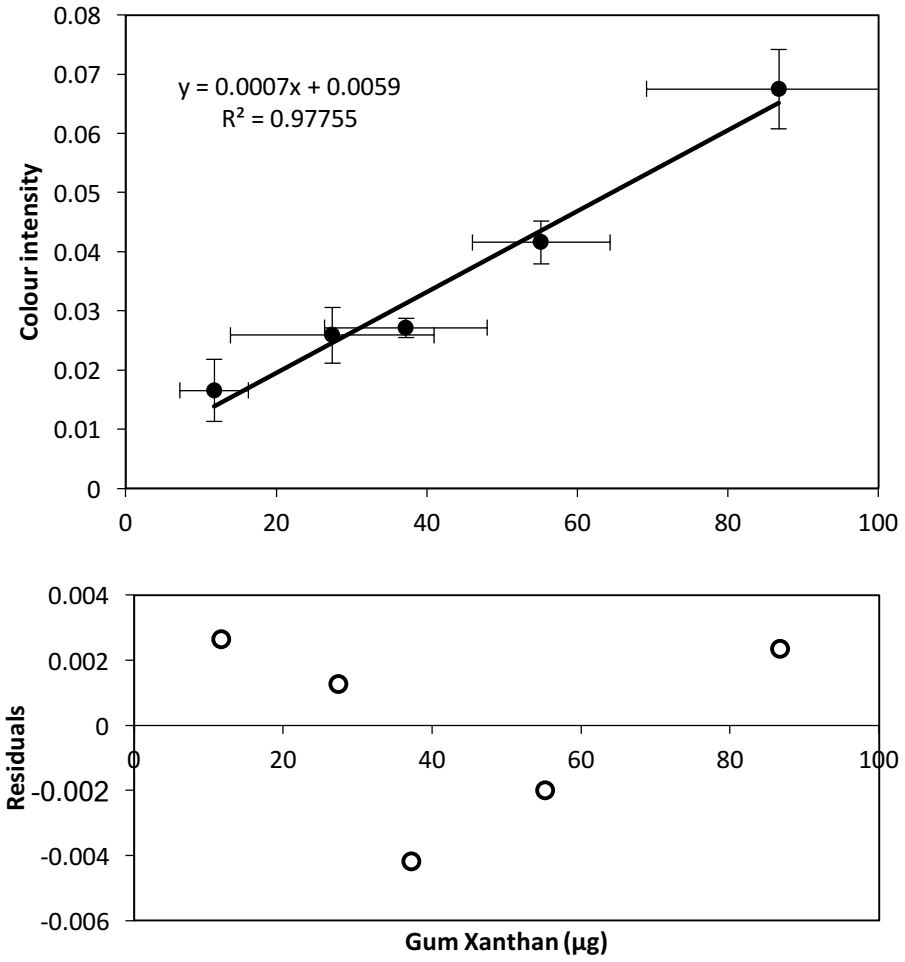

Figure 2.8 Photographic method: Calibration curve, linear regression and residuals of the standard Gum Xanthan.

The statistical analyses of the calibration curve of the photographic method (regression statistics and ANOVA) were performed and are reported in Table 2.4 and Figure 2.8.

Table 2.4 Photographic method: regression statistic and ANOVA of the curve.

Regression Statistics	
Multiple R	0.989
R Square	0.978
Adjusted R Square	0.970
Standard Error	0.003
Observations	5

ANOVA

	df	*SS*	*MS*	*F*	*Significance F*
Regression	1	0.001	0.001	130.62	0.001
Residual	3	3.55E-05	1.18E-05		
Total	4	0.001			

	Coefficients	*Standard Error*	*t Stat*	*p-value*
Intercept	0.005	0.003	1.939	0.147
Slope	0.0007	5.97E-05	11.429	0.001

2.9.4 Standard spectrophotometric method versus photographic method

The photographic method developed for TEP analysis was compared with the spectrophotometric method as shown in Figure 2.9. The comparison showed a coefficient of determination of 0.982, indicating a significant and linear correlation between the two methods.

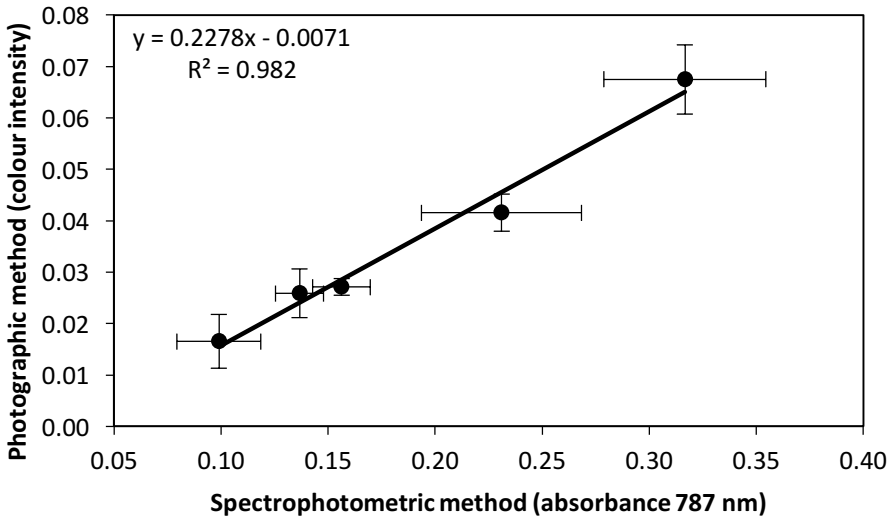

Figure 2.9 The photographic method versus spectrophotometric method.

2.9.5 Conclusion and future work

The photographic method developed has shown to be simple to put in place, reliable and as accurate as the spectrophotometric method. It is also rapid and does not require working with hazardous chemicals such as sulfuric acid. There is no interference observed during the TEP analysis due to high concentrations of suspended particles in the samples. However, this is just a preliminary study and further analysis should be done particularly in the direction of testing a real sample with both methods and comparing the results. The photographic method was developed at a late stage of this research, where more than 50% of TEP samples were already analysed with the standard spectrophotometric method. Therefore, it was not possible to use it as part of this research.

2.10 TEP storage experiment

2.10.1 Introduction

Passow and Alldredge (1995) have shown that formalin is a suitable chemical to preserve TEP and does not interfere with TEP analysis. Since the publication of their paper, formalin has been the only chemical method used for TEP preservation. Here seawater samples collected by Cefas SmartBuoy and preserved with a saturated mercuric chloride solution (commonly used in nutrient preservation) were used to investigate the seasonal cycle of TEP at West Gabbard (51.9569° N, 2.1042° E) and Warp (51.5294° N, 1.0166° E). Storage experiments were carried out to test the suitability of mercuric chloride as an alternative chemical to preserve TEP samples over extended periods. As a first step an experiment was conducted by testing a wide range of unbuffered and buffered formalin solutions along with a solution of saturated mercuric chloride. The best two methods to preserve TEP (unbuffered formalin and saturated mercuric chloride) were further used to carry out an experiment to investigate the suitability of saturated mercuric chloride to preserve TEP for up to six months in sea water collected from different locations and seasons.

2.10.2 Testing various preservatives

Thirty-three litres of sea water were collected during the Cefas cruise Cend 3/15 (February 2015) at the location “off Plymouth” (50.0276° N, 4.3768° W) with Niskin bottles at 3.4 m depth. One litre of sea water (in triplicate) was used as a reference, processed on board according to the method described in section 2.2 and stained filter

were stored frozen at -20°C for later analysis. The other thirty liters of the sea water were stored in five liter carboys and preserved as follows:

- **Exp. 1** sample without preservative.
- **Exp. 2** sample with 2% formalin (2 ml of CH_2O in 100 ml H_2O), buffered with sodium phosphate monobasic ($NaH_2PO_4 \cdot H_2O$) and sodium phosphate di-basic (Na_2HPO_4) at pH of 6.8 (Nagorsen and Peterson, 1980).
- **Exp. 3** sample with 4% (4 ml of CH_2O in 100 ml H_2O) unbuffered formalin.
- **Exp. 4** sample with 4% (4 ml of CH_2O in 100 ml H_2O) formalin, buffered with sodium phosphate monobasic ($NaH_2PO_4 \cdot H_2O$) and sodium phosphate dibasic (Na_2HPO_4) at pH of 6.8 (Nagorsen and Peterson, 1980).
- **Exp. 5** sample with 4% formalin (4 ml of CH_2O in 100 ml H_2O), buffered with sodium tetraborate ($Na_2B_4O_7 \cdot 10H_2O$) at pH of 8.2.
- **Exp. 6** sample with 7.5 ml of saturated mercuric chloride solution (32 g of $HgCl_2$ in 1 L H_2O) (Johnson *et al.*, 2013).

The stored samples were placed in a cool (4°C) and dark place until further analysis. A single sub-sample (1 litre) of the stored sample from each carboy was analyzed and the TEP concentration was determined colorimetrically as described in section 2.6, after one week, two weeks, one month, two months and seven months from collection.

2.10.3 Results

TEP concentration of the reference and from each storage experiment after one week, two weeks, one month, two months and seven months from collection are shown in Table 2.5 and Figure 2.10.

Table 2.5 TEP concentration (µg Xeq. l^{-1}) for each storage experiment at five different time steps and the reference.

Sample ID	1 week TEP (µg Xeq. l^{-1})	2 weeks TEP (µg Xeq. l^{-1})	1 month TEP (µg Xeq. l^{-1})	2 months TEP (µg Xeq. l^{-1})	7 months TEP (µg Xeq. l^{-1})
Reference	108.8 ± 0.02				
Exp. 1	83.3	81.6	53.6	115.0	121.2
Exp. 2	170.2	107.5	80.2	88.9	89.2
Exp. 3	84.7	95.7	100.2	93.9	86.4
Exp. 4	1136.4	1236.3	1302.9	1316.1	1295.8
Exp. 5	100.3	126.8	96.8	97.8	101.4
Exp. 6	85.7	117.6	124.1	91.0	107.2

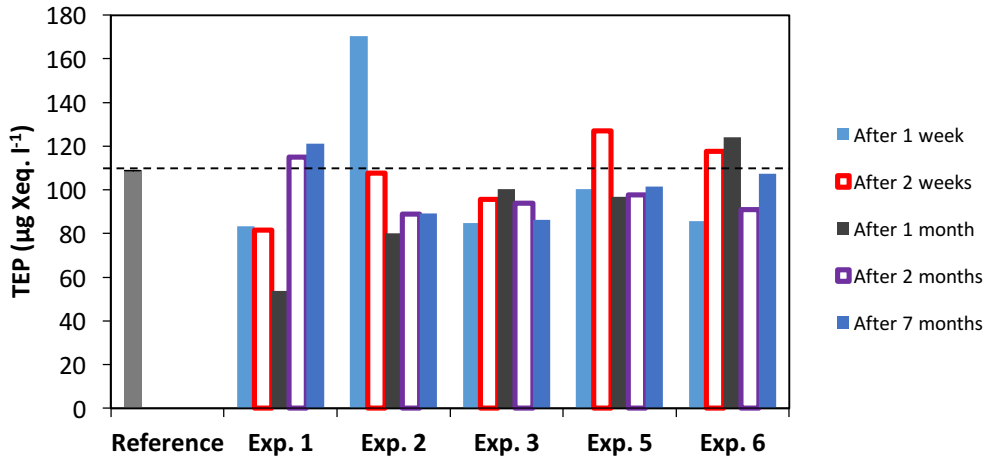

Figure 2.10 Results of TEP concentration detected for each storage experiment at five different time steps; (dashed line) reference threshold. Reference (frozen sample 108.75 ± 0.02 µg Xeq. l^{-1}). The results from experiment four are not shown.

Table 2.6 Mean concentrations of TEP (µg Xeq. l^{-1}), standard deviation and percentage of increase/decrease of TEP concentrations respect to the reference for each storage experiment.

Sample ID	mean TEP (µg Xeq. l^{-1})	increase /decrease %
Exp. 1	83.4 ± 27	↓ 23.3
Exp. 2	111.7 ± 40.6	↑ 2.7
Exp. 3	93.6 ± 6.5	↓ 13.9
Exp. 4	1247.9 ± 82.1	↑ 1047.5
Exp. 5	105.4 ± 14.3	↓ 3.0
Exp. 6	104.6 ± 19.1	↓ 3.8

After a week Exp. 1 has a lower TEP concentration compared to the reference. The TEP concentration decreased over time after one month (Figure 2.10). After two months in Exp. 1 an increase of TEP was observed, reaching the reference concentration. This increase in TEP concentration in the sample without preservative could be explained by the possible lysis of the phytoplankton cells or the variability in the measurements due to a lack of replicates. The lysis of phytoplankton cells causes the release of the cytoplasmatic content of the cells, which can stain with Alcian Blue, resulting in an overestimation of TEP (Passow and Alldredge, 1995). Exp. 2, Exp. 5 and Exp. 6 had mean concentrations relatively close to the reference and with an increase/decrease of average concentrations of 2.7%, 3.0% and 3.8% (Table 2.6). In particular Exp. 3 had a low variability in TEP concentrations over time (Figure 2.10). In Exp. 2 and Exp. 4 precipitates of sodium phosphate monobasic and sodium phosphate dibasic in the samples stained with Alcian Blue may explain the overestimation of TEP (Table 2.5). For instance, Exp. 4 (not shown in the graph) had a high formation of precipitates owing to the high values of TEP (mean value of 1247.94 ± 82.1 µg Xeq. l^{-1}) when compared with the reference (Tables 2.5 and 2.6).

2.10.4 Conclusion

The results show that Exp. 3, Exp. 5 and Exp. 6 with their lower percentage of changes in concentrations in respect to that of the reference are suitable methods to preserve TEP samples for up to seven months. Due to its very low variability in TEP concentrations over time, Exp. 3 may be the most consistent and reliable method for the preservation of TEP samples. Further analysis was carried out in different locations and seasons to

investigate the suitability of unbuffered formalin (Exp. 3) and saturated mercuric chloride (Exp. 6) to preserve TEP for up to six months.

2.10.5 Testing unbuffered formalin and saturated mercuric chloride

Five litres of surface sea water were collected during the Cefas cruises: Cend 8/15 (May 2015) and Cend 24/15 (November 2015) at four different locations on the UK shelf seas using Niskin bottles. A sample of the collected sea water (in triplicate) was used as reference and processed on board as described in section 2.2 and stored frozen at -20°C for later analysis. The experiments took five litres of sea water, which were stored in three five litre carboys: one without preservative and the other two with preservatives: 4% unbuffered formalin solution (4 ml of CH_2O in 100 ml H_2O) and a saturated mercuric chloride solution (32 g of $HgCl_2$ in 1 L H_2O) respectively. Preserved sea water was stored in a cool (4°C) and dark place until further analysis. Different amounts of the stored sample (100 ml - 300 ml) from each experiment were analyzed in triplicate and TEP concentration was determined colorimetrically according to the method described in section 2.6 after one week, two weeks, one month, two months and six months from collection.

2.10.6 Results

TEP concentrations of the reference, the sample without preservative, the sample preserved with 4% unbuffered formalin and the sample preserved with mercuric chloride after one week, two weeks, one month, two months and six months from collection are shown in Figures 2.11, 2.12, 2.13, 2.14 and in Tables 2.7, 2.9, 2.11, 2.13. Tables 2.8, 2.10, 2.12, 2.14 show TEP average concentrations and the percentages of increase/decrease of TEP concentrations for each treatment with respect to that of the reference. In the first three experiments (ST1, ST6 and ST8) the samples without preservative showed a decrease of TEP concentrations of about 50% (Tables 2.8, 2.10, 2.12). In all the experiments (ST1, ST6, ST8 and ST21) the mean values of the samples preserved with mercuric chloride showed smaller variations in the percentages of increase/decrease of TEP concentrations, than those preserved in formalin (Tables 2.8, 2.10, 2.12, 2.14). However, the samples preserved with formalin in all the experiments were more consistent overtime.

Table 2.7 TEP concentration (µg Xeq. l^{-1}) in each storage experiment at five different time steps and the reference for Cend 8/15 Station 1.

Cend 8/15 ST 1	1 week TEP (µg Xeq. l^{-1})	2 weeks TEP (µg Xeq. l^{-1})	1 month TEP (µg Xeq. l^{-1})	2 months TEP (µg Xeq. l^{-1})	6 months TEP (µg Xeq. l^{-1})
Reference	1080.8 ± 259.3				
no preser.	461.6 ± 229.4	655 ± 137.5	318.3 ± 81	366.6 ± 55.3	493.3 ± 23.6
formalin	866.6 ± 100	968.5 ± 75	859.2 ± 32	966.6 ± 260.7	998.1 ± 91.3
mercuric chloride	1036.6 ± 321.8	1130 ± 60.8	916.6 ± 159	1023.3 ± 163.1	953.3 ± 104

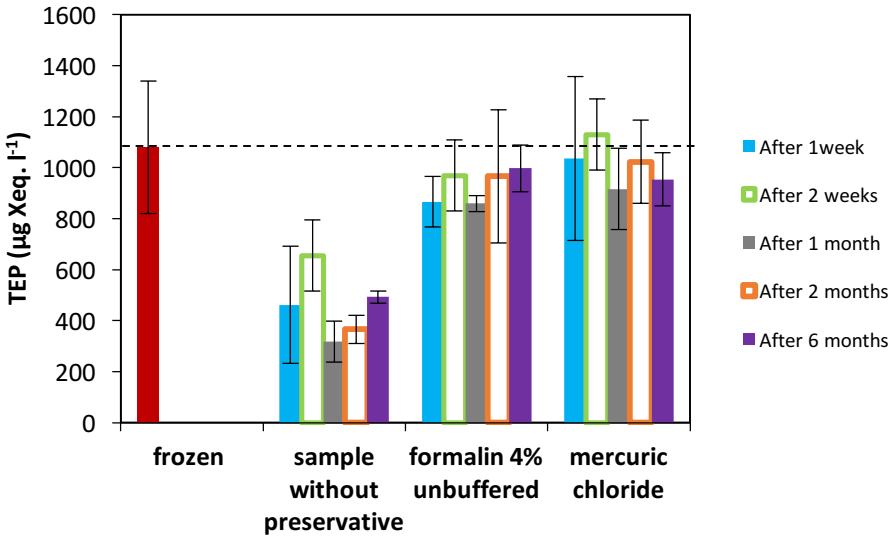

Figure 2.11 Variability of TEP sample concentration collected during Cend 8/15 (ST 1 51.9946° N, 2.1066°E) in May 2015 using different preservation methods for up to six months after collection. The dashed line indicates reference threshold.

Table 2.8 Mean concentrations of TEP (µg Xeq. l^{-1}), standard deviation and percentage of increase/decrease of TEP concentrations with respect to the reference for each storage experiment.

Cend 8/15 ST 1	mean TEP (µg Xeq. l^{-1})	decrease %
no preser.	459 ± 80.9	↓ 57.5
formalin	931.8 ± 87.2	↓ 13.7
mercuric chloride	1012 ± 98.9	↓ 6.3

Table 2.9 TEP concentration (µg Xeq. l^{-1}) in each storage experiment at five different time steps and the reference for Cend 8/15 Station 6.

Cend 8/15 ST 6	1 week TEP (µg Xeq. l^{-1})	2 weeks TEP (µg Xeq. l^{-1})	1 month TEP (µg Xeq. l^{-1})	2 months TEP (µg Xeq. l^{-1})	6 months TEP (µg Xeq. l^{-1})
Reference	325.8 ± 16				
no preser.	174.4 ± 50.4	139.4 ± 44.4	173.8 ± 11	193.8 ± 35.3	191.6 ± 48.4
formalin	252.4 ± 26.7	311.1 ± 61	263.5 ± 22.4	275.3 ± 41.1	259.8 ± 50.5
mercuric chloride	257.7 ± 24.3	339.1 ± 50.6	283.8 ± 33	300.8 ± 31.8	386.6 ± 80.1

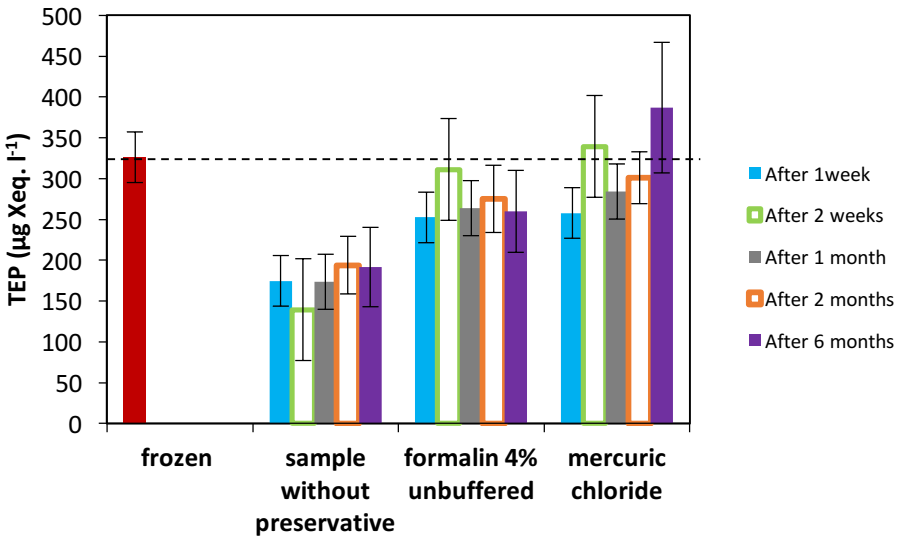

Figure 2.12 Variability of TEP sample concentration collected during Cend 8/15 (ST 6 53.5279° N, 1.0704° E) in May 2015 using different preservation methods for up to six months after collection. The dashed line indicates the reference threshold.

Table 2.10 Mean concentrations of TEP (µg Xeq. l^{-1}), standard deviation and percentage of increase/decrease of TEP concentrations with respect to the reference for each storage experiment.

Cend 8/15 ST 6	mean TEP (µg Xeq. l^{-1})	decrease %
no preser.	174.6 ± 16.1	↓ 46.3
formalin	272.4 ± 16	↓ 16.3
mercuric chloride	313.6 ± 22.4	↓ 3.7

Table 2.11 TEP concentration (µg Xeq. l^{-1}) in each storage experiment at five different time steps and the reference for Cend 24/15 Station 8.

Cend 24/15 ST 8	1 week TEP (µg Xeq. l^{-1})	2 weeks TEP (µg Xeq. l^{-1})	1 month TEP (µg Xeq. l^{-1})	2 months TEP (µg Xeq. l^{-1})	6 months TEP (µg Xeq. l^{-1})
Reference	206 ± 11.6				
no preser.	99.6 ± 41.6	119.6 ± 9	129.2 ± 14.3	158.8 ± 37	213 ± 14.1
formalin	160 ± 34.1	189.2 ± 21.2	171.3 ± 13.5	171 ± 23.1	163.2 ± 8
mercuric chloride	157.4 ± 6.4	203.7 ± 40.7	180.7 ± 15	178.8 ± 25.6	226.3 ± 57.3

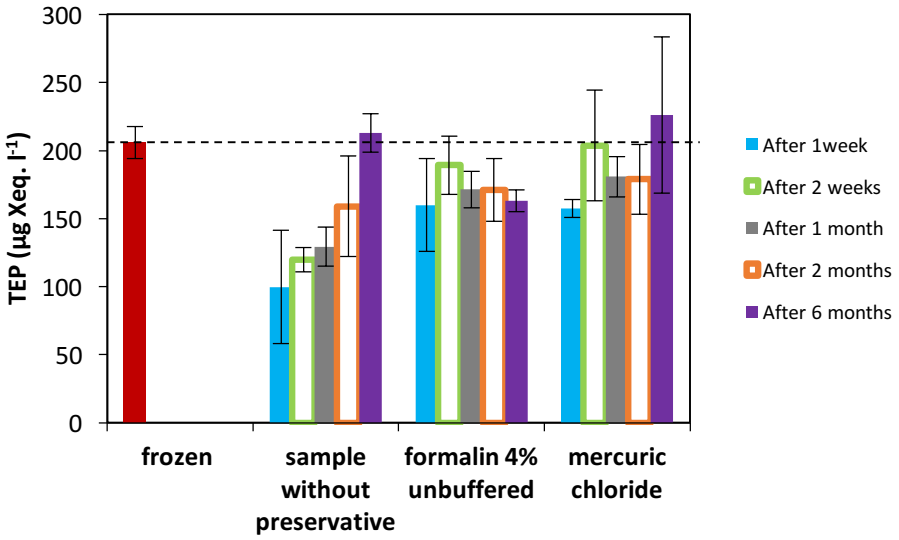

Figure 2.13 Variability of TEP sample concentration collected during Cend 24/15 (ST 8 53.5347° N, 3.3831° E) in November 2015 using different preservation methods for up to six months after collection. The dashed line indicates the reference threshold.

Table 2.12 Mean concentrations of TEP (µg Xeq. l^{-1}), standard deviation and percentage of increase/decrease of TEP concentrations with respect to the reference for each storage experiment.

Cend 24/15 ST 8	mean TEP (µg Xeq. l^{-1})	decrease %
no preser.	144 ± 14.9	↓ 30.0
formalin	171 ± 10	↓ 17
mercuric chloride	189.4 ± 20.3	↓ 8.0

Table 2.13 TEP concentration (µg Xeq. l^{-1}) in each storage experiment at five different time steps and the reference for Cend 24/15 Station 21.

Cend 24/15 ST 21	1 week TEP (µg Xeq. l^{-1})	2 weeks TEP (µg Xeq. l^{-1})	1 month TEP (µg Xeq. l^{-1})	2 months TEP (µg Xeq. l^{-1})	6 months TEP (µg Xeq. l^{-1})
Reference	385.2 ± 53.5				
no preser.	339.2 ± 66.1	316.3 ± 107.1	425.2 ± 54.2	333 ± 99.2	379.6 ± 84.7
formalin	359.3 ± 40	530.7 ± 68.1	484.3 ± 14.7	476.2 ± 99.6	457.8 ± 26.8
mercuric chloride	418.1 ± 31.7	406.3 ± 56.2	476.6 ± 17.8	443.7 ± 41.7	456 ± 40.7

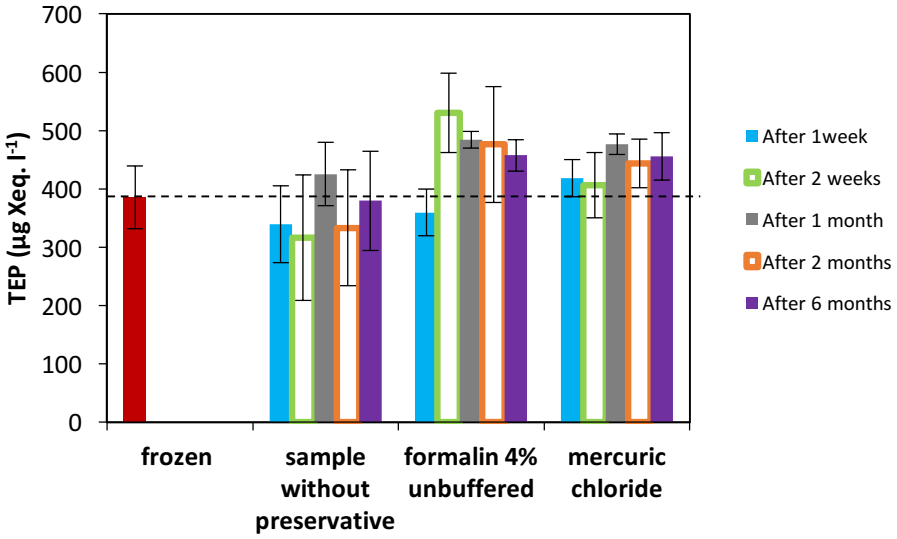

Figure 2.14 Variability of TEP sample concentration collected during Cend 24/15 (ST 21 51.9789° N, 2.0882 E°) in November 2015 using different preservation methods for up to six months after collection. The dashed line indicates the reference threshold.

Table 2.14 Mean concentrations of TEP (µg Xeq. l^{-1}), standard deviation and percentage of increase/decrease of TEP concentrations with respect to the reference for each storage experiment.

Cend 24/15 ST 21	mean TEP (µg Xeq. l^{-1})	increase /decrease %
no preser.	358.6 ± 22.1	↓ 6.9
formalin	461.7 ± 34.1	↑ 19.9
mercuric chloride	440.1 ± 14.1	↑ 14.3

2.10.7 Conclusion

The results show that both mercuric chloride and unbuffered formalin can be suitable preservatives for TEP preservation for up to six months. Mercuric chloride can be a good alternative to unbuffered formalin for the preservation of TEP long term. In the case of the use of formalin a correction needs to be made for the extra volume added to the sample. Such a correction is not necessary for the mercuric chloride method, as only a small volume of mercuric chloride solution is added to the sample.

2.11 Analysis of Particulate Organic Matter (POM)

Particulate organic carbon (POC) and particulate organic nitrogen (PON) samples were collected by filtering a volume of 250 ml of sea water through a glass syringe provided with a filter holder. Pre-combusted glass fiber filters (GF/F) (diameter of 25 mm and pore size of 0.7 μm) were used. After collection samples and blanks were stored at –20°C for later analysis.

In the UEA laboratory the filters containing POC and PON samples were defrosted and half of each filter was analysed. Prior to the analysis clean glass petri dishes were placed in the furnace at 450 °C for 4 hours before usage to avoid possible carbon contamination. During the analysis a single sample from the defrosted filter was used. The filter was placed in the glass petri dishes and dried for 24 hours at 60°C in a clean oven prior to POC and PON analysis.

When completely dry, samples were treated to remove any particulate inorganic carbon (PIC) present due to possible calcite shells of coccolithophorids. For this purpose the vapor acidification method (Hedges and Stern, 1984) was used. Samples in the glass petri dishes were kept in a desiccator containing a beaker with concentrated hydrochloric acid (HCl 36% w/v) for 24 hours. Afterwards the PIC-free samples were dried for 24 hours at 60°C in a clean oven to remove any residual HCl and water, and kept in a desiccator with silica gel until further analysis. Blank filters were processed in the same way as the POC and PON samples and used as control on potential contamination.

Acetanilide (in the range 1500 – 1900 μg) was used as standard and weighed directly into tin capsules by using an electronic ultra-microbalance Sartorius SE2. Samples, standards and blanks were placed into nickel sleeves and analyzed with a CHN Elemental Analyser

(Exeter Analytical Model 440). The concentration of the samples was calculated after blank correction. The limit of detection (LOD) of the instrument for POC and PON was 0.47 µmol C and 0.03 µmol N, respectively and calculated on the basis of three times the standard deviation of the blanks (Miller and Miller, 2010). POC and PON concentrations in µM were calculated based on two times the mass of carbon and nitrogen in the samples analysed (to get the concentration of the whole filter), divided by the volume of sea water filtered.

2.12 Analysis of chlorophyll *a*

Subsurface samples (4 m depth) for chlorophyll *a* determination were collected at 50 stations, distributed at regular intervals within the sampling area during the International Beam Trawl Survey (IBTS) in the North Sea. The IBTS was carried out in August 2014 and 2015 in the North Sea by the Centre for Environment, Fisheries and Aquaculture Science (Cefas). Chlorophyll *a* samples were analyzed by high performance liquid chromatography (HPLC) by Cefas. To calculate chlorophyll *a* concentrations of the 76 sampling stations (surface and bottom) of the survey a linear regression analysis between chlorophyll *a* measurements and fluorescence from the onboard Ferrybox and CTD profiles were used. Figure 2.15 and Figure 2.16 show two examples of the four calibration curves obtained from regression analysis and used to determine chlorophyll *a* concentrations in surface and bottom waters in the two years of the survey (2014 - 2015) in the North Sea. Eq. (2.5) from the linear regression was used to calculate the chlorophyll *a* (µg l^{-1}) for the 76 stations.

$$\boldsymbol{Chl\ a\ (\mu g\ l^{-1}) = \frac{(fluor - b)}{m}} \qquad (\mathbf{2.5})$$

where:

$\boldsymbol{fluor}$ is the Ferrybox or CTD fluorescence

$\boldsymbol{m}$ is the slope of the linear regression curve

$\boldsymbol{b}$ is the y-intercept

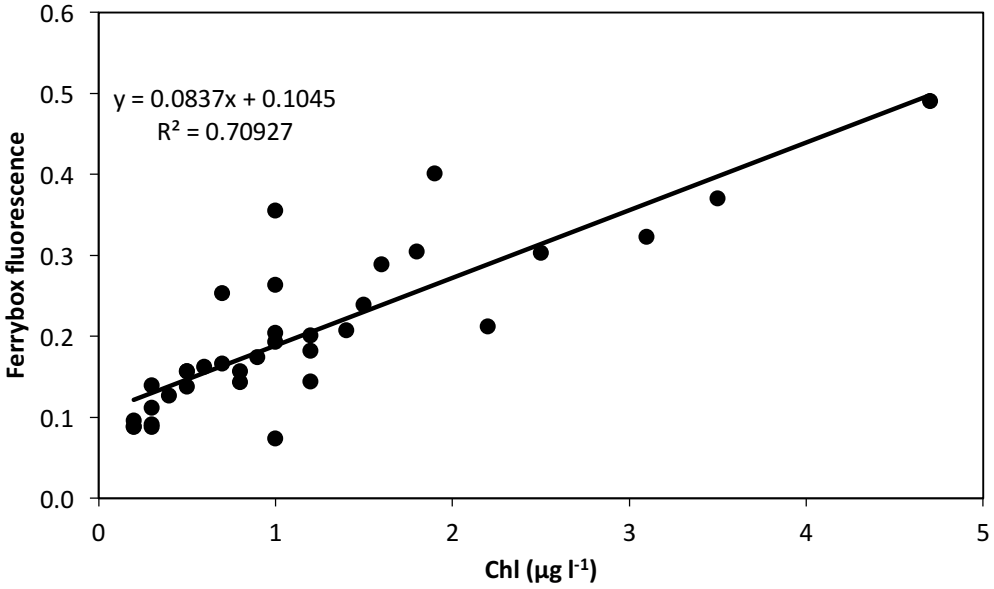

Figure 2.15 The chlorophyll *a* versus fluorescence linear regression analysis used to determine surface chlorophyll *a* concentrations in the year 2014.

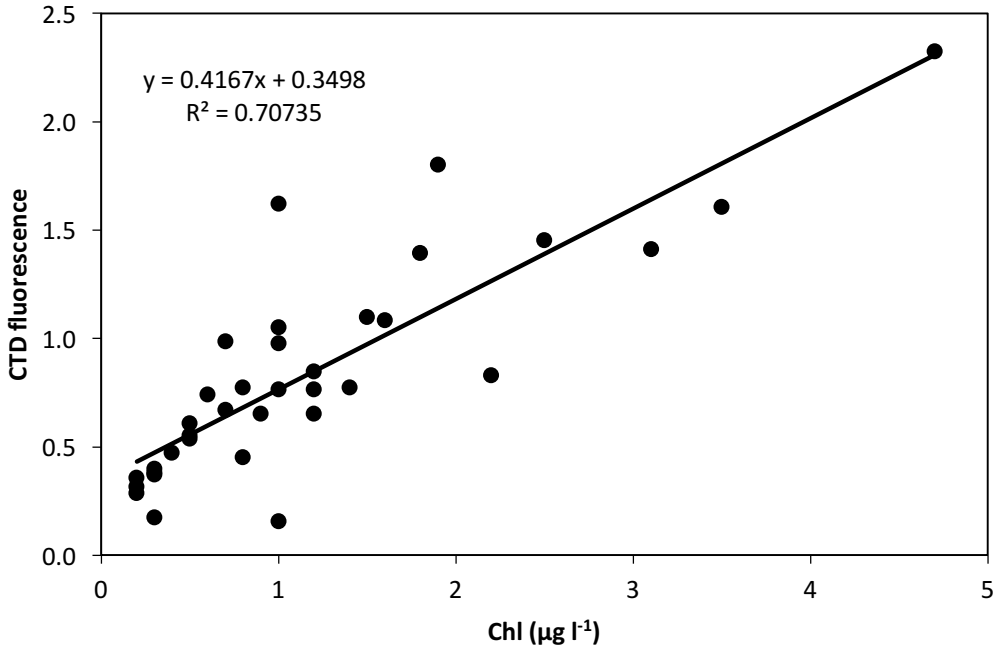

Figure 2.16 The chlorophyll versus fluorescence linear regression analysis used to determine bottom chlorophyll *a* concentrations in the year 2014.

Chapter 3 Modelling the effect of TEP on particle aggregation and export

3.1 Introduction

Dissolved organic carbon (DOC) is a significant reservoir of carbon in the marine ecosystem. Therefore, understanding the processes regulating DOC production and consumption is crucial for a quantitative assessment of the global ocean carbon cycle (Polimene *et al.*, 2006). Marine ecosystem models are valuable tools to mechanistically investigate physiological and biogeochemical processes underpinning DOC dynamics. Transparent Exopolymer Particles (TEP) are ubiquitous in the marine environment (Passow, 2002). Due to its stickiness and low density (Azetsu-Scott and Passow, 2004a) TEP can act as a glue, promoting the formation of large aggregates which when ballasted with negative buoyant particles, may sink out exporting particulate organic carbon and TEP to the seafloor (Passow *et al.*, 2001; Burd and Jackson, 2009; Mari *et al.*, 2017). The approach used to model TEP follows the recently published insight on TEP dynamics by Mari *et al.* (2017). To the best of my knowledge the approach used within this study is new, unique and is applied for the first time to a marine biogeochemical model. In this study the European Regional Seas Ecosystem Model (ERSEM) was chosen for its past applications in regional seas, its variable stoichiometry (C : N : P) and its ability to simulate the major biogeochemical cycles of carbon, nitrogen, phosphorus and silicate. It is also able to simulate a simple microbial food web. Those characteristics make ERSEM highly suitable to simulate the effect of TEP on aggregate formation and sedimentation and therefore on carbon sedimentation fluxes in the UK shelf seas. For the purpose of this work the latest version of ERSEM published by Butenschön *et al.* (2016) was used and a new parameterization for TEP was derived. This chapter explains in detail the development of TEP parameterisation in ERSEM and the approach applied to model TEP into ERSEM. The method is based on the capability of TEP to aggregate solid particles and on the consequent potential formation of sinking or floating aggregates. The addition of TEP equations to the standard ERSEM code is evaluated in Chapter 4, where station A in the Celtic Sea and station L4 in the Western English Channel were used as a test case for model development. *In situ* observations of TEP and chlorophyll *a* collected at station A were used to tune the model. Furthermore, *in situ* observations of nutrients, chlorophyll *a* and particulate organic carbon collected at station A and at station L4 were used to evaluate the effect of TEP on particle aggregation and export.

3.2 The model

3.2.1 The European Regional Seas Ecosystem Model (ERSEM)

ERSEM (Baretta *et al.*, 1995; Blackford *et al.*, 2004; Butenschon *et al.*, 2015) is a marine biogeochemical model based on biomass and functional type describing the carbon and nutrient (N, P, Si and Fe) cycles within the lower trophic levels of the marine ecosystem. Model state variables include living organisms, dissolved nutrients, organic detritus, oxygen and CO_2. Model living organisms are subdivided into three functional groups (Figure 3.1) describing the planktonic trophic chain: primary producers, consumers and decomposers. Primary producers and consumers are subdivided into 4 and 3 size-based functional types respectively, while decomposers are modeled through only one functional type. More specifically the phytoplankton community consists of picophytoplankton, nanoflagellates, dinoflagellates and diatoms. The zooplankton community includes: mesozooplankton, microzooplankton and heterotrophic nanoflagellates. Decomposers are modeled by one type of heterotrophic bacteria. Functional types belonging to the same group share common process descriptions, but different parameterizations.

A key feature of ERSEM is the decoupling between carbon and nutrient dynamics allowing the simulation of variable stoichiometry within the modeled organisms. Chlorophyll is also treated as an independent state variable following the formulation proposed by Geider *et al.* (1997). Consequently, each plankton functional type is modeled throughout by up to five state variables describing each cellular component (C, N, P, Si, Chl *a*).

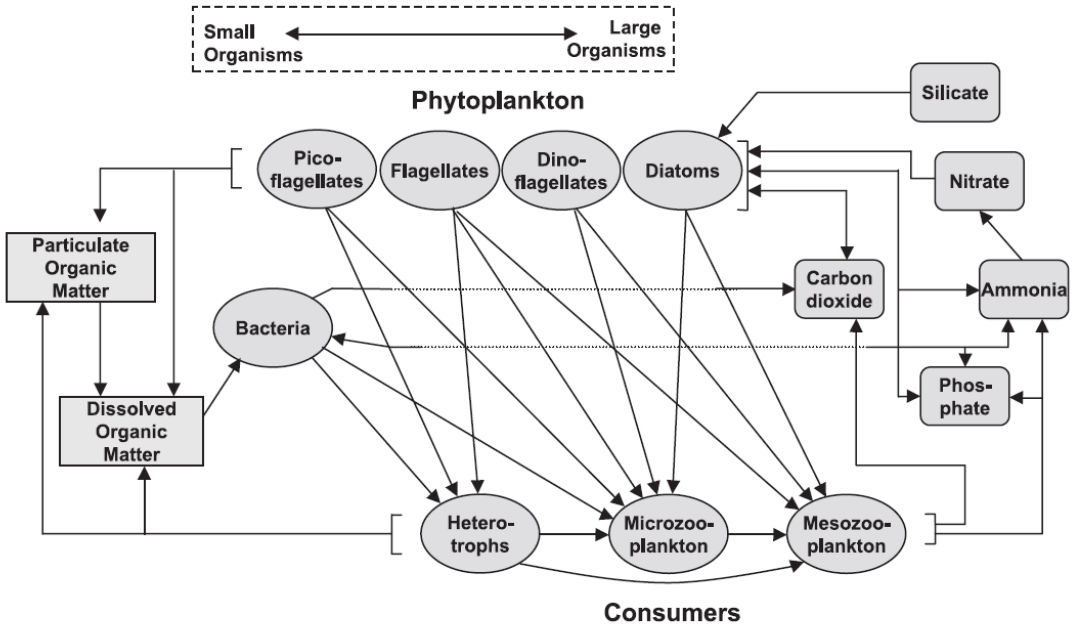

Figure 3.1 The pelagic ecosystem model flow diagram in ERSEM indicating the carbon and nutrient pathways between functional groups (Blackford *et al.*, 2004).

3.2.3 Model set up

In this study, ERSEM was coupled with the General Ocean Turbulence Model (GOTM) (Figure 3.2) and set-up as described in Butenschön *et al.* (2016). More specifically, the model was forced with re-analysis meteorological data from the European Centre for Medium-Range Weather Forecasts (ECMWF) and fluxes were calculated using the bulk formulae of Kondo (1975). The model was initialized with temperature, salinity and nutrient concentrations observed *in situ* (Smyth *et al.*, 2009) and the water column evolution was further constrained by nudging observed temperature and salinity profiles at a weekly interval with a one week relaxation time (Burchard *et al.*, 1999; Torres *et al.*, 2006) The water column was divided into 50 vertical layers, a time step of 900 s was used. Surface radiation was calculated by an astronomical formula (Rosati and Miyakoda, 1988) taking into account latitude, longitude, time, fractional cloud cover and albedo. Light extinction through the water column was assumed to depend on the concentration of organic particulates in the water column for living organisms, detritus, and silt as described in Blackford *et al.* (2004).

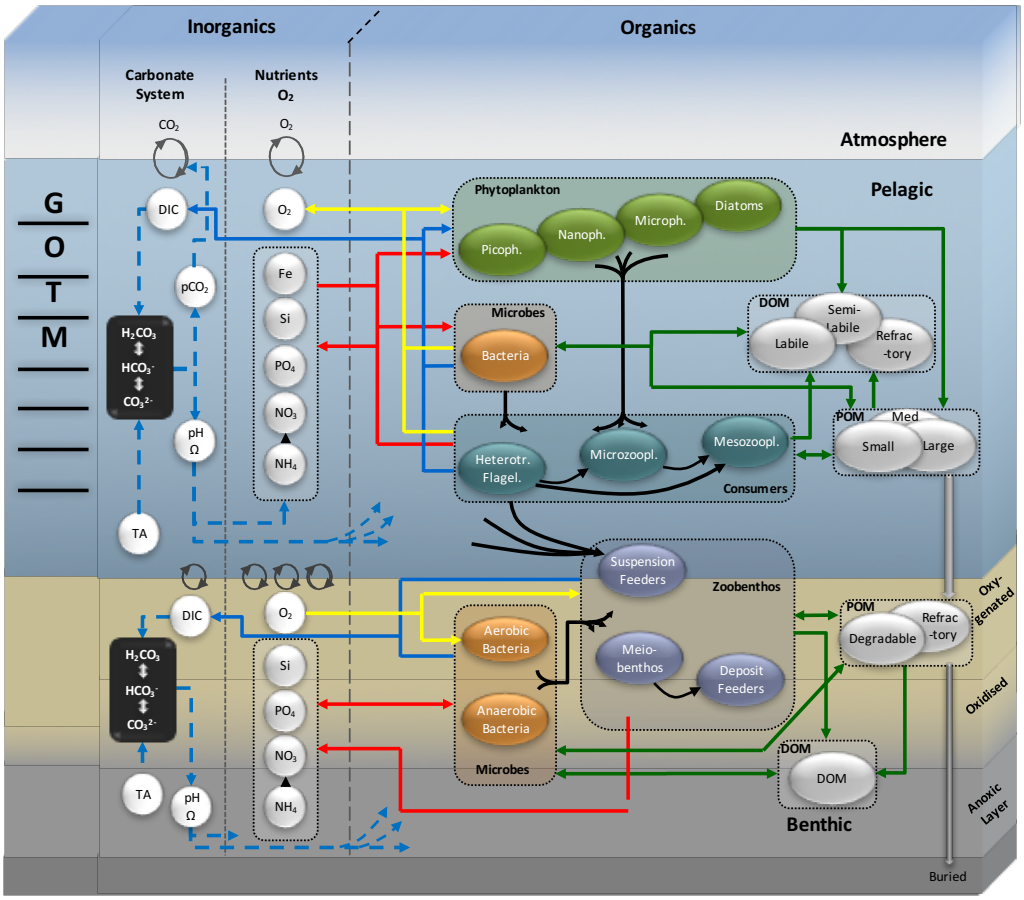

Figure 3.2 The European Regional Seas Ecosystem Model (Butenschön *et al.*, 2016).

3.3 Model development

3.3.1 New parameterization of TEP and aggregates containing TEP

TEP plays a crucial role in the aggregation and potential sinking of particles (Dam and Drapeau, 1995; Logan *et al.*, 1995; Engel, 2000a; Passow *et al.*, 2001; Fabricius *et al.*, 2003; Engel *et al.*, 2004; Mari *et al.*, 2007). In this study a new parameterisation of TEP was developed in ERSEM to simulate the TEP aggregation process and its impact and role in biogeochemical carbon cycling. Figure 3.3 shows the schematic representation of TEP in ERSEM. TEP is produced by the phytoplankton community during nutrient limitation (Mari et al., 2017) in the form of dissolved organic matter (Figure 3.3; pathway a). TEP in the water column can be used by bacteria (Figure 3.3; pathway b) and when ballasted with solid particles can promote sinking of POC and TEP to the seafloor (Figure 3.3; pathway c).

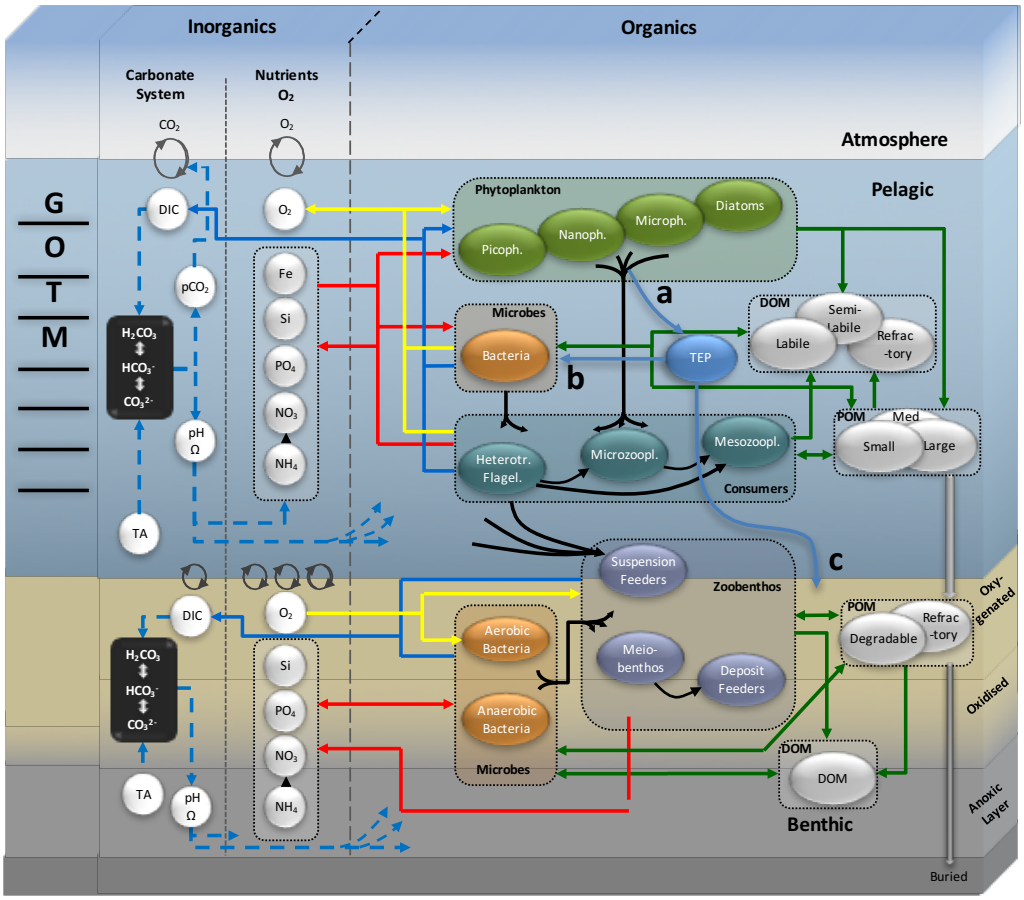

Figure 3.3 Modified version of the European Regional Seas Ecosystem Model (Butenschön et al., 2016) showing the TEP scheme. Pathway a) shows the production of TEP by the phytoplankton community during nutrient limitation in the form of dissolved organic matter (DOM). Pathway b) shows the interaction of TEP in the water column with bacterial food web. Pathway c) shows the fate of TEP when ballasted with solid particles which promote sinking of POC and TEP in form of an aggregate to the seafloor.

Figure 3.4 shows the conceptual diagram describing the TEP aggregation process. The aggregation process starts when a certain concentration of TEP is reached and a threshold is exceeded. The formation of aggregates containing TEP is linked to the probability of collision and adhesion capacity of two particles (stickiness). For the purpose of this work the stickiness coefficient (α) is used as a proxy for aggregates containing TEP formation. In particular the approach developed in this study is based on the assumption that a minimum concentration of TEP is required to form an aggregate. Therefore an aggregate is formed only when the stickiness coefficient (derived from TEP:Chl *a* ratio) is greater than the arbitrary aggregation threshold (α_{aggr}). If this condition is met, an aggregate is formed and it is assumed to be composed of POC, TEP and phytoplankton biomass. The buoyancy/sinking of this aggregate is sensitive to the ratio of TEP (low density) to other particles (high density) in the aggregate (Mari *et al.*, 2017). In our case these other particles consist of phytoplankton biomass and detrital POC. In the last step of the aggregation process the density of the newly formed aggregate ($\boldsymbol{\rho}_{aggr}$) is compared to

the density of seawater ($\boldsymbol{\rho_{seawater}}$) to determine whether the aggregate will float or will sink. The aggregation process also considers that a floating aggregate after being generated, due to mixing and further particles collision can further aggregate forming higher density particles heavy enough to sink.

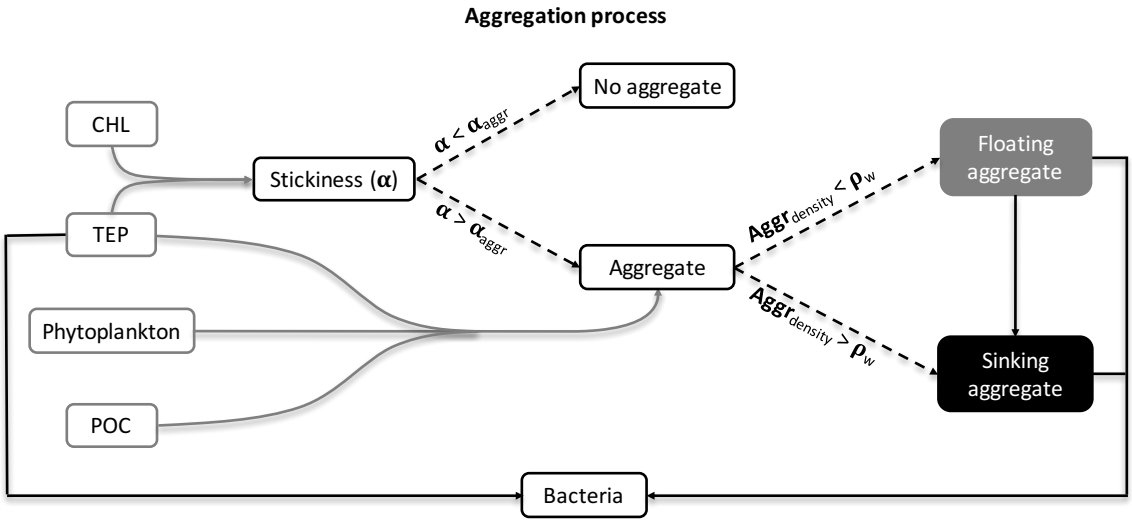

Figure 3.4 Schematic conceptual diagram representing TEP aggregation process. Dashed lines represent processes, solid lines represent fluxes. Stickiness coefficient (α), aggregation threshold ($\boldsymbol{\alpha_{aggr}}$), aggregate density ($\boldsymbol{Aggr_{density}}$) and density of seawater ($\boldsymbol{\rho_w}$).

3.3.1.1 Preliminary version of the TEP aggregation process in ERSEM

The first and preliminary approach developed to model TEP in ERSEM was based on the density of the aggregate formed by TEP. The process of formation of the aggregates was performed by assuming that any concentration of TEP would be enough to form an aggregate. When this approach was compared with the reference (standard ERSEM model without TEP) a change in the distribution of the four phytoplankton functional types was found (Figure 3.5 a and b). The introduction of TEP in ERSEM caused an inversion on the dominance of the phytoplankton groups and a month shift of the algal bloom. In the reference run the phytoplankton bloom was dominated by diatoms with a bloom in May (Figure 3.5a). By contrast in the model with TEP the picophytoplankton was dominant and the bloom had shifted from May to June (Figure 3.5b). To overcome this problem and get a more realistic aggregation process a second approach (used in the rest of this manuscript and represented in Figure 3.4) was developed. This approach introduces a further step in the aggregation process of TEP based on the stickiness coefficient (α) of TEP (Engel, 2000a). The use of the stickiness coefficient introduces a

threshold to the aggregation process, which needs to be exceeded in order to get an aggregate. This implies that the capability of TEP to form aggregates (Mari *et al.*, 2017) will depend on its concentration. This approach with a minimum threshold for aggregation reestablished the distribution of the four phytoplankton functional types (Figure 3.5a and c). The change in the structure of the phytoplankton community in the first approach could be explained by the fact that it did not have an aggregation threshold. This would have caused an excessive removal of phytoplankton biomass during the aggregation process (mainly diatoms), giving more chance to other phytoplankton groups, such as picophytoplankton to grow and to become dominant.

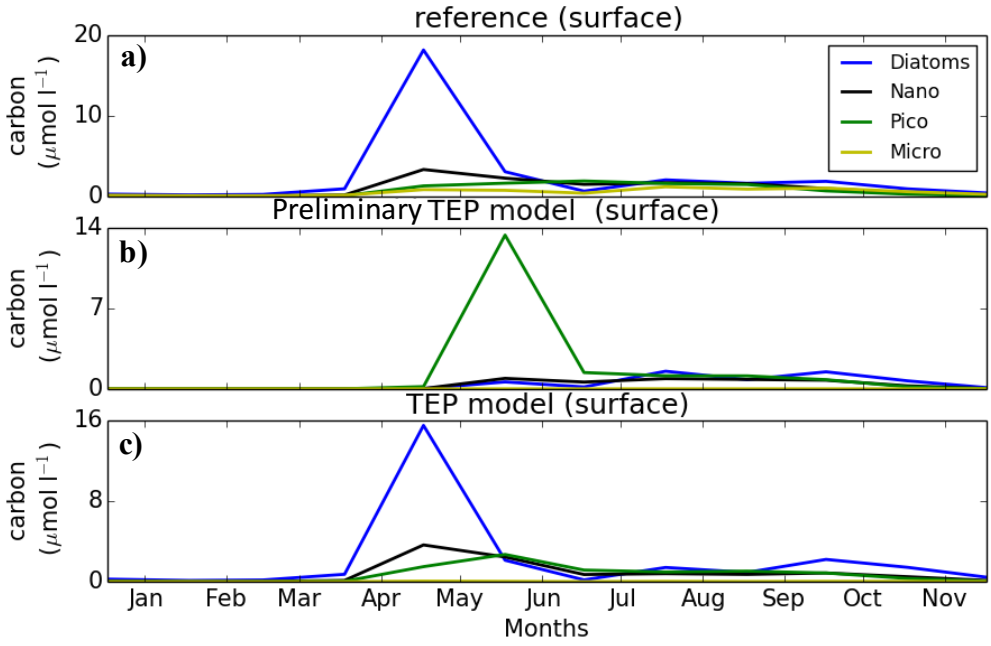

Figure 3.5 Phytoplankton functional types (Diatoms, Nanophytoplankton, Picophytoplankton and Microphytoplankton) in ERSEM for the year 2015 at station L4 in surface waters for a) a reference run without TEP b) a preliminary TEP model with density process only and c) a TEP model with density and stickiness processes.

3.3.2 Aggregation process

The detailed series of equations describing TEP formation and aggregation and the dynamics of aggregates containing TEP are explained in this section.

The total floating aggregate, sinking aggregate and free TEP_c are given in the Eq. (3.1), (3.2) and (3.3).

$$\frac{\partial Af_c}{\partial t}\Big|_{aggr} = \frac{\partial Af_c}{\partial t}\Big|_{prod} - \frac{\partial Af_c}{\partial t}\Big|_{consumption} \qquad (3.1)$$

$$\frac{\partial As_c}{\partial t}\Big|^{aggr} = \frac{\partial As_c}{\partial t}\Big|^{prod} - \frac{\partial As_c}{\partial t}\Big|^{consumption} - \frac{\partial As_c}{\partial t}\Big|^{sink} \quad (3.2)$$

$$\frac{\partial TEP_c}{\partial t}\Big|^{free} = \frac{\partial TEP_c}{\partial t}\Big|^{source} - \frac{\partial As_c}{\partial t}\Big|^{aggr} - \frac{\partial Af_c}{\partial t}\Big|^{aggr} - \frac{\partial TEP_c}{\partial t}\Big|^{consumption} \quad (3.3)$$

where:

$\frac{\partial Af_c}{\partial t}\Big|^{aggr}$ = total floating aggregate (mg C $m^{-3}d^{-1}$)

$\frac{\partial Af_c}{\partial t}\Big|^{prod}$ = TEP_c, phytoplankton biomass and particulate organic carbon going into the floating aggregate (mg C $m^{-3}d^{-1}$)

$\frac{\partial Af_c}{\partial t}\Big|^{consumption}$ = consumption of the floating aggregate by bacteria (mg C $m^{-3}d^{-1}$)

$\frac{\partial As_c}{\partial t}\Big|^{aggr}$ = total sinking aggregate (mg C $m^{-3}d^{-1}$)

$\frac{\partial As_c}{\partial t}\Big|^{prod}$ = TEP_c, phytoplankton biomass and particulate oganic carbon going into the sinking aggregate (mg C $m^{-3}d^{-1}$)

$\frac{\partial As_c}{\partial t}\Big|^{consumption}$ = consumption of the sinking aggregate by bacteria (mg C $m^{-3}d^{-1}$)

$\frac{\partial As_c}{\partial t}\Big|^{sink}$ = sinking of the aggregate (mg C $m^{-3}d^{-1}$)

$\frac{\partial TEP_c}{\partial t}\Big|^{free}$ = total free TEP_c (mg C $m^{-3}d^{-1}$)

$\frac{\partial TEP_c}{\partial t}\Big|^{source}$ = TEP_c produced by phytoplankton during nutrient limitation (mg C $m^{-3}d^{-1}$)

$\frac{\partial TEP_c}{\partial t}\Big|^{consumption}$ = consumption of the free TEP_c by bacteria (mg C $m^{-3}d^{-1}$)

TEP_c is assumed to be produced by phytoplankton under nutrient limitation as given in Eq. (3.4).

$$\frac{\partial TEP_c}{\partial t}\Big|^{source} = \left[(1-\beta_P)\left(1-f_P^{n,p}\right)\right]\frac{\partial P_c}{\partial t}\Big|^{gpp} \qquad (3.4)$$

where:

$\beta_P =$ constant fraction of carbon uptake

$f_P^{n,p} =$ internal nutrient ratio

$\frac{\partial P_c}{\partial t}|^{gpp} =$ gross primary production (mg C $m^{-3}d^{-1}$)

The aggregation process is based on the density of the aggregates. Particulate organic carbon (Eq. (3.6)), TEP_c (Eq. (3.4)) and phytoplankton biomass (Eq. (3.7)) are used for the formation of the aggregate.

$$R_{tot\,c} = R1_c + R2_c + R3_c + R4_c + TEP_c + R6_c + R8_c + As_c + Af_c \qquad (3.5)$$

$$R_c = R4_c + R6_c + R8_c \qquad (3.6)$$

$$P_c = P1_c + P2_c + P3_c + P4_c \qquad (3.7)$$

where:

$R_{tot\,c} =$ total organic carbon (mg C m^{-3})

$R1_c =$ labile dissolved organic carbon (mg C m^{-3})

$R2_c =$ semi $-$ labile dissolved organic carbon (mg C m^{-3})

$R3_c =$ semi $-$ refractory dissolved organic carbon (mg C m^{-3})

$R4_c =$ small $-$ size particulate organic carbon (mg C m^{-3})

$TEP_c =$ free TEP_c concentration (mg C m^{-3})

$R6_c =$ medium $-$ size particulate organic carbon (mg C m^{-3})

$R8_c =$ large $-$ size particulate organic carbon (mg C m^{-3})

$As_c =$ sinking aggregate concentration (mg C m^{-3})

$Af_c =$ floating aggregate concentration (mg C m^{-3})

$P1_c =$ diatom biomass (mg C m^{-3})

$P2_c =$ nanophytoplankton biomass (mg C m^{-3})

$\boldsymbol{P3_c}$ = picophytoplankton biomass (mg C m^{-3})

$\boldsymbol{P4_c}$ = microphytoplankton biomass (mg C m^{-3})

$\boldsymbol{R_c}$ = particulate organic carbon (POC) (mg C m^{-3})

$\boldsymbol{P_c}$ = phytoplankton biomass (mg C m^{-3})

The formation of the aggregate is triggered by the stickiness coefficient (α). More specifically, in this work a linear relationship between the stickiness coefficient and TEP : Chl *a* was used (Engel, 2000a) as a proxy within the aggregation process to determine whether the concentration of TEP is enough to lead to the formation of an aggregate. Chl *a* (Eq. (3.8)) and TEP are used in Eq. (3.9) to calculate the stickiness coefficient (α).

$$\boldsymbol{Chl\ a = P1_{chl} + P2_{chl} + P3_{chl} + P4_{chl}} \quad (\mathbf{3.8})$$

$$\boldsymbol{\alpha = m\left(\frac{\frac{TEP_c}{\omega}}{Chl\ a}\right) - q} \quad (\mathbf{3.9})$$

where:

$\boldsymbol{Chl\ a}$ = chlorophyll *a* (mg m^{-3})

$\boldsymbol{P1_{chl}}$ = diatom chlorophyll *a* (mg m^{-3})

$\boldsymbol{P2_{chl}}$ = nanophytoplankton chlorophyll *a* (mg m^{-3})

$\boldsymbol{P3_{chl}}$ = picophytoplankton chlorophyll *a* (mg m^{-3})

$\boldsymbol{P4_{chl}}$ = microphytoplankton chlorophyll *a* (mg m^{-3})

$\boldsymbol{\omega}$ = 0.63 (conversion factor to convert TEP_c (mg m^{-3}) to TEP (µg Xeq. l^{-1}))

$\boldsymbol{m}$ = slope of equation (6.38×10^{-4} (Engel, 2000a))

$\boldsymbol{q}$ = y − intercept (-3.33×10^{-3} (Engel, 2000a))

$\boldsymbol{\alpha}$ = TEP stickiness (Engel, 2000a)

The process of formation of the aggregate was performed by assuming that only in the case of TEP stickiness (α) being higher than that of the aggregation threshold α_{aggr} ($\boldsymbol{\alpha > \alpha_{aggr}}$), there would be enough TEP_c to form an aggregate, while the aggregate composition depends on the contribution of each single fraction (Eq. (3.10), (3.11), (3.12)).

$$\%\,\boldsymbol{TEP_c} = \frac{\boldsymbol{TEP_c}}{\boldsymbol{R_c + P_c + TEP_c}}\boldsymbol{100} \qquad (\boldsymbol{3.10})$$

$$\%\,\boldsymbol{R_c} = \frac{\boldsymbol{R_c}}{\boldsymbol{R_c + P_c + TEP_c}}\boldsymbol{100} \qquad (\boldsymbol{3.11})$$

$$\%\,\boldsymbol{P_c} = \frac{\boldsymbol{P_c}}{\boldsymbol{R_c + P_c + TEP_c}}\boldsymbol{100} \qquad (\boldsymbol{3.12})$$

The density of the aggregate is calculated using Eq. (3.13), which takes into account the aggregate composition (Eq. (3.10), (3.11) and (3.12)), densities of TEP_c, POC, phytoplankton, seawater density and aggregate porosity.

$$\boldsymbol{Aggr_{density}} = \boldsymbol{\rho_w - p_{aggr} + (1 - p_{aggr})}[\left(\frac{\%_{\boldsymbol{TEP_c}}}{\boldsymbol{100}}\right)\boldsymbol{\rho_{TEP_c}} + \left(\frac{\%_{\boldsymbol{R_c}}}{\boldsymbol{100}}\right)\boldsymbol{\rho_{R_c}} + \left(\frac{\%_{\boldsymbol{P_c}}}{\boldsymbol{100}}\right)\boldsymbol{\rho_{P_c}}] \qquad (\boldsymbol{3.13})$$

where:

$\boldsymbol{TEP_c}$ = TEP_c concentration (mg C m^{-3})

$\boldsymbol{R_c}$ = particulate organic carbon (mg C m^{-3})

$\boldsymbol{P_c}$ = phytoplankton biomass (mg C m^{-3})

$\%\boldsymbol{TEP_c}$ = percentage of TEP_c in the aggregate

$\%\boldsymbol{R_c}$ = percentage of particulate organic carbon in the aggregate

$\%\boldsymbol{P_c}$ = percentage of pytoplankton biomass in the aggregate

$\boldsymbol{\rho_w}$ = density of seawater (kg m^{-3})

$\boldsymbol{p_{aggr}}$ = porosity of the aggregate

$\boldsymbol{\rho_{TEP_c}}$ = density of the TEP_c (kg m^{-3})

$\boldsymbol{\rho_{R_c}}$ = density of the particulate organic carbon(kg m^{-3})

$\boldsymbol{\rho_{P_c}}$ = density of the pytoplankton biomass (kg m^{-3})

$\boldsymbol{Aggr_{density}}$ = density of the aggregate(kg m^{-3})

The formation of a floating aggregate occurs when TEP stickiness (α) is higher than the aggregation threshold α_{aggr} ($\boldsymbol{\alpha > \alpha_{aggr}}$) and the density of the aggregate is lower than

that of seawater ($\boldsymbol{Aggr_{density} < \rho_w}$), then the aggregation factor $\boldsymbol{\vartheta = 1}$ and an aggregate will be formed as described in equations Eq. (3.14) and (3.15).
A fraction $\boldsymbol{\xi}$ of the concentration of POC and phytoplankton (Eq. (3.14)), and a fraction $\boldsymbol{\xi_{TEP}}$ of TEP_c concentration will contribute to the aggregate every day (Eq. (3.15)).

$$\frac{\partial \boldsymbol{Af_c}}{\partial \boldsymbol{t}} \Big|^{\boldsymbol{prod\ PR}} = (\boldsymbol{P_c + R_c})\ \boldsymbol{\xi}\ \boldsymbol{\vartheta} \qquad (\mathbf{3.14})$$

$$\frac{\partial \boldsymbol{Af_c}}{\partial \boldsymbol{t}} \Big|^{\boldsymbol{prod\ TEP}} = \boldsymbol{TEP_c}\ \ \boldsymbol{\xi_{TEP}}\ \boldsymbol{\vartheta} \qquad (\mathbf{3.15})$$

where:

$\frac{\partial \boldsymbol{Af_c}}{\partial \boldsymbol{t}} \Big|^{\boldsymbol{prod\ PR}}$ = phytoplankton biomass and particulate oganic carbon going into the floating aggregate (mg C $m^{-3}d^{-1}$)

$\frac{\partial \boldsymbol{Af_c}}{\partial \boldsymbol{t}} \Big|^{\boldsymbol{prod\ TEP}}$ = TEP_c going into the floating aggregate (mg C $m^{-3}d^{-1}$)

$\boldsymbol{\vartheta}$ = aggregation factor

$\boldsymbol{\xi}$ = daily fraction of carbon (POC and Phytoplankton) forming aggregates

$\boldsymbol{\xi_{TEP}}$ = daily fraction of TEP_c forming aggregates (d^{-1})

In this process a daily fraction of the floating aggregate can be assembled with other particles, forming heavier particles which can sink out and become part of the sinking aggregate (Eq. (3.16)).

$$\frac{\partial \boldsymbol{Af_c}}{\partial \boldsymbol{t}} \Big|^{\boldsymbol{sink}} = \boldsymbol{Af_c}\ ß \qquad (\mathbf{3.16})$$

where:

$\frac{\partial \boldsymbol{Af_c}}{\partial \boldsymbol{t}} \Big|^{\boldsymbol{sink}}$ = flux of floating aggregate moving to the sinking aggregate (mg C $m^{-3}d^{-1}$)

ß = daily fraction of floating aggregate going into sinking aggregate (d^{-1})

The production of floating aggregates (Eq. (3.17)) is given by the sum of phytoplankton/POC production and the production of TEP_c, minus the flux of floating aggregates going into the pool of the sinking aggregates.

$$\frac{\partial Af_c}{\partial t}\Big|^{prod} = \frac{\partial Af_c}{\partial t}\Big|^{prod\,PR} + \frac{\partial Af_c}{\partial t}\Big|^{prod\,TEP} - \frac{\partial Af_c}{\partial t}\Big|^{sink} \qquad (3.17)$$

The consumption of the floating aggregate by bacteria (Eq. (3.18)) is proportional to the amount of the aggregates relative to the total carbon substrate available for bacteria (Eq. (3.5)), the fraction of the sinking aggregate available to bacteria and bacterial uptake.

$$\frac{\partial Af_c}{\partial t}\Big|^{consumption} = [(\frac{Af_c}{R_{tot\,c}})\, P^B_{Af_c}]\frac{\partial B_c}{\partial t}\Big|^{upt} \qquad (3.18)$$

where:

$P^B_{Af_c}$ = fraction of the floating aggregate available to bacteria (d^{-1})

$\frac{\partial B_c}{\partial t}\Big|^{upt}$ = bacterial uptake (mg C $m^{-3}d^{-1}$)

The formation of a sinking aggregate occurs when TEP stickiness (α) is higher than the aggregation threshold α_{aggr} ($\alpha > \alpha_{aggr}$) and the density of the aggregate is higher than that of seawater ($Aggr_{density} > \rho_w$), then the aggregate factor $\vartheta = 1$ and an aggregate will be formed as described in the Eq. (3.19) and (3.20).

A fraction ξ of the concentration of POC and phytoplankton (Eq. (3.19)), and a fraction ξ_{TEP} of TEP_c concentration will contribute to the aggregate every day (Eq. (3.20)).

$$\frac{\partial As_c}{\partial t}\Big|^{prod\,PR} = (P_c + R_c)\ \xi\ \vartheta \qquad (3.19)$$

$$\frac{\partial As_c}{\partial t}\Big|^{prod\,TEP} = TEP_c\ \ \xi_{TEP}\ \vartheta \qquad (3.20)$$

where:

$\frac{\partial As_c}{\partial t}\Big|^{prod\ PR}$ = phytoplankton biomass and detrital POC going into the aggregate (mg C $m^{-3}d^{-1}$)

$\frac{\partial As_c}{\partial t}\Big|^{prod\ TEP}$ = TEP_c going into the aggregate (mg C $m^{-3}d^{-1}$)

The production of sinking aggregate (Eq. (3.21)) is given by the sum of phytoplankton/POC production, the production of TEP_c. and the flux of floating aggregate moved to the pool of the sinking aggregate.

$$\frac{\partial As_c}{\partial t}\Big|^{prod} = \frac{\partial As_c}{\partial t}\Big|^{prod\ PR} + \frac{\partial As_c}{\partial t}\Big|^{prod\ TEP} + \frac{\partial Af_c}{\partial t}\Big|^{sink} \quad (3.21)$$

As for the floating aggregate the consumption of the sinking aggregate by bacteria (Eq. (3.22)) is proportional to the amount of the aggregates relative to the carbon substrate available for bacteria (Eq. (3.5)), the fraction of the floating aggregate available to bacteria and bacterial uptake.

$$\frac{\partial As_c}{\partial t}\Big|^{consumption} = [(\frac{As_c}{R_{tot\ c}})\ P^B_{As_c}]\frac{\partial B_c}{\partial t}\Big|^{upt} \quad (3.22)$$

The loss/gain term due to sinking (Eq. (3.23)) depends on the concentration gradient of the sinking aggregate along the water column and the sedimentation velocity of the aggregate.

$$\frac{\partial As_c}{\partial t}\Big|^{sink} = \frac{As_c}{\partial z} V_{As_c} \quad (3.23)$$

where:

$P^B_{As_c}$ = fraction of the sinking aggregate available to bacteria (d^{-1})

$\frac{As_c}{\partial z}$ = sinking aggregate gradient concentration (mg C m^{-3})

V_{As_c} = sinking velocity of the sinking aggregate (m d^{-1})

The consumption of the free TEP_c, (TEP_c not associated with the aggregates and still in form of DOM) by bacteria (Eq. (3.24)) is proportional to the amount of the aggregate relative to the carbon substrate available for bacteria (Eq. (3.5)), the fraction of the TEP_c available to bacteria and bacteria uptake.

$$\frac{\partial TEP_c}{\partial t} \Big|^{cosumption} = [(\frac{TEP_c}{R_{tot\,c}})\, P^B_{TEP_c}] \frac{\partial B_c}{\partial t} \Big|^{upt} \qquad (3.24)$$

where:

$P^B_{TEP_c}$ = fraction of TEP_c available to bacteria (d^{-1})

A fraction of nitrogen, phosphorus and silicium proportional to that of TEP_c goes into the aggregates. Furthermore, in order to track the amount of TEP_c into each aggregate a specific new currency (t) was added to the model, which expresses the content of TEP_c in both sinking and floating aggregates. The specific parameters used during TEP simulations are listed in the Table 3.1.

Table 3.1 Summary of the specific parameters (symbol, description and unit) used to represent TEP in ERSEM.

Symbol	Description	Unit
ρ_{TEP_c}	TEP density	kg m^{-3}
ρ_{POC}	POC density	kg m^{-3}
ρ_{Phyto}	Phytoplankton density	kg m^{-3}
$porosity$	Aggregate porosity	-
rm	Sinking velocity of the sinking aggregate	m d^{-1}
$aggr$	Daily fraction of POC and Phytoplankton going to the aggregate	d^{-1}
$aggr_{TEP}$	Daily fraction of TEPc going to the aggregate	d^{-1}
α_{aggr}	Aggregation threshold	-
ϑ	Aggregation factor	-
ß	Daily fraction of floating aggregate going to the sinking aggregate	d^{-1}
$rR5$	Fraction of TEPc available to bacteria	d^{-1}
$rR10$	Fraction of sinking aggregate available to bacteria	d^{-1}
$rR11$	Fraction of floating aggregate available to bacteria	d^{-1}

Chapter 4 Vertical distribution of TEP at Celtic Sea sites during spring and summer 2015

4.1 Introduction

TEP exuded by phytoplankton as a carbon-rich compound (Mari *et al.*, 2017) may play an important role in the Continental shelf seas for the uptake, export and storage of organic carbon. TEP production is thought to be associated with carbon overconsumption, which occurs in summer when the phytoplankton community is nutrient limited (Mari *et al.*, 2017). Due to its stickiness and low density (Azetsu-Scott and Passow, 2004a) TEP can act as a glue by promoting the formation of large aggregates, which when ballasted with negatively buoyant particles may sink out, exporting particulate organic carbon and TEP to the seafloor (Passow *et al.*, 2001; Burd and Jackson 2009; Mari *et al.*, 2017).

This study was carried out during the Shelf Sea Biogeochemistry programme (SSB), co-funded by the Natural Environment Research Council (NERC) and the Department for Environment, Food and Rural Affairs (Defra). The aim of the SSB programme was to increase understanding of the cycling of nutrients and carbon and the controls on primary and secondary production in NW European shelf seas and their role in biogeochemical cycles. Within the SSB programme, samples for TEP were collected from the seasonally stratified Celtic Sea during spring and summer 2015 to investigate the role of TEP in carbon cycling in NW European shelf seas. In particular, the vertical distribution of TEP in spring and summer, at three Celtic Sea sites was studied.

This Chapter presents the results and discussion of the vertical distribution of TEP in the Celtic Sea during spring and summer. The Chapter is divided into two parts, observations and modelling approaches. The first part is focused on the field observations of TEP which were used to discover the vertical distribution of TEP at three different sites in the Celtic Sea. TEP observations were also used to address the key processes that control the vertical dynamics of TEP, with the use of linear regression analyses of TEP versus chlorophyll *a* and other variables. Furthermore, the TEP to chlorophyll *a* relationship and ratio is used to investigate their possible use as indicators of TEP production. In the second part of the Chapter three different modelling approaches were used in combination with TEP observations to explore the processes controlling TEP dynamics in the shelf sea. The first modelling approach uses a simple box model to estimate TEP formation, accumulation rate, residence time, sinking rate, TEP export and bacterial

remineralization. The second modelling approach was used to investigate the role of TEP in the formation of marine aggregates, aggregates containing TEP composition sinking and export. The third modelling approach was used to reproduce the observed TEP concentrations and model the effect of TEP on particle aggregation in the Celtic Sea by means of the European Regional Seas Ecosystem Model (ERSEM). To this end a new formulation for TEP dynamics was developed in ERSEM and used to investigate the fate of carbon exported and its effects on CO_2 uptake from the atmosphere, carbon sequestration and C : N stoichiometry of the particulate organic carbon .

4.2 Observations

4.2.1 Method: TEP sample collection and processing

Water samples were collected at three stations: Station A, Station CCS and Station CS2 along a transect from the coast to the open ocean in the Celtic Sea (Figure 4.1).

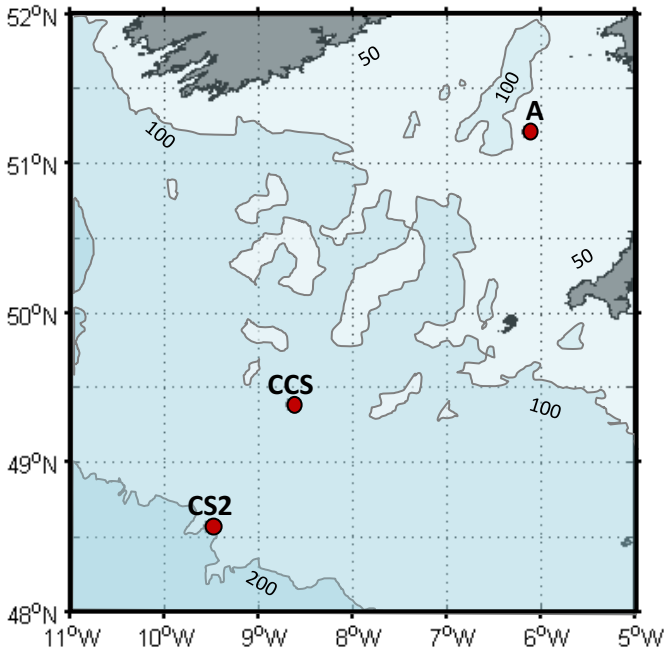

Figure 4.1 Sampling area: Celtic Deep (A); Candyfloss (CCS); Shelf Edge (CS2).

TEP samples were collected as part of the Shelf Sea Biogeochemistry research program during spring 2015 (DY029) and summer 2015 (DY033) on the RRS Discovery at three study sites in the Celtic Sea. Discrete samples for TEP were collected at the three main process sites, which were the focus of the SSB cruise programme: Celtic Deep,

Candyfloss and Shelf Edge (Figure 4.1). The samples were collected from 20 L Niskin bottles filled at different depths during CTD casts, along a transect from the coast to the shelf edge (Figure 4.1). TEP samples (1 L) were fixed with a 4% formaldehyde final concentration in the sample and stored at 4 °C in the dark until analysis was undertaken in the UEA laboratory as described in sections 2.2 and 2.6. TEP values shown in this chapter are based on a single measurement at each depth due to the low volume of sample collected and low concentration of TEP. However, a standard deviation of ± 15% of the TEP value was estimated to be the uncertainty associated to the measurements as described in (section 2.6). During the two cruises samples of water were collected for chlorophyll *a*, nutrients and Particulate Organic Matter (POM) determination. Chlorophyll *a* was collected by filtering 200 - 250 ml of sea water through 25 mm diameter Whatman GF/F filters. Filters were extracted in 8 ml of 90% acetone for 18-20 h and the resulting chlorophyll *a* fluorescence was measured on a Turner Trilogy fluorometer calibrated against a solid standard and a chlorophyll *a* extract (Sigma) by Dr. Alex Poulton at the NOC (National Oceanography Centre), Southampton. Nutrients were analysed by Carolyn Harris from PML (Plymouth Marine Laboratory) during the research cruise DY029 and by Malcolm Woodward from PML during the cruise DY033. Nutrient concentrations were determined by the analytical method described in Woodward and Rees (2001). The typical precision of the analytical results was between 2-3%. The limits of detection for nitrate and phosphate were 0.02 μmol l^{-1}, nitrite 0.01 μmol l^{-1}, ammonia 0.05 μmol l^{-1} and silicate did not ever approach the limits of detection. Particulate organic carbon and nitrogen samples were analysed by Dr. Clare Davis and Dr. Claire Mahaffey at Liverpool University in duplicate after vapour phase decarbonation using a Carlo Erba Instruments NC2500 elemental analyser (Yamamuro and Kayanne, 1995). The results uncertainty limits were 7.17 ± 0.09 % for POC and 0.57 ± 0.02 % for PON. CTD profiles data for physical variables such as temperature, salinity and turbidity were downloaded from the British Oceanographic Data Centre (BODC).

In order to investigate the potential biological and physicochemical factors controlling TEP_c dynamics the relationship between TEP_c and chlorophyll *a*, nutrients, temperature and salinity were determined by means of regression analysis. For comparison with the existing literature, TEP and chlorophyll *a* were log-transformed. TEP stickiness (α) was calculated using the empirical equation Eq. (4.1) (Engel, 2000a).

$$\boldsymbol{\alpha = 6.38\times10^{-4}\left(\frac{TEP}{Chl\ a}\right) - 3.3\times10^{-3}} \qquad (\mathbf{4.1})$$

where:

$\boldsymbol{TEP} =$ concentration of TEP ($\mu g\ Xeq.\ l^{-1}$)

$\boldsymbol{Chl\ a} =$ concentration of chlorophyll a ($\mu g\ l^{-1}$)

The Surface Mixed Layer Depth (SMLD) was determined by Dr. Joanne Hopkins at NOC, Liverpool using the vertical density of water masses from the CTD profiles and applying a threshold for the potential change in density relative to that at 10 metres. For the cruise in summer 2015 (DY033) a threshold of 0.02 kg m^{-3} was used. For spring 2015 (DY029) the threshold was reduced to 0.01 kg m^{-3}. The SMLD calculated at Station CS2 was not very clear due to strong vertical mixing. Therefore for this station SMLD was determined using the vertical profiles of chlorophyll *a*, temperature, salinity and density.

4.2.2 Results

TEP_c concentrations and other variables are shown in Figure 4.2, 4.3 and 4.4. Spring TEP_c concentration ranged from 1.3 μmol l^{-1} (137 m depth) on Station CCS to 7.3 μmol l^{-1} (15 m depth) on Station CCS, with an average of 3.7 μmol l^{-1}. Summer TEP_c concentration ranged from 1.2 μmol l^{-1} (192 m depth) on Station CS2 to 12.3 μmol l^{-1} (7 m depth) on Station A, with an average of 4.5 μmol l^{-1}. The SMLD at Station A was calculated to be at 31 metres depth in spring and at 27 metres depth in summer. At Station CCS the SMLD was at 53 metres depth in spring and at 28 metres depth in summer. At Station CS2 the SMLD was at 10 metres depth in summer. However, due to high vertical mixing this result was not very clear. Therefore for this station the SMLD was inferred to be at 20 metres depth by taking into account the vertical profiles of chlorophyll *a*, temperature, salinity and density. TEP_c concentrations were generally higher in the Surface Mixed Layer (SML) in spring and summer at stations CCS and CS2, and decreased with depth. Station A showed high TEP_c concentrations near the bottom (~ 100 m depth) in spring (6.2 μmol l^{-1}) and summer (7.5 μmol l^{-1}). This may suggest a potential benthic interaction and resuspension of old TEP from the seafloor. At stations CCS and CS2, TEP_c vertical profiles generally tracked those of chlorophyll *a*, decreasing with increasing depth in the Bottom Mixed Layer (BML). TEP_c concentration increased with depth in the BML at Station A in spring and summer and did not follow the profile of chlorophyll *a*. In all

stations TEP_c production in the SML in summer was consistent with the hypothesis that TEP is linked to nutrient depletion due to its higher concentrations in the SML respect to that of the BML. Nutrient concentrations were much lower in summer in the SML compared to spring due to drawdown by primary producers. The TEP_c profile at Station CCS in spring, in surface waters showed concentrations of TEP_c very different from each other, despite being taken from samples at similar depths (the difference in concentration being approximately doubled). Such a difference was not observed in the chlorophyll *a* profile at the same depth. This may be explained by the observed net decrease in temperature of 0.05 ˚C (Figure 4.3a).

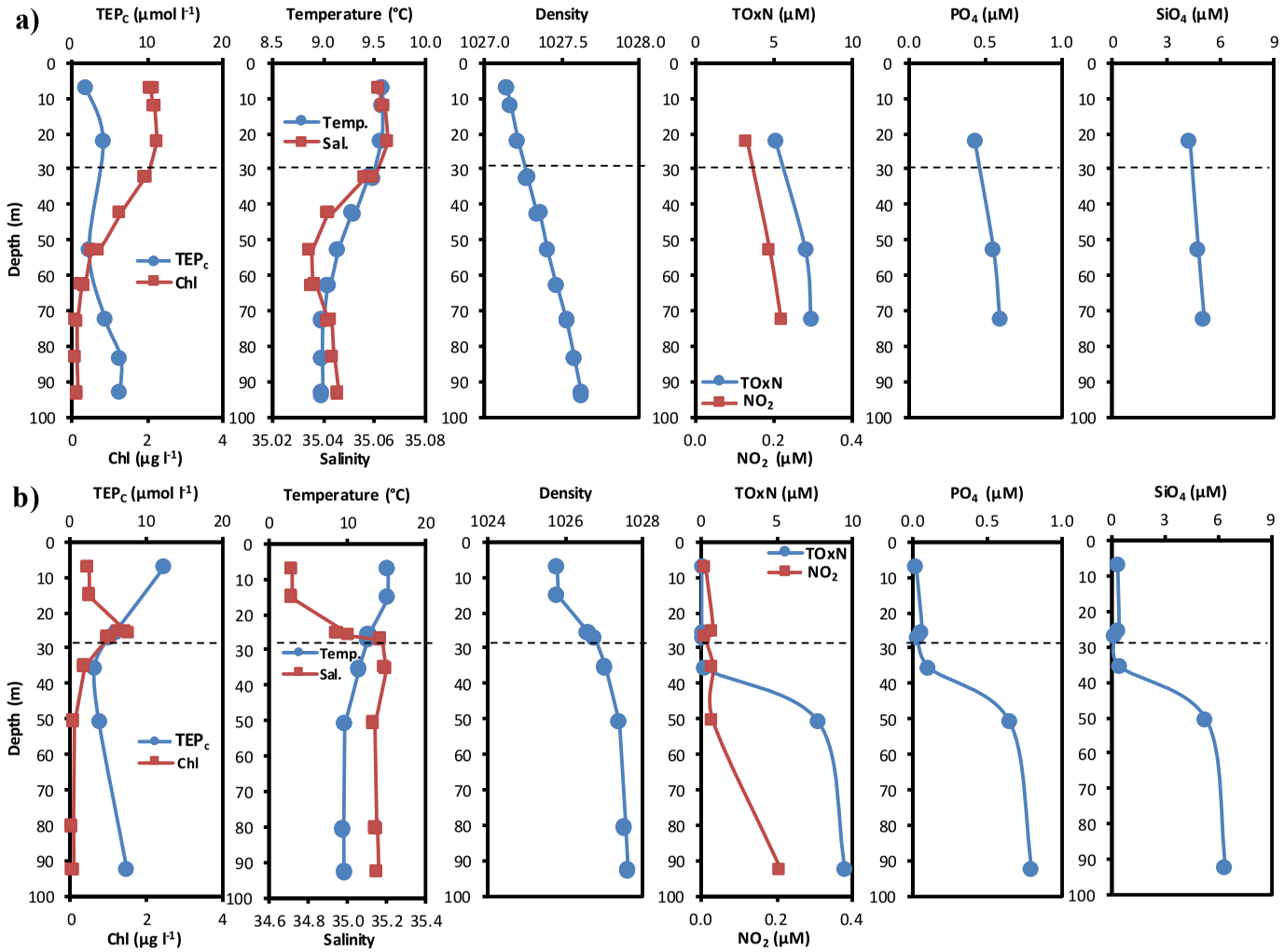

Figure 4.2 Vertical distribution of TEP$_c$ content (µmol l^{-1}), chlorophyll *a* (µg l^{-1}), temperature (°C), salinity, density (kg m^{-3}), TOxN (µM), NO_2 (µM), PO_4 (µM) and SiO_4 (µM), in a) spring and b) summer 2015 at Station Celtic Deep (A). TEP values are based on a single measurement at each depth. The dashed line indicates the Surface Mixed Layer Depth (SMLD).

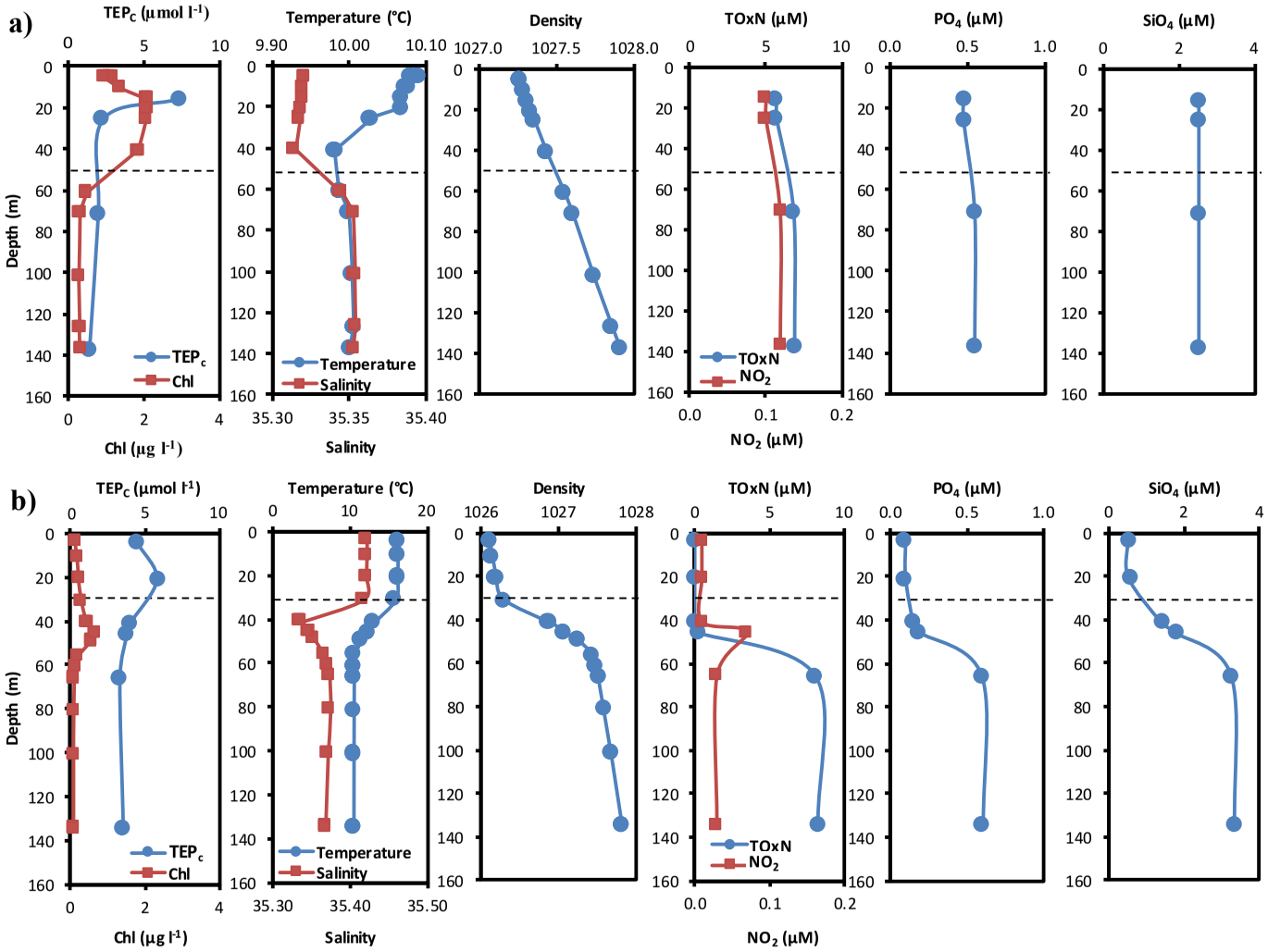

Figure 4.3 Vertical distribution of TEP_c content (µmol l^{-1}), chlorophyll *a* (µg l^{-1}), temperature (°C), salinity, density (kg m^{-3}), TOxN (µM), NO_2 (µM), PO_4 (µM) and SiO_4 (µM), in a) spring and b) summer 2015 at Station Candy Floss (CCS). TEP values are based on a single measurement at each depth. The dashed line indicates the Surface Mixed Layer Depth (SMLD).

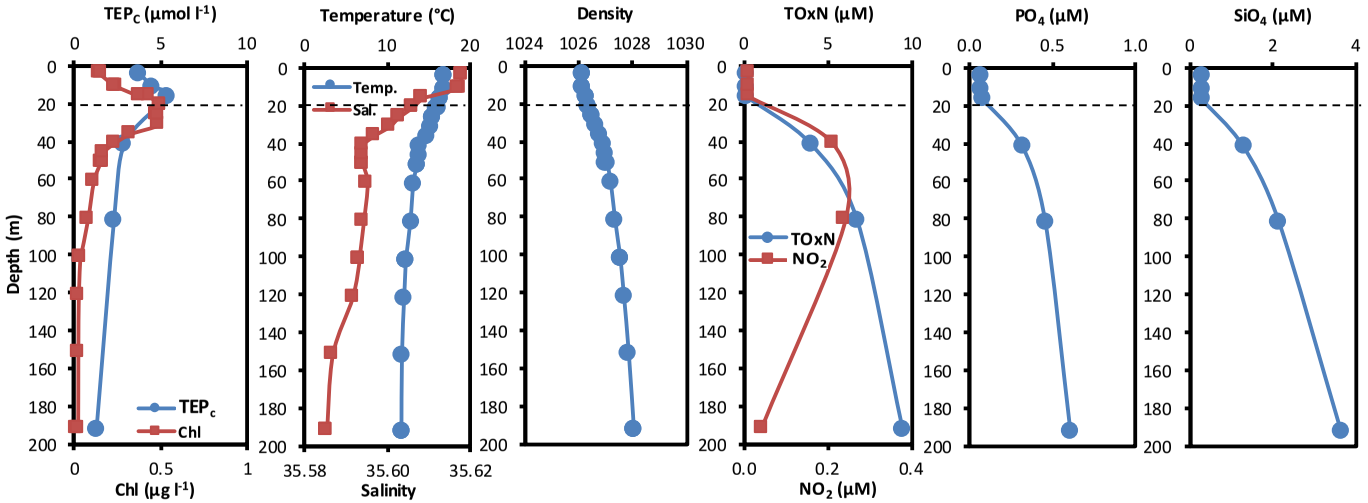

Figure 4.4 Vertical distribution of TEP_c content (µmol l^{-1}), chlorophyll *a* (µg l^{-1}), temperature (°C), salinity, density (kg m^{-3}), TOxN (µM), NO_2 (µM), PO_4 (µM) and SiO_4 (µM), in summer 2015 at Station Shelf Edge (CS2). TEP values are based on a single measurement at each depth. The dashed line indicates the Surface Mixed Layer Depth (SMLD).

The highest average chlorophyll *a* concentration (2.1 ± 0.1 µg l^{-1}) in the SML was found at Station A in spring, without a corresponding high average TEP_c concentration (2.9 ± 1.6 µmol l^{-1}) (Table 4.2). TEP_c concentration was associated to chlorophyll *a* at Station CS2 in summer, where a significant and positive linear relationship between TEP_c and chlorophyll *a* was found (Figure 4.5; $R^2 = 0.816$, n = 6, $p < 0.05$). Relationship between TEP_c and biological and physicochemical variables (temperature, salinity, density, chlorophyll *a*, TOxN, nitrite, ammonium, phosphate and silicate) at the stations A, CCS and CS2 in spring and summer 2015 are reported in appendix 4.

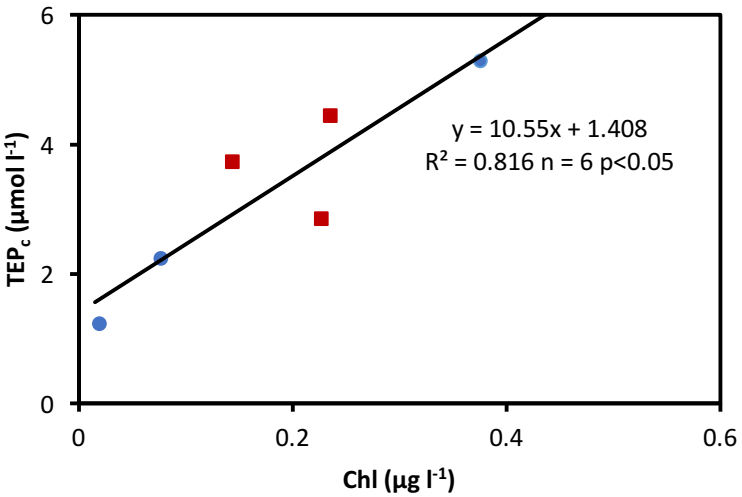

Figure 4.5 TEP_c (µmol l^{-1}) versus chlorophyll *a* (µg l^{-1}) at station CS2 in summer (whole water column, ■ red squares indicate samples in the SML; ● blue circles indicate samples in the BML).

TEP_c concentration decreased along the transect from coast to the shelf edge in summer, associated with an increase in salinity (Figure 4.6b). However, no similar pattern was found in spring (Figure 4.6a) nor for chlorophyll *a* in both seasons. The mean TEP : Chl *a* ratio was generally lower in the SML with respect to the BML except for the Station CCS in summer (Table 4.1). Very low TEP : Chl *a* ratio averages in the SML at stations A (24.9 ± 12.7 µg Xeq. µg chl^{-1}) and CCS (43.7 ± 33 µg Xeq. µg chl^{-1}) in spring were observed (Table 4.1). TEP to chlorophyll ratio showed much higher values in summer in comparison to the spring in surface waters at all stations (Table 4.1). This is consistent with the hypothesis that TEP is a by-product of primary production in spring and an overflow production during nutrient limitation in summer. The contribution of TEP_c to the pool of POC was estimated as the percentage of TEP-carbon present in POC. This was calculated by dividing the concentration of TEP_c by the sum of the concentration of POC, plus half of the concentration of TEP_c, multiplied by hundred. Half of the

concentration of TEP_c was used to take into account that standard GF/F filters used for POC determination may retain only ~ 50% of TEP (Passow and Alldredge, 1995). The percentage of TEP_c in the pool of POC was ~ 30% at the stations A and CCS in the SML in spring and at Station CS2 in the SML and in the BML. A much higher percentage ~ 50% was found at the stations A and CCS in spring in the SML and in the BML and in summer in the SML (Table 4.1).

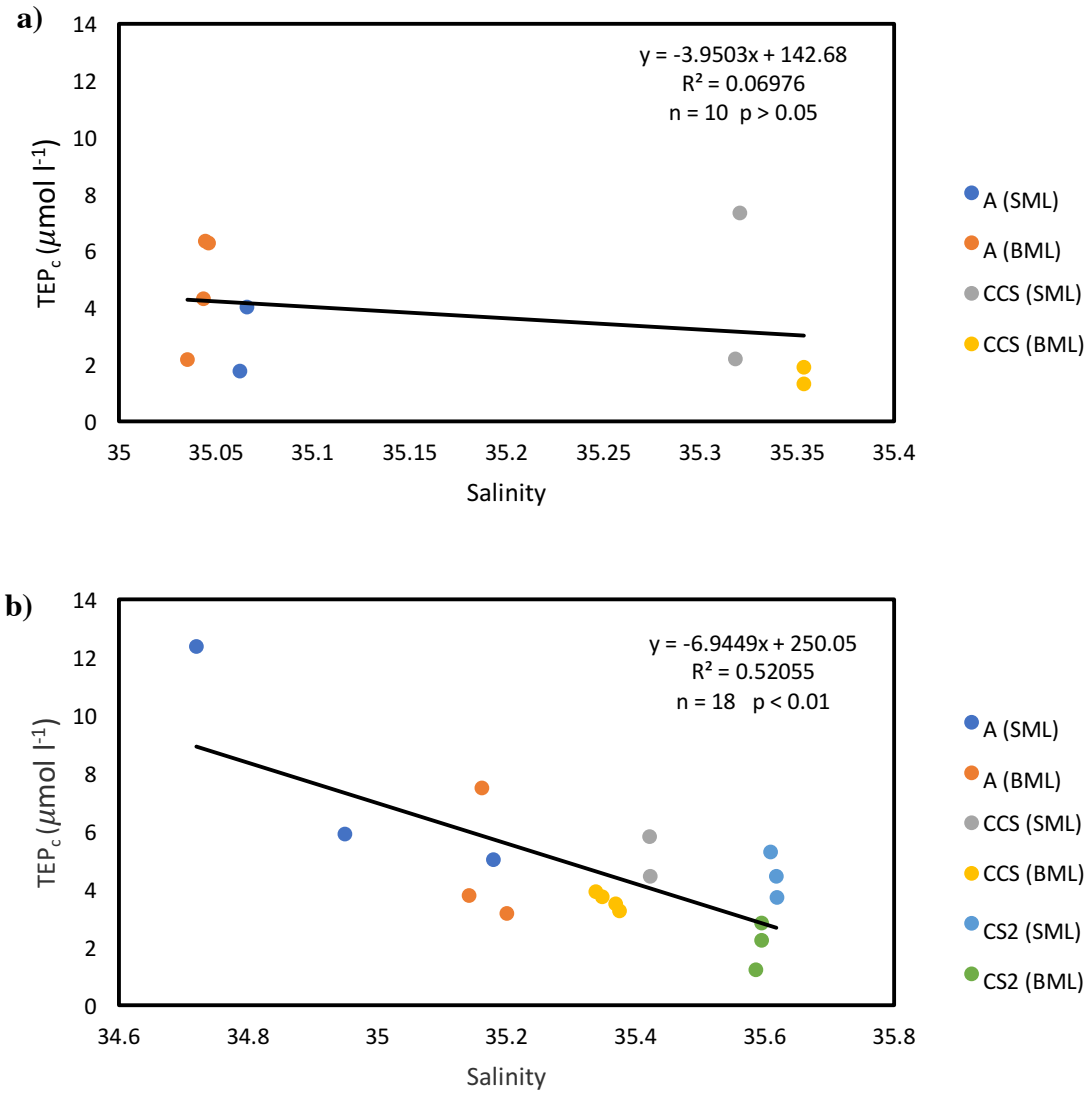

Figure 4.6 Relationship between TEP_c (µmol l^{-1}) and salinity along the transect from coast to shelf edge for the SML and the BML in a) spring and b) summer.

Table 4.1 Results of TEP (µg Xeq. l^{-1}), TEP_c (µmol l^{-1}), chlorophyll *a* (µg l^{-1}), Particulate Organic Carbon (POC) (µmol l^{-1}), Particulate Organic Nitrogen (PON) (µmol l^{-1}), % of TEP_c in the pool of POC, TEP:Chl ratio (µg Xeq. µg Chl *a* $^{-1}$), Stickiness (α), Salinity and Temperature (°C) (minimum, maximum and average) for each station during spring and summer, in the SML and in the BML.

		A	**Spring**					**SMLD**	**31**	**m**		**A**					**Summer**	**SMLD**	**27**	**m**	
		TEP	**TEP_c**	**Chl *a***	**POC**	**PON**	**TEP_c %***	**TEP:Chl**	**α**	**Salinity**	**Temp.**	**TEP**	**TEP_c**	**Chl *a***	**POC**	**PON**	**TEP_c %***	**TEP:Chl**	**α**	**Salinity**	**Temp.**
SML	**min**	33.5	1.7	1.9	11.3	1.6	14.4	15.9	0.01	35.06	9.4	95.9	5	0.4	8.4	1.3	16.6	88.1	0.05	34.7	12.7
	max	76.8	4	2.2	11.4	1.7	29.9	33.9	0.02	35.07	9.5	235.9	12.3	1.5	32.4	3.7	84.4	485.8	0.3	35.1	15.2
	average	55.1	2.9	2.1	11.3	1.6	22.1	24.9	0.01	35.06	9.5	148.1	7.7	0.8	20.4	2.5	50.5	223.4	0.1	34.9	14
	St.dev	±30.6	±1.6	±0.1	±0.1	±0.03	±10.9	±12.7	±0.01	±0.02	±0.05	±76.4	±4.01	±0.4	±16.9	±1.7	±47.8	±227.3	±0.1	±0.2	±1.3
	values	2	2	11	2	2	2	2	2	11	11	4	4	12	4	4	4	4	4	12	12
BML	**min**	41.3	2.1	0.1	4.5	0.7	38.3	81.5	0.05	35.04	8.9	60.6	3.1	0.06	4.1	0.4	25.7	167.9	0.1	35.1	9.6
	max	120.7	6.3	1.2	5.9	0.8	71.7	1102.9	0.7	35.05	9.3	142.8	7.5	0.3	10.7	1.5	73.4	2018.2	1.2	35.2	11.5
	average	91	4.7	0.4	5.3	0.7	54.4	694.9	0.4	35.04	9	91.9	4.8	0.1	7.1	0.8	53.8	992.7	0.6	35.1	10.1
	St.dev	±37.6	±1.9	±0.4	±0.7	±0.03	±16.7	±436.2	±0.2	±0.004	±0.1	±44.4	±2.3	±0.1	±3.3	±0.6	±24.9	±941.3	±0.6	±0.02	±0.8
	values	4	4	13	4	4	4	4	4	13	13	3	3	12	3	3	3	3	3	12	12

Continued

					CCS	Spr.		SMLD	53	m					CCS		Sum.	SMLD	28	m	
		TEP	**TEP_c**	**Chl *a***	**POC**	**PON**	**TEP_c %***	**TEP:Chl**	**α**	**Salinity**	**Temp.**	**TEP**	**TEP_c**	**Chl *a***	**POC**	**PON**	**TEP_c %***	**TEP:Chl**	**α**	**Salinity**	**Temp.**
	min	41.9	2.2	0.9	6.8	1.9	23	20.4	0.01	35.31	9.9	84.8	4.4	0.1	6	0.8	52.4	494.8	0.3	35.42	15.8
SML	**max**	139.7	7.3	2.1	28.1	4.1	27.8	67.1	0.04	35.32	10	110.9	5.8	0.3	8.1	1.3	53.6	662.4	0.4	35.42	16.1
	average	90.8	4.7	1.6	17.4	3	25.4	43.7	0.02	35.32	10	97.9	5.1	0.2	7.1	1.1	53	578.6	0.3	35.42	16
	St.dev	±69.1	±3.6	±0.4	±15	±1.5	±3.3	±33	±0.02	±0.002	±0.03	±18.4	±0.9	±0.06	±1.4	±0.3	±0.8	±118.5	±0.07	±0.001	±0.1
	values	2	2	14	2	2	2	2	2	14	14	2	2	7	2	2	2	2	2	7	7
	min	25	1.3	0.2	3.1	0.5	34.6	81.7	0.05	35.34	9.9	62.1	3.2	0.09	4	0.3	41.8	110.1	0.07	35.34	10.4
BML	**max**	36.3	1.9	0.4	3.1	0.6	46.4	126.1	0.08	35.35	10	74.9	3.9	0.6	7.4	0.9	57.1	728	0.4	35.37	13
	average	30.7	1.6	0.3	3.1	0.5	40.5	103.9	0.06	35.35	10	68.8	3.6	0.2	5.7	0.6	49.3	390.5	0.2	35.36	11.1
	St.dev	±7.9	±0.4	±0.08	±0.007	±0.08	±8.3	±31.3	±0.02	±0.004	±0.007	±5.5	±0.2	±0.2	±1.7	±0.2	±8.6	±300.2	±0.1	±0.01	±0.9
	values	2	2	10	2	2	2	2	2	10	10	4	4	16	4	4	4	4	4	16	16

Continued

		CS2 Spr.										CS2 Sum.									
		TEP	TEP_c	Chl *a*	POC	PON	TEP_c %*	TEP:Chl	α	Salinity	Temp.	TEP	TEP_c	Chl *a*	POC	PON	TEP_c %*	TEP:Chl	α	Salinity	Temp.
	min											71.2	3.7	0.1	12.5	1.4	23.8	268.5	0.1	35.61	15.9
SML	**max**											100.8	5.2	0.5	13.8	1.5	34.9	496.8	0.3	35.62	16.7
	average											85.59	4.4	0.3	13.1	1.4	29.4	375.2	0.2	35.61	16.5
	St.dev											±14.8	±0.7	±0.1	±0.9	±0.1	±7.8	±114.8	±0.7	±0.01	±0.3
	values											3	3	7	3	3	3	3	3	7	7
	min											23.4	1.2	0.02	3.4	0.08	30.2	239.6	0.1	35.59	11.6
BML	**max**											54.3	2.8	0.5	6.2	0.4	37.2	1221.7	0.7	35.61	15.3
	average											40.1	2.1	0.1	5	0.2	33.6	673.2	0.4	35.59	13.3
	St.dev											±15.5	±0.8	±0.1	±1.4	±0.1	±3.5	±501	±0.3	±0.01	±1.4
	values											3	3	17	3	3	3	3	3	17	17

(*) % of TEP_c was calculated by taking into account that only ~ 50% of TEP is retained on GF/F filters (Passow and Alldredge, 1995). Therefore it was assumed that only 50% of TEP is present in the pool of POC.

4.3 Box model: Estimation of the production and fate of TEP

4.3.1 Description and method

Within this study a simple box model is used to estimate TEP_c formation and accumulation rates, export flux, consumption and residence time at three stations in the Celtic Sea. The box model (Figure 4.7) considers a steady state system where the export rate of TEP_c at the SML is equal to the deposition rate at the bottom of the water column. The only loss term considered in the model is TEP_c degradation due to bacterial remineralization and implicitly deposition to the sea-bed. Estimations of TEP_c fluxes and relative sinking rates at SML and bottom are calculated with and without bacterial consumption to evaluate the potential impact of the bacterial remineralization on TEP export.

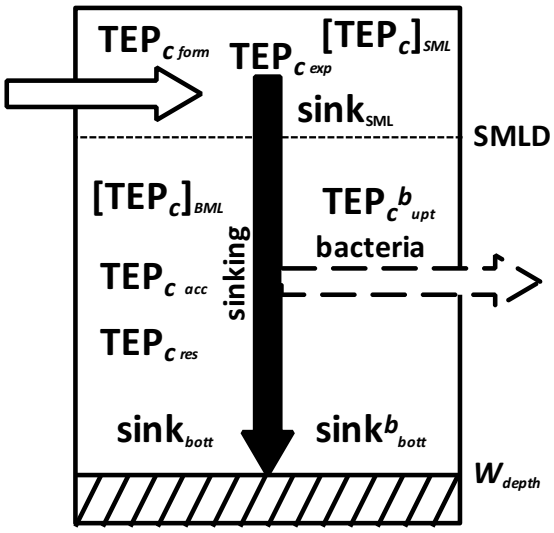

Figure 4.7 Box model describing the fate of the TEP_c and fluxes. The white arrow indicates TEP_c production, the black arrow indicates export of TEP_c from the SML, white dashed arrow indicates the fraction of TEP_c removed due to potential bacterial remineralization. $[\boldsymbol{TEP_c}]_{\boldsymbol{SML}}$ - average TEP_c concentration in the SML (µmol l^{-1}), $\boldsymbol{TEP_{c\,form}}$ - TEP_c formation rate in the SML (µmol l^{-1} d^{-1}), $\boldsymbol{TEP_{c\,exp}}$ - TEP_c export flux (mmol m^{-2} d^{-1}), $\boldsymbol{sink_{SML}}$ - TEP_c sinking rate at the SML (m d^{-1}), $[\boldsymbol{TEP_c}]_{\boldsymbol{BML}}$ - average TEP_c concentration in the BML (µmol l^{-1}), $\boldsymbol{TEP_{c\,acc}}$ - potential accumulation rate of TEP_c in the BML (µmol l^{-1} d^{-1}) without bacterial uptake, $\boldsymbol{TEP_{c\,res}}$ - TEP_c residence time (days), $\boldsymbol{TEP^{b}_{c\,upt}}$ - TEP_c loss due to bacterial uptake (mmol m^{-2} d^{-1}), $\boldsymbol{sink_{bott}}$ - potential TEP_c sinking rate without bacterial uptake (m d^{-1}), $\boldsymbol{sink^{b}_{bott}}$ - potential TEP_c sinking rate with bacterial uptake (m d^{-1}) , $\boldsymbol{SMLD}$ - Surface Mixed Layer Depth (m), $\boldsymbol{W_{depth}}$ - total depth of the water column (m).

Given the average concentration of TEP_c in the SML, in order to calculate the potential flux of TEP_c, an estimation of its formation rate is needed. A study conducted by Wurl *et al.* (2011), estimated TEP_c formation rates at three different locations (North Pacific, Offshore Hawaii and Arctic Ocean) from June 2009 to April 2010. Analysis of the Wurl *et al.* (2011) data in this present study reveals a linear relationship between TEP_c

concentrations and TEP_c formation rates in the SML. Due to the fact that the dataset reported by Wurl *et al.* (2011) covers a different areas of the globe, in this work it has been assumed that this relationship can be universally applicable. This relationship (Figure 4.8) was used in this study to estimate the TEP_c formation rate in the SML.

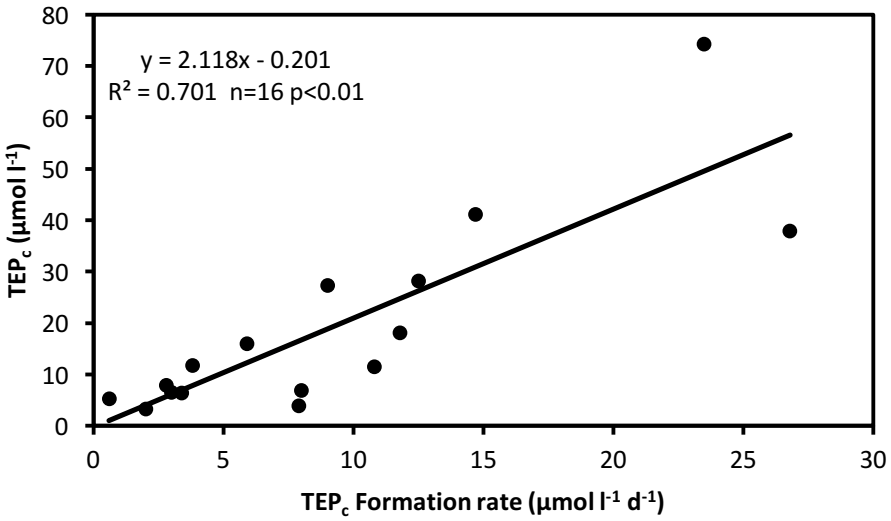

Figure 4.8 Relationship between TEP_c (µmol l^{-1}) concentration and TEP_c formation rate (µmol l^{-1} d^{-1}) extrapolated from data published in Wurl *et al.* (2011).

TEP_c formation rate (µmol l^{-1} d^{-1}) in the SML is calculated using the Eq. (4.2) derived from the linear regression in Figure 4.8.

$$\boldsymbol{TEP_{c\,form}} = \frac{[\boldsymbol{TEP_c}]_{\boldsymbol{SML}} + \boldsymbol{b}}{\boldsymbol{m}} \qquad (\mathbf{4.2})$$

where:

$\boldsymbol{m} = 2.118$ (slope of the linear regression curve)

$\boldsymbol{b} = -0.201$ (y axis intercept)

$[\boldsymbol{TEP_c}]_{\boldsymbol{SML}}$ = average TEP_c concentration in the SML (µmol l^{-1})

$\boldsymbol{TEP_{c\,form}}$ = TEP_c formation rate in the SML (µmol $l^{-1}d^{-1}$)

The TEP_c formation rate estimated in the SML is used in Eq. (4.3) to calculate the flux of TEP_c exported from the SML and its associated sinking rate Eq. (4.4)

$$\boldsymbol{TEP_{c\,exp}} = \boldsymbol{TEP_{c\,form}}\ \boldsymbol{SMLD} \qquad (\mathbf{4.3})$$

$$\boldsymbol{sink_{SML}} = \frac{\boldsymbol{TEP_{c\,exp}}}{[\boldsymbol{TEP_c}]_{\boldsymbol{SML}}} \qquad (\mathbf{4.4})$$

where:

$\boldsymbol{SMLD}$ = Surface Mixed Layer Depth (m)

$\boldsymbol{TEP_{c\,exp}}$ = TEP_c export flux (mmol $m^{-2}d^{-1}$)

$[\boldsymbol{TEP_c}]_{\boldsymbol{SML}}$ = average TEP_c concentration in the SML (µmol l^{-1})

$\boldsymbol{sink_{SML}}$ = TEP_c sinking rate at the SML (m d^{-1})

The potential TEP_c accumulation rate and TEP_c residence time in the BML are calculated in Eq. (4.6, 4.7 and 4.5) by assuming that TEP_c produced in the SML is not consumed by bacteria.

$$\mathbf{BMLD} = \boldsymbol{W_{depth}} - \boldsymbol{SMLD} \qquad (\mathbf{4.5})$$

$$\boldsymbol{TEP_{c\,acc}} = \frac{\boldsymbol{TEP_{c\,exp}}}{\boldsymbol{BML}} \qquad (\mathbf{4.6})$$

$$\boldsymbol{TEP_{c\,res}} = \frac{[\boldsymbol{TEP_c}]_{\boldsymbol{BML}}}{\boldsymbol{TEP_{c\,acc}}} \qquad (\mathbf{4.7})$$

where:

$\boldsymbol{W_{depth}}$ = total depth of the water column (m)

$\boldsymbol{BMLD}$ = depth of the water column between the SMLD and the bottom (m)

$\boldsymbol{TEP_{c\,acc}}$ = potential accumulation rate of TEP_c in the BML (µmol $l^{-1}d^{-1}$)

$[\boldsymbol{TEP_c}]_{\boldsymbol{BML}}$ = average TEP_c concentration in the BML (µmol l^{-1})

$\boldsymbol{TEP_{c\,res}}$ = TEP_c residence time (days)

The sinking rate of TEP_c at the bottom of the water column is calculated by taking into account no bacterial consumption (Eq. (4.8)).

$$\boldsymbol{sink_{bott}} = \frac{\boldsymbol{TEP_{c\,exp}}}{[\boldsymbol{TEP_c}]_{\boldsymbol{BML}}} \qquad (\mathbf{4.8})$$

where:

$\boldsymbol{sink_{bott}}$ = potential TEP_c sinking rate without bacterial uptake (m d^{-1})

The potential loss of TEP_c due to bacterial uptake and the resulting TEP_c sinking rate at the bottom of the water column are also calculated in Eq. (4.9 and 4.10). Due to the lack of information in literature on the degradation rate of TEP_c, two different approaches were used to quantify the most likely losses of TEP_c due to bacterial remineralization. The first approach assumes that the bacteria degradation rate of TEP_c is similar to that of semi-refractory POC of 0.008 d^{-1} (Fujii *et al.*, 2002). This value was chosen on the basis of a study which indicates that the degradation rate of TEP should be similar to that of POC (Passow *et al.*, 2001). The second approach uses a degradation rate determined for a generic carbohydrate of 0.53 d^{-1} (Mari *et al.*, 2017).

$$\boldsymbol{TEP^{b}_{c\,upt} = TEP_{c\,exp}\ P^{b}} \qquad (\mathbf{4.9})$$

$$\boldsymbol{sink^{b}_{bott} = \frac{TEP_{c\,exp} - TEP^{b}_{c\,upt}}{[TEP_c]_{BML}}} \qquad (\mathbf{4.10})$$

where:

$\boldsymbol{P^b}$ = TEP_c degradation rate by bacteria (d^{-1})

$\boldsymbol{TEP^{b}_{c\,upt}}$ = TEP_c losses due to bacterial uptake (mmol $m^{-2}d^{-1}$)

$\boldsymbol{sink^{b}_{bott}}$ = potential TEP_c sinking rate with bacterial uptake (m d^{-1})

4.3.2 Results

The highest and lowest TEP_c formation rate were estimated at Station A in summer (3.8 µmol l^{-1} d^{-1}) and spring (1.5 µmol l^{-1} d^{-1}), respectively (Table 4.2 and Figure 4.9). The flux of TEP_c from the SML to the bottom of the water column ranges from 44 mmol m^{-2} d^{-1} in summer at Station CS2 to 112 mmol m^{-2} d^{-1} in spring at Station CCS (Table 4.2 and Figure 4.9). The sinking velocity of TEP_c was generally lower in the SLM than near the bottom at each Station and season, except for the Station A in spring where a net decrease of ~ 6 m d^{-1} was established. Station CCS in spring showed an increase in the sinking velocity from the SML to the BML of ~ 50 m d^{-1} (Table 4.2 and Figure 4.9). The highest accumulation rate and the lowest residence time of TEP_c were found at Station CCS in

spring (1.4 µmol l^{-1} d^{-1} and 1.1 d). Conversely the lowest accumulation rate and the highest residence time of TEP_c were predicted at the Station CS2 in summer (0.2 µmol l^{-1} d^{-1} and 8.3 d) (Table 4.2 and Figure 4.9). Residence time in the BML was only ~ 5 days, which indicates that processes such as bacterial remineralization and/or sinking may have an important role in removing TEP_c from the water column in the Celtic Sea. After applying the bacterial remineralization factor of 0.08 d^{-1} no significant decrease of TEP_c flux was established. Also no significant change on the sinking velocity of TEP_c was detected in any station or season. By contrast, the bacterial remineralization factor of 0.53 d^{-1}, leads to a substantial net decrease of TEP_c flux reaching the bottom, with a consequent decrease in the apparent sinking velocity of TEP_c close to the bottom at each station and season (Table 4.2 and Figure 4.9).

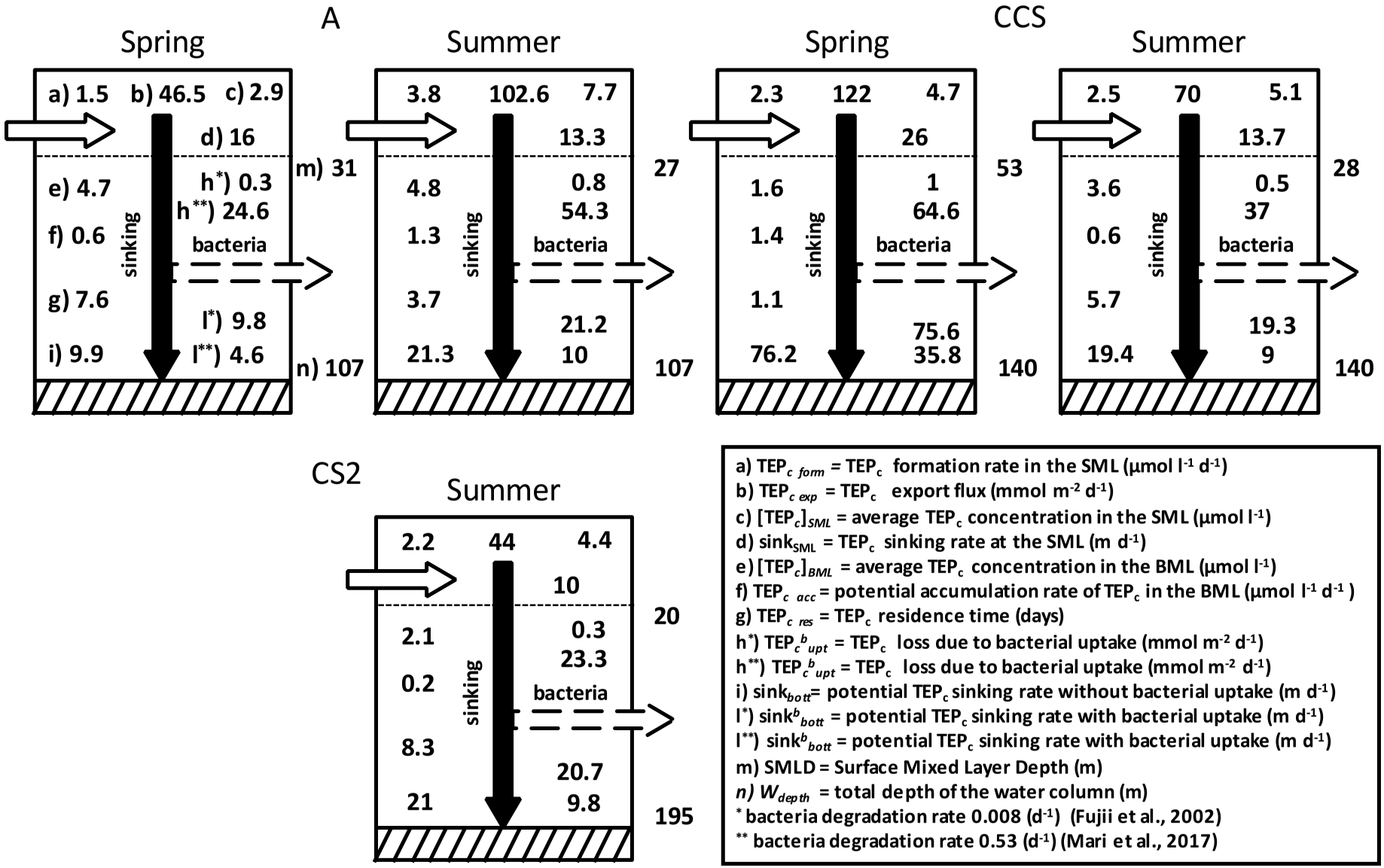

Figure 4.9 Schematic representation showing the results from the box model describing the fate of TEP$_c$ and fluxes at three stations in the Celtic Sea in spring and summer 2015.

Table 4.2 Table summarising the results from the box model describing the fate of TEP_c and fluxes at three stations in the Celtic Sea. $[\boldsymbol{TEP_c}]_{\boldsymbol{SML}}$ - average TEP_c concentration in the SML (µmol l^{-1}), $\boldsymbol{TEP_{c\,form}}$ - TEP_c formation rate in the SML (µmol l^{-1} d^{-1}), $\boldsymbol{TEP_{c\,exp}}$ - TEP_c export flux (mmol m^{-2} d^{-1}), $\boldsymbol{sink_{SML}}$ - TEP_c sinking rate at the SML (m d^{-1}), $[\boldsymbol{TEP_c}]_{\boldsymbol{BML}}$ - average TEP_c concentration in the BML (µmol l^{-1}), $\boldsymbol{TEP_{c\,acc}}$ - potential accumulation rate of TEP_c in the BML (µmol l^{-1} d^{-1}) without bacterial uptake, $\boldsymbol{TEP_{c\,res}}$ - TEP_c residence time (days), $\boldsymbol{TEP^b_{c\,upt}}$ - TEP_c loss due to bacterial uptake (mmol m^{-2} d^{-1}), $\boldsymbol{sink_{bott}}$ - potential TEP_c sinking rate without bacterial uptake (m d^{-1}), $\boldsymbol{sink^b_{bott}}$ - potential TEP_c sinking rate with bacterial uptake (m d^{-1}) .

Station	Season	$[TEP_c]_{SML}$	$TEP_{c\,form}$	$TEP_{c\,exp}$	$sink_{SML}$	$[TEP_c]_{BML}$	$TEP_{c\,acc}$	$TEP_{c\,res}$	$TEP^b_{c\,upt}$*	$TEP^b_{c\,upt}$**	$sink_{bott}$	$sink^b_{bott}$*	$sink^b_{bott}$**
A	spring	2.9	1.5	46.5	16	4.7	0.6	7.6	0.3	24.6	9.9	9.8	4.6
	summer	7.7	3.8	102.6	13.3	4.8	1.3	3.7	0.8	54.3	21.3	21.2	10
CCS	spring	4.7	2.3	122	26	1.6	1.4	1.1	1	64.6	76.2	75.6	35.8
	summer	5.1	2.5	70	13.7	3.6	0.6	5.7	0.5	37	19.4	19.3	9.1
CS2	summer	4.4	2.2	44	10	2.1	0.2	8.3	0.3	23.3	21	20.7	9.8

* TEP_c degradation rate by bacteria assumed to be similar to that of semi-refractory POC, $\boldsymbol{P^b = 0.008\ (d^{-1})}$, (Fujii *et al.*, 2002)

** TEP_c degradation rate by bacteria assumed to be similar to that of a generic carbohydrate, $\boldsymbol{P^b = 0.53\ (d^{-1})}$, (Mari *et al.*, 2017)

4.4 TEP in the aggregation model

4.4.1 Description

Several studies have reported the crucial role of TEP for the aggregation and potential sinking of particles (Dam and Drapeau, 1995; Logan *et al.*, 1995; Engel, 2000a; Fabricius *et al.*, 2003; Engel *et al.*, 2004; Engel, 2004). Due to its stickiness TEP can act as a glue (Passow, 2002) and being responsible for the formation of fast sinking aggregates (Mari *et al.*, 2017). However, because the density of TEP is lower than that of seawater the buoyancy/sinking of these aggregates has been proposed to be sensitive to the ratio of TEP to other particles (of different density) in the aggregate (Mari *et al.*, 2017). Furthermore, the formation rate of these aggregates depends on the size and concentration of particles (e.g. phytoplankton cells, POC and detritus) in seawater (Jackson, 1990; Hill, 1992; Logan *et al.*, 1995). In this study a novel approach was used to model the TEP aggregation process and its impact on POC and TEP flux. The sinking and buoyancy of aggregates containing TEP was investigated at the Stations A, CCS and CS2 in spring and summer. Theoretical aggregate composition, aggregate density, sinking rate and the flux of TEP and POC were estimated.

4.4.2 Method

The analysis was performed by assuming that the concentration of TEP_c at each depth and station was enough to form an aggregate (i.e. all material was in aggregated particles, rather than free particles). Following the experiment conducted by Mari *et al.* (2017), the aggregate was assumed to be composed of TEP_c, particulate organic matter and minerals (i.e. inorganic fraction). This inorganic fraction may be composed of carbonate from coccolithophores and foraminifera, or a siliceous compound called opal from diatoms (Mari *et al.*, 2017). For each Station and at each depth TEP_c, POM and mineral masses were used to calculate the relative contribution of each fraction to the aggregate and the density and sinking rate of the aggregate. Furthermore, TEP_c and POC concentrations were used to calculate the potential fluxes of TEP_c and POC respectively. Given the uncertainty in various parameters used in the estimation of particle density, sinking rate and fluxes, a Monte Carlo style approach was used to explore parameter space and present densities, sinking rates and fluxes with representative uncertainties. Due to the unknown distribution of each parameter, some assumptions were made and a uniform distribution was used. For each parameter 10,000 values were randomly sampled from the uniform distributions. The ensemble of parameters was used to compute density, sinking rate and

fluxes of the aggregate. Equation symbols with description and unit are given in Table 4.3. Parameter symbols, description, range and unit are given in Table 4.4.

The concentration of POM which does not contain TEP_c ($\boldsymbol{POM_{non\,TEP}}$) was computed as described in equation Eq. (4.11). Following evidence that standard GF/F filters used for POC determination may retain only ~ 50% of TEP (Passow and Alldredge, 1995), the concentration of POC was corrected by taking into account that the amount of TEP retained on a GF/F filter may vary from 50% to 100% of its original amount. To this end the concentration of TEP_c was reduced in a range from 100% to 50% of its original value. This was obtained by multiplying the concentration of TEP_c for the variable percentages of TEP_c in POC ($\boldsymbol{TEP_{c\,POC}}$; Table 4.4). This new concentration of TEP_c was subtracted from the pool of POC to quantify the fraction of POC which does not contain TEP_c. Afterwards $\boldsymbol{POM_{non\,TEP}}$ was estimated as two times the corrected POC (Riley, 1971; McCave, 1975; Klaas and Archer, 2002), to account for the non-carbon component of POM (e.g. N and P) (Eq. (4.11)).

$$\boldsymbol{POM_{non\,TEP} = \left(POC - (TEP_c \cdot TEP_{c\,POC})\right) \cdot 2} \qquad \textbf{(4.11)}$$

Little is known of TEP composition. The only thing that is well known is that TEP is an acidic polysaccharides which may contain fucose, rhamnose, arabinose and galactose (Myklestad *et al.*, 1972; Myklestad, 1995; Zhou *et al.*, 1998). Therefore, to convert the concentration of TEP_c to that of its mass the molar weight of a generic polysaccharide ($C_6H_{12}O_6$) was used, which has similar carbon percentage by mass to Gum Xanthan. The mass of $TEP_{c\,m}$ was determined by dividing the molar weight of $C_6H_{12}O_6$ by the number of moles of carbon in the polysaccharide and multiplying by the TEP_c concentration (Eq. (4.12)).

$$\boldsymbol{TEP_{c\,m} = TEP_c \left(\frac{Molar\ mass_{C_6H_{12}O_6}}{n\ moles_{C_6H_{12}O_6}}\right)} \qquad \textbf{(4.12)}$$

To determine the fraction of mineral, measurements of turbidity from a turbidity meter (WET Labs, ECO-BB) from CTD casts in m^{-1} sr^{-1} (metre per steradian -"standard unit of radiant intensity") were used. A conversion factor of 321.207 (from the manufacturer) was used to convert the turbidity unit from m^{-1} sr^{-1} to Nephelometric Turbidity Units (NTU). Subsequently, a range of calibration factors ($\boldsymbol{Turb_{cal}}$; Table 4.4) were used to

convert the turbidity in (NTU) to the Total Suspended Solids (TSS) (µg l^{-1}) (Eq. (4.13)). Afterwards, the mineral mass was estimated by subtracting $\boldsymbol{POM_{non\,TEP}}$ and TEP from the TSS (Eq. (4.14)).

$$\boldsymbol{TSS = Turb_{NTU}\, Turb_{cal} \cdot 1000} \qquad (4.13)$$

$$\boldsymbol{Mineral = TSS - POM_{non\,TEP} - TEP_{c\,m}} \qquad (4.14)$$

The relative contribution of each fraction to the aggregate (%) was calculated using the equations Eq. (4.15), Eq. (4.16) and Eq. (4.17).

$$\%_{TEP_c} = \frac{\boldsymbol{TEP_{c\,m}}}{\boldsymbol{TEP_{c\,m} + POM_{non\,TEP} + Mineral}} \times 100 \qquad (4.15)$$

$$\%_{POM} = \frac{\boldsymbol{POM}}{\boldsymbol{TEP_{c\,m} + POM_{non\,TEP} + Mineral}} \times 100 \qquad (4.16)$$

$$\%_{Mineral} = \frac{\boldsymbol{TEP_{c\,m}}}{\boldsymbol{TEP_{c\,m} + POM_{non\,TEP} + Mineral}} \times 100 \qquad (4.17)$$

The density of the aggregate containing TEP, $\boldsymbol{\rho_{aggr}}$ (kg m^{-3}), was calculated using the equation Eq. (4.18) adapted from Mari *et al.* (2017). To constrain the porosity the range reported in Table 4.4 was used. This range was chosen based on the typical values of porosity reported in the literature for various aggregate types, shown in Table 4.5.

$$\boldsymbol{\rho_{aggr} = \rho_w - p_{aggr} + (1 - p_{aggr})\left[\left(\frac{\%_{TEP_c}}{100}\right)\rho_{TEP_c} + \left(\frac{\%_{POM}}{100}\right)\rho_{POM} + \left(\frac{\%_{Mineral}}{100}\right)\rho_{Mineral}\right]} \qquad (4.18)$$

The aggregate density along with the sea water density were used in Stoke's Law to calculate the sinking velocity, $\boldsymbol{V_{aggr}}$ (m d^{-1}) of the aggregate (Eq. (4.19)). The range of seawater viscosity was calculated by using the minimum and maximum values of temperature and salinity observed at the three Stations during the sampling period. The aggregate was assumed to be spherical and three different ranges of particle size were investigated: small (⌀ 4 - 10 µm), medium (⌀ 10 - 40 µm) and large (⌀ 40 - 160 µm). The

three ranges of particle size were chosen from the Table 4.5, where the smallest and biggest size of TEP particles from three different studies and locations (Santa Barbara Channel, Monterey Bay and Diatom culture) were considered as a representative sample of an aggregate containing TEP.

$$V_{aggr} = \frac{2}{9}\, g\, \frac{\rho_{aggr} - \rho_w}{\mu}\, r^2 \qquad (4.19)$$

TEP and POC fluxes were calculated by multiplying their respective concentrations by the calculated aggregate velocity (Eq. (4.20) and Eq. (4.21)). All fluxes were converted to mmol m^{-2} d^{-1} for literature comparison purposes.

$$TEP_{c\,flux} = TEP_c\, V_{aggr} \qquad (4.20)$$

$$POC_{flux} = POC\, V_{aggr} \qquad (4.21)$$

As part of this study the ballast effect of dense particles (e.g. mineral) on aggregate composition, sinking rate and fluxes was investigated. Its more likely, it seems that there is a lot of mineral in the aggregates when using this method. This may or may not be reasonable. Therefore, to investigate this assumption a variant of the approach described above was used, where the mineral fraction was removed and the aggregate was only composed of TEP_c and POM.

Table 4.3 Equation symbols, description and units.

Symbol	Description	Unit
TEP_c	concentration of TEP_c	µmol l^{-1}
POC	concentration of POC	µmol l^{-1}
$Mineral$	concentration of mineral	µg l^{-1}
$POM_{non\,TEP}$	concentration of POM without TEP_c	µmol l^{-1}
TSS	Total Suspended Solids	µg l^{-1}
$Turb_{NTU}$	turbidity	NTU
$TEP_{c\,m}$	concentration of TEP_c	µg l^{-1}
$\%_{TEP_c}$	percentage of TEP in the aggregate	%
$\%_{POM}$	percentage of POM in the aggregate	%
$\%_{Mineral}$	percentage of mineral in the aggregate	%
ρ_{aggr}	density of the aggregate	kg m^{-3}
ρ_w	density of the seawater	kg m^{-3}
V_{aggr}	sinking velocity of the aggregate	m d^{-1}
$TEP_{c\,flux}$	flux of TEP_c	mmol m^{-2} d^{-1}
POC_{flux}	flux of POC	mmol m^{-2} d^{-1}

Table 4.4 Parameter symbols, description, range and unit.

Symbol	Description	Range	Unit	Ref.*
ρ_{TEP_c}	density of the TEP_c	700 - 840	kg m^{-3}	[4]
ρ_{POM}	density of the POM	1080 - 1700	kg m^{-3}	[1] [3] [5]
$\rho_{Mineral}$	density of mineral	2100- 2600	kg m^{-3}	[6]
p_{aggr}	porosity of the aggregate	90 – 99	%	[8]
$TEP_{c\,POC}$	TEP present in the pool of POC	50 - 100	%	[2]
$Turb_{cal}$	range of calibration factors	1 - 3	mg l^{-1}	[7]
r	aggregate radius	small 2-5 medium 5-20 large 20-80	µm	[8]
µ	seawater viscosity	1.26×10^{-3} - 1.41×10^{-3}	kg m^{-1} s^{-1}	**
g	acceleration of gravity	9.81	m s^{-2}	-

**Calculated by using min and max values of temperature and salinity observed at the three stations

* References

[1] Bruland and Silver, 1981
[2] Passow and Alldredge, 1995
[3] Turner, 2002
[4] Azetsu-Scott and Passow, 2004
[5] Ploug *et al.*, 2008
[6] Chen *et al.*, 2011
[7] Nasrabadi *et al.*, 2016
[8] see Table 4.3

Table 4.5 Porosity and particle size values from different aggregate types, from different studies at different locations.

Location	Aggregate type	Porosity (%)**	Particle size (diameter)**	Ref.*
-	Activated sludge	99.9	100 µm	[8] [11]
-	Activated sludge	91 ± 0.15	100 µm	[2] [11]
-	Zoogloea ram igera	66 ± 0. 10	100 µm	[3] [11]
-	Mold pellets	83 ± 0.03	100 µm	[1] [11]
-	Computer-generated aggregate	98.4	100 µm	[6] [11]
-	Computer-generated aggregate	97.5	100 µm	[5] [11]
-	Necessary for advective flow in sheared fluid	98.4	100 µm	[9] [11]
-	-	99.5	100 µm	[11]
-	Marine snow particles	99.3	up to 1mm	[4] [7]
Santa Barbara Channel	TEP	-	11 ± 10 µm, 161 ± 222 µm,11 ±8 µm	[12]
Monterey Bay	TEP	-	8 ± 9 µm, 13 ± 6 µm, 10 ± 4 µm, 10 ± 9 µm	[12]
Diatom culture	TEP	-	4 ± 2 µm, 4 ± 3 µm	[12]
Northern California	Suspended aggregates	-	Median 600 µm Modal 300 µm	[13]
Panama Basin	Marine snow	-	2 mm, 3.4 mm, 4.6 mm	[10]
Southern California Bight	Marine snow	99.6	2.9 ± 1.3 mm	[14]
phytoplankton-derived aggregates (lab.)	S. costatum (2 weeks)	99.2 ± 0.003	2.8 ± 0.5 mm	[15]
phytoplankton-derived aggregates (lab.)	S. costatum (5 weeks)	98.9 ± 0.009	2 ± 0.7 mm	[15]
phytoplankton-derived aggregates (lab.)	S. costatum (2 weeks)	98.4 ± 0.004	1.7 ± 0.3 mm	[15]

phytoplankton-derived aggregates (lab.)	E. huxleyi (3 weeks)	0.959 ± 0.018	1.5 ± 0.3 mm	[15]
fecal pellets (lab.)	Appendicularian fp	43.4 ± 0.1	0.63 ± 0.09 mm	[15]
fecal pellets (lab.)	Copepod fp	65	0.10 ± 0.02 mm	[15]
Culture (lab.)	S. costatum	-	2.51 ± 0.83 mm	[16]
Culture (lab.)	E. huxleyi	-	1.67 ± 0.68 mm	[16]
Culture (lab.)	Mix of S. costatum and E. huxleyi	-	2.02 ± 0.48 mm	[16]

[**] value (mean ± SD)
[*] References

[1] Yano *et al.*, 1961
[2] Mueller *et al.*, 1966
[3] Mueller *et al.*, 1967
[4] Kajihara, 1971
[5] Goodarz-Nia, 1977
[6] Tambo and Watanabe, 1979
[7] Alldredge, 1979
[8] Smith and Coackley, 1984
[9] Logan, 1986
[10] Asper, 1987
[11] Logan and Hunt, 1987
[12] Alldredge *et al.*, 1993
[13] Sternberg *et al.*, 1999
[14] Ploug *et al.*, 1999
[15] Ploug *et al.*, 2008
[16] Iversen and Ploug, 2010

4.4.3 Results

Overall the results showed that in both approaches, (aggregate with and without the mineral fraction) in the majority of the cases the aggregate was positively or neutrally buoyant with ascending velocity and upward fluxes of TEP and POC. To give an idea of the results an example with aggregate particle size ranging from 40 to 160 μm is reported in Figure 4.10 for the Station A in summer. When the aggregate was composed of TEP_c and POM, TEP_c had to reach ~ 60% of the total composition of the aggregate in order to make the aggregate neutrally buoyant (Figure 4.10a). With the addition of the mineral fraction, mineral had to reach ~ 60% of the total aggregate composition to make the aggregate negatively buoyant and get it to sink. (Figure 4.10b). However, in both approaches (with or without the mineral fraction) TEP_c had to be less than 40 % of the total aggregate composition to allow the aggregate to sink. The results for the aggregate sinking velocity from the model with the mineral and no mineral and three particle size ranges were compared with that estimated from the box model for the three stations (see section 4.3.2) and reported in Table 4.6. Although all of them showed non-comparable velocity values, on the basis of the results of sinking velocity from the box model it was assumed that the model with TEP, POM and mineral and particle size ranging from 40 to 160 μm may be the one closer to reality. To this end it was necessary to increase the mineral fraction in the aggregate by acting on the calibration factor ($\boldsymbol{Turb_{cal}}$). Due to no

data being available on the mineral for the study area, the TSS used to estimate the mineral fraction in this modeling approach was inferred to be from 1 to 3 times the turbidity values. Furthermore, the conversion factor used to convert the turbidity unit from m^{-1} sr^{-1} to Nephelometric Turbidity Units (NTU) is a rough approximation. This produced a considerable uncertainty in the fraction of the mineral in the model results. For comparison purpose with the box model the mineral fraction in the aggregate was increased by changing the range of the calibration factors ($\boldsymbol{Turb_{cal}}$) from 1 to 3 to 1 to 20 for the particle size ranging from 40 to 160 μm. The results produced and reported in Table 4.6 for all the stations gave velocity values consistent with that of the box model in each station. An example of aggregate composition, density, velocity and fluxes of TEP_c and POC for Station A in summer is reported in Figure 4.10c. Results showed that at Station A in summer the aggregate should sink at an average velocity of ~ 19 m d^{-1}, which was close to that estimated for the same station in summer with the box model. The mean TEP_c and POC fluxes in Station A in summer estimated by this method were 83.3 ± 89.6 mmol m^{-2} d^{-1} and 292.3 ± 332 mmol m^{-2} d^{-1} (Figure 4.10c). Results of the TEP in the aggregation model with and without the mineral fraction for the three Stations in spring and summer have been inconclusive, therefore are not shown here. This was caused by the huge computational uncertainties of this modeling approach in estimating aggregates containing TEP sinking rate and TEP and POC fluxes. For the above reasons these results will not be further discussed in this Chapter. However, this simple modeling exercise shows how TEP dynamics is complex to resolve and that future work needs to be done in the direction of getting turbidity measurements. This will allow to constrain the mineral fraction in the aggregate, reducing the computational error and getting more appreciable and realistic results.

Table 4.6 Comparison of aggregate velocity (m d^{-1}) results from the TEP in the aggregation model and the box model at the Stations A, CCS and CS2 in spring and summer. Three possible ranges of particle size 4 - 10, 10 - 40 and 40 - 60 µm in diameter were investigated. Aggregates were composed of Transparent Exopolymer Particle (TEP), Particular Organic Matter (POM) and mineral (min).

		Box model	**TEP in aggr. model**	**TEP in aggr. model**	**TEP in aggr. model**	**TEP in aggr. model**	**TEP in aggr. model**	**TEP in aggr. model**	**TEP in aggr. model**
Station	**Season**	**Velocity***	**TEP - POM Velocity* 4 - 10 (µm)**	**TEP – POM Velocity* 10 - 40 (µm)**	**TEP – POM Velocity* 40 - 160 (µm)**	**TEP – POM -min Velocity* 4 - 10 (µm)**	**TEP –POM - min Velocity* 10 - 40 (µm)**	**TEP – POM -min Velocity* 40 - 160 (µm)**	**TEP – POM -min Velocity* 40 - 160 (µm)****
A	spring	16	0.006	0.007	1.2	0.1	1.6	25.4	27.2±25.5
	summer	13.3	0.01	0.1	2.7	-0.03	-0.4	-6.4	18.6±21.2
CCS	spring	26	0.001	0.01	0.2	0.01	0.2	3.4	21.2±21.8
	summer	13.7	-0.02	-0.3	-4.6	-0.01	-0.2	-3.8	19.7±21
CS2	summer	10	-0.003	-0.04	-0.7	-0.1	-1.6	-25.9	13.1±23.7

(*) Mean velocity estimated in the SML

(**) Assuming a turbidity calibration factor much greater (range 1 to 20)

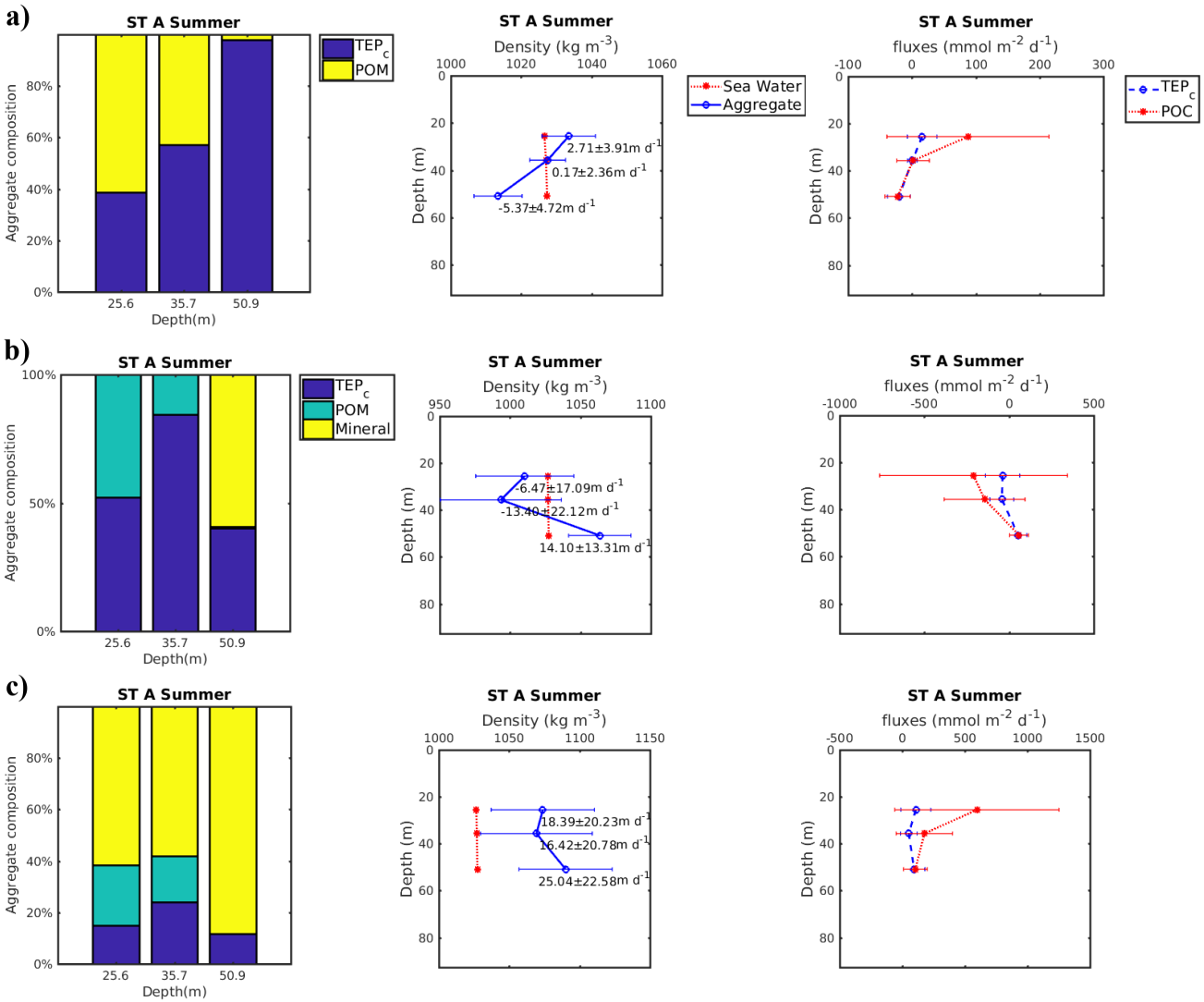

Figure 4.10 Example of aggregate composition, aggregate density, aggregate velocity and fluxes of TEP_c and POC estimated in summer 2015 at Station A (Celtic Deep), in three different scenarios: a) aggregate composed of TEP and POM and particle size range from 40 to 160 µm, b) aggregate composed of TEP, POM and mineral with turbidity calibration factor range from 1 to 3 and particle size range from 40 to 160 µm, c) aggregate composed of TEP, POM and mineral with turbidity calibration factor range from 1 to 20 and particle size range from 40 to 160 µm. The horizontal line indicates standard deviation (SD).

4.5 Modelling the effect of TEP on particle aggregation and export

4.5.1 Method

An experimental-modelling approach was used for the mechanistic investigation of the fate of carbon exported, due to TEP and the potential effect of TEP on the marine ecosystem in terms of CO_2 uptake, carbon sequestration and C : N stoichiometry of organic matter. For this purpose the latest version of ERSEM published by Butenschön *et al.* (2016) was used to derive a new formulation describing TEP dynamics. A comprehensive description of the development of TEP in ERSEM, the equations and the approach used to model TEP into ERSEM is given in Chapter 3. In this Chapter the addition of TEP to the standard ERSEM is evaluated. Station A in the Celtic Sea and Station L4 in the Western English Channel were used as test cases for model development. *In situ* observations of TEP collected at Station A were used to conduct a sensitivity study and to tune the parameters of the TEP model. The skills of the TEP model in reproducing general ecosystem properties (chlorophyll *a*, nutrients distribution) were assessed at Station L4 against both observations and a reference simulation carried out with the standard ERSEM. It should be stressed that the model developed in this study is a preliminary tool meant to explore the potential impact of TEP on carbon export and not to make TEP predictions.

4.5.2 Model assessment: test case Celtic Sea (Station A)

The TEP model (ERSEM with the TEP parameterisation) and the standard ERSEM were implemented in the Celtic Sea and run for 10-years (2006 – 2015). Both models were run by using the set-up developed for the Celtic Deep (Station A) under the UK Shelf Seas Biogeochemistry programme and described in Aldridge *et al.* (2017). The TEP model was run by using the set-up of the reference with the addition of the specific parameters for the representation of TEP dynamics in the standard ERSEM, which are reported in Table 4.7.

Table 4.7 Parameter symbols, description, value and unit used in the TEP model.

Symbol	Description	Value	Unit	Ref.*
ρ_{TEP_c}	TEP density	770	kg m^{-3}	[1]
ρ_{POC}	POC density	1390	kg m^{-3}	[2]
ρ_{Phyto}	Phytoplankton density	1120	kg m^{-3}	[3]
$porosity$	Aggregate porosity	90	%	[4]
rm	Sinking velocity of the sinking aggregate	10	m d^{-1}	[5]
$aggr$	Daily fraction of POC and Phytoplankton going to the aggregate	0.045	d^{-1}	[6]
$aggr_{TEP}$	Daily fraction of TEP_c going to the aggregate	0.18	d^{-1}	[5]
α_{aggr}	Aggregation threshold	0.01	-	[6]
ϑ	Aggregation factor	1 or 0	-	-
ß	Daily fraction of floating aggregate going to the sinking aggregate	0.1	d^{-1}	[6]
$rR5$	Daily fraction of TEPc available to bacteria	0.008	d^{-1}	[7]
$rR10$	Daily fraction of sinking aggregate available to bacteria	0.008	d^{-1}	[7]
$rR11$	Daily fraction of floating aggregate available to bacteria	0.008	d^{-1}	[7]

* References
[1] [2] average value of the range of values reported in literature Table 4.4
[3] Van Ierland and Peperzak, 1984
[4] average value of the range of values of porosity reported in Table 4.6
[5] Oguz, 2017
[6] no available value from literature, value chosen on the basis of a sensitivity analysis
[7] Fujii *et al.*, 2002

TEP density (ρ_{TEP_c}) was calculated by averaging the values from literature reported in Table 4.4. Due to a lack of information on the specific density of POC (ρ_{POC}) in literature, its value was chosen as an average of the range of values reported in Table 4.4 for POM, which includes a variety of different sinking particles ranging from fecal pellets to marine snow. The density of phytoplankton (ρ_{Phyto}) was assumed to be similar to that of diatoms (Van Ierland and Peperzak, 1984). The value of porosity ($porosity$) used for the aggregates containing TEP was extrapolated as an average value from the range of porosity values reported in Table 4.3, which covers a wide range of possible aggregate types. The values of the sinking aggregate velocity (rm) and the instantaneous rate of TEP_c going to the

aggregate per day ($aggr_{TEP}$) used in this study were obtained from Oguz, (2017b). No information on the daily aggregation rate of POC and phytoplankton was found in literature. For this reason, the parameters regulating aggregation and mass exchanges between the two aggregate pools (floating and sinking) were manually tuned to maximize the agreement between observed and simulated TEP (Figure 4.11).

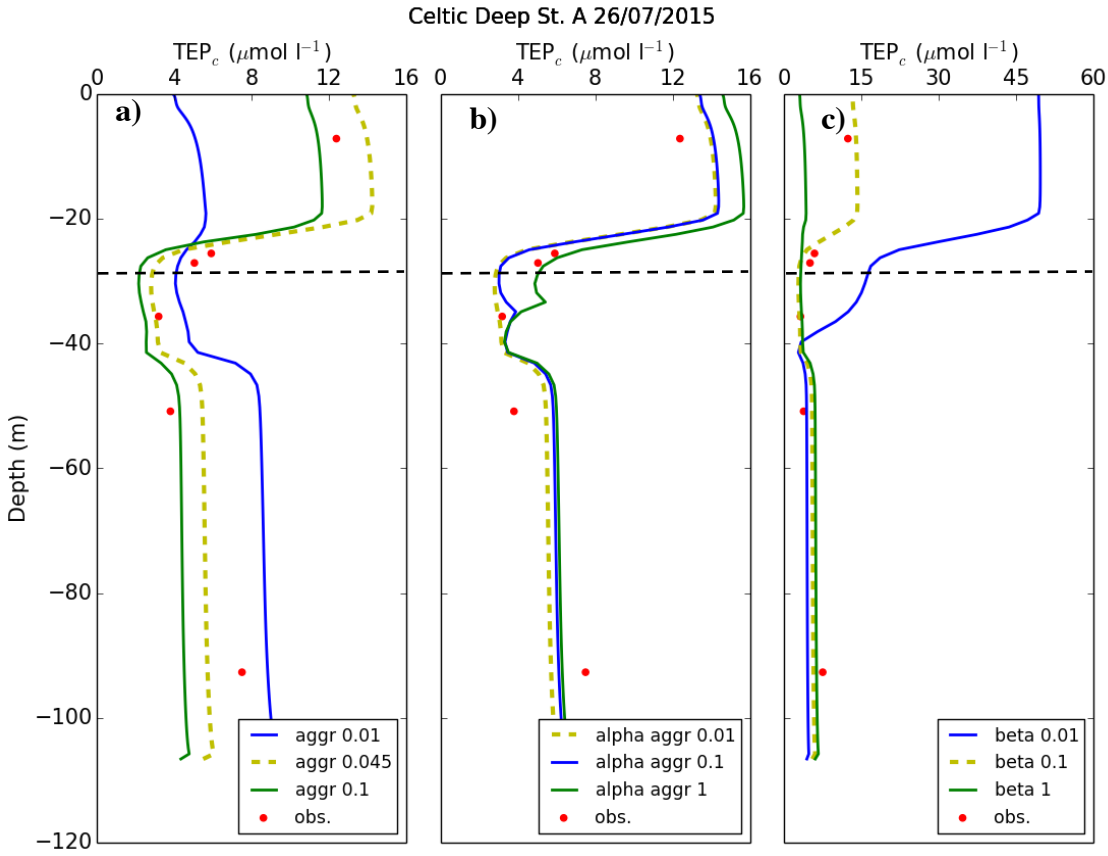

Figure 4.11 Sensitivity analysis conducted at Station A in the Celtic Sea on the 26th July 2015 for the following parameters: a) daily fraction of POC and Phytoplankton aggregate going to the aggregate per day ($aggr$), b) aggregation threshold (α_{aggr}) and c) daily fraction of floating aggregate going to the sinking aggregate per day (ß). Each line indicates a TEP$_c$ profile from the TEP model run with the different parameters setting used against the TEPc observations (obs.). The yellow dashed line in a), b) and c) represents the TEP$_c$ profile closest to the TEP observations from which $aggr$, α_{aggr} and ß values are used in the TEP model to simulate TEP dynamics and results are presented in this chapter. The black dashed line indicates observed Surface Mixed Layer Depth (SMLD).

A sensitivity analysis was carried out by using *in situ* observations of TEP collected at Station A in summer 2015 (26th July 2015) during the SSB programme. The analysis was used to test sensitivity of the simulated TEP$_c$ to the variation of each single unknown parameter (Figure 4.11a, b, c). For this purpose, three different runs of the TEP model were performed with different values (about an order of magnitude from each other) for each individual parameter and the results were plotted against the TEP$_c$ observations. The

analysis revealed that the modelled TEP_c is sensitive to the daily fraction of POC and phytoplankton going to the aggregate everyday ($\boldsymbol{aggr}$) (Figure 4.11a) and the daily fraction of the floating aggregate going to the sinking aggregate everyday (ß) (Figure 4.11c) in the SML. A lower variation of TEP_c was found for $\boldsymbol{aggr}$ in the BML (Figure 4.1a). Conversely, TEP_c is less sensitive to the variation of the aggregation threshold ($\boldsymbol{\alpha_{aggr}}$) (Figure 4.11b). Parameters allowing the model to achieve agreement between simulated and observed TEP_c (Figure 4.11a, b, c yellow dashed line) were used to simulate TEP at Station A in the Celtic Sea and at Station L4 in the Western English Channel and the results are presented in this chapter (section 4.5.3 Model assessment: test case Western English Channel (Station 4) and section 4.5.4 Results simulation at Station A).

The daily fractions of sinking ($\boldsymbol{rR10}$) and floating aggregate ($\boldsymbol{rR11}$) and the fraction of the "free" TEP_c ($\boldsymbol{rR5}$) (i.e. TEP non-associated to other particles) available to bacteria are assumed to have a similar bacterial degradation rate to that of the semi-refractory POC (Fujii *et al.*, 2002). However, this assumption may not reflect reality because the "free" TEP still in the form of DOC might be more accessible to bacteria in respect to the aggregates with a consequent higher degradation rate. The TEP model with the parameters reported in Table 4.5, along with the reference were used to investigate the effect of TEP on particle aggregation and carbon export at Station A in the Celtic Sea for the year 2015 after a 9 years spin-up period.

4.5.3 Model assessment: test case Western English Channel (Station L4)

Station L4 in the Western English Channel was used as a test case to develop the new parameterization of TEP into ERSEM and test its skills. Although there is no information on TEP for that area L4 is a well studied and characterized area, with a long time-series of oceanographic data collected by the Western Channel Observatory (WCO) and ERSEM has been used and improved at L4 for a long time by the Plymouth Marine Laboratory (PML) with good results (Polimene *et al.*, 2013; Polimene *et al.*, 2015; Sailley *et al.*, 2015; Butenschön *et al.*, 2016). For the above reasons Station L4 was the ideal place to assess the skills of the TEP model.

Station L4 (4° 13' W 50° 15' N) is located about 16 km southwest of Plymouth, in the Western English Channel (Figure 4.12). It has a maximum depth of 50 m and it is

characterized by a strong seasonality with deep vertical mixing in winter and strong stratification during summer. Two distinct algal blooms are regularly observed. The first in spring, dominated by diatoms and the second in late summer, dominated by dinoflagellates (Widdicombe *et al.*, 2010). Summer is characterized by low nutrient concentrations (Smyth *et al.*, 2009).

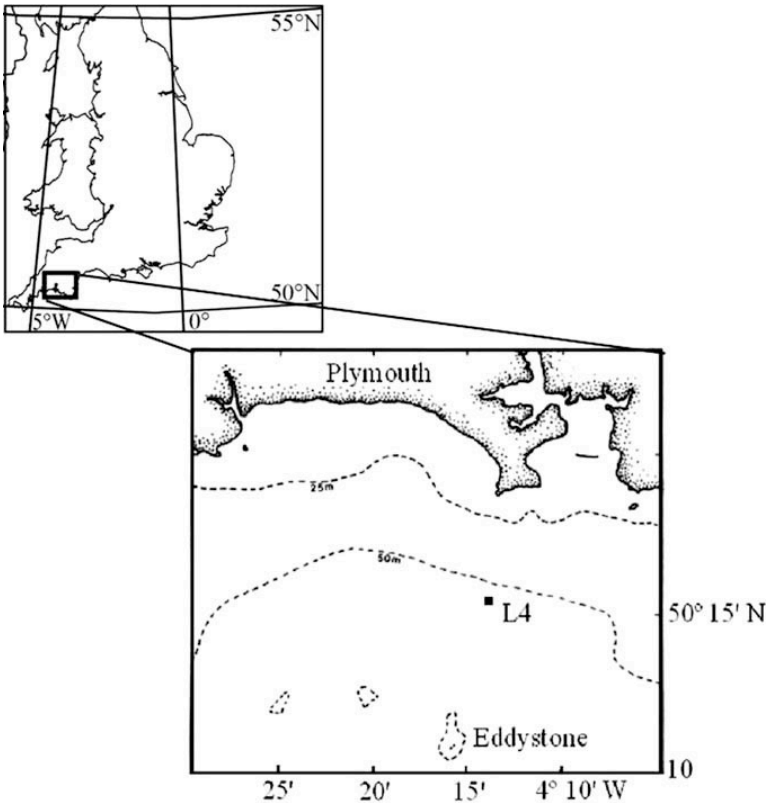

Figure 4.12 Western English Channel, Station L4 (Wyatt *et al.*, 2010).

In the Western English Channel at Station L4 both the TEP model and the reference ERSEM were run for a 13-year period (2003-2015). Here, model simulations are presented from the year 2005 onwards when all the main biogeochemical state variables had reached a stable seasonal cycle, without spurious trends due to initial conditions. Model parameters (for both the TEP model and standard ERSEM) were taken from Butenschön *et al.* (2016) while the TEP-specific parameters are those reported in Table 4.7.

The mass balances for carbon (Figure 4.13a), nitrogen (Figure 4.13b), phosphorus (Figure 4.13c) and silicium (Figure 4.13d) from the TEP model were compared with that of the reference to evaluate that the introduction of TEP into the standard ERSEM does not

cause imbalances in mass conservation. The analysis highlighted no significant differences between the reference and the TEP model for all the investigated variables (Figure 4.13). To assess the TEP model skill, TEP model results were compared to results from the reference and *in situ* observations of chlorophyll *a* (Figure 4.14a), particulate organic carbon (Figure 4.14b), nitrate (Figure 4.14c), ammonium (Figure 4.14d), phosphate (Figure 4.14e) and silicate (Figure 4.14f) collected at Station L4 in surface waters by the Western Channel Observatory (WCO) from 2005 to 2015. Statistical analysis, Pearson correlation (Figure 4.15a) and RMSE (Figure 4.15b) were performed. A complete evaluation of the model skill for the reference at L4 is presented in Butenschön *et al.* (2016). Therefore, this study has only investigated the differences in performance between the reference and TEP model. Overall the metrics results reported in Figure 4.15, indicate a mild deterioration of the model performance due to the introduction of TEP. All the variables analyzed perform less well in the TEP model in respect to that of the reference. *In situ* observations of chlorophyll *a*, particulate organic carbon and nutrients collected at Station L4 in surface waters from 2005 to 2015 reported in Figure 4.14 are monthly averages. Therefore in order to give an idea of the variability of these observations the same data for the year 2015 only are shown in Figure 4.16 with the relative error bars.

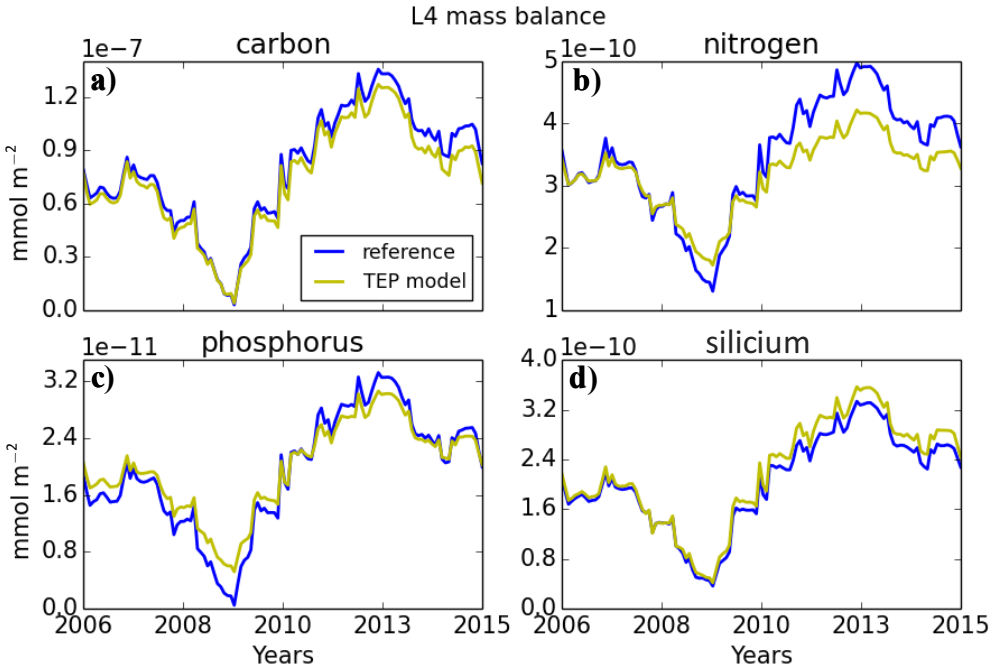

Figure 4.13 Mass balance for a) carbon, b) nitrogen, c) phosphorus and d) silicium at Station L4 in the Western English Channel from the 2006 to the 2015 for the reference (standard ERSEM) and the TEP model. Note the low scale of the y axis.

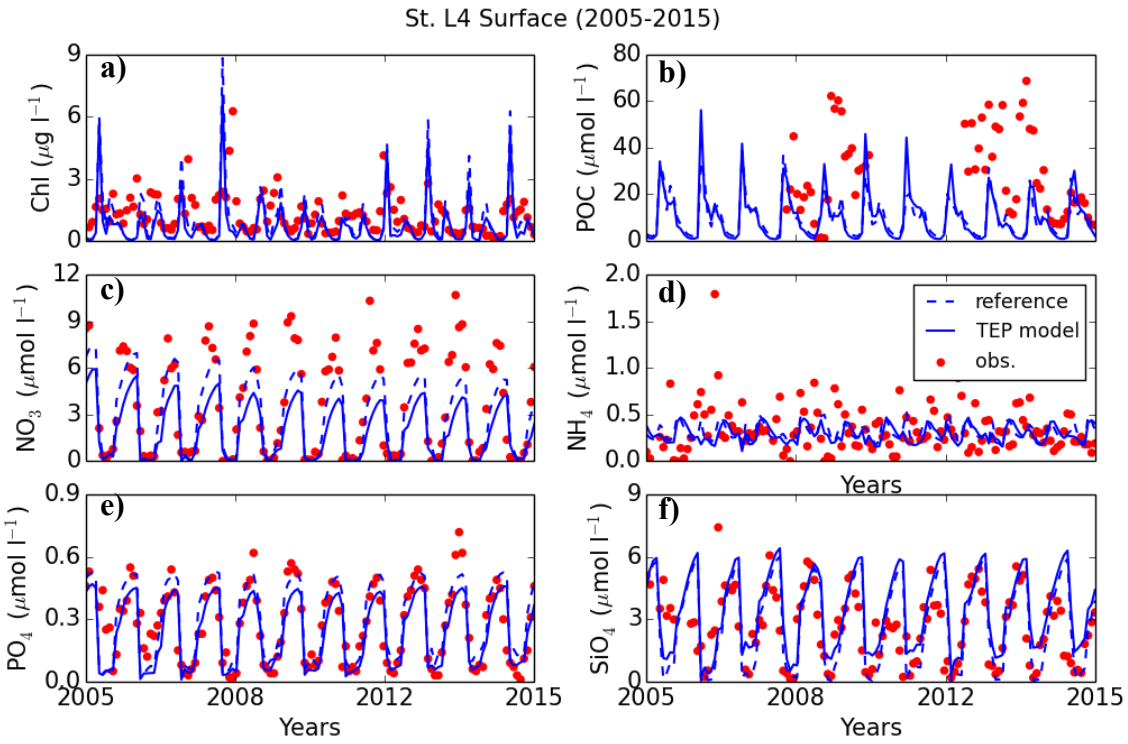

Figure 4.14 Surface: a) chlorophyll *a*, b) particulate organic carbon, c) nitrate, d) ammonium, e) phosphate and f) silicate concentrations at Station L4 from 2005 to 2015 from fieldwork observations, reference and TEP model. For comparison with POC from observations the modelled POC from the reference and TEP model includes: particulate carbon from phytoplankton (diatoms, nano-, pico- and micro-phytoplankton), zooplankton (micro-zooplankton and nano-flagellates), bacteria and particulate organic matter (small-, medium- and large size). Plus particulate carbon from sinking and floating aggregates (only for TEP model).

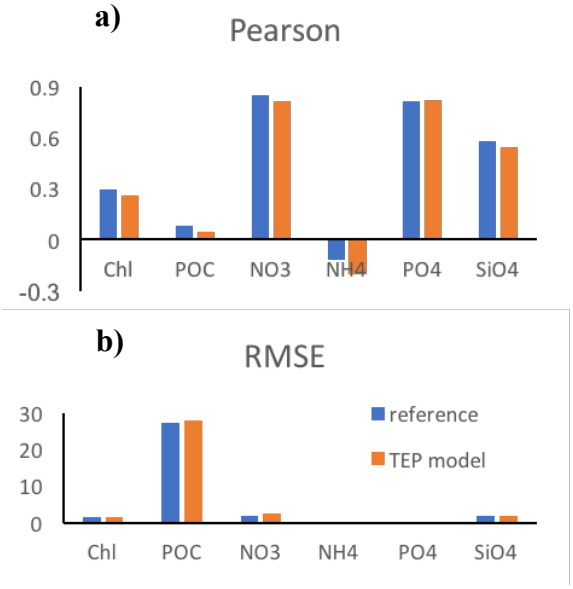

Figure 4.15 Statistical analysis: a) Pearson correlation, b) root mean square error (RMSE) of surface chlorophyll *a*, particulate organic carbon and nutrients at Station L4 from 2005 to 2015 of fieldwork observations against reference and TEP model.

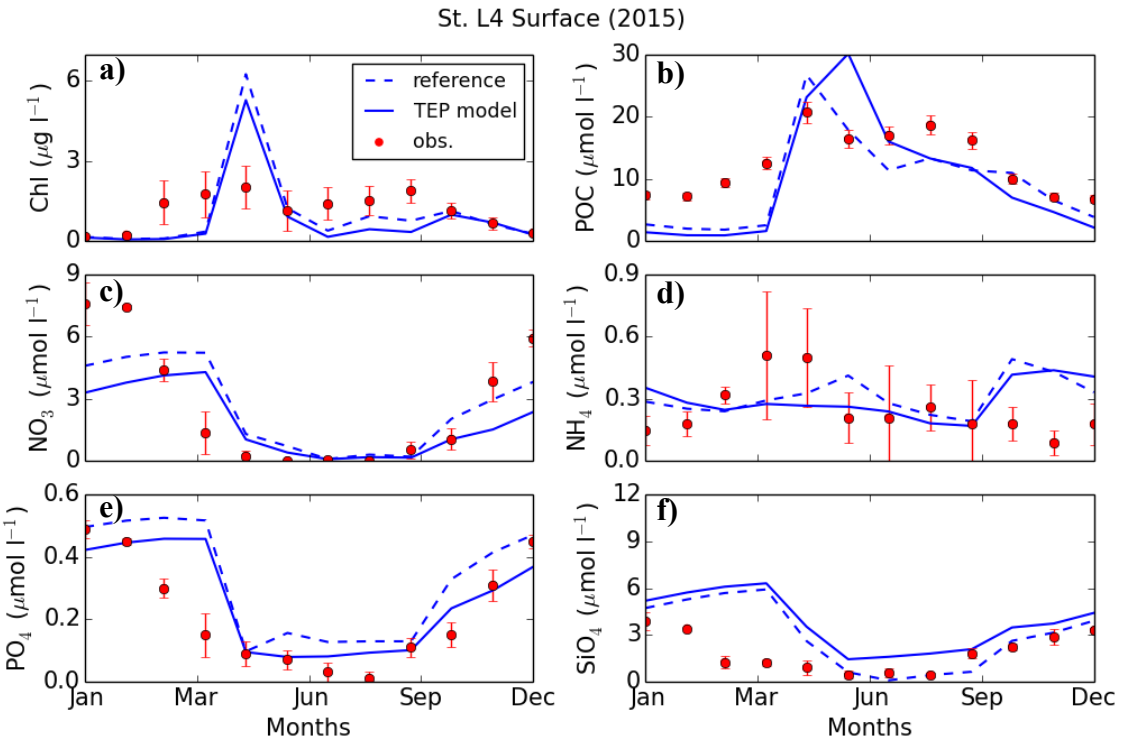

Figure 4.16 Surface: a) chlorophyll *a*, b) particulate organic carbon (POC), c) nitrate, d) ammonium, e) phosphate and f) silicate concentrations at Station L4 for the year 2015 from fieldwork observations, reference and TEP model. The red error bar indicates the SD of the monthly averaged values. See Figure 4.14 for information on modelled POC.

4.5.4 Results simulation at Station A

4.5.4.1 TEP configuration versus observation and reference

To investigate the capability of the TEP model to reproduce the observed surface chlorophyll in the years 2014 and 2015 at Station A in the Celtic Sea, the modeled chlorophyll from the TEP model was compared with the observed chlorophyll and the chlorophyll from the reference. Results highlight that the TEP model underestimates the surface observed chlorophyll, especially during peak times (Figure 4.17).

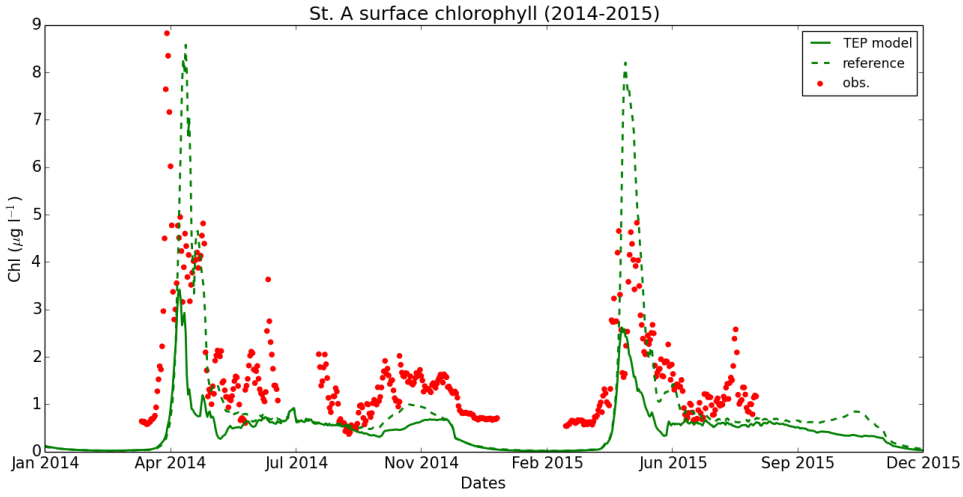

Figure 4.17 Surface chlorophyll *a* (1 m depth) observed (Celtic Deep 2 SmartBuoy) at Station A in the Celtic Sea, compared with the reference and TEP model.

The TEP_c profiles (Figure 4.18a), show the concentration of the TEP_c in sinking and floating aggregate, the concentration of the "free" TEP_c (TEP non-associated to other particles) and the sum of the sinking and floating TEP_c. The match of TEP_c (sinking plus floating) with the observations shown in Figure 4.18 a, suggests that the model is based on reasonable assumptions. However, it needs to be considered that TEP observations displayed in Figure 4.18 are not independent data as they were also used in the tuning process of the model. Consequently, further analyses using totally independent observations are required to properly assess the model capability to simulate TEP. Both models (reference and TEP model) were able to reproduce the observed chlorophyll profile (Figure 4.18b). However, none of them was able to simulate the deep chlorophyll maximum (DCM) at the correct depth. When comparing the modeled chlorophyll with the observed chlorophyll, the results indicate that the reference overestimates the concentration of chlorophyll at the DCM. Conversely the TEP model produces values closer to the observations. Modeled POC in both models (reference and TEP model) was not in good agreement with the observations (Figure 4.18c). This is due to the fact that

even the standard ERSEM is not able to reproduce POC dynamics. The Figure 4.19 gives an overview of the distribution of TEP_c and chlorophyll concentrations in the water column in July 2015. The observed DCM was at 27 metres depth (Figure 4.18b). However, the TEP model predicted the DCM at 40 metres depth (Figure 4.18b and Figure 4.19b). Looking at the simulation of TEP_c for the whole of July (Figure 4.19a) the results indicated a high concentration of TEP_c from the surface up to ~ 20 metres depth, followed by a net decrease of TEP_c to the DCM (~ 40 meters depth) and an increase of TEP_c from the DCM to the bottom.

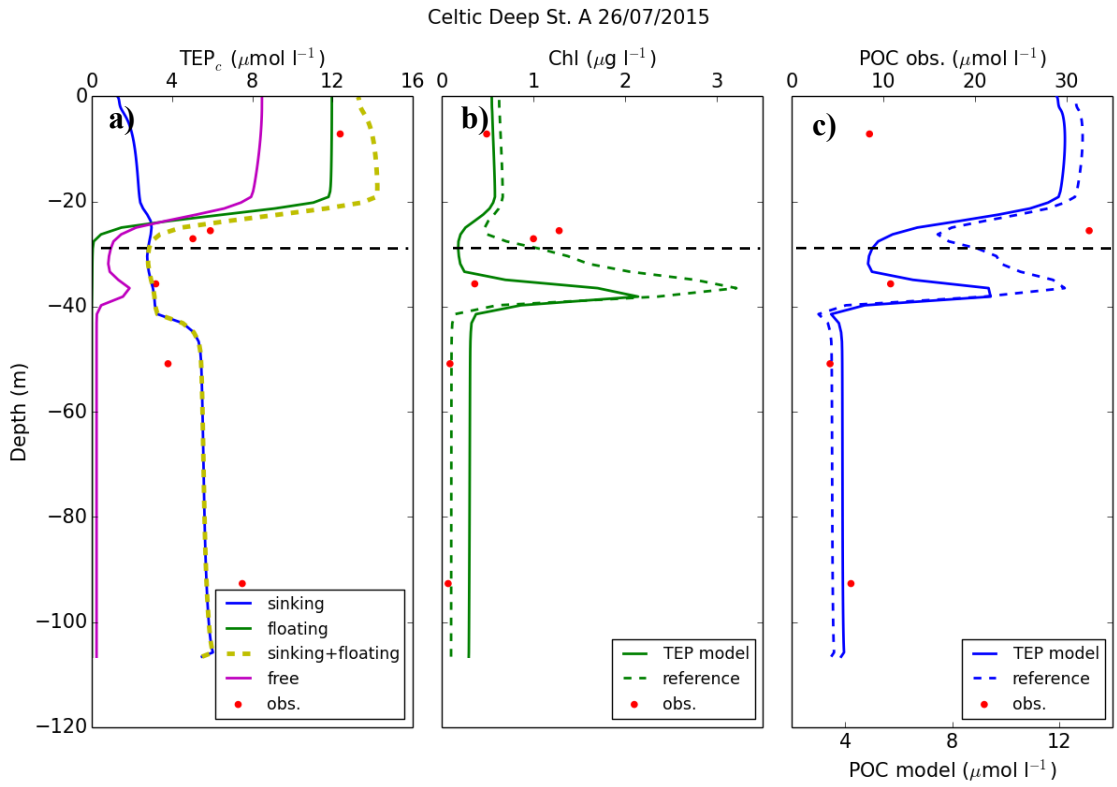

Figure 4.18 Vertical profiles of a) TEP_c, b) chlorophyll and c) POC from fieldwork observations and model (reference and TEP model) at Station A in the Celtic Sea on the 26th July 2015. TEP_c profiles show: the concentration of TEP_c in sinking and floating aggregates, the concentration of the "free" TEP_c (non-associated to other particles) and the sum of the sinking and floating TEP_c. The latter was used to compare the TEP_c model output with the observations. The black dashed line indicates observed Surface Mixed Layer Depth (SMLD). See Figure 4.14 for information on modelled POC.

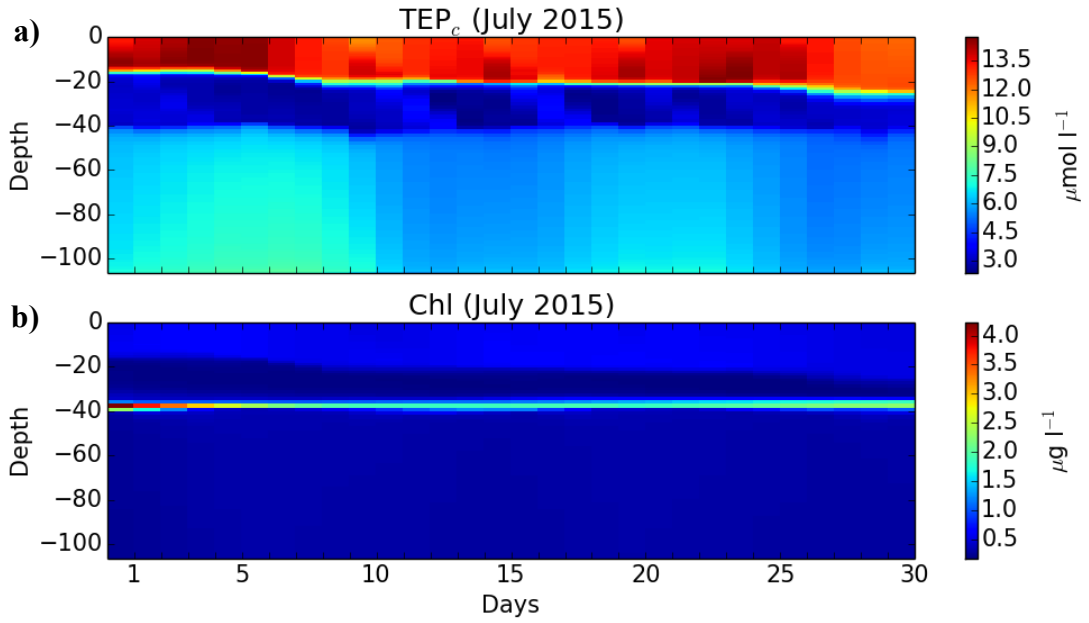

Figure 4.19 Simulation results from the TEP model of a) TEP_c and b) chlorophyll *a* in July 2105 at Station A in the Celtic Sea.

Observed TEP concentrations from the 13th April 2015 were used to test the capability of the TEP model to reproduce the observed vertical profiles of TEP_c, chlorophyll and POC (Figure 4.20). TEP_c results (Figure 4.20a) showed that on the 13th April the TEP model was not able to reproduce the TEP_c, chlorophyll and POC profiles. The TEP model simulation of TEP_c and chlorophyll concentrations in the water column for April 2015, showed very low concentrations of TEP (Figure 4.21a) and chlorophyll (Figure 4.21b) in the water column from the beginning of the month to about the 20th of April. The seasonal stratification occurred at the end of the month with the consequent development of a phytoplankton bloom (Figure 4.21b). The higher concentration of chlorophyll observed on the 13th April without a correspondence in the TEP model simulation (Figure 4.20b) indicates a temporal shift of the TEP model in predicting the seasonal stratification and the spring bloom. This shift may explain the low concentrations of TEP_c, chlorophyll and POC predicted by the TEP model (Figure 4.20).

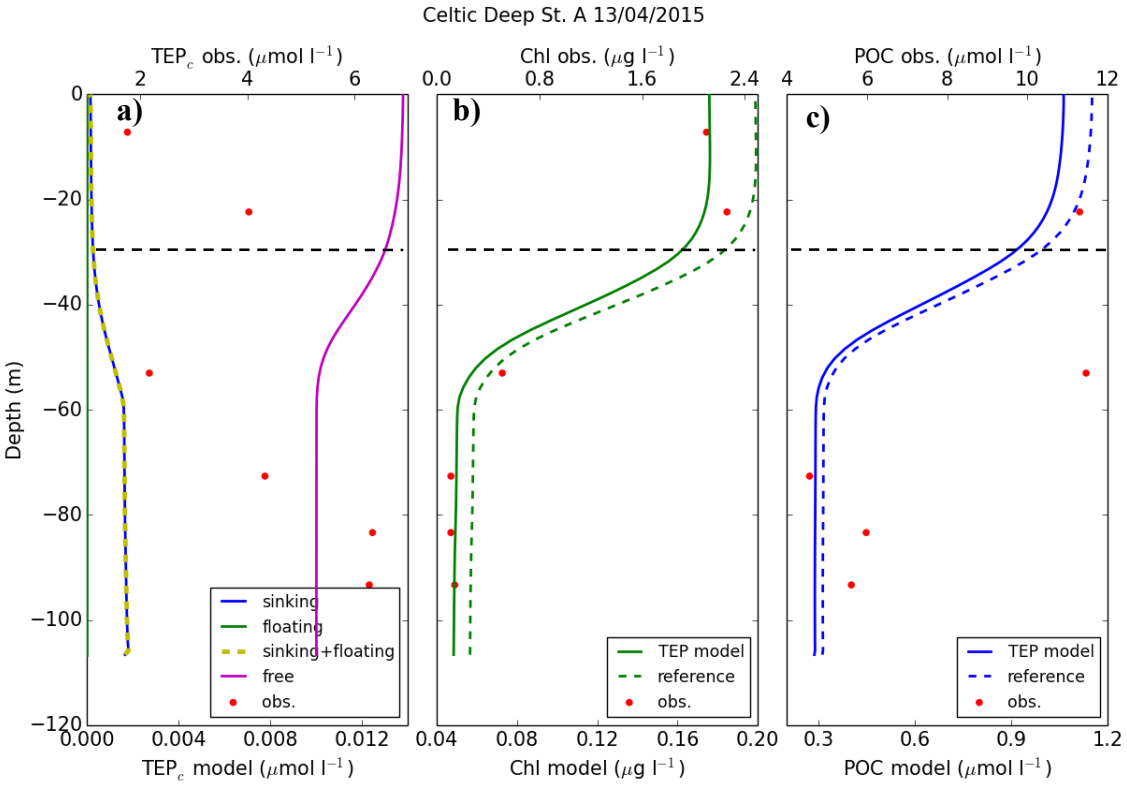

Figure 4.20 Vertical profiles of a) TEP_c, b) chlorophyll and c) POC from fieldwork observations and model (reference and TEP model) at Station A in the Celtic Sea on the 13th April 2015. TEP_c profiles show: the concentration of TEP_c in sinking and floating aggregates, the concentration of the "free" TEP_c (non-associated to other particles) and the sum of the sinking and floating TEP_c. The latter was used to compare the TEP_c model output with the observations. The black dashed line indicates the observed Surface Mixed Layer Depth (SMLD). See Figure 4.14 for information on modelled POC.

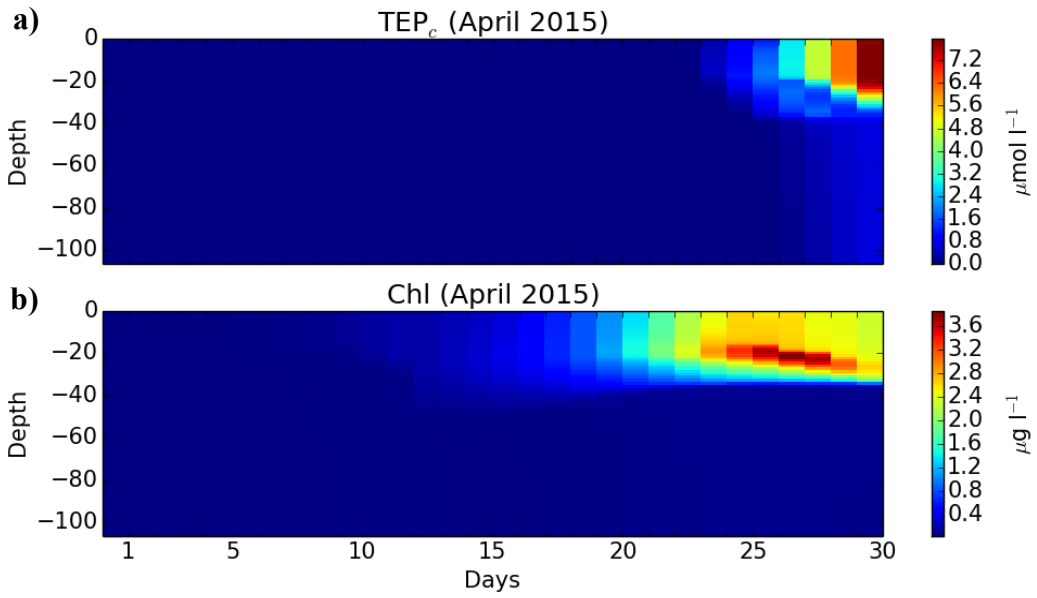

Figure 4.21 Simulation results from the TEP model of a) TEP_c and b) chlorophyll *a* in April 2105 at Station A in the Celtic Sea.

4.5.4.2 CO_2 air-sea flux, DIC and NO_3

A year-long simulation of the TEP model against the reference for the year 2015 was investigated. The modeled CO_2 flux between the atmosphere and the sea surface indicated an uptake of CO_2 from the atmosphere from April to November and a release of CO_2 from the sea to the atmosphere during the rest of the year in both model runs (Figure 4.22a). The change in direction of the flux of CO_2 during the year is highlighted by a spike in the variation in percentage between the two models in April and November (Figure 4.22b). The CO_2 fluxes were in good agreement with each other (Figure 4.22a). The only significant difference in the flux of CO_2 between the TEP model and the reference was found in November with a value of ~ 20 mmol C m^{-2} d^{-1} (Figure 4.22b). Both models estimated that on an annual scale Station A in the year 2015 was a source of CO_2 to the atmosphere and released 886 mmol m^{-2} y^{-1} of CO_2 (reference) and 927 mmol m^{-2} y^{-1} of CO_2 (TEP model).

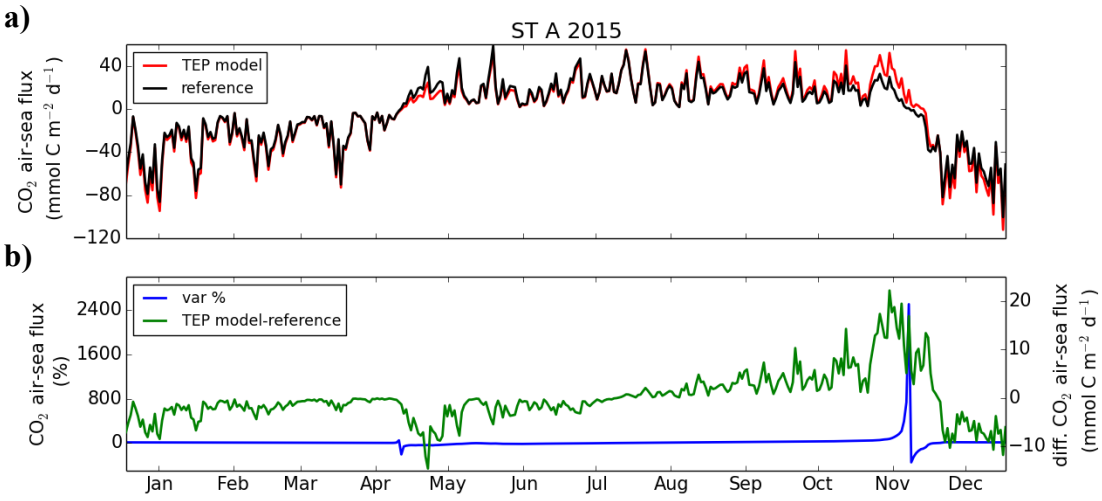

Figure 4.22 Simulation results from the TEP model and the reference of a) CO_2 air-sea flux, b) variation in percentage of the CO_2 air-sea flux (TEP model and reference) and CO_2 air-sea flux difference between the TEP model and the reference at Station A in the Celtic Sea for the year 2015.

Results of surface water DIC and NO_3 showed that from April to November for a given amount of nitrogen there was more uptake of DIC in the TEP model (Figure 4.23). The NO_3 estimated from the TEP model (~ 3 µmol l^{-1}) was about half of that of the reference (~ 7 µmol l^{-1}) during winter months (from January to April and from November to December) (Figure 4.23b). In contrast, no significate difference in the concentration of NO_3 in surface waters was found from April to November between the reference and the TEP model (Figure 4.23b). In surface waters TEP_c reached a peak value of 22 µmol l^{-1} in

May and a second lower peak of 14 µmol l^{-1} between June and July. The highest peak of TEP_c corresponded to a period of NO_3 limitation and an increase DIC uptake. Overall, the nitrogen concentration in the TEP model (Figure 4.24b) was lower compared to that of the reference (Figure 4.24a) in the whole of 2015. Aggregates containing TEP do not export only TEP, POC and phytoplankton biomass. A fraction of nitrogen, phosphorus and silicium proportional to that of TEP_c goes into the aggregates. Therefore, it also acts to remove nutrients from the surface, causing a lower NO_3 concentration in the TEP model compared to the reference run in winter (Figure 4.23b).

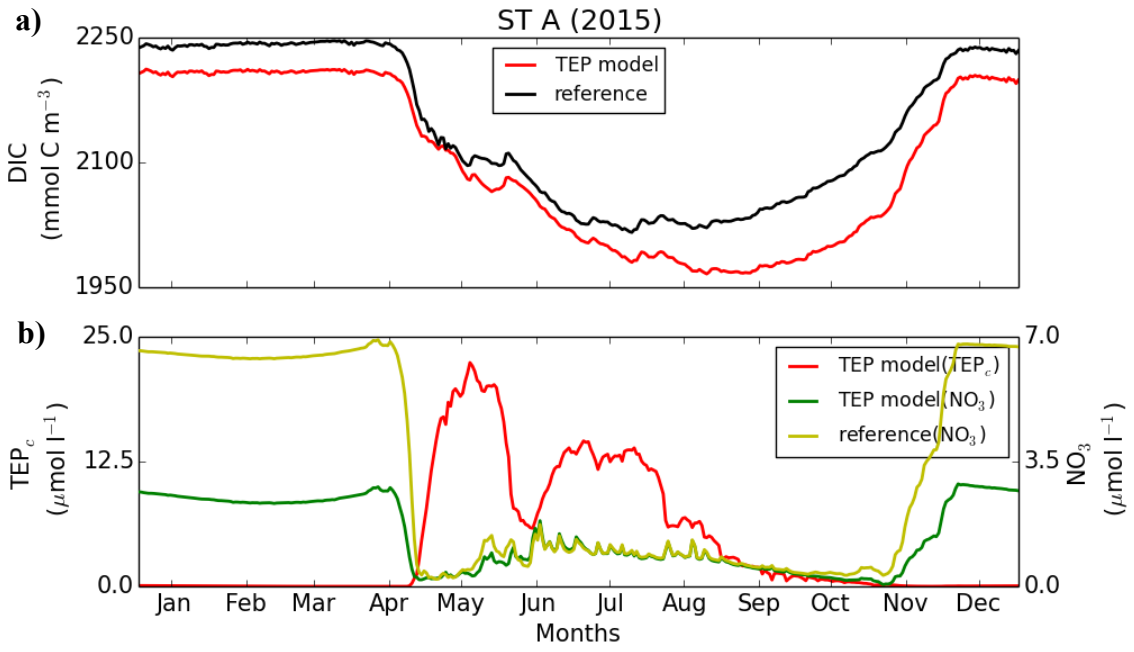

Figure 4.23 Simulation results from the TEP model and the reference of surface water a) Dissolved Inorganic Carbon (DIC), b) nitrate (NO_3) and TEP_c at Station A in the Celtic Sea for the year 2015.

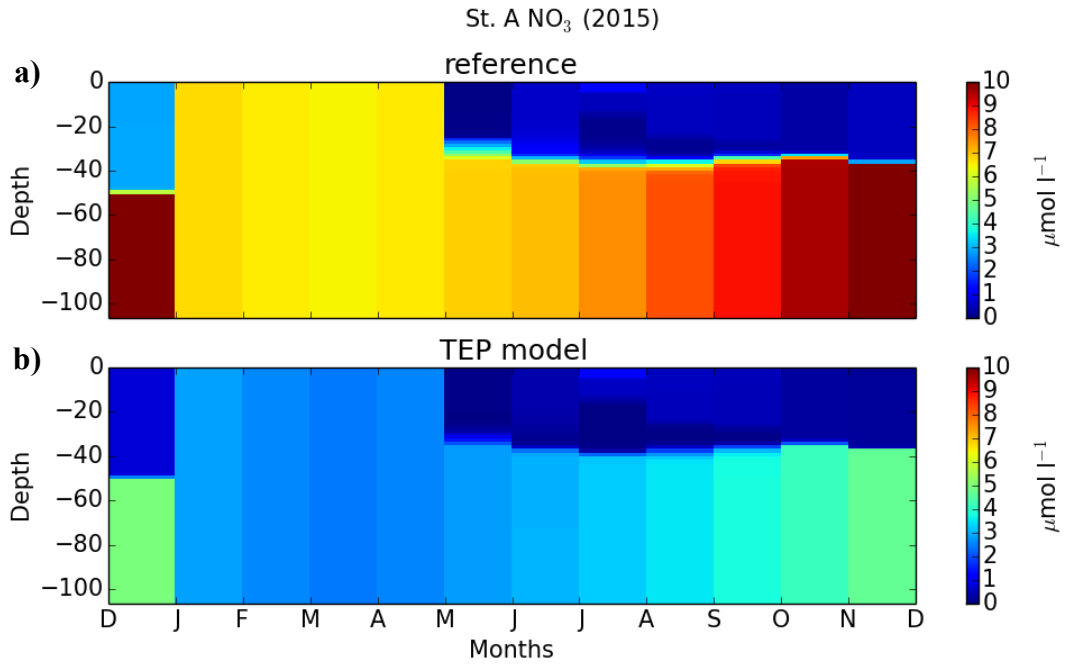

Figure 4.24 Simulation results of nitrate (NO_3) for a) the reference and b) the TEP model at the Station A in the Celtic Sea for the year 2015.

4.5.4.3 TEP and POC fluxes and sinking POC molar ratio

The simulated export of TEP_c ranged from 0.002 mmol C m^{-2} d^{-1} during winter months to 102 mmol C m^{-2} d^{-1} in June, with an annual export of 5304 mmol C m^{-2} y^{-1} (Figure 4.25a). The exported POC in the TEP model was much higher than that of the reference from April to November. POC export in the TEP model ranged from 0.06 mmol C m^{-2} d^{-1} during winter months to 137 mmol C m^{-2} d^{-1} in June, with an annual export of 8107 mmol C m^{-2} y^{-1} (Figure 4.25b). In contrast POC export in the reference ranged from 0.3 mmol C m^{-2} d^{-1} during winter months to 23.5 mmol C m^{-2} d^{-1} in June, with an annual export of 2151 mmol C m^{-2} y^{-1} (Figure 4.25 b). Exported TEP was subtracted from the total exported POC in the TEP model to determine the contribution of TEP_c to the total carbon export. This new POC no TEP export ranged from 0.06 mmol C m^{-2} d^{-1} during winter months to 35.3 mmol C m^{-2} d^{-1} in June, with an annual export of 2802 mmol C m^{-2} y^{-1} (Figure 4.25b). When comparing POC export in both models without the contribution of TEP_c, results indicate that both models give similar results. In the TEP model, TEP_c contributed ~ 65% to the export of POC on an annual basis in the year 2015.

The presence of TEP_c in aggregates increased the export of carbon-rich POC (Figure 4.25b), with a higher C : N ratio than to that of the reference (Figure 4.26). The molar ratio of the sinking POC from the TEP model (Figure 4.26) showed a high C : N ratio

from May to November in the BML, with the highest ratio of 30 in June. In contrast, the molar ratio of the sinking POC from the reference was closer to the Redfield ratio of 6.6.

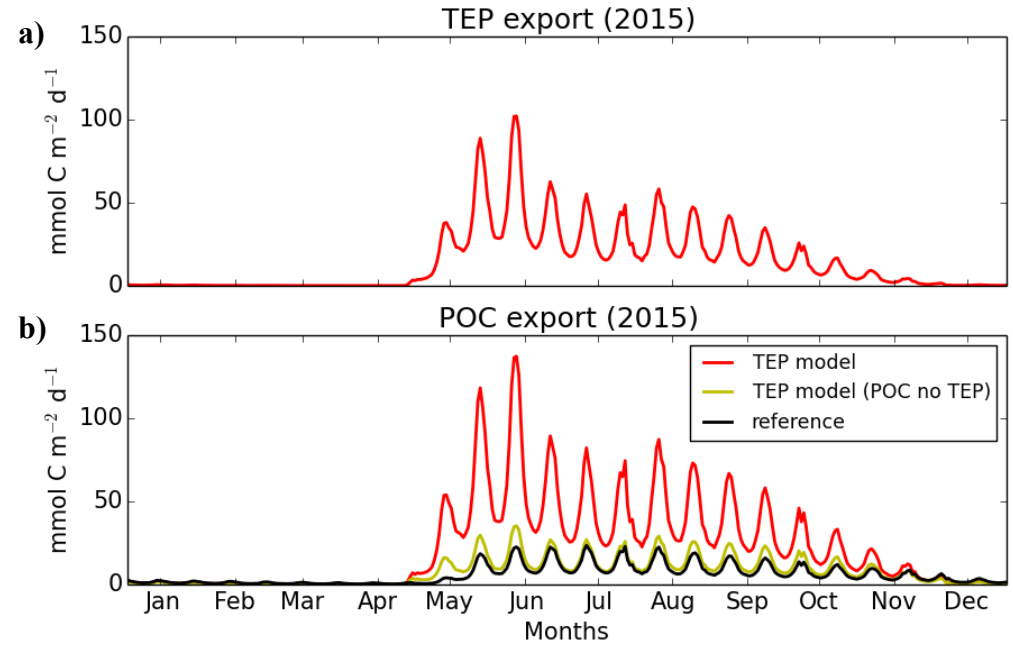

Figure 4.25 Simulation results from the TEP model and the reference of fluxes of a) TEP_c and b) Particulate organic carbon and the flux of POC minus TEP_c). The cyclic pattern of TEP and POC export in both the TEP model and the reference may be determined by the fact that the exported primary production is consumed by microorganisms (i.e. zooplankton and bacteria).

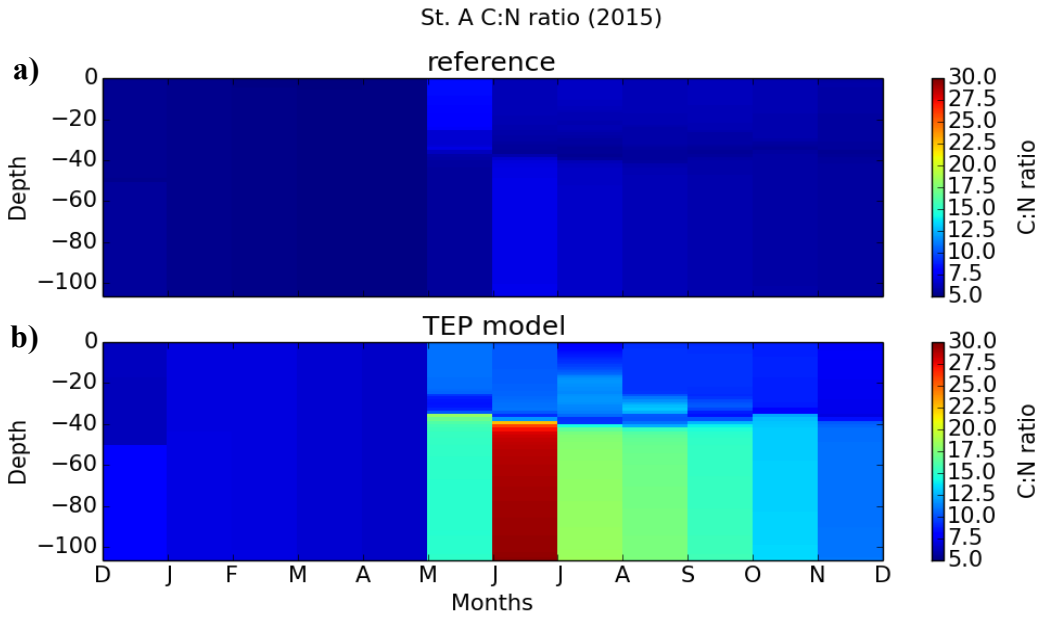

Figure 4.26 Simulation results of the molar ratio of particulate organic carbon : particulate nitrogen (C : N) for a) the reference and b) the TEP model.

4.5.4.4 Carbon budget

To investigate the fate of the organic carbon exported with the aggregates, a carbon budget of the TEP model was performed and compared with that of the reference model (Figure 4.27). The results showed that the addition of TEP in the standard ERSEM (reference) changes the dynamics of the system. In particular, TEP increases the export of organic carbon and nutrient from the water column to the sediments. This caused a decrease in the percentage of gross primary production respired by the planktonic community in the water column from 94% to 68%. This decrease is mirrored by an increase in benthic respiration in the TEP model, which is ~ 30% higher in respect to the reference. The TEP model also simulates an increase of organic carbon and biomass in the benthic system.

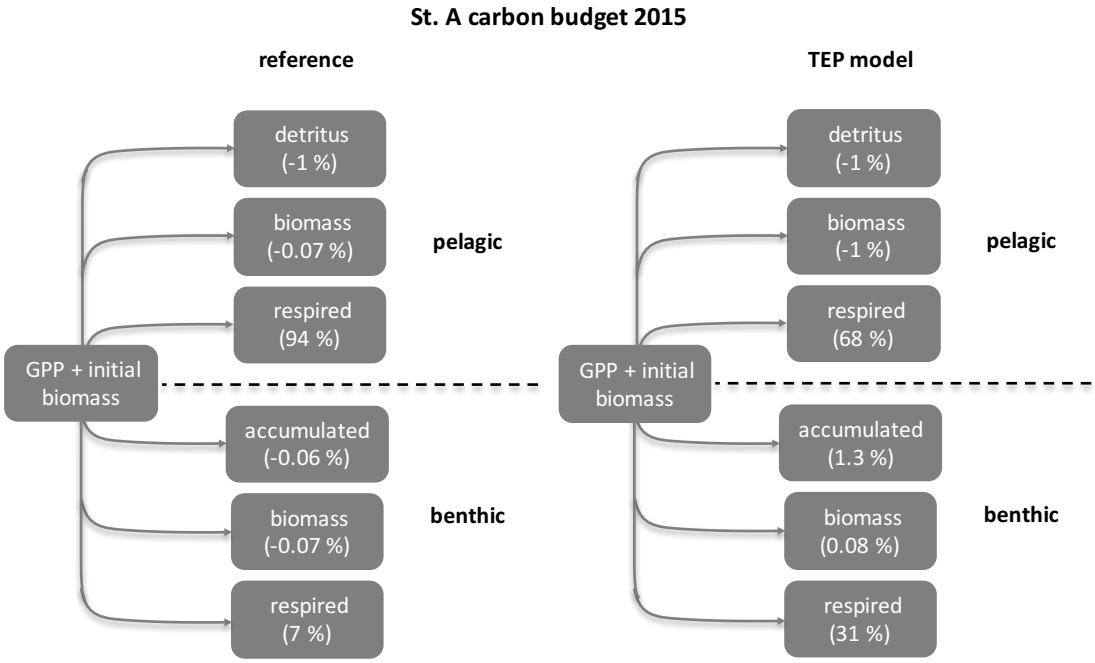

Figure 4.27 Simulation results of the carbon budget for the reference and the TEP model at Station A in the Celtic Sea for the year 2015.

4.6 Discussion

TEP observations collected in spring and summer at three Stations in the Celtic Sea along with three different modeling approaches were used to address the following objectives:

- Discover the vertical distribution of TEP in the Celtic Sea.
- Determine the major key processes controlling TEP vertical dynamics.
- Understand how TEP dynamics can affect particle aggregation and sinking.

- Estimate the fate of carbon exported by aggregates containing TEP in the Celtic Sea.
- Estimate TEP formation, accumulation rate and residence time.

Observations

TEP concentrations in the Celtic Sea have been reported for the first time and they are within the range of previous studies with a similar water column depth (Table 4.8). The concentration of TEP was generally higher in the SML than in the BML, and tended to be higher at the stations where chlorophyll *a* concentration was also higher, as also reported in other field studies (Passow and Alldredge, 1995; Hong *et al.*, 1997; Passow, 2002). During this study no correlation between TEP and chlorophyll *a* was found at stations A and CCS in summer. Similar cases were reported in literature for coastal Antarctic waters (Passow *et al.*, 1995) and in the Adriatic Sea (Schuster and Herndl, 1995). However, at the Station CS2 in summer TEP_c was associated to chlorophyll *a*, with a significant and positive linear relationship (Figure 4.5). The TEP/Chlorophyll relationship varies over time and space and can be predicted at the horizontal scale, but not at the vertical scale (Ortega-Retuerta *et al.*, 2017). This relationship is also species specific (Jennings *et al.*, 2017), indicating that the TEP/Chlorophyll relationship cannot be used as a reliable indicator of TEP production due to the interaction of multiple factors.

The relationship between TEP and autotrophic biomass was investigated through the analysis of TEP : Chlorophyll *a* ratio and the regression equation between both variables. This was compared with information available in literature (Table 4.8). Several studies reported a strong connection between the TEP : Chlorophyll *a* ratio and the stage of phytoplankton blooms. Generally during the first stage of the bloom a low TEP : Chlorophyll *a* ratio is observed, as the bloom develops nutrients are depleted, resulting in a decrease of the phytoplankton biomass and the increase of the TEP : Chlorophyll *a* ratio (Corzo *et al.*, 2000). A low TEP : Chlorophyll *a* ratio was observed in the SML at stations A and CCS in spring (Table 4.2). This may suggest an early phytoplankton growth stage, due to the fact that nutrients were not limiting (Figure 4.2; Figure 4.3) (Prieto *et al.*, 2006).

The slope of the linear regression (*b*) of TEP and chlorophyll *a* (log-transformed) relationship at the Station CCS in spring (0.48 µg Xeq. µg Chl a^{-1}) and at the Station CS2 in summer (0.47 µg Xeq. µg Chl a^{-1}) were within the range reported in the literature (0.65 ± 0.26 µg Xeq. µg Chl a^{-1}, Passow, 2002; Corzo *et al.*, 2005) and close to those reported

in Table 4.8. The slope of the linear regression (*b*) is generally larger than one (Passow, 2002) and is used for comparison across different systems (Corzo *et al.*, 2005).

Table 4.8 Comparison of TEP concentration (µg Xeq. l^{-1}), TEP : Chlorophyll *a* ratio (µg Xeq. µg Chl a $^{-1}$), TEP (log_{10} µg Xeq. l^{-1}) versus chlorophyll *a* (log_{10} µg l^{-1}) equation between different studies with comparable water column depth. For TEP concentration these values are indicated: average (minimum – maximum). The TEP to chlorophyll fits are for logarithms to base 10.

Location	Season	Depth (m)	TEP (µg Xeq. l^{-1})	TEP : Chl *a* (µg Xeq. µg Chl a^{-1})	TEP/Chl *a* (log_{10} µg Xeq. l^{-1})	ref.**
Santa Barbara Channel	winter, summer	0-75	- (29-252)	27.8	-	[1]
Otsuchi Bay	spring	-	1344 (24-2321)	206.8	-	[2]
Gulf of Cadiz	summer	0-100	118 (25-609)	281.5	-	[3]
Gerlache Strait	-	0-100	- (0-283)	32.7	log TEP = 0.67* log Chl + 1.52	[4]
Gulf of Cadiz/ Strait of Gibraltar	-	0- 200	- (25-205)	- (42-2708)	log TEP = 2.14* log Chl + 0.20	[5]
Antarctic Peninsula	-	0- 200	15.4 (0-48.9)	40.9 (0-1492)	log TEP = 0.38* log Chl + 1.08	[6]
Mediterranean Sea	-	0-200	21 (5-94)	453 (0-12,368)	log TEP = 0.17* log Chl + 1.43	[7]
Celtic Sea St. A	spring	0-100	79.1 (33-120)	471.6 (15-1102)	log TEP = -0.26* log Chl + 1.74	[8]
Celtic Sea St. A	summer	0-100	120 (60-235)	608.1 (88-2018)	Not related	[8]
Celtic Sea St. CCS	spring	0-150	60.7 (25-139)	73.9 (20-126)	log TEP = 0.48* log Chl + 1.73	[8]
Celtic Sea St. CCS	summer	0-150	78.5 (62-111)	453.2 (110-728)	Not related	[8]
Celtic Sea St. CS2	summer	0-195	62.8 (23-100)	524.2 (239-1221)	log TEP = 0.47* log Chl + 2.17	[8]

(*) Slope of the linear regression (*b*)

** References

[1] Passow and Alldredge, 1995
[2] Ramaiah *et al.*, 2001
[3] Garcia *et al.*, 2002
[4] Corzo *et al.*, 2005
[5] Prieto *et al.*, 2006
[6] Ortega-Retuerta *et al.*, 2009
[7] Ortega-Retuerta *et al.*, 2010
[8] This study

TEP is usually associated with primary producers (Passow and Alldredge, 1994; Mari and Kiørboe, 1996; Mari and Burd, 1998; Passow *et al.*, 2001) and higher concentrations are found within the euphotic zone and in the coastal areas compared to the open ocean (Passow and Alldredge, 1994; Engel and Passow, 2001). This is in agreement with the results from this study, showing a clear decreasing pattern of TEP_c concentration found along the transect from coast to the shelf edge in the SML and in the BML in summer (Figure 4.6b), which is also associated with an increase of salinity. This suggests that TEP may be produced in coastal seas or transported from land and exported to the open ocean via surface mixing. This mechanism might depend on TEP lifetime, considering that TEP can include refractory compounds (i.e. sulfated polysaccharides) difficult to be consumed quickly (Alldredge *et al.*, 1993; Passow, 2002a; Radić *et al.*, 2005b). Morever, the box model suggests that its residence time in the water column is probably quite short (~ 5 days).

The contribution of TEP_c to the pool of POC for the Southern Ocean has been estimated by the use of chlorophyll *a* to carbon ratio (Ortega-Retuerta *et al.*, 2009). The estimation established that TEP_c can contribute about 18% to the total detrital POC pool, suggesting that TEP has a longer residence time compared to that of phytoplankton or bacterial POC. In this study the contribution of TEP_c to the pool of POC was investigated by taking into account that only ~ 50% of TEP_c may be retained on GF/F filters (Passow and Alldredge, 1995). The estimation for the Celtic Sea during spring and summer showed that TEP_c can contribute up to 50% to the total pool of POC, which is much higher than that reported by Ortega-Retuerta *et al.* (2009) for the Southern Ocean. However, this number is uncertain considering that it is only a rough estimation of the potential contribution of TEP.

In this study Station A showed an irregular vertical pattern with an increase of TEP_c concentrations near the bottom of the water column for spring and summer. Typically, TEP_c concentration is highest in the SML and decreases with depth (Corzo *et al.*, 2005; Ortega-Retuerta *et al.*, 2009). This increase of TEP_c may be explained by the peculiarity of the seafloor (muddy site), which may determine an interaction between the water column and the seafloor, leading to a re-suspension of TEP_c particles stored in it. It may also be attributed to abiotic processes of aggregation of aged Dissolved Organic Matter (DOM) (Wurl *et al.*, 2011) such as detritus aggregation, disaggregation and degradation

which can provide a constant supply of DOM that can coagulate enriching the pool of TEP_c (Biddanda and Pomeroy, 1988).

Box model

TEP_c abiotic formation, residence time and turnover rate depend on environmental factors such as POC concentration, UV radiation and microbial activity (Wurl *et al.*, 2011). Aggregates containing TEP produced by diatoms have shown a residence time of more than 11 days and bacteria seem to be able to produce refractory TEP_c with an even longer residence time (Piontek *et al.*, 2009). In the Celtic Sea TEP_c residence time in the BML at the three stations ranged from 1.1 day in spring at the station CCS to 8.3 days in summer at the Station CS2, with an average value of 5.2 days which is closer to that estimated (4.6 days) in the North Pacific, Offshore Hawaii and Arctic Ocean from June 2009 to April 2010 (Wurl *et al.*, 2011) and is within the range reported in the literature (from 0.3 to 34 days) (Wurl *et al.*, 2011).

An important quantity of TEP sinking in the form of aggregates has been observed in sediment traps (Newton *et al.*, 1994; Passow *et al.*, 2001). In the Santa Barbara Channel estimated sedimentation rate of TEP_c at 500 m depth ranged from 0.54 to 5.4 mmol m^{-2} d^{-1}, which contributes ~ 30 % to the flux of POC (Engel and Passow, 2001). The flux of TEP_c in a North Norwegian Fjord at 100 m depth reached a maximum of 32 mmol m^{-2} d^{-1} (Reigstad and Wassmann, 2007). In the absence of information on the direct measurement of TEP flux in the Celtic Sea, the results from the box model were compared with Primary Production (PP) estimated in the Celtic Sea during spring and summer phytoplankton blooms. The PP at the shelf edge in the Celtic Sea at the beginning of the spring bloom is estimated to be ~ 70 mmol m^{-2} d^{-1}, reaching 120 mmol m^{-2} d^{-1} during a late bloom (Rees *et al.*, 1999). However, the PP in summer in the Celtic Sea ranges from 16 to 32 mmol m^{-2} d^{-1} (Hickman *et al.*, 2012). In the Celtic Sea the box model estimated an average TEP flux of 84±53 mmol m^{-2} d^{-1} in spring, 72 ± 29 mmol m^{-2} d^{-1} in summer. The potential maximum share of TEP in PP in the Celtic Sea in spring and summer can be inferred from the highest PP value reported in the literature for the area (120 mmol m^{-2} d^{-1}) and the average flux of TEP in spring and summer (77 mmol m^{-2} d^{-1}) from the box model. This suggests that ~ 64 % of the PP could potentially support TEP production in the Celtic Sea during spring and summer phytoplankton booms. This high percentage could be in part explained by the fact that the carbon content of TEP is on the same order of magnitude as that of phytoplankton (Engel and Passow, 2001).

The box model was assumed to be a steady state system, with a loss of TEP due to bacterial remineralization. Evidence indicates that the TEP degradation rate is similar to that of POC (Passow *et al.*, 2001) and the TEP can include refractory compounds (i.e. sulfated polysaccharides) (Alldredge and Passow, 1993; Passow *et al.*, 1994; Radić *et al.*, 2005b). Therefore, the degradation rate of TEP may be similar to that of semi-refractory POC of 0.008 d^{-1} (Fujii *et al.*, 2002). However, in literature a degradation rate much higher of 0.53 d^{-1} for a generic carbohydrate (i.e. TEP) has been reported (Harvey *et al.*, 1995; Hamanaka *et al.*, 2002; Mari *et al.*, 2017). Due to this contrasting information on the TEP degradation rate both values were used. Only the flux of TEP_c at the bottom of the water column, calculated after bacterial uptake by using higher degradation rate (0.53 d^{-1}) made a noticeable reduction in the TEP fluxes. While applying this high degradation rate the average flux of TEP in the Celtic Sea in spring and summer at the bottom of the water column was 36.2 ± 16.2 mmol m^{-2} d^{-1}. Comparing this new flux of TEP_c with the highest PP value, the result showed that TEP_c can make up for ~ 30% of the PP in the Celtic Sea in spring and summer blooms. This is half of the value estimated without considering bacterial uptake. Bacterial consumption of TEP_c increased from ~ 0.7% (by using the lower degradation rate) to ~ 40% (by using the highest degradation rate). However, TEP_c losses in the water column might be much higher due to other potential losses from zooplankton grazing and photodegradation, none of them considered in this study.

ERSEM

TEP dynamics are poorly studied in marine ecosystem models (Oguz, 2017b). In this study a novel formulation describing TEP dynamics was implemented within ERSEM in order to improve a mechanistic understanding of the role of TEP in the biogeochemical carbon cycle. The standard ERSEM model implemented at Station A in the Celtic Sea successfully reproduced the major features of the site. The introduction of TEP reduced the performance of the model in reproducing chlorophyll *a* and nutrient concentrations, which are less representative of reality. This was mainly caused by the fact that the formation of aggregates containing TEP and their export removes TEP, POC and phytoplankton biomass as well as nutrients from the surface waters, making the ecosystem more oligotrophic. The TEP model increased the carbon and nutrient export from the water column to the sediments, resulting in an increase of the benthic respiration of ~30% in respect to the reference. This change from pelagic to benthic respiration, can

be explained by the modelled decrease in DIC in surface waters, which was more in the TEP model respect to the reference. This was caused by the fact that much less of the organic carbon (~30%) was respired back to the water column. The decrease in surface DIC should lead to an increase of the CO_2 uptake from the atmosphere into the sea. However, this effect may be partially balanced by the reduced GPP, due to reduced nutrients in the TEP model. The 30% increase of the benthic respiration in the TEP model in respect to the standard version of the model, suggested that TEP as a source of extra sinking organic carbon may have a very important role in carbon sinking and per-nitrate carbon drawdown and may play a significant role in the Biological Shelf Sea Carbon Pump (BSSCP). However, in the Celtic Sea the nitrate concentration in winter is much more likely to be ~ 7 μmol l^{-1} as predicted by the reference, than ~ 3 μmol l^{-1} as predicted by the TEP model. Therefore, this suggests that without TEP the system would keep and remineralise more material in the water column, with higher nitrate concentration and less drawdown of CO_2. The peak value of TEP_c in surface waters in May, which corresponded to a period of NO_3 limitation and increased DIC uptake, may be linked to the process of carbon overconsumption (Mari *et al.*, 2017). The presence of TEP_c in aggregates increased the export of carbon-rich POC with a higher C : N ratio in respect to that of the reference. C : N ratio of TEP has a mean value above 20, which is above the Redfield ratio (Engel and Passow, 2001; Mari *et al.*, 2001).The molar ratio of the sinking POC from the TEP model showed a high C : N ratio in the BML from May to November, reaching a maximum of 30. Due to a lack of observations on TEP and POC export in the Celtic Sea it has been difficult to estimate if the values predicted by the model are realistic for the area of study. However, POC export in both models (reference and TEP model), the latter upon removal of TEP_c to POC export, gave similar results. This indicates that TEP_c may account for ~ 65% of total exported POC on an annual basis in the year 2015.

Models comparison

Strengths, weaknesses and usability of the three different modeling approaches are reported in Table 4.9. The section below compares and discusses the results from the box model and ERSEM with TEP parameterisation (Table 4.10) at Station A in the Celtic Sea in spring and summer. Each modeling approach has different limitations, this produced uncertainty in the results, that made it difficult to estimate the aggregates containing TEP sinking rate and TEP export. Furthermore, the lack of direct measurements made it difficult to quantify carbon export at Station A. Nonetheless, the two independent approaches produced results with the same order of magnitude, suggesting that TEP_c

export at Station A on the 26th July 2015 ranged from 48 to 102 mmol C m^{-2} d^{-1}. In spring, TEP_c export from ERSEM was not comparable with the results from the box model, because of the reduced performance of the model in reproducing spring variables. The results of the sinking rate of the aggregates containing TEP from the box model showed a sinking velocity range from 13 to 17 m d^{-1}, with an average of ~ 15 m d^{-1}. In contrast in ERSEM a fixed sinking rate of 10 m d^{-1} was used, which was extrapolated as an approximation of the maximum sinking flux of aggregates in the euphotic zone reported in Oguz (2017b). These results indicate that the most likely sinking rate of aggregates containing TEP in this study should be ~ 10 m d^{-1}. However, aggregates collected *in situ* with a size smaller than 500 μm had a sinking rate from 4 to 42 m d^{-1} (Kriest, 2002).

Table 4.9 Comparison of the three different modelling approaches (box model, TEP in the aggregation model and TEP model in ERSEM).

Model	Strengths	Weaknesses	Usability
Box model	- Simple to put in place - Uses TEP observations - Provides some useful information on the TEP dynamics	- Assumes that all TEP formed is exported - Assumes that potential export rate of TEP from the SML is equal to its deposition rate - Does not consider TEP buried in the sediments - Considers only an empirical loss of TEP due to bacterial remineralization - Does not consider loss of TEP due to zooplankton and production of TEP from bacteria - Does not consider processes that may happen in the surface microlayer (e.g. photodegradation and injection of air bubbles in surface waters)	- Provides an estimation of TEP export, sinking rate, bacterial uptake, accumulation rate and residence time of TEP
TEP in the aggregation model	- Gives useful information on the most likely composition of aggregates containing TEP - Helps to simulate the role of TEP for particle aggregation - Provides understanding of how aggregate composition and ratio of TEP to other particles in the aggregate can affect the fate of aggregates containing TEP (sinking vs floating)	- Assumes that all TEP is in the form of an aggregate and finally exported - Uncertainty in the estimation of the aggregates containing TEP composition - Huge uncertainty in the estimation of the mineral fraction	- Not usable at this stage. Needs an in-depth assessment of the estimation of the aggregates containing TEP composition in particular the contribution of the mineral fraction to the aggregate

TEP model in ERSEM	- Ecosystem model - Provides useful information on TEP dynamics - Used as a diagnostic model it helps to understand the sensitivity of the model to the introduction of new processes (e.g. TEP dynamics)	- 1-Dimensional model (does not consider lateral advection and input from rivers) - Does not consider production of TEP from bacteria and consumption of TEP from zooplankton - Does not consider process that may happen in surface microlayer (e.g. photodegradation and injection of air bubbles in surface waters)	- Useful to investigate and improve understanding of processes at ecosystem level (e.g. TEP dynamics, carbon export)

Table 4.10 Summary of the different approaches (box model and TEP model in ERSEM) used at the Station A in the Celtic Sea in spring and summer to discover the role played by TEP in carbon cycling

Station A (03/04/2015)	**Box model**	**ERSEM**
Aggregates containing TEP sinking rate (m d^{-1})	13*	10**
Carbon export (mmol C m^{-2} d^{-1})	-	0.2
TEP_c export (mmol C m^{-2} d^{-1})	46	0.01

Station A (26/07/2015)	**Box model**	**ERSEM**
Aggregates containing TEP sinking rate (m d^{-1})	17*	10**
Carbon export (mmol C m^{-2} d^{-1})	-	74
TEP_c export (mmol C m^{-2} d^{-1})	102	48

(*) mean sinking rate (in the SML and bottom) without bacterial uptake
(**) fixed sinking rate

4.6 Conclusion

The vertical distribution of TEP in the Celtic Sea was mapped for the first time and appears to be site specific. The observations highlight that the three stations have different characteristics. Station CCS showed an export of TEP from spring to summer in the BML. Station A showed a potential benthic interaction due to possible resuspension of TEP from the seafloor. Station CS2 showed a strong relationship between TEP and chlorophyll *a* in summer, suggesting that at this site chlorophyll *a* may be a good biological indicator of TEP concentration in summer. However, this is only a particular case since chlorophyll *a* cannot be used as a reliable indicator of TEP at the other sites investigated. The horizontal distribution of TEP showed a decrease pattern of TEP concentration along the transect from the coast to the shelf edge in both SML and BML, highlighting that TEP is mainly produced in coastal seas and eventually exported to the open ocean via surface mixing.

TEP plays a crucial role in particle aggregation process and consequent carbon export. In the Celtic TEP is potentially very important in driving the sinking of carbon and per-nitrate carbon drawdown. This process may play a significant role in the Biological Shelf

Sea Carbon Pump by increasing the export of organic carbon with higher C : N ratio and by changing the partitioning of the exported organic carbon and its fate in the marine ecosystem (i.e. increasing benthic respiration).

These results suggest that TEP dynamics is quite complex. However, in the three investigated areas of the Celtic Sea TEP appears to be controlled by the phytoplankton community in the SML. Conversely in the BML, TEP dynamics seem most likely controlled by physical forcing such as export (Station CCS) and benthic interaction (Station A).

Chapter 5 Distribution of TEP in the North Sea in summer

5.1 Introduction

Shelf seas cover only 7% of the global ocean surface area and they are accountable for 10-30% of the global marine primary production (Gattuso *et al.*, 1998), playing a key role in the global carbon cycle (Walsh, 1991; Mackenzie *et al.*, 2004). The North Sea makes an important contribution to sequestration of CO_2 from the atmosphere, through physical and biological processes, i.e. the Continental Shelf Pump (CSP) (Tsunogai *et al.*, 1999; Thomas *et al.*, 2004; Borges *et al.*, 2005). Nevertheless, the mechanisms and their seasonality are still not fully understood (Prowe *et al.*, 2009). The North Sea has a shallow permanently mixed southern region and a seasonally stratified northern region. It has been recognised as a heterotrophic system (Thomas *et al.*, 2005) with a strong sink for atmospheric CO_2 (Thomas *et al.*, 2004). The CO_2 taken up from the atmosphere by the North Sea is exported to the North Atlantic Ocean, making the North Sea a very efficient CSP (Thomas *et al.*, 2005). The North Sea in summer has been characterized by an excess of Dissolved Inorganic Carbon (DIC) uptake (~ 40 μmol kg^{-1}) without a corresponding nutrient uptake (Prowe *et al.*, 2009), which may involve a non-Redfield pathway for carbon fixation (carbon overconsumption) (Toggweiler, 1993; Thomas *et al.*, 1999; Koeve, 2005). This process could be particularly effective if carbon-rich material, such as gel-like Transparent Exopolymer Particles (TEP) are formed, as these sink out of the surface layer and could increase the CSP efficiency.

This study was conducted during the International Beam Trawl Survey (IBTS) in August 2014 and 2015 and during SmartBuoy cruises in the year 2015 carried out by the Centre for Environment, Fisheries and Aquaculture Science (Cefas) on board of the RV Cefas Endeavour in the North Sea. In this Chapter the spatial distribution of TEP in the North Sea in summer during the two years of the survey and the seasonal cycle of TEP at SmartBuoy sites will be shown and discussed. To the best of my knowledge this was the first survey of its kind and it will supplement the lack of literature on the distribution and role played by TEP in the North Sea in summer. The main objectives of this Chapter are to discover and investigate the seasonality and dynamics of TEP in the North Sea in the context of the carbon cycling. To this end TEP observations were used to study the spatial and temporal distribution of TEP in the North Sea. Furthermore, physicochemical factors controlling TEP distribution were evaluated and discussed. In the last part of the Chapter processes controlling TEP dynamics and the implications of TEP cycling for the North

Sea productivity were evaluated. This was achieved by using a combination of different approaches (i.e. observations, statistical analysis and modelling).

5.2 Materials and methods

5.2.1 Data collection

Discrete samples of seawater for TEP analysis were collected from the 76 sampling stations (Figure 5.1) at the subsurface (from 4 m depth from a continuous water supply, part of the Ferrybox) and at the bottom (using a 10 L Niskin bottle) across the North Sea. In the year 2014 five replicates of a TEP sample were collected from the Ferrybox and the Niskin bottle to evaluate the comparability of the two different sampling methods (e.g. to determine if possible TEP particle disaggregation occurred in the sample from the continuous water supply). The results indicate a variation between the two methods of ± 1.2 % in terms of TEP concentrations. Seawater samples for TEP detection were processed onboard as described in section 2.2 and later analysed in the UEA laboratory as described in section 2.6. Particulate Organic Matter (POM) samples from surface and bottom were collected (only in the year 2015) from 45 stations equally distributed over the sampling area and analyzed with a CHN analyzer to determine Particulate Organic Carbon (POC) and Particulate Organic Nitrogen (PON), as described in section 2.11. Subsurface samples for chlorophyll *a* determination were collected at 50 stations distributed at regular intervals within the sampling area and analysed by high liquid performance chromatography (HPLC), as described in section 2.12 by Cefas. Information on the surface water characteristics (temperature, salinity, fluorescence, turbidity and photosynthetic yield) were obtained by the Ferrybox system installed onboard. CTD casts were used to obtain the physico-chemical properties (temperature and salinity) of the water masses in the North Sea. Samples for phosphate (PO_4), silicate (SiO_4), nitrate and nitrite (TOxN), were collected from surface and bottom waters, equally distributed over the sampling area. Nutrient concentrations were determined using the analytical method described in Woodward and Rees, (2001). The typical precision of the analytical results was between 2-3%. The detection limits for nitrate and phosphate were 0.02 μmol l^{-1}, for nitrite 0.01 μmol l^{-1}, for ammonia 0.05 μmol l^{-1}, while silicate concentrations were well above the limit of detection. A weekly median composite map of chlorophyll *a* from MODIS (Figure 5.2) was provided by Plymouth Marine Laboratory, showing the spatial distribution of chlorophyll *a* during the last week of the survey (from 29th August to 04th September 2014). The map highlights the beginning of an algal bloom off the east coast

of England, at 55.85° N, 1° W (Figure 5.2). On 4th September 2014 water samples for analysis of TEP, chlorophyll *a* and phytoplankton community were collected at 55.8° N, 1° E from the Ferrybox. The sample for phytoplankton community determination was fixed in Lugol iodine solution and subsequently analysed under an inverted microscope, at the Cefas Laboratory in Lowestoft. The results show a concentration of *Karenia mikimotoi* in the sample of approximately 900,000 cell l^{-1} (Elisa Capuzzo, personal communication).

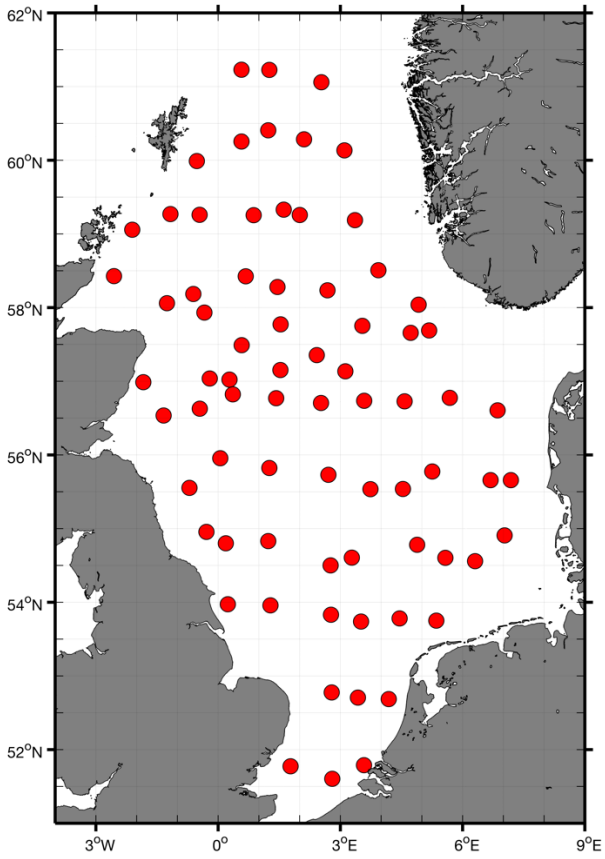

Figure 5.1 Map of the 76 sampling stations within the North Sea.

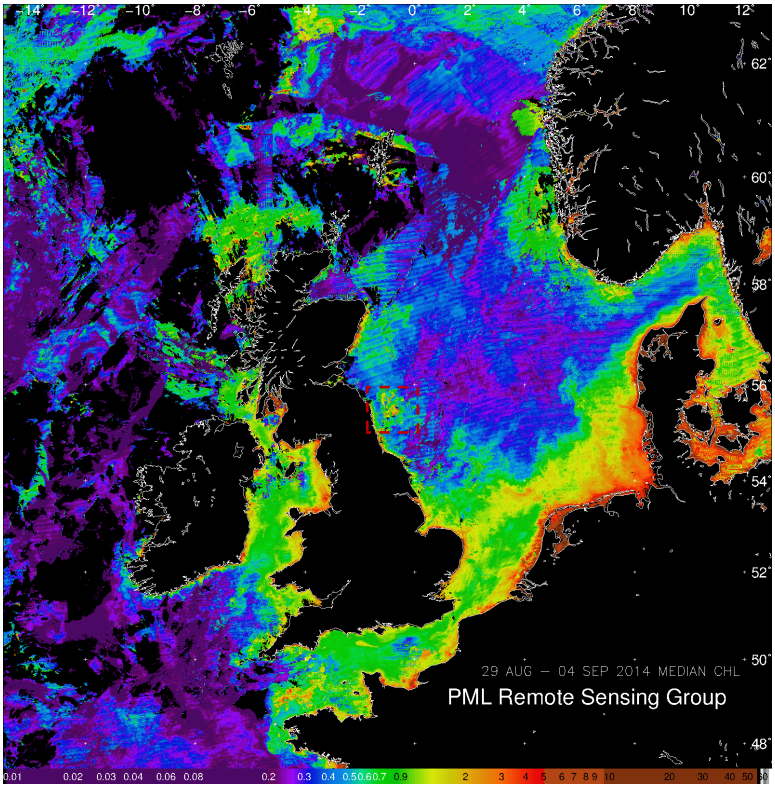

Figure 5.2 MODIS weekly median composite map of chlorophyll *a* (µg l^{-1}) from 29th August to 04th September 2014 (Plymouth Marine Laboratory – Remote Sensing Group). The frame highlights the beginning of an algal bloom.

5.2.2 Cluster analysis

The North Sea covers a vast area with different regions. Therefore, in this study a cluster analysis was used in order to split the entire North Sea dataset of each variable (TEP, chlorophyll *a*, temperature, salinity, nutrients, POC and PON) into different regions with similar characteristic. Sea surface temperature (SST), surface salinity and density differences between the bottom and the surface of the water column were used to perform the cluster analysis. Before the cluster analysis sea surface temperature (SST), surface salinity and density differences were standardized to zero mean and unit variance, in order to get the same numerical scale for these three variables. Afterwards these variables were used in the clustering algorithm to divide the data into classes. These variables were chosen for two reasons. Firstly, surface temperature and salinity provided information on the spatial variation of the surface water masses. Secondly, the differences between bottom and surface densities of the water provided information on the vertical stratification of the water column. The clustering algorithm was described in Oliver *et al.* (2004). This method groups data according to Ward's linkage (Ward, 1963). This method was able to pick up distinct features of the North Sea area within the dataset. The cluster

analysis was applied to the two different years of the survey (2014 and 2015) and was performed by using the computer program Matlab. The resulting clusters are reported in Figure 5.3a for the year 2014 and in Figure 5.3b for the year 2015. A major difficulty in this cluster analysis was to determine how many clusters (or regions) should be used to describe the main features of the North Sea. For this purpose analysis from two to five different clusters was performed (not shown). The results indicated that using five clusters was the best way to pick up the main features of the North Sea (Figure 5.3). The following five regions were identified within the North Sea: Southern Coastal (SC), Southern Mixed (SM), Transitional (T), Northern Stratified (NS) and Northern Coastal (NC).

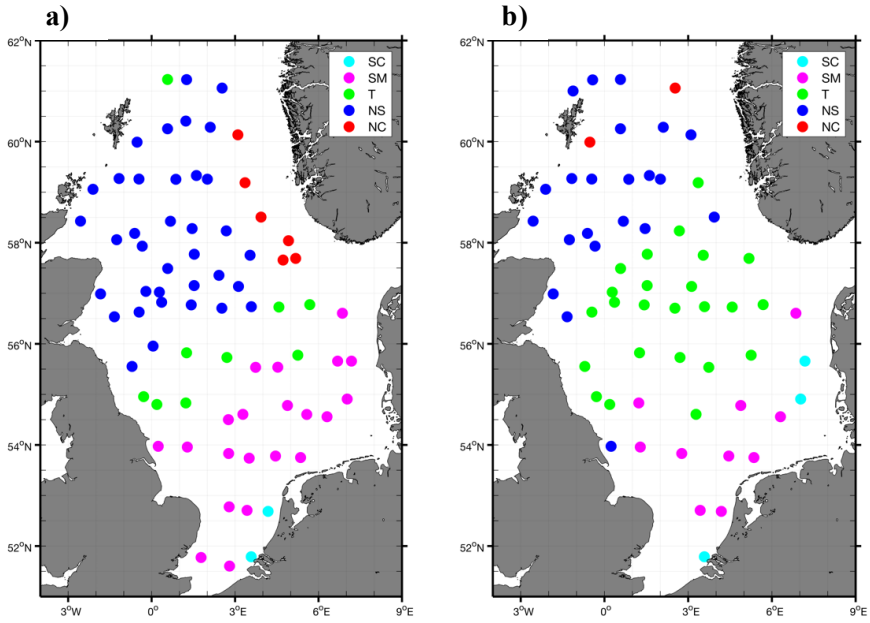

Figure 5.3 Cluster analysis describing the five different regions of the North Sea: Southern Coastal (SC), Southern Mixed (SM), Transitional (T), Northern Stratified (NS) and Northern Coastal (NC) in the year a) 2014 and b) 2015.

To evaluate the reproducibility of the cluster analysis between the two years of the survey, the variation of temperature and salinity in the surface and the bottom of the water column in the two different years (2014-2015) for each of the five regions were compared. The cluster analysis has given similar results for both years. The results in Figure 5.4 show the variation in temperature and salinity in the five different regions within the North Sea. In particular, a clear difference between the southern mixed region and the southern coastal region of the North Sea and the northern stratified region and the northern coastal region of the North Sea was found for the temperature. Salinity showed similar, low variation in all regions except for the northern coastal region. This high variation in

salinity in the region northern coastal region might be linked to the exchange of water masses with the Atlantic along the Norwegian coast.

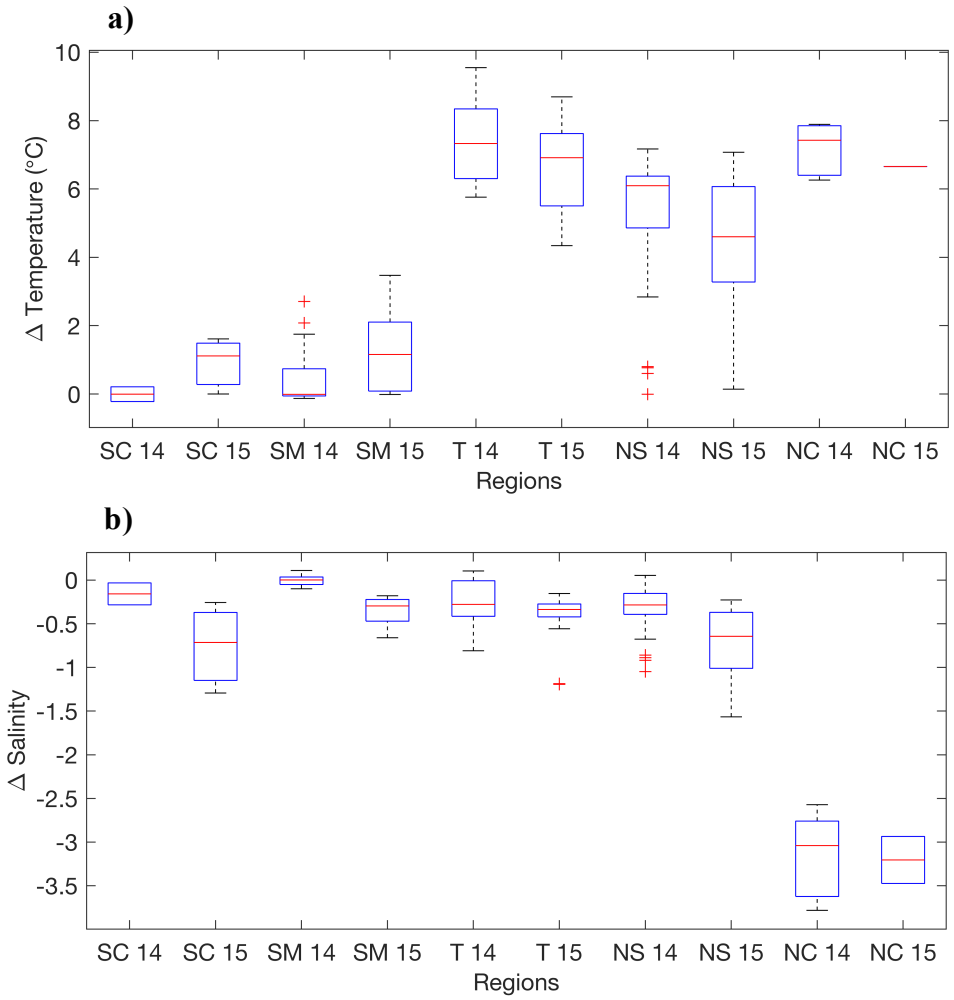

Figure 5.4 Box-whisker plot of the cluster analysis describing the five different regions of the North Sea: Southern Coastal (SC), Southern Mixed (SM), Transitional (T), Northern Stratified (NS) and Northern Coastal (NC) in the year a) 2014 and b) 2015. The box indicates the lower and the upper quartile. The horizontal line within the box represents the median. The whiskers indicate the lower and higher data points. The red crosses indicate outliers. The outliers were classified as two times the interquartile range from the median.

5.2.3 Box model

The box model method described in section 4.3.1 was applied in this chapter to estimate TEP_c formation/accumulation rate, export flux, consumption and residence time at all the sampling stations of the survey in the North Sea for the years 2014 and 2015. Profiles of temperature at each sampling station were used to determine if the water column was mixed or seasonally stratified. The box model equations were applied within the cluster analysis, along with the information on the water column. The results were divided into the five different regions and classified as mixed or stratified according to the profile of

the temperature. The scheme shown in Figure 5.5a was applied at stations with stratification. Otherwise the scheme shown in Figure 5.5b was applied. The box model consists of a steady state system where even in mixed water column particles can sink and reach the bottom and no re-suspension occurs.

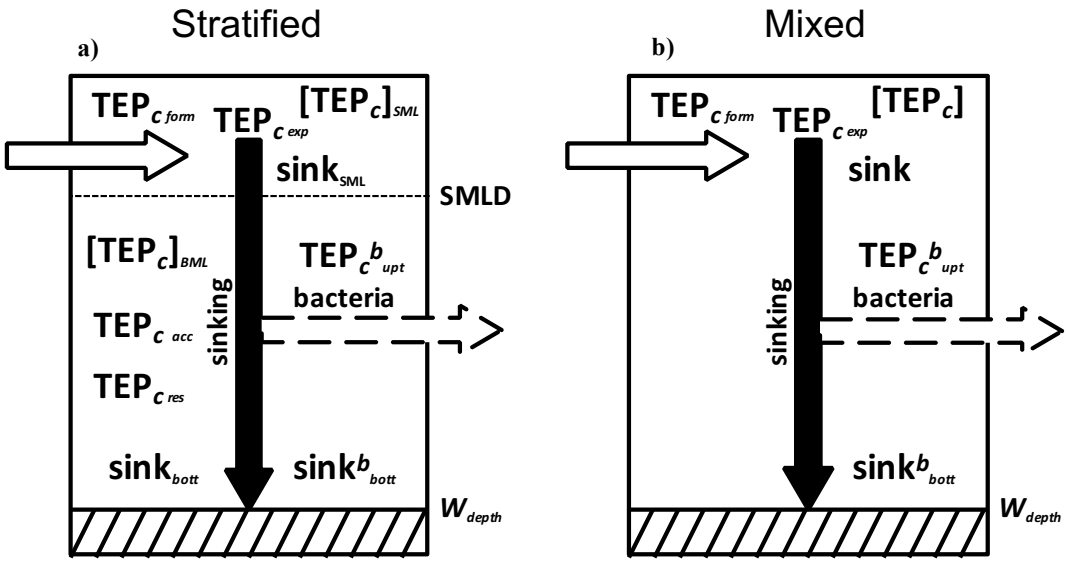

Figure 5.5 Box model describing the fate of TEP_c and fluxes in a) stratified region and a b) mixed region of the North Sea. White arrow indicates TEP_c input, the black arrow indicates export of TEP_c from the SML, the white dashed arrow indicates the fraction of TEP_c removed due to potential bacterial remineralization. $[\boldsymbol{TEP_c}]_{\boldsymbol{SML}}$ - average TEP_c concentration in the SML (µmol l^{-1}), $\boldsymbol{TEP_{c\,form}}$ - TEP_c formation rate in the SML (µmol l^{-1} d^{-1}), $\boldsymbol{TEP_{c\,exp}}$ - TEP_c export flux (mmol m^{-2} d^{-1}), $\boldsymbol{sink_{SML}}$ - TEP_c sinking rate at the SML (m d^{-1}), $[\boldsymbol{TEP_c}]_{\boldsymbol{BML}}$ - average TEP_c concentration in the BML (µmol l^{-1}), $\boldsymbol{TEP_{c\,acc}}$ - potential accumulation rate of TEP_c in the BML (µmol l^{-1} d^{-1}) without bacterial uptake, $\boldsymbol{TEP_{c\,res}}$ - TEP_c residence time (d), $\boldsymbol{TEP^{b}_{c\,upt}}$ - TEP_c loss due to bacterial uptake (mmol m^{-2} d^{-1}), $\boldsymbol{sink_{bott}}$ - potential TEP_c sinking rate without bacterial uptake (m d^{-1}), $\boldsymbol{sink^{b}_{bott}}$ - potential TEP_c sinking rate with bacterial uptake (m d^{-1}) , $\boldsymbol{SMLD}$ - Surface Mixed Layer (m), $\boldsymbol{W_{depth}}$ - total depth of the water column (m).

5.2.4 Statistical analyses

To explore the potential factors controlling TEP distribution, statistical analyses were performed using different software packages. Data were considered together or separated into different groups, according to the result from the cluster analysis. Figures were created in Microsoft Office Excel, Matlab and PRIMER 7 (Plymouth Routines In Multivariate Ecological Research). Regression analysis, t-test and cluster analysis were performed using Matlab. Multivariate analysis was conducted using PRIMER 7 statistical software with PERMANOVA+. Data were normalized before further analysis, with resemblance matrices constructed based on Euclidean distances. Relationships between regions with similar characteristics were visualised by principal coordinates analysis (PCO), with data significance assessed by PERMANOVA (999 permutations). Data

vectors were overlaid onto PCO plots of regions. Vector direction indicated correlated data, whilst vector length indicated the degree of data correlation. Relationships were considered to be significant when $p < 0.05$.

5.4 Results: distribution of TEP in summer 2014

5.4.1 Characterisation of environmental conditions

Environmental condition of the North Sea in summer 2014 are shown in Figure 5.6. Surface and bottom temperature indicated a clear division between the northern seasonally stratified region and the southern mixed region of the North Sea (Figure 5.6a and b). Temperature was higher in surface waters (range 12.71-20.58 ºC, mean 15.60 ± 1.95 ºC, Figure 5.6a) respect to that of bottom waters (range 7.32-20.80 ºC, mean 11.42 ± 4.44 ºC, Figure 5.6b). The warmest water was found along the Dutch and German coastline. The lowest temperature was observed in the bottom waters of the northern region of the North Sea. Lower salinity was observed in surface waters (range 31.54-35.13, mean 34.36 ± 0.75, Figure 5.6c) in respect to that of bottom waters (range 32.94-35.39, mean 34.84 ± 0.47, Figure 5.6d). Lower salinity was found in the southern North Sea along the Dutch and German coastlines, which is linked to the presence of river inputs. Low salinity was observed in surface waters near the Norwegian coastline, which results from the outflow of surface waters from the Baltic. Nutrient concentrations were generally low in surface waters. TOxN concentration in surface waters ranged from 0.1 to 3.1 μmol l^{-1} with a mean value of 0.3 ± 0.6 μmol l^{-1} (Figure 5.6e). A high peak of TOxN concentration (3.1 μmol l^{-1}) was found in the middle of the northern North Sea region and a second peak of lower intensity was recorded in the northwest area of the North Sea along the UK coastline. However, TOxN remained low within the southern region of the North Sea. PO_4 and SiO_4 in surface waters followed similar spatial patterns ranging from 0.01 to 0.32 μmol l^{-1}, with a mean value of 0.08 ± 0.09 μmol l^{-1} (Figure 5.6f) and from 0.1 to 0.64 μmol l^{-1}, with a mean value of 1.21 ± 1.18 μmol l^{-1} (Figure 5.6g) respectively. Both presented a high concentration in the southern North Sea region and close to the coastline, suggesting the important contribution of riverine inputs. PO_4 also showed a peak concentration in the northwest North Sea area close to the UK coastline.

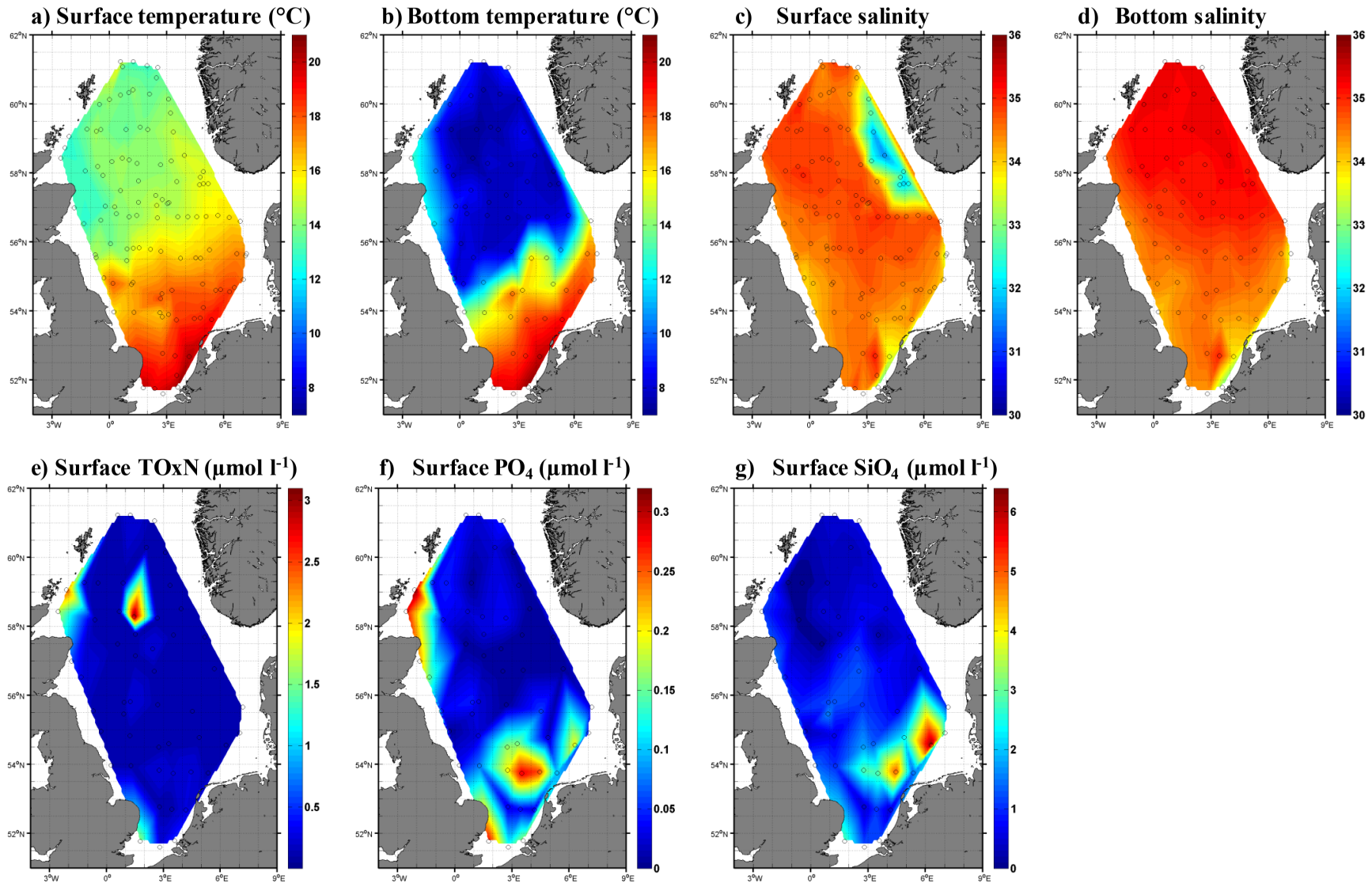

Figure 5.6 Environmental condition of the North Sea in summer 2014. a-b) temperature (°C) in surface and bottom waters, c-d) salinity in surface and bottom waters, e) nitrate plus nitrite in surface waters (µmol l^{-1}), f) phosphate in surface waters (µmol l^{-1}), g) silicate in surface waters (µmol l^{-1}).

5.4.2 TEP observations in 2014

Analyses of water samples revealed high TEP_c concentrations in surface waters (average of 14 ± 4.8 µmol l^{-1}) relative to bottom (average of 11.8 ± 4.9 µmol l^{-1}) waters (Figure 5.7a, b), with the highest concentrations near the Netherlands coast for both surface (35.8 µmol l^{-1}; Figure 5.7a) and bottom (34.4 µmol l^{-1}; Figure 5.7b) waters and at 10 meters depth (34.7 µmol l^{-1}) in the algal bloom (Figure 5.7 c; 55.8 °N, 1°E). The phytoplankton community determination analysis, showed a concentration of *Karenia mikimotoi* of approximately 900,000 cell l^{-1}. Blooms of *Karenia mikimotoi* have long been reported to produce prolonged blooms in the North Sea between July and August (Davidson *et al.,* 2009). Distribution of TEP_c was correlated with that of chlorophyll in the southern mixed region (Figure 5.7c, d). Peaks of chlorophyll *a* were observed in the algal bloom (Figure 5.7 c; 55.8°N, 1°E) (12.2 µg l^{-1}) and surface (5.9 µg l^{-1}) and bottom (4.5 µg l^{-1}) waters of the Netherlands coast, which were associated with high TEP_c concentrations. Extremely low chlorophyll *a* concentrations (below the detection limit) were observed in the central North Sea in surface and bottom waters.

The seasonally stratified northern region (Figure 5.8) showed higher TEP_c concentrations in surface with respect to the bottom waters, with the highest difference along the Shetland Isles (16.4 µmol l^{-1}). A second high difference in TEP_c concentrations was found in the algal bloom (12.8 µmol l^{-1}). The southern mixed region (Figure 5.8) had generally higher TEP_c in the bottom waters, however this did not apply to southern coastal waters of the Netherlands coast. Overall the TEP_c concentration in surface and bottom waters was significantly positively correlated ($R^2 = 0.33$, $p < 0.001$, $n = 76$).

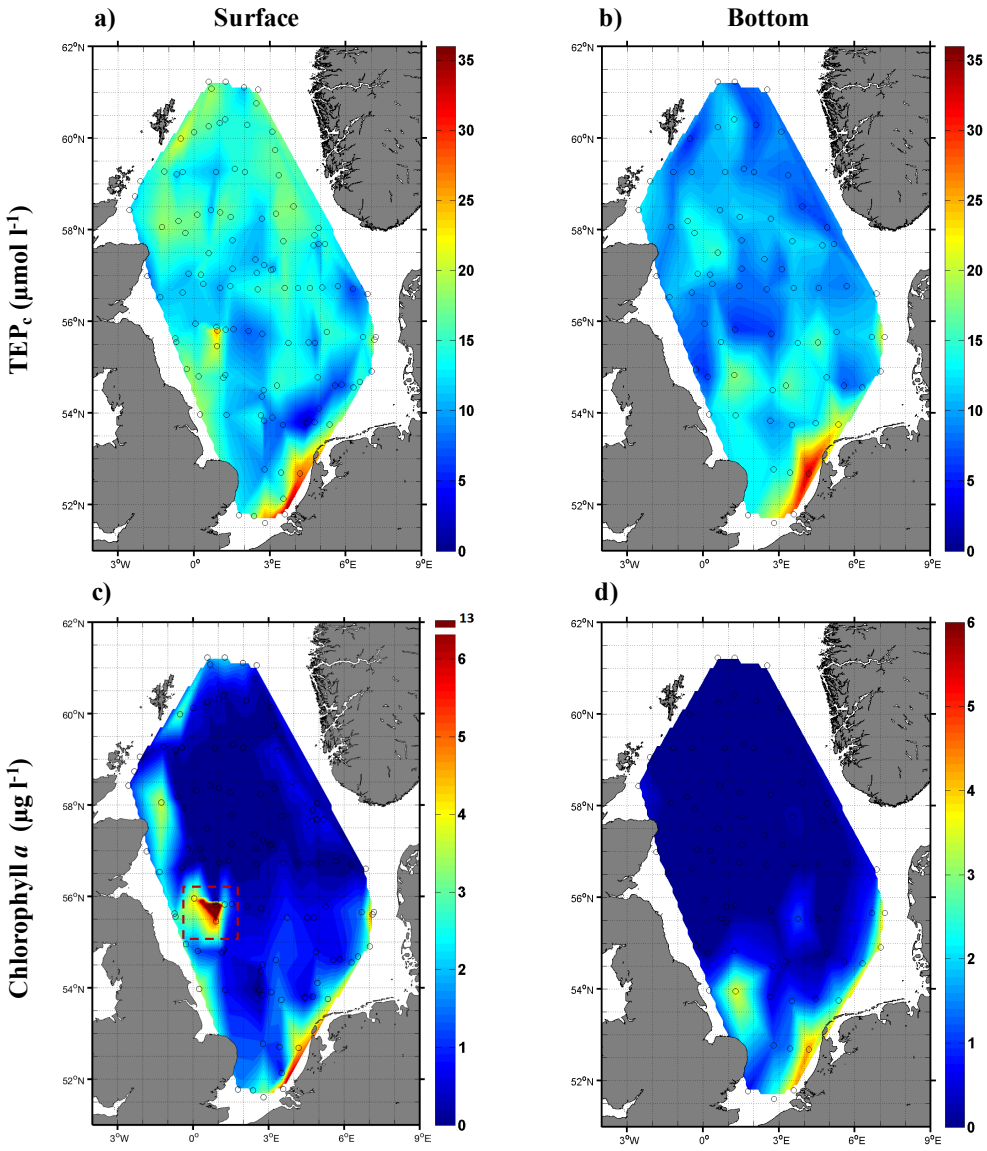

Figure 5.7 Spatial distribution of TEP_c content (µmol l^{-1}) for a) surface (4 meters depth) and b) bottom waters; c) chlorophyll (µg l^{-1}) surface and d) bottom waters during summer 2014 in the North Sea. The frame highlights an algal bloom (55.8°N, 1°E) of *Karenia mikimotoi*.

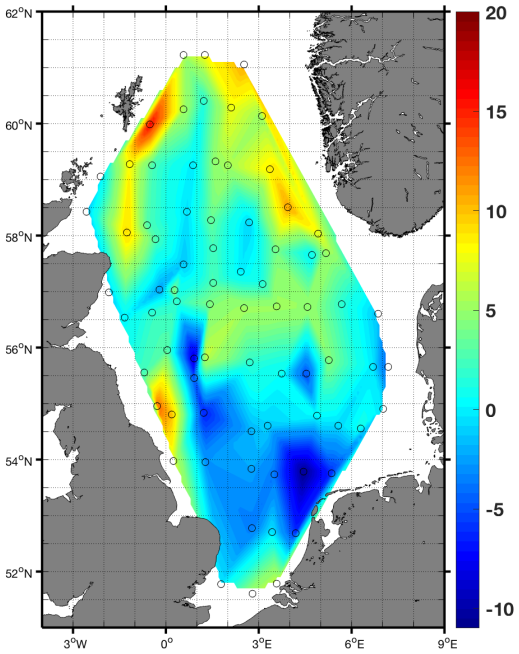

Figure 5.8 TEP_c concentration (µmol l^{-1}) differences between surface and bottom waters during summer 2014 in the North Sea.

5.4.3 Cluster analysis for 2014

A box plot of TEP_c concentrations in surface and bottom waters for each of the five regions of the North Sea is shown in Figure 5.9. Surface and bottom waters in all regions had a similar median TEP_c concentration of ~ 10 µmol l^{-1}, except for the southern coastal region where surface and bottom waters had a median concentration of TEP_c of ~ 30 µmol l^{-1} (Figure 5.9). The southern mixed region had the widest range of TEP_c concentrations in surface waters (Figure 5.9a). Results from the cluster analysis in the North Sea for the year 2014 are shown in graphs (Figures 5.10, 5.11, 5.12 and 5.13) and summarised in tables (Tables 5.1, 5.2 and 5.3). Only regressions of variables which showed statistically significant correlations within the five different regions of the North Sea for the year 2014 are reported in tables and presented here.

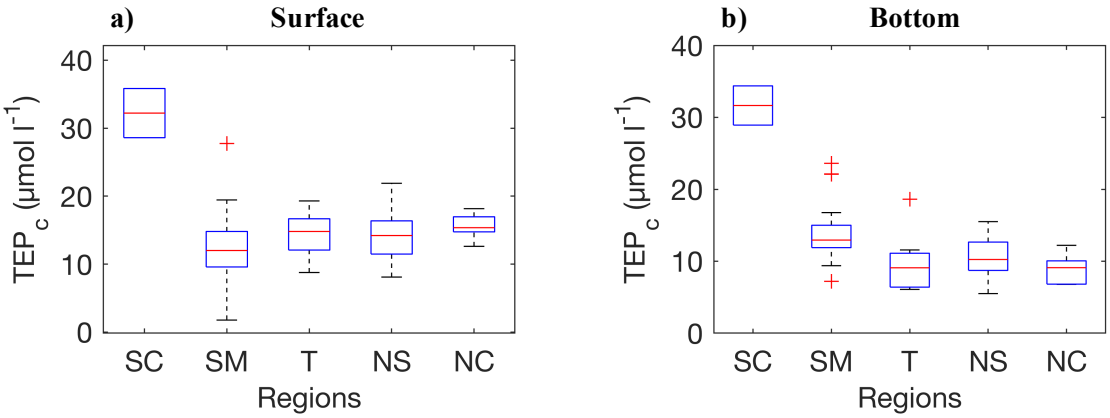

Figure 5.9 Box-whisker plots of TEP_c (µmol l^{-1}) concentrations in a) surface and b) bottom waters during summer 2014 in the five different regions of the North Sea: Southern Coastal (SC), Southern Mixed (SM), Transitional (T), Northern Stratified (NS) and Northern Coastal (NC). See Figure 5.4 for an explanation of box and whisker plots.

A significant positive relationship between the concentrations of TEP_c and chlorophyll *a* (Figure 5.10 and Table 5.1) was observed in the North Sea in surface ($R^2 = 0.35$, $p < 0.001$, $n = 54$; Figure 5.10b and Table 5.1) and bottom waters ($R^2 = 0.52$, $p < 0.001$, $n = 25$; Figure 5.10b and Table 5.1). From the five identified regions within the North Sea area a significant positive relationship between TEP_c and chlorophyll *a* was found only in the southern mixed region in surface ($R^2 = 0.49$, $p < 0.001$, $n = 20$; Figure 5.10a and Table 5.1) and bottom waters ($R^2 = 0.29$, $p < 0.05$, $n = 19$; Figure 5.10b and Table 5.1). A positive relationship between the TEP_c concentration and temperature was found in the North Sea in bottom waters ($R^2 = 0.35$, $p < 0.001$, $n = 74$; Figure 5.11b and Table 5.2). Salinity and the TEP_c concentration had a negative significant correlation in the North Sea in bottom waters ($R^2 = 0.37$, $p < 0.001$, $n = 74$; Figure 5.11d and Table 5.2). Negative significant correlations were found between the concentration of TEP_c and inorganic nutrients (Figure 5.12 and Figure 5.13) in surface and bottom waters. TEP_c was negatively correlated with NH_4 in surface waters in the North Sea ($R^2 = 0.13$, $p < 0.05$, $n = 51$; Figure 5.12b and Table 5.3) and in the southern mixed region ($R^2 = 0.24$, $p < 0.05$, $n = 17$; Figure 5.12b and Table 5.3). SiO_4 showed a negative correlation with TEP_c in the North Sea in surface ($R^2 = 0.12$, $p < 0.05$, $n = 51$; Figure 5.12d and Table 5.3) and bottom waters ($R^2 = 0.26$, $p < 0.05$, $n = 24$; Figure 5.13c and Table 5.3). A further significant negative correlation for SiO_4 was observed in surface in the southern mixed region ($R^2 = 0.25$, $p < 0.05$, $n = 17$; Figure 5.12d and Table 5.3) and in the northern stratified region ($R^2 = 0.14$, $p < 0.05$, $n = 22$; Figure 5.12d and Table 5.3). No correlation was found for TOxN and PO_4 in surface (Figure 5.12a, c) and bottom waters (Figure 5.13a, b). However, TEP_c

concentrations increased when surface nutrients became limited for phytoplankton (Figure 5.12).

In addition to the regression analyses between single paired variables a multivariate analysis (PCO) was carried out in order to obtain an in depth understanding of the relationships among all variables. Due to a lack of data points in the years 2014 for the bottom waters, principal coordinates analysis (PCO) was only applied to surface data. The PCO analysis (Figure 5.14) revealed that PCO1 and PCO2 accounted for 57 % of the total variation in the analysis. The distribution of the five regions of the North Sea (Figure 5.14) reflected the results of the cluster analysis. Spatial distribution of the different regions in the North Sea indicated a statistically significant difference between regions (PERMANOVA; $p = 0.001$). PCO also showed similar relationships between variables which were addressed previously by the single paired regression analysis. However, PCO analysis provides a summary of relationships and interactions among variables.

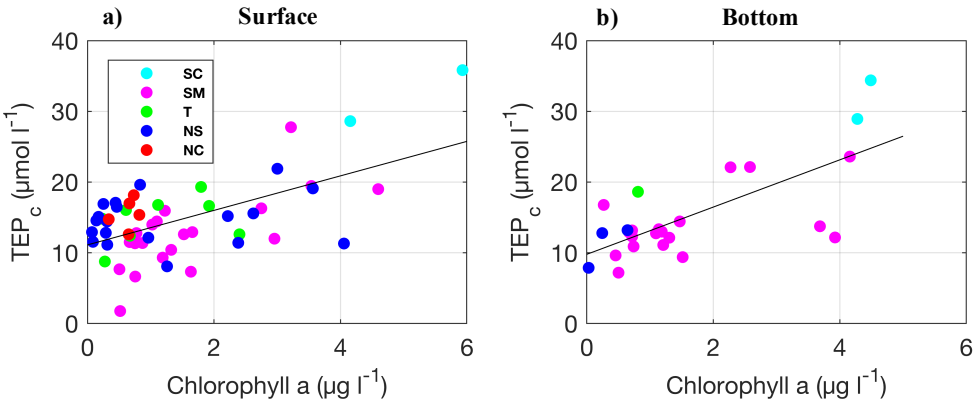

Figure 5.10 Plots of TEP_c (µmol l^{-1}) versus chlorophyll *a* (µg l^{-1}) concentrations in a) surface and b) bottom waters during summer 2014 in the five different regions of the North Sea: Southern Coastal (SC), Southern Mixed (SM), Transitional (T), Northern Stratified (NS) and Northern Coastal (NC). The black line represents the linear regression curve for all the data points.

Table 5.1 Regression analysis of TEP_c (µmol l^{-1}) versus chlorophyll *a* (µg l^{-1}) concentrations in surface and bottom waters during summer 2014 in the five different regions of the North Sea: Southern Coastal (SC), Southern Mixed (SM), Transitional (T), Northern Stratified (NS) and Northern Coastal (NC).

Variable	Depth	Region	Regression	R^2	n	pvalue
Chlorophyll *a*	**Surface**	All regions	y = 2.44x + 11.12	0.35	54	< 0.001
		SM	y = 3.32x + 7.36	0.49	20	< 0.001
Chlorophyll *a*	**Bottom**	All regions	y = 3.34x + 9.79	0.52	25	< 0.001
		SM	y = 1.97x + 10.77	0.29	19	< 0.05

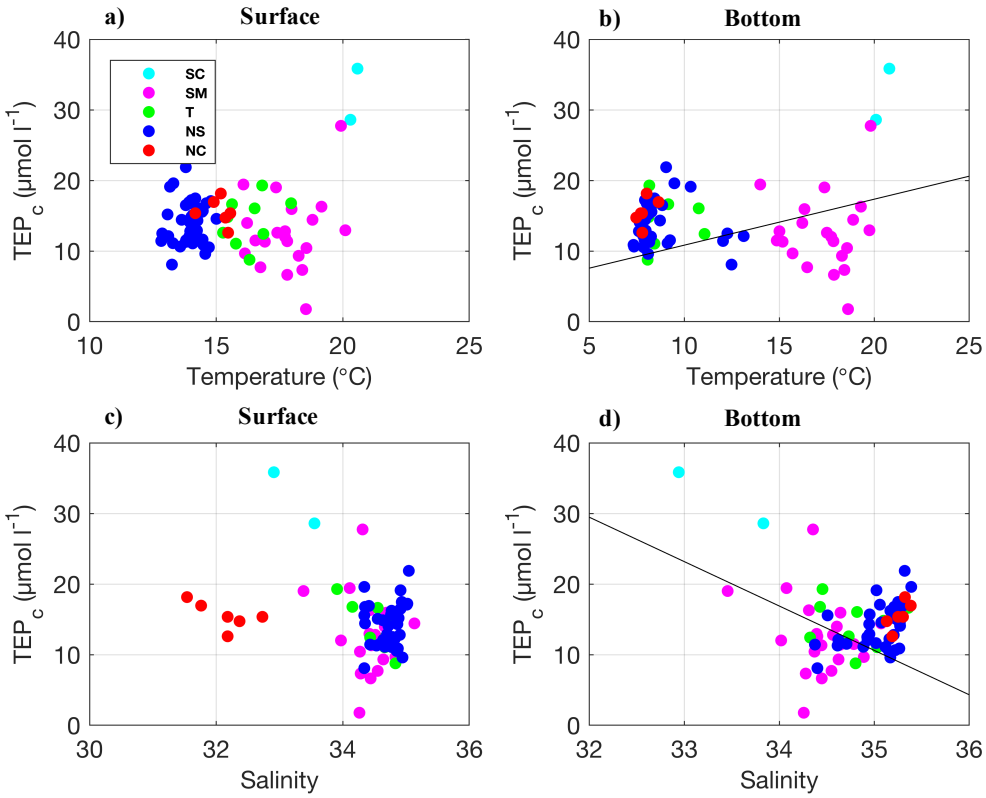

Figure 5.11 Plots of TEP_c concentration (µmol l^{-1}) versus temperature (ºC) and salinity in a-c) surface and b-d) bottom waters during summer 2014 in the five different regions of the North Sea: Southern Coastal (SC), Southern Mixed (SM), Transitional (T), Northern Stratified (NS) and Northern Coastal (NC). The black line represents the linear regression curve for all the data points.

Table 5.2 Regression analysis of TEP_c concentration (µmol l^{-1}) versus temperature (ºC) and salinity in surface and bottom waters during summer 2014 in the five different regions of the North Sea: Southern Coastal (SC), Southern Mixed (SM), Transitional (T), Northern Stratified (NS) and Northern Coastal (NC).

Variable	Depth	Region	Regression	R^2	n	pvalue
Temperature	**Bottom**	All regions	y = 0.65 x+ 4.33	0.35	74	< 0.001
Salinity	**Bottom**	All regions	y = -6.29x + 230.6	0.37	74	< 0.001

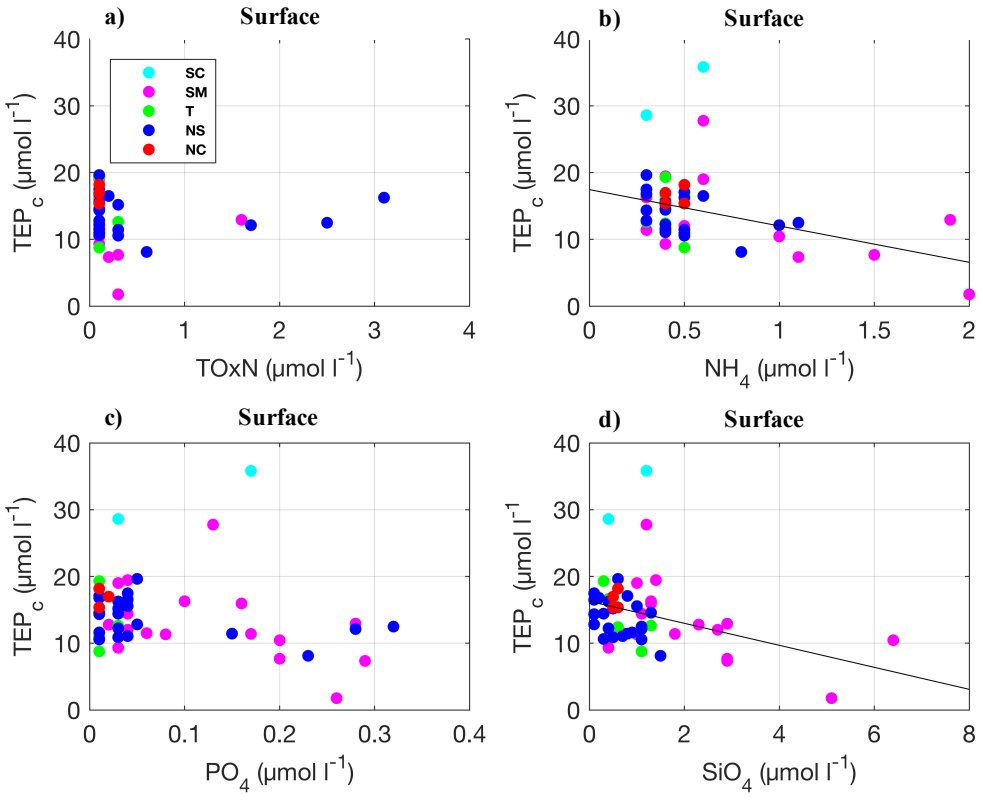

Figure 5.12 Plots of TEP_c (µmol l^{-1}) versus nutrient concentrations a) TOxN, b) NH_4, c) PO_4, d) SiO_4 in surface waters during summer 2014 in the five different regions of the North Sea: Southern Coastal (SC), Southern Mixed (SM), Transitional (T), Northern Stratified (NS) and Northern Coastal (NC). The black line represents the linear regression curve for all the data points.

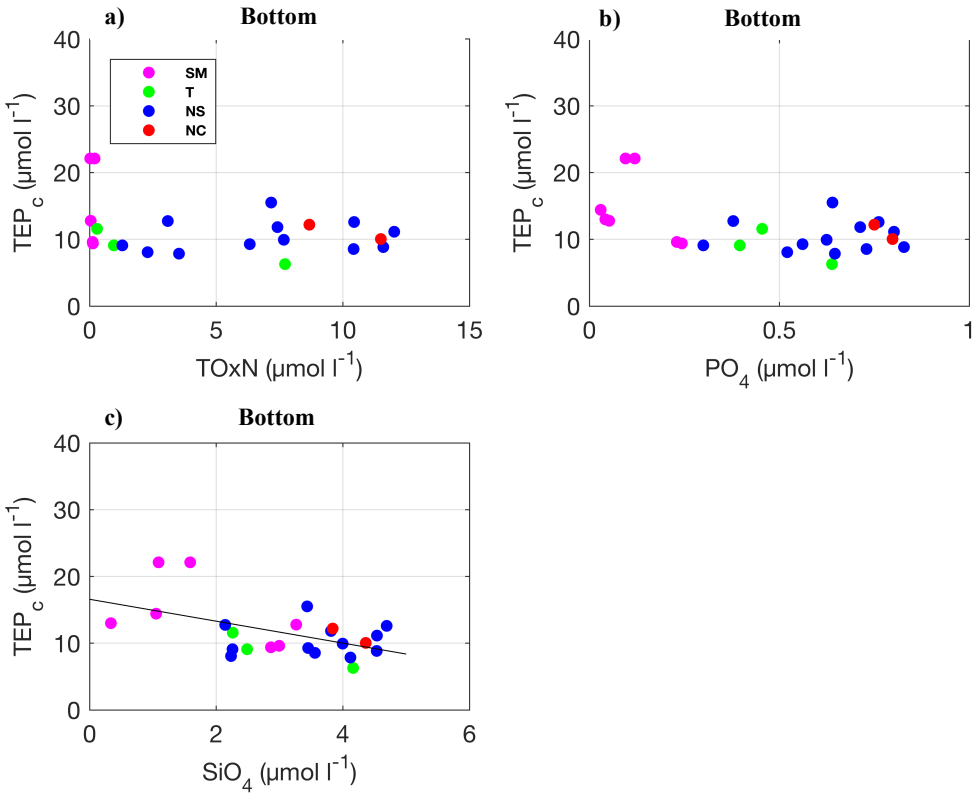

Figure 5.13 Plots of TEP_c (µmol l^{-1}) versus nutrient (µmol l^{-1}) concentrations a) TOxN, b) PO_4, c) SiO_4 in bottom waters during summer 2014 in the five different regions of the North Sea: Southern Coastal (SC), Southern Mixed (SM), Transitional (T), Northern Stratified (NS) and Northern Coastal (NC). The black line represents the linear regression curve for all the data points.

Table 5.3 Regression analysis of TEP_c (µmol l^{-1}) versus nutrient (µmol l^{-1}) concentrations in surface and bottom waters during summer 2014 in the five different regions of the North Sea: Southern Coastal (SC), Southern Mixed (SM), Transitional (T), Northern Stratified (NS) and Northern Coastal (NC).

Variable	Depth	Region	Regression	R^2	n	p-value
NH_4	**Surface**	All regions	y = -5.44x + 17.5	0.14	51	< 0.05
		SM	y = -5.14x + 16.83	0.25	17	< 0.05
SiO_4	**Surface**	All regions	y = -1.648x + 16.28	0.13	51	< 0.05
		SM	y = -1.83x + 16.94	0.26	17	< 0.05
		NS	y = -2.92x + 15.56	0.15	22	< 0.05
SiO_4	**Bottom**	All regions	y = -1.64x + 16.58	0.26	24	< 0.05

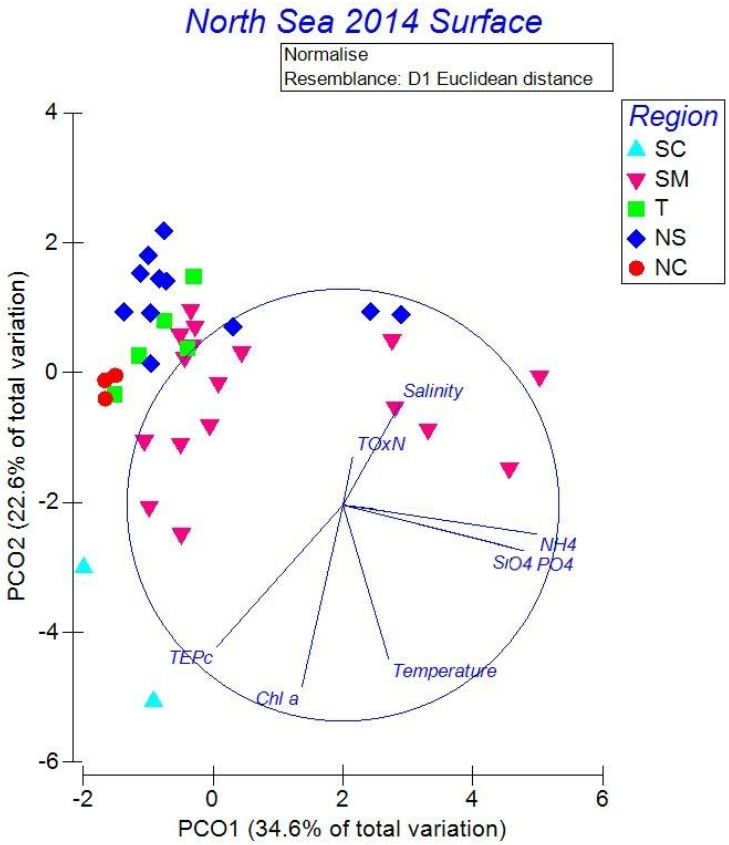

Figure 5.14 Principal coordinates plot (PCO) showing relationships between variables in the five different regions of the North Sea: Southern Coastal (SC), Southern Mixed (SM), Transitional (T), Northern Stratified (NS) and Northern Coastal (NC); in surface waters in the year 2014.

5.4.4 Box model for 2014

Results from the box model for the year 2014 are summarised in Table 5.4. The SMLD in the stratified regions was ~ 30 meters depth. The water column depth ranged from 20.4 ± 1.9 meters in the southern coastal region to 123.9 ± 56.7 meters in the northern coastal region. The highest and lowest TEP_c formation rate were estimated in the southern coastal region (15.1 ± 0.3 µmol l^{-1} d^{-1}) and in the transitional mixed region (5.7 ± 1.2 µmol l^{-1} d^{-1}) respectively. The export of TEP_c from the surface to the bottom of the water column ranges from 189.2 ± 50.5 mmol l^{-1} m^{-2} d^{-1} in the transitional stratified region to 308.8 ± 23 mmol l^{-1} m^{-2} d^{-1} in the southern coastal region. The lowest and the highest potential sinking velocity of TEP_c was predicted in the mixed regions Southern Coastal (9.7 ± 0.9 m d^{-1}) and transitional (22.8 ± 1.5 m d^{-1}). Accumulation of TEP_c below the mixed layer deep in the stratified regions ranged from 2.6 ± 1.5 µmol l^{-1} d^{-1} in the northern coastal region to 6.0 ± 2.7 µmol l^{-1} d^{-1} in the transitional stratified region. On the contrary the residence time of TEP_c ranged from 1.9 ± 1.2 days in the Transitional stratified region to 4.2 ± 1.9 days in the northern coastal region. The use of a bacterial remineralization factor

of 0.08 d^{-1} did not result in a significant decrease in TEP_c flux, nor in change in the sinking velocity of TEP_c. In contrast the bacterial remineralization factor of 0.53 d^{-1} produced an increase on the loss of TEP_c, a substantial net decrease in TEP_c flux and a consequent decrease in the sinking velocity of TEP_c.

Table 5.4 Table summarising the results from the box model describing the fate of TEP_c and fluxes in the North Sea in stratified and mixed waters for the year 2014 in the five regions of the North Sea: Southern Coastal (SC), Southern Mixed (SM), Transitional (T), Northern Stratified (NS) and Northern Coastal (NC). $[\boldsymbol{TEP_c}]_{\boldsymbol{SML}}$ - TEP_c concentration in the SML (µmol l^{-1}), $\boldsymbol{TEP_{c\,form}}$ - TEP_c formation rate in the SML (µmol l^{-1} d^{-1}), $\boldsymbol{TEP_{c\,exp}}$ – TEP_c export flux (mmol m^{-2} d^{-1}), $\boldsymbol{sink_{SML}}$ – TEP_c sinking rate at the SML (m d^{-1}), $[\boldsymbol{TEP_c}]_{\boldsymbol{BML}}$ - TEP_c concentration in the BML (µmol l^{-1}), $\boldsymbol{TEP_{c\,acc}}$ – potential accumulation rate of TEP_c in the BML (µmol l^{-1} d^{-1}) without bacterial uptake, $\boldsymbol{TEP_{c\,res}}$ - TEP_c residence time (d), $\boldsymbol{TEP^{b}_{c\,upt}}$ – TEP_c loss due to bacterial uptake (mmol m^{-2} d^{-1}), $\boldsymbol{sink_{bott}}$ – potential TEP_c sinking rate without bacterial uptake (m d^{-1}), $\boldsymbol{sink^{b}_{bott}}$ – potential TEP_c sinking rate with bacterial uptake (m d^{-1}).

Region	Area	$[TEP_c]_{SML}$	$TEP_{c\,form}$	$TEP_{c\,exp}$	$sink_{SML}$	$[TEP_c]_{BML}$	$TEP_{c\,acc}$	$TEP_{c\,res}$	$TEP^{b}_{c\,upt}$*	$TEP^{b}_{c\,upt}$**	$sink_{bott}$	$sink^{b}_{bott}$*	$sink^{b}_{bott}$**	SMLD	W_{depth}
SC	Mixed (2)	31.9 ± 0.6	15.2 ± 0.3	308.8 ± 23	9.7 ± 0.9	-	-	-	2.5 ± 0.2	163.7 ± 12.2	-	9.6 ± 0.9	4.5 ± 0.43	-	20.4 ± 1.9
SM	Mixed (20)	13.3 ± 4.6	6.3 ± 2.1	199.9 ± 77.1	15.2 ± 2.9	-	-	-	1.6 ± 0.6	106 ± 40.9	-	15.1 ± 2.9	7.1 ± 1.4	-	31.7 ± 6.1
T	Mixed (2)	11.9 ± 2.6	5.7 ± 1.2	270.8 ± 42.3	22.8 ± 1.5	-	-	-	2.2 ± 0.3	143.5 ± 22.4	-	22.6 ± 1.5	10.7 ± 0.7	-	47.5 ± 3.0
T	Stratified (7)	14.5 ± 3.5	6.9 ± 1.6	189.2 ± 50.5	13.3 ± 3.1	9.2 ± 4.5	6.0 ± 2.7	1.9 ± 1.2	1.5 ± 0.4	100.2 ± 26.7	23.8 ± 8.5	23.6 ± 8.4	11.2 ± 4	27.8 ± 6.3	69.1 ± 33.8
NS	Stratified (31)	14.0 ± 3.1	6.7 ± 1.4	215.1 ± 68.5	15.1 ± 2.8	10 ± 2.2	4.2 ± 2.4	3.1 ± 2.5	1.7 ± 0.5	114 ± 36.3	23 ± 11.4	22.8 ± 11.3	10.8 ± 5.4	31.4 ± 5.9	90.5 ± 23.5
NC	Stratified (6)	15.5 ± 2.0	7.4 ± 0.9	205.2 ± 56.8	13.1 ± 3.3	9.0 ± 2.1	2.6 ± 1.5	4.2 ± 1.9	1.6 ± 0.4	108.7 ± 30.1	23.9 ± 7.7	23.7 ± 7.6	11.2 ± 3.6	27.5 ± 6.9	123.9 ± 56.7

* TEP_c degradation rate by bacteria similar to that of semi-refractory POC, $\boldsymbol{P^b = 0.008\ (d^{-1})}$, (Fujii *et al.*, 2002)

** TEP_c degradation rate by bacteria similar to that of a generic carbohydrate, $\boldsymbol{P^b = 0.53\ (d^{-1})}$, (Mari *et al.*, 2017)

( ) Number of stations in the specific region

(mean value ± standard deviation)

5.5 Results: distribution of TEP in summer 2015

5.5.1 Characterisation of environmental conditions

Environmental conditions of the North Sea in summer 2015 are shown in Figure 5.15. Surface and bottom temperature in summer 2015 showed similar patterns to those found in summer 2014. The temperature was higher in surface waters (range 12.10 - 19.13 ºC, mean 15.12 ± 1.61 ºC, Figure 5.15a) in respect to that of bottom waters (range 7.07 - 19.13 ºC, mean 10.54 ± 3.48 ºC, Figure 5.15b). Lower salinity was observed in surface waters (range 32.79 - 35.28, mean 34.73 ± 0.48, Figure 5.15c) in respect to that of bottom waters (range 33.63 - 38.73, mean 35.36 ± 0.82, Figure 5.15d). Similar to 2014 a low salinity was found in surface and bottom waters in 2015 in the southern North Sea along the Dutch and German coasts. No clear evidence of low salinity in surface waters near the Norwegian coast was detected in the year 2015. Nutrient concentrations were generally low in surface waters. TOxN concentration in surface waters ranged from 0.04 to 2.15 μmol l^{-1}, with a mean value of 0.32 ± 0.48 μmol l^{-1} (Figure 5.15e). A peak concentration of TOxN (2.15 μmol l^{-1}) was found in the southern region of the North Sea along the UK coast. However, TOxN remained low elsewhere within the North Sea area. PO_4 in surface waters ranged from 0.01 to 0.28 μmol l^{-1}, with a mean value of 0.08 ± 0.08 μmol l^{-1} (Figure 5.15f). PO_4 presented high concentrations along the UK coast, with peaks in the southern North Sea region (0.28 μmol l^{-1}) and along the Orkney Isles (0.25 μmol l^{-1}). SiO_4 was very low in the North Sea except for a peak concentration (3.79 μmol l^{-1}) in the southern North Sea along the Dutch and German coasts.

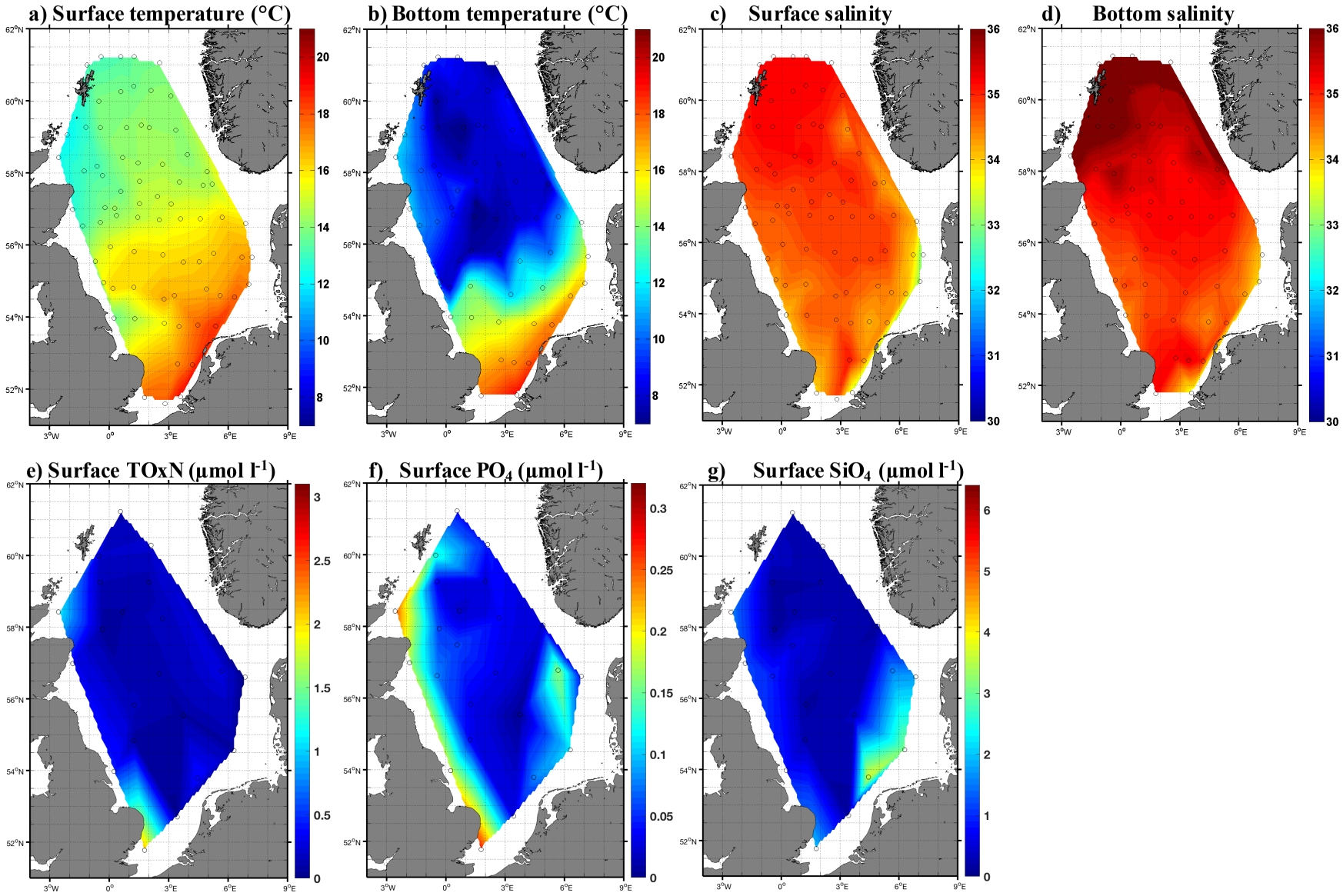

Figure 5.15 Environmental condition of the North Sea in summer 2015. a-b) temperature (°C) in surface and bottom waters, c-d) salinity in surface and bottom waters, e) nitrate + nitrite in surface waters (µmol l^{-1}), f) phosphate in surface waters (µmol l^{-1}), g) silicate in surface waters (µmol l^{-1}).

5.5.2 TEP observations in 2015

In 2015, as for the year 2014, TEP_c showed high concentrations in surface (average of 10.4 ± 4.4 µmol l^{-1}) relative to bottom waters (average of 7.6 ± 3.2 µmol l^{-1}) (Figure 5.16a, b). The highest TEP_c concentrations were found in surface waters along the Scottish coast (26.4 µmol l^{-1}) and near the Shetland Isles (24.1 µmol l^{-1}). These high TEP_c concentrations were associated with high surface chlorophyll *a* concentrations (~ 2 µg l^{-1}) and may be linked to an algal bloom. Chlorophyll *a* concentrations (Figure 5.16c, d) ranged from 0.19 µg l^{-1} to 2.11 µg l^{-1}, with a mean value of 0.62 ± 0.43 µg l^{-1} in surface waters and from 0.04 µg l^{-1} to 3.61 µg l^{-1}, with a mean value of 0.52 ± 0.79 µg l^{-1} in bottom waters. Bottom waters of the northern stratified North Sea region showed extremely low chlorophyll *a* concentrations. Overall the North Sea (Figure 5.17) showed higher TEP_c concentrations in the surface waters with respect to the bottom waters, with the highest difference along the Scottish coast (19 µmol l^{-1}) and the Shetland Isles (16.9 µmol l^{-1}).

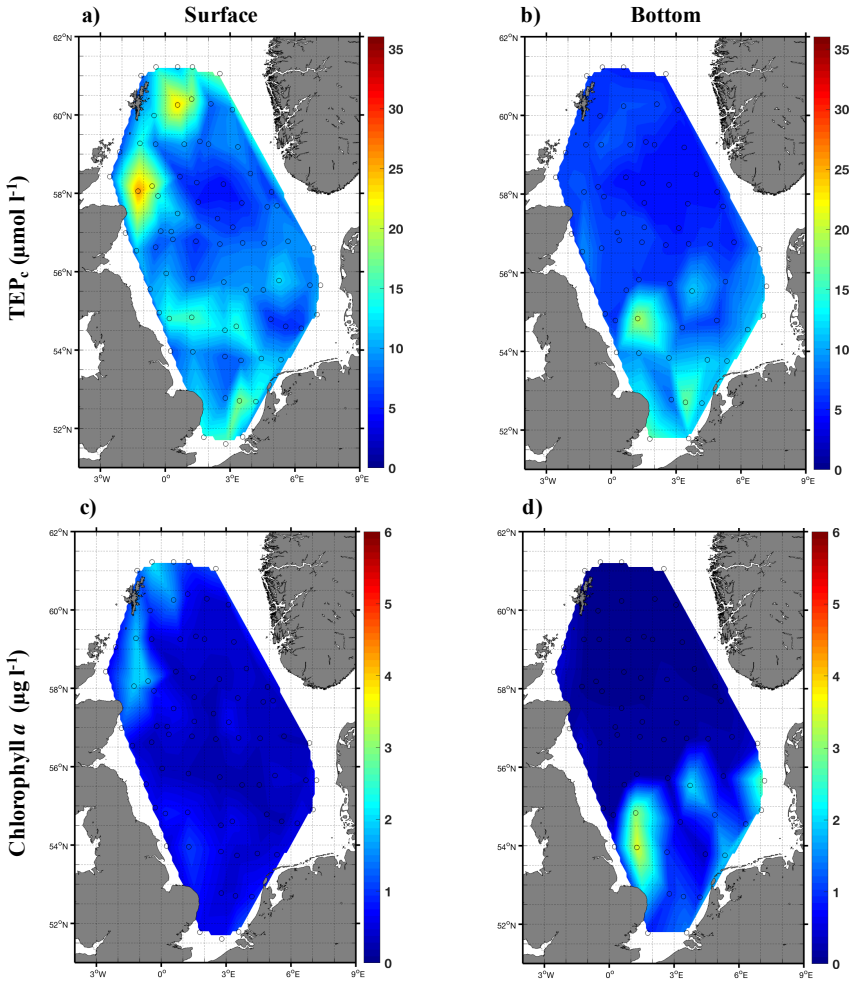

Figure 5.16 Spatial distribution of TEP_c content (µmol l^{-1}) for a) surface (4 meters depth) and b) bottom waters; c) chlorophyll *a* (µg l^{-1}) surface and d) bottom waters during summer 2015 in the North Sea.

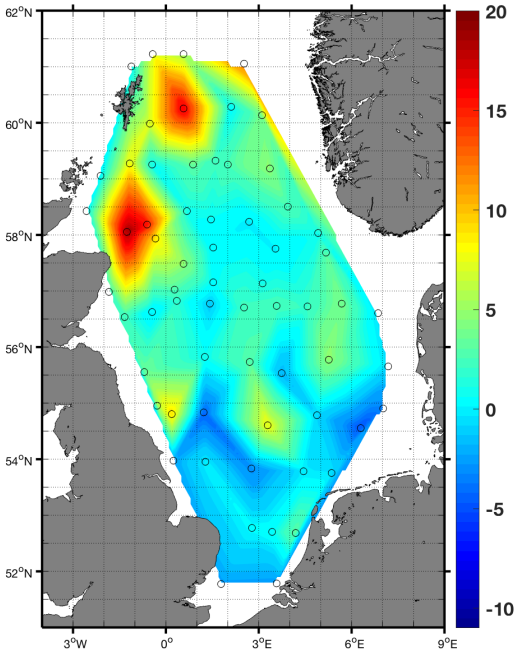

Figure 5.17 TEP_c concentration (µmol l^{-1}) differences between surface and bottom waters during summer 2015 in the North Sea.

5.5.3 Cluster analysis for 2015

Results from the cluster analysis in the North Sea for the year 2015 are shown in graphs and summarised in tables. Only regressions of variables which showed statistically significant correlations within the five different regions of the North Sea for the year 2015 are reported in the tables and presented here. Box plots of TEP_c concentrations in surface and bottom waters for each of the five regions of the North Sea are shown in Figure 5.18. Surface TEP_c in all regions had a similar median TEP_c concentration of ~ 10 µmol l^{-1}, expect for the northern coastal region which showed a median value of TEP_c of ~ 15 µmol l^{-1} (Figure 5.18a). The northern stratified region had the widest range of TEP_c concentrations in surface waters. In the bottom waters the median TEP_c concentrations decreased with the increase of latitude from the southern coastal region, to the northern coastal region (Figure 5.18b).

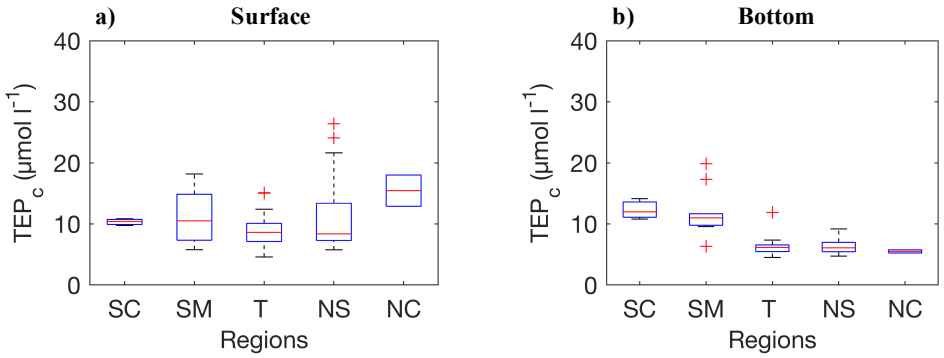

Figure 5.18 Box-whisker plots of TEP_c (µmol l^{-1}) concentrations in a) surface and b) bottom waters during summer 2015 in the five different regions of the North Sea: Southern Coastal (SC), Southern Mixed (SM), Transitional (T), Northern Stratified (NS) and Northern Coastal (NC). See Figure 5.4 for an explanation of box and whisker plots.

TEP_c concentrations showed a significant positive relationship with chlorophyll *a* in surface and bottom waters in all the North Sea area ($R^2 = 0.43$, $p < 0.001$; $R^2 = 0.56$, $p < 0.001$, n=61; Figure 5.19a, b and Table 5.5), the transitional region ($R^2 = 0.299$, $p < 0.05$; $R^2 = 0.77$, $p < 0.001$, $n = 24$; Figure 5.19a, b and Table 5.5) and northern stratified region ($R^2 = 0.55$, $p < 0.001$; $R^2 = 0.42$, $p < 0.001$, $n = 22$; Figure 5.19a, b and Table 5.5). No significant correlations were detected between TEP_c and chlorophyll *a* concentrations in surface and bottom waters in other regions of the North Sea. TEP_c was positively correlated with temperature in the North Sea in bottom waters ($R^2 = 0.61$, $p < 0.001$, $n = 61$; Figure 5.20b and Table 5.6). Another positive significant correlation with temperature was found in the transitional region in surface waters ($R^2 = 0.28$, $p < 0.05$, $n = 24$; Figure 5.20a and Table 5.6) and bottom waters ($R^2 = 0.21$, $p < 0.05$, $n = 24$; Figure 5.20b and Table 5.6). On the contrary salinity showed a negative significant correlation in the North Sea in bottom waters ($R^2 = 0.18$, $p < 0.001$, $n = 61$; Figure 5.20d and Table 5.6) and in the transitional region in surface ($R^2 = 0.22$, $p < 0.05$, $n = 24$; Figure 5.20c and Table 5.6) and bottom waters ($R^2 = 0.23$, $p < 0.05$, $n = 24$; Figure 5.20d and Table 5.6). Negative significant correlations were found between TEP_c and inorganic nutrients (Figure 5.22) in bottom waters. TEP_c was negatively correlated with PO_4 in the North Sea ($R^2 = 0.32$, $p < 0.05$, $n = 22$; Figure 5.22b and Table 5.7) and SiO_4 in the North Sea ($R^2 = 0.26$, $p < 0.05$, $n = 22$; Figure 5.22c and Table 5.7), in the transitional region ($R^2 = 0.58$, $p < 0.05$, $n = 7$; Figure 5.22c and Table 5.7) and in the southern mixed region ($R^2 = 0.88$, $p < 0.05$, $n = 5$; Figure 5.22c and Table 5.7). No correlation was found for TOxN in surface (Figure 5.21a) and bottom waters (Figure 5.22a). However, TEP_c concentrations increased when surface nutrients became limited for phytoplankton (Figure 5.21). POC was positively

correlated with TEP_c in surface in the North Sea area ($R^2 = 0.27$, $p < 0.05$, $n = 31$; Figure 5.23a and Table 5.8), in the northern stratified region ($R^2 = 0.48$, $p < 0.05$, $n = 17$; Figure 5.23a and Table 5.8) and in bottom waters in the transitional region ($R^2 = 0.93$, $p < 0.001$, $n = 9$; Figure 5.23b and Table 5.8). PON showed a positive significant correlation with TEP_c in surface in the North Sea ($R^2 = 0.35$, $p < 0.001$, $n = 31$; Figure 5.23c and Table 5.8), in the northern stratified region ($R^2 = 0.43$, $p < 0.05$, $n = 17$; Figure 5.23c and Table 5.8), in bottom waters in the North Sea area ($R^2 = 0.45$, $p < 0.001$, $n = 34$; Figure 5.23d and Table 5.8) and in the transitional region ($R^2 = 0.6$, $p < 0.05$, $n = 9$; Figure 5.23d and Table 5.8).

The PCO analysis conducted in the year 2015 in surface (Figure 5.24a) and bottom (Figure 5.24b) waters, revealed that PCO1 and PCO2 accounted for 60% in the surface waters and for 74% in the bottom waters of the total variation in the analysis. The spatial distribution of the different regions in surface and bottom waters of the North Sea indicated a statistically significant difference between regions (PERMANOVA; surface waters $p = 0.012$; bottom waters $p = 0.0041$). PCO also showed similar relationships between variables, which were addressed previously by the single paired regression analysis.

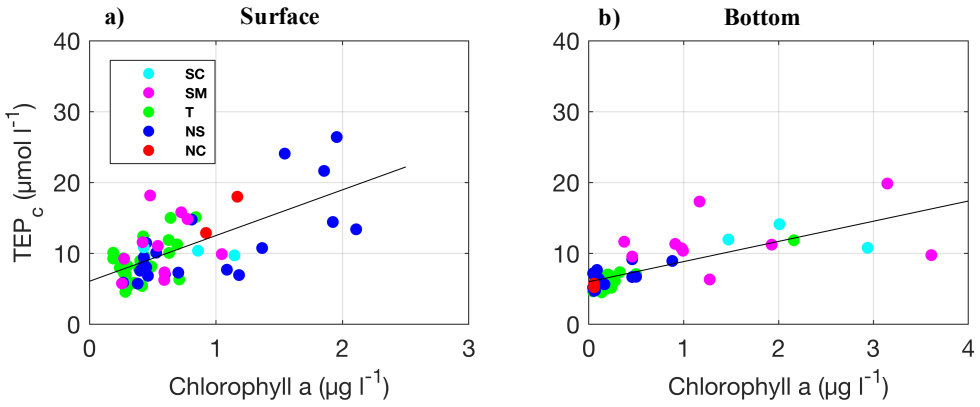

Figure 5.19 Plots of TEP_c (µmol l^{-1}) versus chlorophyll *a* (µg l^{-1}) concentrations in a) surface and b) bottom waters during summer 2015 in the five different regions of the North Sea: Southern Coastal (SC), Southern Mixed (SM), Transitional (T), Northern Stratified (NS) and Northern Coastal (NC). The black line represents the linear regression curve for all the data points.

Table 5.5 Regression analysis of TEP_c (µmol l^{-1}) versus chlorophyll *a* (µg l^{-1}) concentrations in surface and bottom waters during summer 2015 in the five different regions of the North Sea: Southern Coastal (SC), Southern Mixed (SM), Transitional (T), Northern Stratified (NS) and Northern Coastal (NC).

Variable	Depth	Region	Regression	R^2	n	p-value
Chlorophyll *a*	**Surface**	All regions	y = 6.45x + 6.08	0.43	61	< 0.001
		T	y = 8.51x + 5.30	0.30	24	< 0.05
		NS	y = 7.11x + 4.72	0.55	22	< 0.001
Chlorophyll *a*	**Bottom**	All regions	y = 2.85x + 6.0	0.56	61	< 0.001
		T	y = 3.04x + 5.45	0.77	24	< 0.001
		NS	y = 3.69x + 5.74	0.43	22	0.001

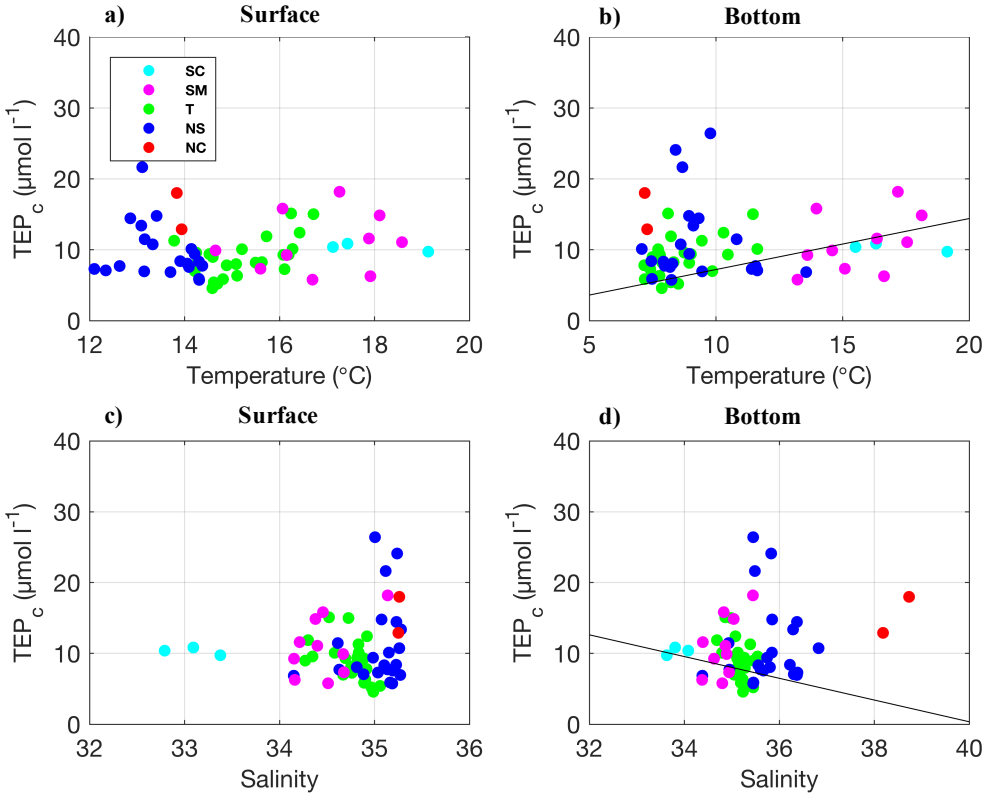

Figure 5.20 Plots of TEP_c (µmol l^{-1}) versus temperature (ºC) and salinity concentrations in a-c) surface and b-d) bottom during summer 2015 in the five different regions of the North Sea: Southern Coastal (SC), Southern Mixed (SM), Transitional (T), Northern Stratified (NS) and Northern Coastal (NC). Black line represents linear regression curve for all the data points.

Table 5.6 Regression analysis of TEP_c concentration (µmol l^{-1}) versus temperature (ºC) and salinity in surface and bottom waters during summer 2015 in the five different regions of the North Sea: Southern Coastal (SC), Southern Mixed (SM), Transitional (T), Northern Stratified (NS) and Northern Coastal (NC).

Variable	Depth	Region	Regression	R^2	n	p-value
Temperature	**Surface**	T	y = 1.77x + 18.05	0.28	24	< 0.05
Temperature	**Bottom**	All regions	y = 0.72x + 0.02	0.62	61	< 0.001
		T	y = 1.0x + 0.27	0.22	24	< 0.05
Salinity	**Surface**	T	y = -6.15x + 222.7	0.22	24	< 0.05
Salinity	**Bottom**	All regions	y = -1.53x + 61.73	0.18	61	< 0.001
		T	y = -6.66x + 243.10	0.23	24	< 0.05

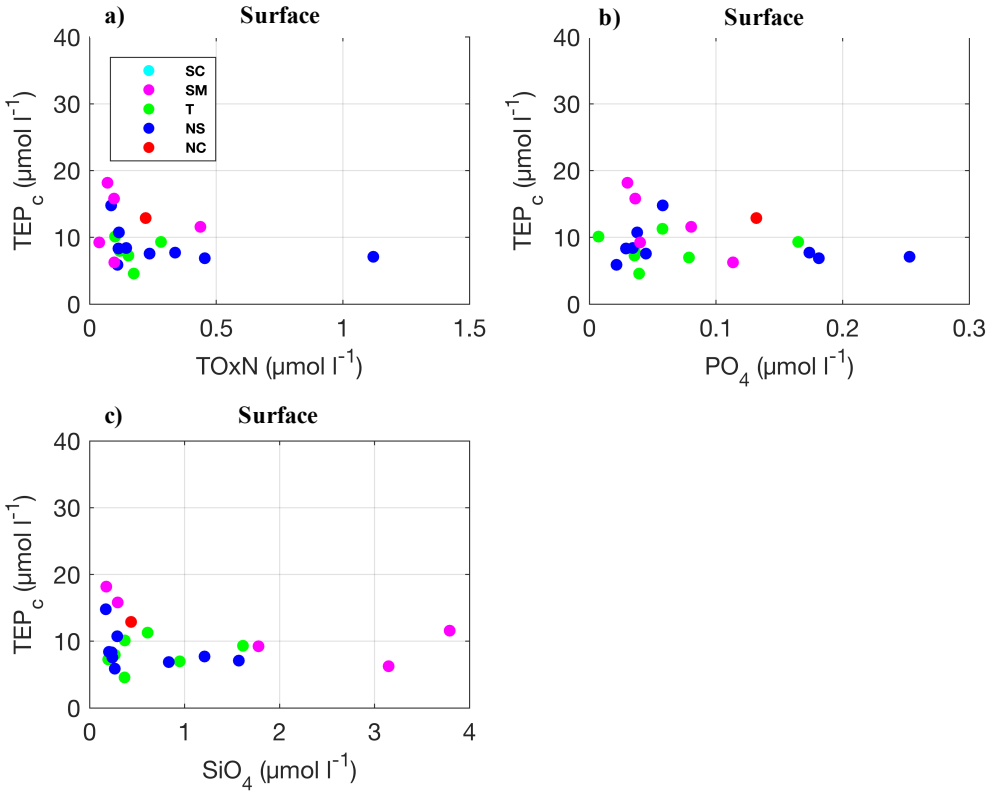

Figure 5.21 Plots of TEP_c (µmol l^{-1}) versus nutrients concentrations a) TOxN, b) PO_4, c) SiO_4 in surface during summer 2015 in the five different regions of the North Sea: Southern Coastal (SC), Southern Mixed (SM), Transitional (T), Northern Stratified (NS) and Northern Coastal (NC). The black line represents the linear regression curve for all the data points.

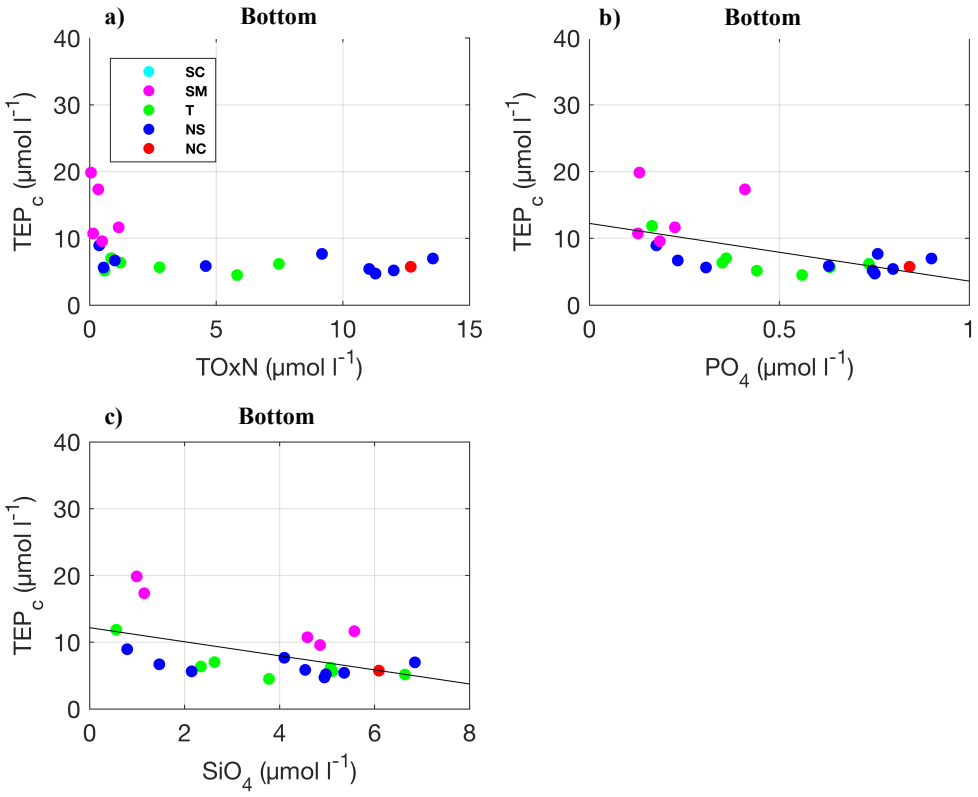

Figure 5.22 Plots of TEP_c (µmol l^{-1}) versus nutrient (µmol l^{-1}) concentrations a) TOxN, b) PO_4, c) SiO_4 in bottom waters during summer 2015 in the five different regions of the North Sea: Southern Coastal (SC), Southern Mixed (SM), Transitional (T), Northern Stratified (NS) and Northern Coastal (NC). The black line represents the linear regression curve for all the data points.

Table 5.7 Regression analysis of TEP_c (µmol l^{-1}) versus nutrient (µmol l^{-1}) concentrations in surface and bottom waters during summer 2015 in the five different regions of the North Sea: Southern Coastal (SC), Southern Mixed (SM), Transitional (T), Northern Stratified (NS) and Northern Coastal (NC).

Variable	Depth	Region	Regression	R^2	n	p-value
PO_4	**Bottom**	All regions	y = -8.64x + 12.24	0.32	22	< 0.05
SiO_4	**Bottom**	All regions	y = -1.053x + 12.17	0.27	22	< 0.05
		T	y = -0.90x +10.05	0.59	7	< 0.05
		SM	y = -1.93x + 20.46	0.88	5	< 0.05

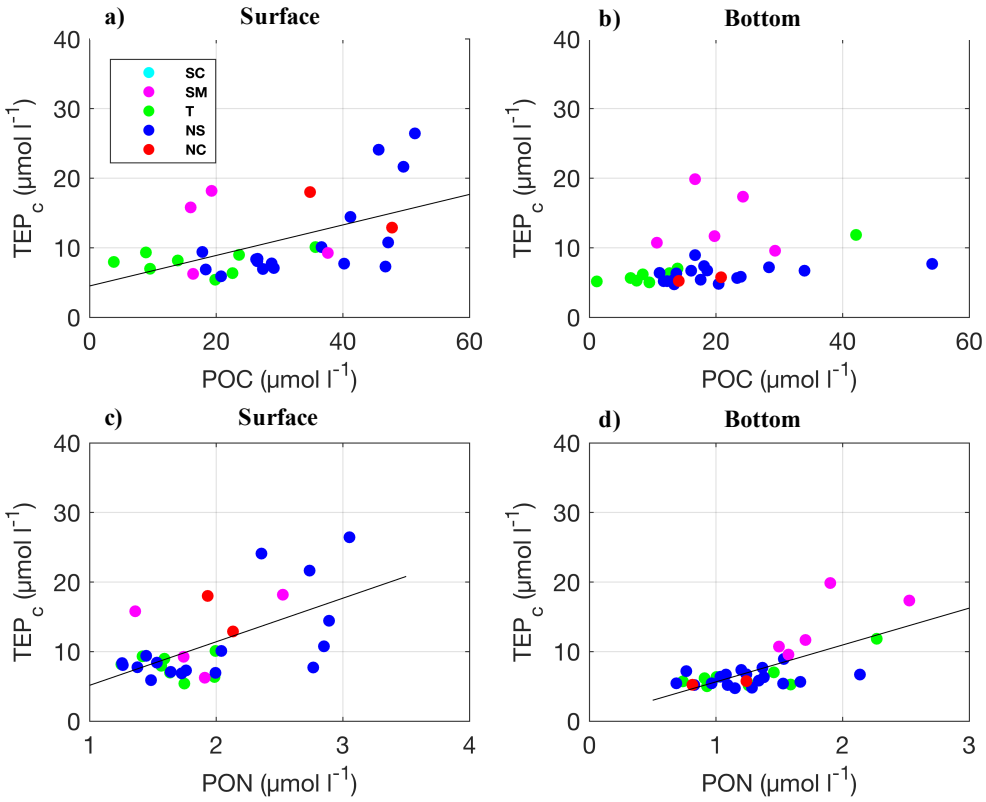

Figure 5.23 Plots of TEP_c (µmol l^{-1}) versus POC (µmol l^{-1}) and PON (µmol l^{-1}) concentrations in a-c) surface and b-d) bottom waters during summer 2015 in the five different regions of the North Sea: Southern Coastal (SC), Southern Mixed (SM), Transitional (T), Northern Stratified (NS) and Northern Coastal (NC). The black line represents the linear regression curve for all the data points.

Table 5.8 Regression analysis of TEP_c (µmol l^{-1}) versus POC (µmol l^{-1}) and PON (µmol l^{-1}) concentrations in surface and bottom waters during summer 2015 in the five different regions of the North Sea: Southern Coastal (SC), Southern Mixed (SM), Transitional (T), Northern Stratified (NS) and Northern Coastal (NC).

Variable	Depth	Region	Regression	R^2	n	p-value
POC	**Surface**	All regions	y = 0.22x + 4.51	0.27	31	< 0.05
		NS	y =0.40x - 2.34	0.49	17	< 0.05
POC	**Bottom**	T	y = 0.18x + 4.26	0.94	9	< 0.001
PON	**Surface**	All regions	y = 6.26x - 1.11	0.36	31	< 0.001
		NS	y = 6.76x - 2.33	0.44	17	< 0.05
PON	**Bottom**	All regions	y = 5.30x + 0.36	0.46	34	< 0.001
		T	y = 3.55x + 1.98	0.61	9	< 0.05

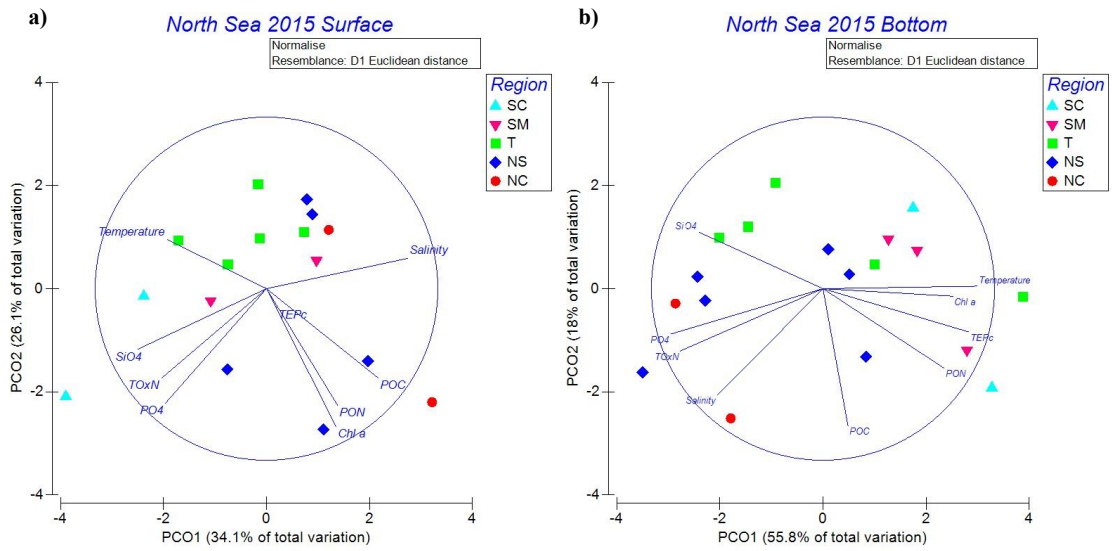

Figure 5.24 Principal coordinates plot (PCO) showing relationships between variables in the five different regions of the North Sea: Southern Coastal (SC), Southern Mixed (SM), Transitional (T), Northern Stratified (NS) and Northern Coastal (NC); in a) surface and b) bottom waters in the year 2015.

5.5.4 Box model 2015

Results from the box model for the year 2015 are summarised in Table 5.9. The SMLD in the stratified regions was ~ 30 meters depth. The water column depth ranged from 20 metres in the southern coastal region to 192 metres in the northern coastal region. The highest and lowest TEP_c formation rate were estimated in the northern coastal region (8.6 µmol l^{-1} d^{-1}) and in the transitional stratified region (4.2 ± 1.2 µmol l^{-1} d^{-1}) respectively. The export of TEP_c from the surface to the bottom of the water column ranged from 104.4 mmol m^{-2} d^{-1} in the southern coastal region to 429.8 mmol m^{-2} d^{-1} in the northern coastal region. The lowest and the highest sinking velocity of TEP_c was predicted in the southern coastal (9.6 m d^{-1}) and northern coastal region (23.9 m d^{-1}). Accumulation of TEP_c below the mixed layer deep in the stratified regions ranged from 3 µmol l^{-1} d^{-1} in the northern coastal region to 3.2 ± 1.1 µmol l^{-1} d^{-1} in the transitional stratified region. The residence time of TEP_c ranged from 1.7 days in the Northern Coastal region to 3.3±1.1 days in the Northern Stratified region. As in the section 5.4.4 the application of the bacterial remineralization factor of 0.08 d^{-1} did not have a significant impact on TEP_c flux, nor in the sinking velocity of TEP_c. By contrast the bacterial remineralization factor of 0.53 d^{-1} produced an increase in the loss of TEP_c, with a consequent net decrease in TEP_c flux and sinking velocity of TEP_c.

Table 5.9 Table summarising the results from the box model describing the fate of TEP_c and fluxes in the North Sea in stratified and mixed waters for the year 2015 in the five regions of the North Sea: Southern Coastal (SC), Southern Mixed (SM), Transitional (T), Northern Stratified (NS) and Northern Coastal (NC). $[\boldsymbol{TEP_c}]_{\boldsymbol{SML}}$ - TEP_c concentration in the SML (µmol l^{-1}), $\boldsymbol{TEP_{c\,form}}$ - TEP_c formation rate in the SML (µmol l^{-1} d^{-1}), $\boldsymbol{TEP_{c\,exp}}$ - TEP_c export flux (mmol m^{-2} d^{-1}), $\boldsymbol{sink_{SML}}$ - TEP_c sinking rate at the SML (m d^{-1}), $[\boldsymbol{TEP_c}]_{\boldsymbol{BML}}$ -TEP_c concentration in the BML (µmol l^{-1}), $\boldsymbol{TEP_{c\,acc}}$ - potential accumulation rate of TEP_c in the BML (µmol l^{-1} d^{-1}) without bacterial uptake, $\boldsymbol{TEP_{c\,res}}$ - TEP_c residence time (d), $\boldsymbol{TEP^b_{c\,upt}}$ - TEP_c loss due to bacterial uptake (mmol m^{-2} d^{-1}), $\boldsymbol{sink_{bott}}$ - potential TEP_c sinking rate without bacterial uptake (m d^{-1}), $\boldsymbol{sink^b_{bott}}$ - potential TEP_c sinking rate with bacterial uptake (m d^{-1}).

Region	Area	$[TEP_c]_{SML}$	$TEP_{c\,form}$	$TEP_{c\,exp}$	$sink_{SML}$	$[TEP_c]_{BML}$	$TEP_{c\,acc}$	$TEP_{c\,res}$	$TEP^b_{c\,upt}$*	$TEP^b_{c\,upt}$**	$sink_{bott}$	$sink^b_{bott}$*	$sink^b_{bott}$**	SMLD	W_{depth}
SC	Mixed (1)	10.8	5.2	104.4	9.6	-	-	-	0.8	55.3	-	9.5	4.5	-	20
SM	Mixed (8)	12 ± 3.3	5.7 ± 1.5	200.4 ± 58.7	17.8 ± 7.6	-	-	-	1.6 ± 0.4	106.2 ± 31.1	-	17.7 ± 7.5	8.4 ± 3.5	-	37 ± 15.6
T	Stratified (18)	8.7 ± 2.5	4.2 ± 1.2	126 ± 51.7	14.5 ± 4	5.8 ± 0.7	3.2 ± 1.1	1.9 ± 0.5	1 ± 0.4	66.8 ± 27.8	21.6 ± 9.6	21.5 ± 9.5	10.2 ± 4.5	29.9 ± 8.4	70.9 ± 25.7
NS	Stratified (17)	11.2 ± 5.6	5.4 ± 2.6	160 ± 73.3	14.9 ± 3.7	6.1 ± 1.1	2.1 ± 1.1	3.3 ± 1.1	1.8 ± 0.6	84.8 ± 38.8	26.2 ± 10.7	26 ± 10.6	12.3 ± 5	30.9 ± 7.7	110.1 ± 26.8
NC	Stratified (1)	18	8.6	429.8	23.9	5.2	3	1.7	3.4	227.8	82.2	81.5	38.6	50	192

* TEP_c degradation rate by bacteria similar to that of semi-refractory POC, $\boldsymbol{P^b = 0.008\ (d^{-1})}$, (Fujii *et al.*, 2002)
** TEP_c degradation rate by bacteria similar to that of a generic carbohydrate, $\boldsymbol{P^b = 0.53\ (d^{-1})}$, (Mari *et al.*, 2017)
( ) Number of stations in the specific region
(mean value ± standard deviation)

5.6 TEP incubation experiments

5.6.1 Method

During the survey in the year 2015 onboard incubation experiments were conducted by James Fox (University of Essex). Seawater samples were collected from different regions across the North Sea in order to obtain a representative sample of the phytoplankton community for the North Sea. Samples were taken from the underway non-toxic seawater supply (~ 4 metres depth) onboard, filtered through a 200 μm mesh in order to remove mesozooplankton (Sieburth *et al.*, 1978; Calbet, 2008) and placed into an acid washed 25 litre polycarbonate (Nalgene) carboy. From this start point (0 h) samples were taken for TEP, chlorophyll *a* and inorganic nutrient concentration determinations. For each treatment 5 litres of this water was spiked with nutrients, added alone and in combination, at concentrations of F/2 algal growth medium (8.82 x 10^{-4} M $NaNO_3$, 3.62 x 10^{-5} M NaH_2PO_4, 1.06 x 10^{-4} M Na_2SiO_3; Guillard, 1975). Treatments were divided in (Figure 5.23) treatment one (N + P + Si) comprised of nitrogen (N), silica (Si) and phosphorus (P) addition, as well as F/2 trace metals and vitamins. Treatment two also contained P, Si, vitamins and metals, but no N. Treatment three consisted of only N addition. Following nutrient spiking, water was distributed into 1.2 L polycarbonate (Nalgene) bottles, sealed and placed in an on-deck incubator. Bottles were incubated for a period of 48 h at 20% surface irradiance and cooled by surface seawater. At end point (48 h) samples were taken for TEP analysis. In-between experiments all bottles and sampling equipment were thoroughly rinsed and acid-washed. An Orion 3-star benchtop pH metre (Thermo Scientific, USA) was used to measure the pH of all treatment bottles at the start (0 h) and end (48 h) of all experiments and no significant changes were recorded. TEP samples were collected in triplicate and analysed at UEA laboratory following the method described in sections 2.2 and 2.6. Chlorophyll *a* and nutrient concentrations at the starting point (0 h) were collected and analysed by James Fox at the University of Essex. No information on the chlorophyll *a* and nutrient concentrations is available for the end point (48 h) of each bioassay.

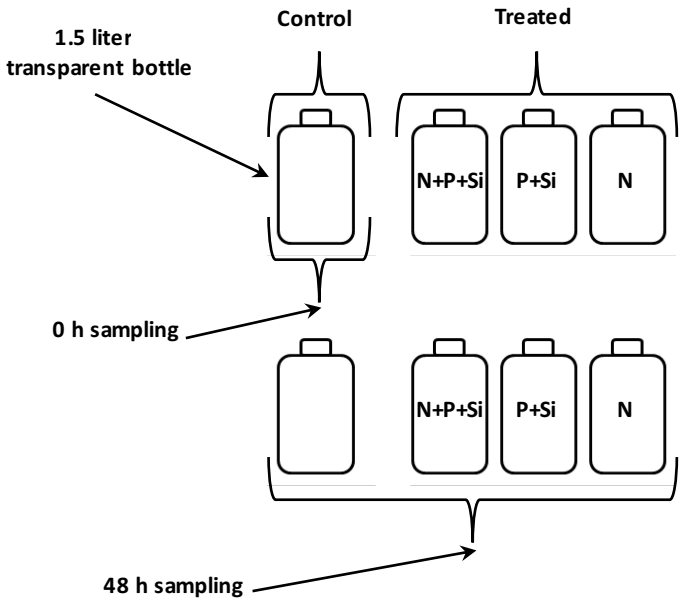

Figure 5.25 Scheme of the on-deck incubation experiment conducted in the North Sea in the year 2015. Three different treatments were used: (N + P + Si) comprised of nitrogen, phosphorus and silica, (P + Si) comprised of phosphorus and silica and (N) comprised of only nitrogen.

5.6.2 Results

Results from the four incubation experiments are reported in Figure 5.25 and summarised in Table 5.10. The addition of nutrients clearly stimulated the production of TEP_c in respect to the control at the end (48 h) of the incubation experiments. Treatment two (P + Si) showed the highest concentration of TEP_c at the end point (48 h) during experiments one, two and three. Treatment three (N) at the end point (48 h) had the lowest concentration of TEP_c in all four experiments. Nevertheless, it was higher in all four experiments with respect to the control. These results suggest that the addition of phosphorus and silica might have created an imbalance in the available nutrients. This led to a consequent increase of TEP_c production in 48 h. This may be explained by the fact that in all the experiments (Figure 5.26 and Table 5.10) nitrogen was limiting to phytoplankton from the beginning of the experiment due to an N : P ratio < of 16 in the water sample (Table 5.10). The addition of phosphorus and silica, but not nitrogen by increasing the imbalance in the nutrient ratio enhanced the release of TEP_c. The lower concentration of TEP_c in treatment two for experiment four (Figure 5.26d) might be explained by the fact that it was the only sample where nitrogen at the beginning of the experiment was higher in respect to the other experiments (Table 5.10). In contrast the addition of only nitrogen may have caused an inhibition of TEP_c production.

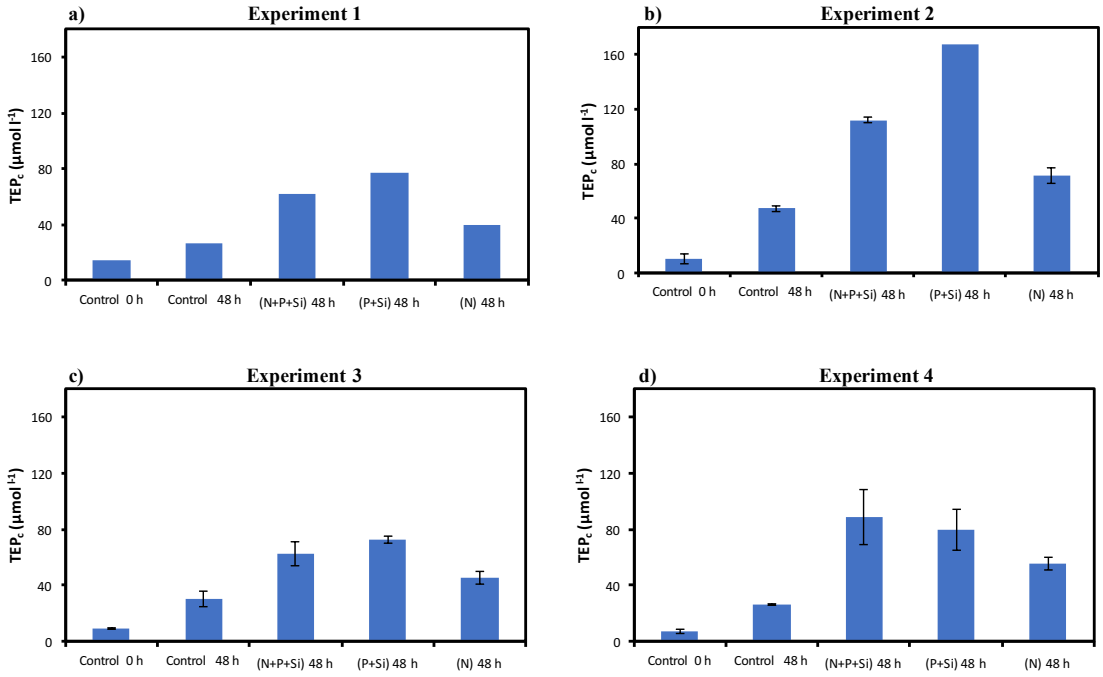

Figure 5.26 Plots of TEP_c (µmol l^{-1}) concentrations in the four experiments (a, b, c and d) at starting point control 0 h and after 48 h for the control and the three different treatments: (N + P + Si) comprised of nitrogen, phosphorus and silica, (P + Si) comprised of phosphorus and silica and (N) comprised of only nitrogen.

Incubation experiments where specific nutrients were added to a natural phytoplankton community are well documented in literature and show a relationship between nutrient limitation and the concentration of nutrient (Moore *et al*., 2013). A lack of nutrient may cause stress (physiological response to nutrient limitation), deficiency (alteration of the elemental stoichiometry N : P = 16) and nutrient co-limitation (lack of two or more nutrients all necessary to phytoplankton growth) in a phytoplankton community. This affects the growth rate of phytoplankton cells and phytoplankton yield (Moore *et al*., 2013) and may stimulate phytoplankton to release of TEP. Even though no information of chlorophyll *a* and nutrient concentrations is available for the end point (48 h) of each bioassay, the results highlighted that nutrient limitation is not the only mechanism that enhance the release of TEP by phytoplankton. Several other processes may be also implicated in the mechanism that release TEP (e.g. the co-limitation of one or two nutrients or a secondary response from phytoplankton due to the addition of a nutrient).

Table 5.10 Table summarising the results of the four different incubation experiments in the North Sea in year 2015. Location of the sample (latitude and longitude), temperature (ºC), salinity, chlorophyll *a* (µg l^{-1}), nitrate (NO_3), phosphate (PO_4), silicate (SiO_4) and TEP_c (µmol l^{-1}) at starting point 0 h. TEP_c concentrations after 48 h for control and the three different treatments: (N +P + Si) comprised of nitrogen, phosphorus and silica, (P + Si) comprised of phosphorus and silica and (N) comprised of only nitrogen.

Experiment	Latitude	Longitude	Temperature	Salinity	Chlorophyll	NO_3	PO_4	SiO_4	TEP_c control 0 h	TEP_c control 48h	TEP_c (N + P + Si) 48h	TEP_c (P + Si) 48h	TEP_c (N) 48h
1	52.68º N	4.18º E	18.11	34.86	0.68	0.43	0.13	0.64	14.8	26.9	62.9	77.1	39.8
2	55.65º N	7.18º E	17.12	32.72	0.88	0.48	0.06	1.41	10.4 ± 3.4	47.2 ± 2.4	112 ± 1.6	166.9	71.4 ± 5.7
3	59.18º N	3.35º E	14.62	34.35	0.31	0.34	0.05	0.25	9.6 ± 0.5	30.4 ± 5.4	62.1 ± 8.4	72.7 ± 2.4	46 ± 4.5
4	59.05º N	2.10º W	12.10	35.05	0.55	2.44	0.32	1.10	7.3 ± 1.2	26.2 ± 0.7	88.67 ± 19.2	79.6 ± 14.2	55.7 ± 4.7

(mean value ± standard deviation)

5.7 Seasonal cycle of TEP

5.7.1 Method: TEP sample collection and analysis

In the year 2015 TEP samples were collected during cruises servicing the SmartBuoy. Samples of TEP were collected from three different SmartBuoy sites (Figure 5.27): West Gabbard (51.94º N, 2.10º E), Warp (51.50º N, 1.03º E) and Dowsing (53.53º N, 1.05º E). Samples were obtained using a Niskin bottle and the Cefas SmartBuoy. A Cefas SmartBuoy is a floating buoy equipped with instruments to provide high frequency measurements of physicochemical parameters (e.g. temperature, salinity, fluorescence etc.) of the surface seawater (~ 1 m depth). It is also equipped with an autonomous water sampler, which at regular time steps take samples of seawater and preserves them in bags prefilled with a saturated solution of mercuric chloride (Johnson *et al.*, 2013). TEP samples from the Niskin were processed onboard, as described in section 2.2 and later analysed in the UEA laboratory as described in section 2.6. Bags of seawater from the SmartBuoys were provided by Cefas and analysed at UEA following the same protocol used for the sample collected with the Niskin. Chlorophyll *a* data was provided by Cefas and analysed as described in Greenwood *et al.* (2010).

Figure 5.27 Map showing the location of the SmartBuoy sites: West Gabbard, Warp and Dowsing along the UK coast (Cefas, 2018).

5.7.2 Results

The SmartBuoy sites exhibit the highest concentrations of TEP_c of the North Sea. All three sites showed similar concentrations in surface and bottom waters in each season with a lower TEP_c concentration during spring and summer, in respect to winter (Figure 5.28). Those comparable TEP_c concentrations in surface and bottom waters were determined by the physicochemical characteristics of the water column (well mixed area). West Gabbard and Warp (Figure 5.28a, b) showed high concentrations of TEP_c in February and November 2015, which may be attributed to riverine inputs from the Thames and Scheldt/Rhine. Alternatively, TEP_c could have been resuspendend from sediments during winter storms due to the shallow water column and the well-mixed water column. Dowsing (Figure 5.28c) had the lowest TEP_c concentration in surface and bottom waters, which might be explained by the fact that it receives waters from the North Atlantic though a southward transport along the east coast of the UK. This causes rapid biological processes during summer time (Johnson *et al.*, 2013) that could have removed TEP from the water column. Samples collected with Niskin do not always agree with the samples collected from SmartBuoy (Figure 5.29). This was further investigated with a TEP aggregation experiment described in section 5.7.2.1. The maximum TEP_c concentration value at the SmartBuoy sites was recorded in surface waters in October 2015 for Warp (Figure 5.29b), which is closer to the maximum concertation of TEP_c observed in the Ross Sea in spring (Hong *et al.*, 1997). West Gabbard TEP_c showed a decoupling with chlorophyll *a* in surface waters (Figure 5.30), which has been observed in culture experiments (Kahl *et al.*, 2008).

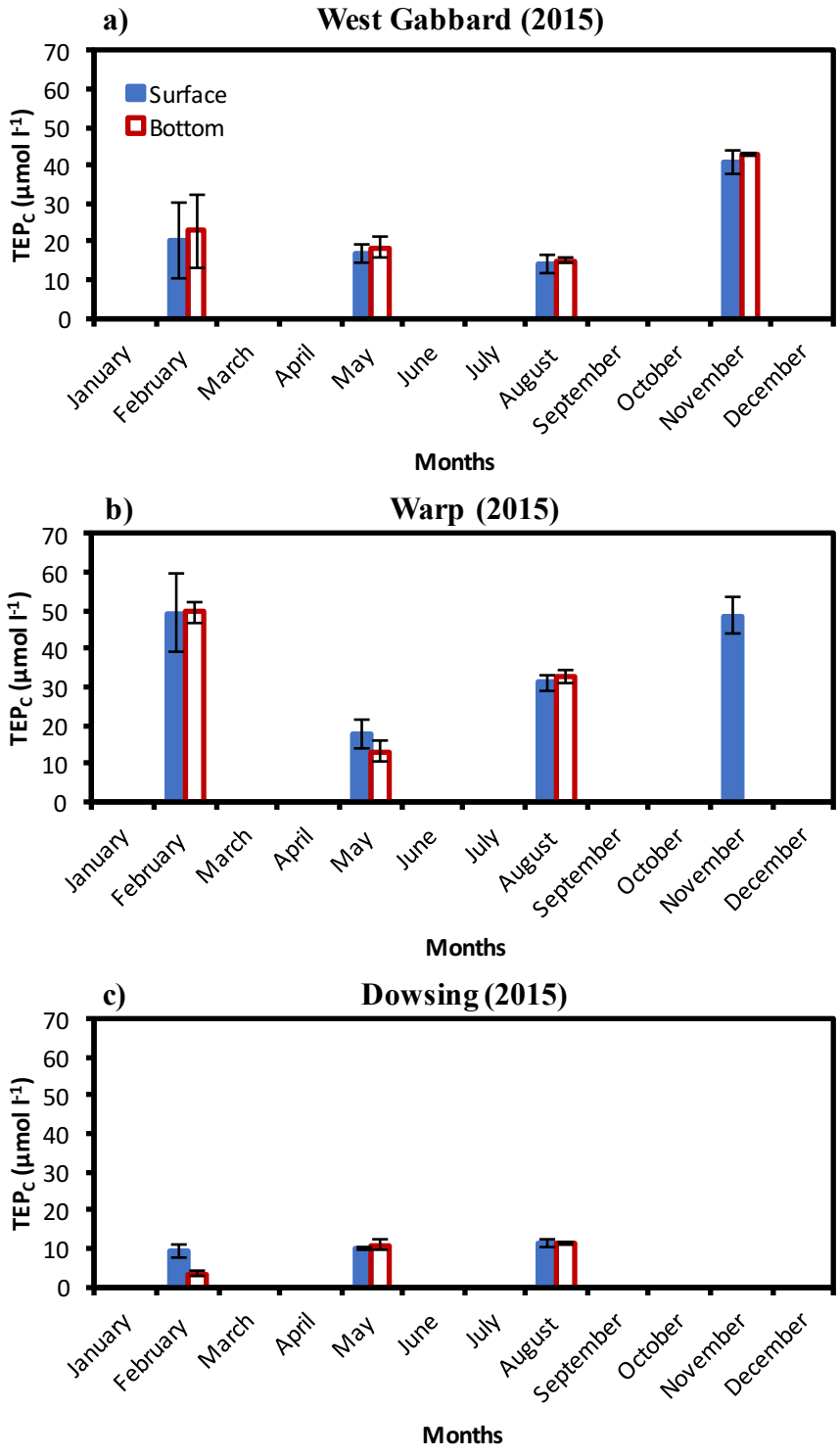

Figure 5.28 Seasonal cycle of TEP_c concentration (µmol l^{-1}) collected with Niskin bottle (4 m depth) at three different Smartbuoy sites, a) West Gabbard, b) Warp and c) Dowsing in surface and bottom waters in the year 2015.

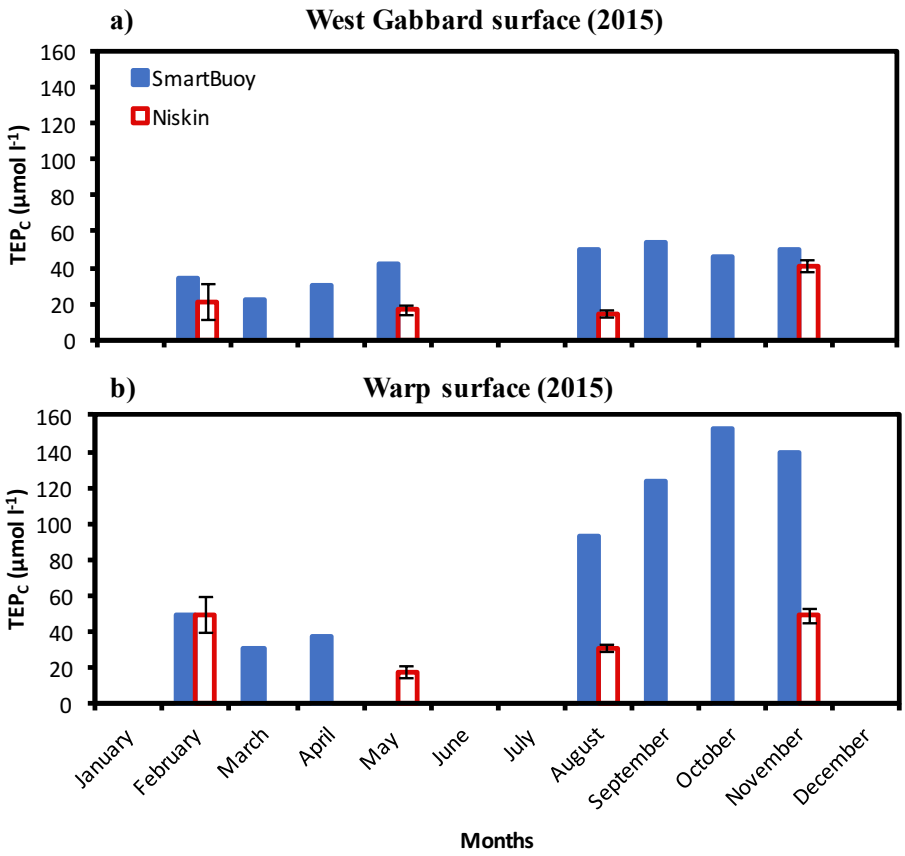

Figure 5.29 Seasonal cycle of TEP_c concentration (µmol l^{-1}) at the SmartBuoy sites, a) West Gabbard, b) Warp and in surface waters in the year 2015. Comparison between samples of TEP_c collected with the Niskin bottle (4 m depth) and from the SmartBouy (~ 1 m depth).

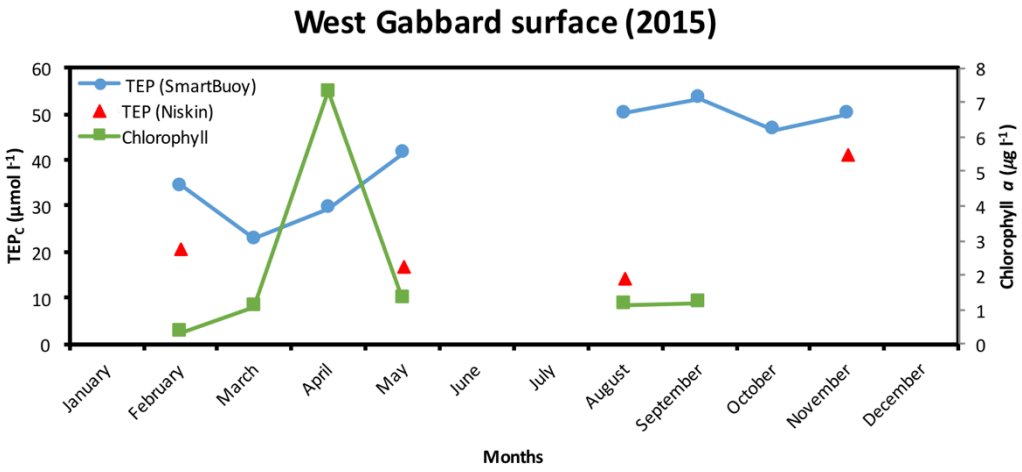

Figure 5.30 Seasonal cycle of TEP_c (µmol l^{-1}) and chlorophyll *a* (µg l^{-1}) concentrations at the SmartBuoy site West Gabbard in surface waters in the year 2015. Comparison between samples of TEP_c (collected with the Niskin bottle and from the SmartBuoy) with chlorophyll *a*.

5.7.2.1 SmartBuoy bag testing

To investigate the differences found between the samples of TEP collected with the Niskin bottle and the samples collected by the SmartBuoy, three experiments were undertaken. It was hypothesized that the higher concentration showed by the sample collected by the SmartBuoy, in respect to that collected with the Niskin could be attributed to the aggregation process of the TEP precursor in the SmartBuoy bag during the months (1 - 3 months) after water collection, due to the wave motion of the SmartBuoy in the sea. To test this hypothesis the same plastic bags used in the SmartBuoy (provided by Cefas) were filled with a sample of seawater previously spiked with a saturated mercuric chloride solution and placed on a shaker for different periods of time to reproduce wave motion and enhance TEP aggregation processes. In order to exclude any interference or alteration produced by the addition of mercuric chloride to the sample a subsample was taken before and after the addition of the preservative and used as a reference. Previously mercuric chloride had been tested as a suitable method to preserve TEP sample (section 2.10.6).

5.7.2.2 Method and results

Seawater (20 litres) was collected from Sheringham beach (59.94º N, 1.21º E) on 1st July 2016. 300 ml of that seawater was analysed in triplicate to determine TEP concentration. The remaining seawater was preserved with saturated mercuric chloride solution (32 g of $HgCl_2$ in 1 L H_2O) (Johnson *et al.*, 2013) and used to fill 250 ml plastic bags to carry out the three different experiments. In the first experiment (Figure 5.31a) the bags were horizontally placed in a shaker, agitated at the speed of 100 RPM and sampled at the beginning of the experiment (0 h) and after 12, 24, 48 and 168 hours. In the second experiment (Figure 5.31b) the speed was reduced to 50 RPM, the bags were placed vertically and sampled after 12 and 24 hours from the starting point. In the third experiment (Figure 5.31c) the bags were placed in a rotatory shaker at two different speeds, 5 and 10 RPM and sampled after 48 hours and one month. Due to a lack of information on the aggregation of TEP in preserved seawater a variety of approaches and durations were used to cover a spectrum of possible aggregation mechanisms. The three experiments gave similar results. Treatments were close to the reference indicating no further aggregation had occurred. However, experiment one showed lower TEP_c concentration in all the treatments in respect to that of the reference, which may be related to the high speed used (100 RPM). This might have produced the opposite effect of

breaking up TEP particles. During flocculation experiments in the laboratory with phytoplankton cultures or seawater with wild phytoplankton, TEP is produced from the coagulation of TEP precursors released by phytoplankton (Passow, 2000). This is achieved by producing a laminar shear which enhance particle aggregation. The fact that the three experiments did not show an increase in TEP_c concentration may be explained by the use of a preservative, that by killing microorganism in the sample did not allow the production of TEP precursors and the increase of TEP concentration. In contrast in culture experiments there is a continuous release of TEP precursors, which can coagulate to form TEP. Furthermore, it is quite likely that in the sample of seawater used in those experiments precursors where already aggregated in the form of TEP.

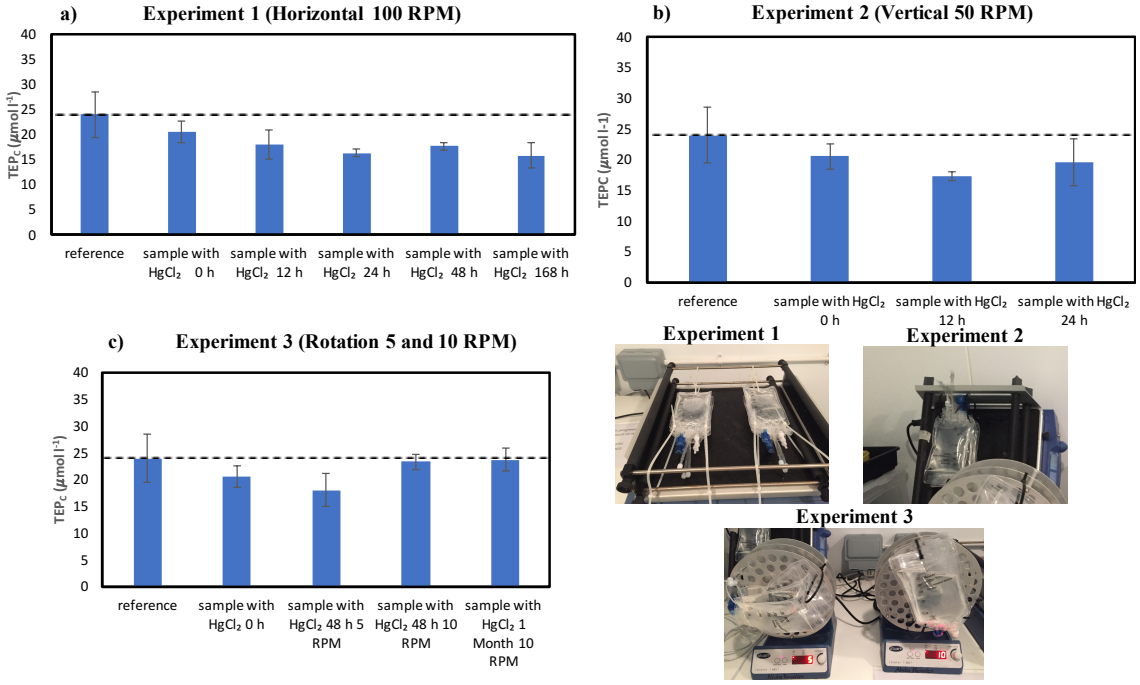

Figure 5.31 TEP_c concentrations (µmol l^{-1}) during the SmartBuoy bag testing experiments. Three experiments: a) experiment 1 reference and sample treated with $HgCl_2$ placed in a horizontal shaker and agitated from 0 h to 168 h at 100 RPM (Revolutions Per Minute); b) experiment 2 reference and sample treated with $HgCl_2$ placed in a vertical shaker and agitated from 0 h to 24 h at 50 RPM; c) experiment 3 reference and sample treated with $HgCl_2$ placed in a rotation shaker and agitated from 0 h to 48 h at 5 and 10 RPM and up to a month at 10 RPM.

5.8 Discussion

Spatial and temporal distribution of TEP

This study is the first attempt to investigate the spatial and temporal distribution and the role of TEP in the North Sea. A single modelling study conducted in the North Sea showed that summers are characterized by an excess of DIC uptake (~ 40 µmol kg^{-1}),

without a corresponding nutrient uptake (Prowe *et al.*, 2009). This phenomenon, called carbon overconsumption (Toggweiler, 1993; Thomas *et al.*, 1999; Koeve, 2005) has been associated with the formation of TEP. This study observed an average concentration of TEP_c of ~ 10 µmol l^{-1} in summers 2014 and 2015 in surface and bottom waters, which is close and may explain the DIC overconsumption (~ 40 µmol kg^{-1}) predicted for the North Sea in summer by Prowe *et al.* (2009).

In the North Sea in the two years of the survey TEP_c showed concentrations ranging from 1.8 µmol l^{-1} to 35.8 µmol l^{-1} in surface waters and from 4.5 µmol l^{-1} to 34.4 µmol l^{-1} in bottom waters. However, samples of TEP collected from Cefas SmartBuoy had much higher concentrations in surface waters reaching ~ 100 µmol l^{-1} in August 2015 and a maximum of ~ 160 µmol l^{-1} in October 2015 at the Warp site. Those concentrations are in line with the one reported in literature for comparable areas. In 2015 TEP_c exhibited a background concentration of ~ 5 µmol l^{-1} in respect to the 2014, which might be liked to an interannual variability in DOC due to the accumulation of DOC on the shelf between years (Chaichana, 2017). This accumulation of DOC may lead to the formation of TEP from abiotic processes and explain why appears to be a background concentration of TEP_c in 2015 but not in 2014. In both years surface and bottom TEP_c were correlated with higher TEP_c concentrations in surface waters with respect to that of the bottom waters. The variation in the concentration of TEP_c in surface and bottom waters was correlated positively with latitude and negatively with longitude, which might be explained by the hydrodynamic characteristics of the North Sea of a shallow southern region and a seasonally stratified northern region (Thomas *et al.*, 2004). TEP_c concentrations in surface and bottom waters between the two years of the survey demonstrated statistically significant positive correlation ($R^2 = 0.13$ $p = 0.001$ $n = 74$ and $R^2 = 0.25$ $p = < 0.001$ $n = 62$ respectively; Figure 5.32). The North Sea showed strong interannual variation in TEP_c concentrations in coastal regions, which was driven by the presence of specific annual algal blooms (i.e. the algal boom along the Dutch coast in the year 2014 and the algal bloom along the Scottish coast and near the Shetland Isles in the year 2015).

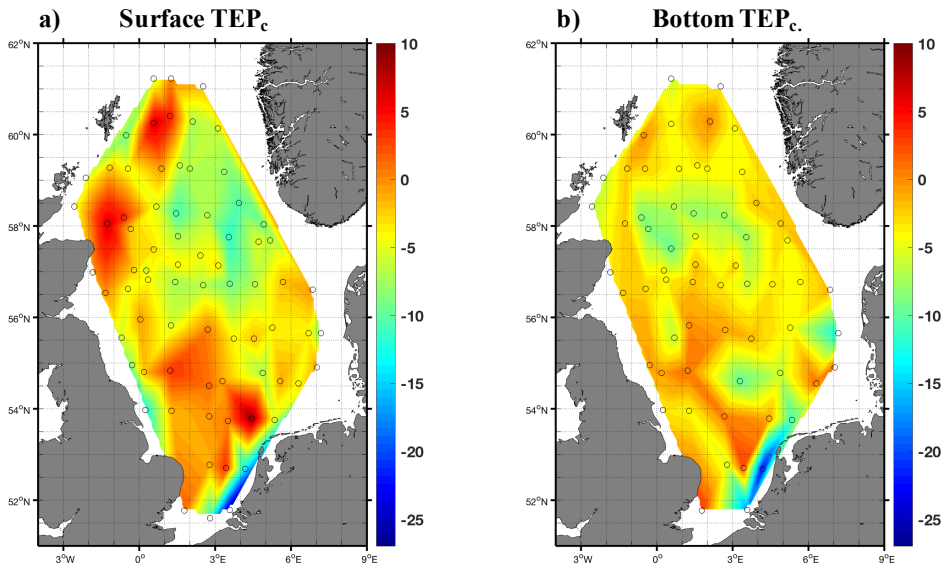

Figure 5.32 Spatial distribution of TEP_c concentration (µmol l^{-1}) differences in a) surface and b) bottom waters in the North Sea between summer 2015 and 2014.

The phytoplankton community in the northern North Sea is often nutrient limited (Lenhart et al., 2004). Coastal regions of the southern North Sea have a high input of nutrients due to mixing, (responsible for organic matter resuspension from the sediment) along with river input. Despite this high nutrient input, the high concentrations of suspended matter determine light limited conditions for the phytoplankton (Lenhart *et al.*, 2004) resulting in an extracellular release of TEP by phytoplankton with a significant source of dissolved organic carbon (DOC) (Aluwihare *et al.*, 1997). This may explain the higher concentrations of TEP found in the coastal regions of the North Sea in both 2014 and 2015. High TEP concentrations have often been observed during diatom blooms (Passow and Alldredge, 1994; Passow and Alldredge, 1995; Grossart *et al.*, 1997; Mari and Burd, 1998; Passow *et al.*, 2014), as well as during blooms dominated by dinoflagellates (Alldredge *et al.*, 1998). The southern North Sea along the Netherlands coast, shows two areas with a specific phytoplankton taxonomic composition: a coastal area dominated by diatoms during the whole year and an offshore area dominated by dinoflagellates during the summer and autumn. In recent years, especially in coastal areas, a change in the phytoplankton taxonomic composition has been observed, with an increase in the dominance of dinoflagellates during summer (Alvarez-Fernandez and Riegman, 2014). The results of this study showed highest TEP_c concentrations associated with the algal bloom of the dinoflagellate *Karenia mikimotoi* in the year 2014. In the same year a further algal bloom associated with high TEP_c productions was detected along the Netherlands

coast. The year 2015 showed high TEP_c concentrations in surface waters along the Scottish coast and near the Shetland Isles were also associated to algal blooms.

Physico-chemical factors controlling TEP distribution

Seasonal stratification or mixing of the water column may be responsible for the vertical and spatial distribution of TEP across the whole North Sea. Moreover, high TEP concentrations have been reported in the presence of a salinity gradient, which might increase the formation of TEP (Passow, 2002; Radić *et al.*, 2005). However, the gradient of salinity recorded in the northern coastal region in the year 2014 was not associated with high TEP concentrations.

With phytoplankton being the most likely source of TEP (Passow *et al.*, 2001; Passow, 2002), a direct relationship between TEP and chlorophyll *a* concentrations might be expected (Passow and Alldredge, 1995; Ramaiah and Furuya, 2002; Wurl and Holmes, 2008; Ortega-Retuerta *et al.*, 2009). Nevertheless, several studies reported a temporal or spatial decoupling between TEP and chlorophyll *a* concentrations with a negative relationship (Garcia, 2002; Corzo *et al.*, 2005). For instance, Malpezzi *et al.* (2013) observed a positive correlation between TEP and chlorophyll *a* concentrations at Chesapeake Bay in the year 2007. However, no clear relationship was found in 2008. During an algal bloom chlorophyll *a* can be used as a reliable predictor of TEP production (Passow *et al.*, 2001). However, since TEP production by phytoplankton is highly variable and influenced by a variety of factors including: the physiological state of phytoplankton (Passow and Alldredge, 1995) , the environmental conditions (Hong *et al.*, 1997), species composition (Passow and Alldredge, 1994) and turbulence (Passow, 2002), phytoplankton biomass could be a poor indicator of TEP production. Furthermore, a study conducted in the NW Mediterranean Sea suggested that TEP can be predicted from chlorophyll *a* concentration on a horizontal scale (Ortega-Retuerta *et al.*, 2017). In this study, a clear relationship between TEP_c and chlorophyll *a* was found on a spatial scale in surface and bottom waters in 2014 and 2015. However, looking at the five different regions of the North Sea it is evident that the southern mixed region in the year 2014 (surface and bottom) and the transitional and northern stratified regions in the year 2015 (surface and bottom) dominated the TEP_c to chlorophyll *a* relationship. This indicates that the TEP_c/Chlorophyll *a* relationship is quite variable and generally depends on the spatial scale. Therefore, this relationship cannot be used as a reliable indicator of TEP production.

According to several experimental studies TEP is mainly released during nutrient limitation (Mari *et al.*, 2005; Ortega-Retuerta *et al.*, 2010; Pedrotti *et al.*, 2010; Ortega-Retuerta *et al.*, 2017). However, is not clear how nutrient stoichiometry affects TEP production (Gärdes *et al.*, 2012). Ortega-Retuerta *et al.* (2010) reported a negative correlation between TEP and phosphorus concentrations in the NW Mediterranean Sea. In this study only in 2015 in the North Sea was found a negative correlation between TEP_c and PO_4 in bottom waters. Usually phosphate is limiting to phytoplankton productivity only when it is lower than 0.06 μmol l^{-1} (Moll, 1998; Johnson *et al.*, 2013). In the two years of the survey most of the time PO_4 in surface waters was lower than 0.06 μmol l^{-1}. No correlation was found between TEP_c and NO_3. This might be explained by the fact that the North Sea is a nitrogen limited system and NO_3 in surface waters was quite low (~ 0.3 μmol l^{-1}). Nitrogen limitation in the North Sea was confirmed by the Redfield stoichiometry (N : P = 16 : 1). The N : P ratio in surface waters in both years was below 16, making the North Sea nitrogen limited (Moore *et al.*, 2013). Furthermore, TEP incubation experiment showed that when nitrogen is limiting to primary production or when there is an imbalance in the available nutrients, phytoplankton increases the release of TEP. Negative correlations were found between TEP_c and SiO_4 in the North Sea in surface and bottom waters in 2014 and in bottom waters in 2015, which were not linked to riverine influences. The positive correlation found between TEP_c and the POC and PON in surface and bottom water supported the hypothesis that TEP is an extra source of sinking carbon. However, TEP being a carbon rich compound a positive relationship with POC : PON ratio would be expected. This study did not show clear evidence of that. In this study, the contribution of TEP to the pool of POC in the North Sea might have been underestimated. Indeed GF/F filters used for POC sampling only retain ~ 50% of TEP (Passow and Alldredge, 1995).

TEP seasonal cycle in the year 2015, showed high concentrations of TEP in winter at the SmartBuoy sites: West Gabbard and Warp. This high TEP during winter time could in part be explained by riverine inputs from the Thames and Scheldt/Rhine that during winter storms may have transported TEP previously produced in rivers or TEP precursors to the SmartBuoy sites. Another explanation of this may be that during winter storms, due to the shallow water column and the well-mixed water masses TEP or TEP precursors could be re-suspended in the water column from sediments. Despite the estimated residence time of TEP in the North Sea waters is days, the SmartBuoy sites are located in

an area where a continuous supply of TEP may occur from terrestrial inputs even during the absence of *in situ* phytoplankton blooms. These results reinforced the evidence that TEP distribution is controlled by environmental factors.

Processes controlling TEP dynamics

In the marine environment TEP dynamics is controlled by several processes such as formation rate, residence time, turnover and sinking which depend on POC concentration, UV radiation, microbical activity (Wurl *et al.*, 2011), TEP_c age and its chemical composition (Passow, 2002). TEP residence time in seawater has been reported to be variable, ranging from 0.3 to 34 days (Wurl *et al.*, 2011). This seems linked to the nature of the aggregates containing TEP. For instance, aggregates containing TEP produced by diatoms have a residence time of more than 11 days and bacteria may produce aggregates containing TEP with an even longer residence time (Piontek *et al.*, 2009). The North Sea showed a residence time of TEP ranging from a minimum of 1.9 ± 1.2 days in the transitional region to a maximum of 4.2 ± 1.9 days in the northern coastal in 2014 and from a minimum of 1.7 days in the northern coastal region to a maximum of 3.3 ± 1.1 days in the northern stratified region in 2015. The average residence time for the North Sea was 2.7 ± 1 days, which is about half of that estimated (4.6 days) in the North Pacific, offshore Hawaii and the Arctic Ocean from June 2009 to April 2010 (Wurl *et al.*, 2011). This indicates that in the North Sea TEP may be quickly consumed and/or exported from the surface water to the sediments.

An important fraction of TEP sinks in the form of aggregates (Newton *et al.*, 1994; Passow *et al.*, 2001). Therefore, it is of primary importance to estimate the export of TEP and its contribution to the total carbon export. Several studies have reported estimations of TEP flux. For instance in the Santa Barbara Channel the estimation of the sedimentation rate of TEP_c at 500 m ranges from 0.54 to 5.4 mmol C m^{-2} d^{-1}, with a contribution of ~ 30 % to the flux of POC (Engel and Passow, 2001). Flux of TEP_c in a North Norwegian Fjord at 100 m depth reached a maximum of 32 mmol C m^{-2} d^{-1} (Reigstad and Wassmann, 2007). However, no information is available on TEP flux in the North Sea. Therefore, in this study the results from the box model were compared with the Primary Production (PP) estimated for the North Sea in other studies. Average PP in the North Sea in summer has been reported to be 75 mmol C m^{-2} d^{-1}, reaching 10.8 mol C m^{-2} during three months of summer (Fernand *et al.*, 2013). In this study the North Sea showed similar TEP export in all the five regions and in the two different years. The

estimation of TEP export had a high uncertainty. The box model results estimated a TEP export of ~ 0.2 mol C m^{-2} d^{-1} for the North Sea and an export of ~ 28 mol C m^{-2} for three months in summer. That was about three times higher than the PP reported for the North Sea in previous studies. This huge discrepancy could be determined by different factors, such as the relationship extrapolated from Wurl *et al.* (2011) used to estimate the formation rate of TEP in this study, the assumption that all TEP produced in surface is exported, difficulty in quantifying the loss of TEP due to bacterial and zooplankton consumption and/or the steady state assumption used in this analysis which may not be applicable to the North Sea. TEP export estimated in 2014 was consistent with the export estimated in 2015, but both values are an overestimation of the real export of TEP for the North Sea. Another challenge that the scientific community is facing is the determination of the sinking rate of aggregates containing TEP. A few studies have reported some values and related assumptions, ranging from upward sinking velocity of aggregates containing TEP (Mari *et al.*, 2017) to modelling the aggregates containing TEP sinking rate in the euphotic zone (10 m d^{-1}; Oguz, 2017b), to aggregates smaller than 500 μm with a sinking velocity of 4 to 42 m d^{-1} (Kriest, 2002). Aggregates containing TEP in the North Sea showed a similar sinking velocity between regions and years with an average of ~ 15 m d^{-1}, which is in line with the sinking velocities reported in literature.

5.9 Conclusions

The distribution of TEP was mapped for the first time in the North Sea. TEP_c concentrations observed in summers 2014 and 2015 in the North Sea may explain the overconsumption of dissolved inorganic carbon observed during summer in the North Sea. The results indicated that elevated TEP production occurs during algal blooms, i.e. the bloom of the dinoflagellate *Karenia mikimotoi* observed in 2014 along the UK coast. The results also highlighted that in the coastal areas of the southern North Sea, where the phytoplankton community in summer was dominated by the dinoflagellates *Karenia mikimotoi* in 2014, TEP production was comparable to that of diatoms.

A clear relationship between TEP_c and chlorophyll *a* concentrations was found within this study in areas of the North Sea, southern mixed region (surface and bottom waters) in 2014 and in transitional and northern stratified regions (surface and bottom) in 2015, but not in the other regions within the North Sea. However, due to the high variability of the TEP/Chlorophyll *a* relationship, this study supported evidence that phytoplankton

biomass cannot be used as a suitable indicator of TEP production, as it strongly depends on the physiological state of phytoplankton, as well as being affected by a wide range of physico-chemical and biological variables.

TEP sinking rate estimated from the observations suggested that TEP was likely in the form of large sinking aggregates. This study highlighted that TEP export is high and may account for a considerable fraction of the total exported carbon. It was not clear how nutrient stoichiometry affects TEP production, results suggested that nutrient limitation and other environmental factors were responsible for high TEP production in the North Sea. This high TEP production seems to be associated with carbon overconsumption and may enhance the efficiency of the Continental Shelf Pump (CSP) for the export of organic carbon to the seafloor, making the North Sea more efficient in the sequestration of atmospheric CO_2 and the export of carbon from the shelf to the Atlantic Ocean.

Chapter 6 Discussion and synthesis

6.1 Introduction

The main aim of this research was to investigate the role played by TEP in carbon cycling in NW European shelf seas. To this end, cruise surveys and experimental-modelling approaches have been used. This last chapter summarises and discusses the main findings in relation to the research hypotheses and objectives stated in section 1.9.3. Furthermore, suggestions for further research are presented.

6.2 TEP in the NW European shelf seas: evaluation of the hypotheses

Hypothesis 1: *Transparent exopolymer particles are produced in situ in shelf seas as a by-product of phytoplankton productivity and will therefore have similar spatial and temporal patterns as primary productivity and related variables, e.g. chlorophyll.*

In this study the spatial and temporal distribution of TEP in the NW European shelf seas was investigated in two different systems (North Sea and Celtic Sea). The Celtic Sea is a system characterised by a low river input, with waters reaching 200 m depth and a primary production during the stratified period ranging from 16 to 32 mmol m^{-2} d^{-1} (Hickman *et al.*, 2012) with an average of ~24 mmol m^{-2} d^{-1}. In contrast, the North Sea is a more complicated system characterised by two different regions, a shallow southern region (<50 m) affected by terrestrial and anthropogenic nutrient inputs, with a permanently mixed water column throughout the year (Emeis *et al.*, 2015) and a northern seasonally stratified region, influenced by Atlantic waters (Emeis *et al.*, 2015), with a net export of particulate organic matter and nutrient to the deeper layers (Thomas *et al.*, 2004). The North Sea during summer exhibits a primary production of 75 mmol m^{-2} d^{-1}, which is ~ 3 times higher than that of the Celtic Sea. In the North Sea TEP_c concentration was ~ 4 times higher than that of the Celtic Sea, which is consistent with the idea that higher primary production would lead to higher TEP production. This finding reinforces the evidence of a link between primary production and the production of TEP and its abundance in the euphotic zone and in coastal seas in comparison to the open ocean (Passow and Alldredge, 1994; Engel and Passow, 2001).

Due to the complexity of the North Sea, with its northern stratified and southern mixed regions, five regions with different properties were identified in the data collected during this study: a Southern Coastal region (SC), a Southern Mixed region (SM), a Transitional region (T), a Northern Stratified region (NS) and a Northern Coastal region (NC). Concentrations of TEP_c detected during this study in the two shelf seas, in bottom and surface waters are shown in Figure 6.1.

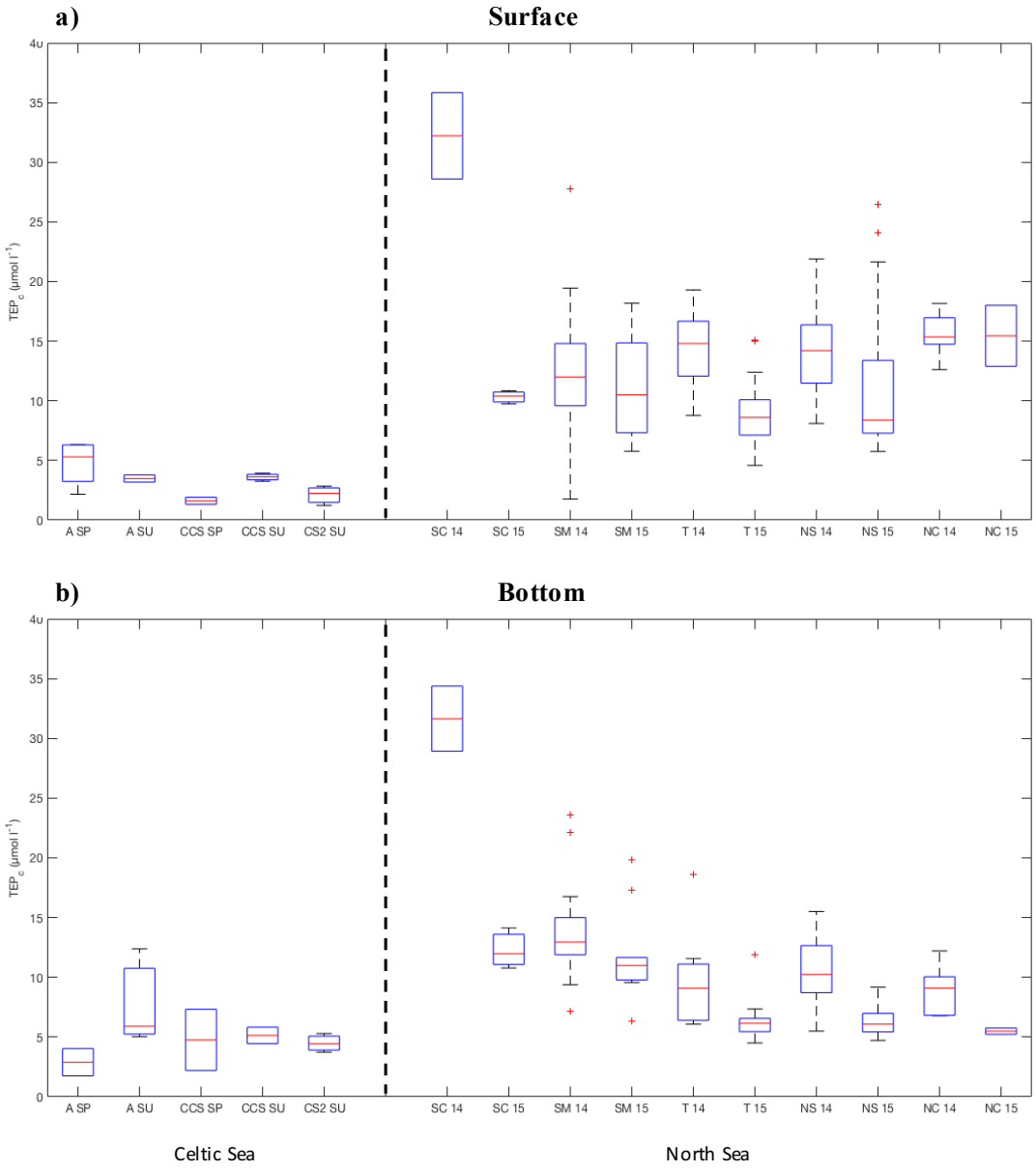

Figure 6.1 Box and whisker plots of TEP_c (µmol l^{-1}) concentrations in a) surface and b) bottom waters in the Celtic Sea and the North Sea. Celtic Sea three stations: Station A in spring (A SP) and summer (A SU), Station CCS in spring (CCS SP) and summer (CCS SU), Station CS2 in summer (CS2 SU) in the year 2015. For the North Sea five different regions are shown: Southern Coastal (SC), Southern Mixed (SM), Transitional (T), Northern Stratified (NS) and Northern Coastal (NC) in the year 2014 and 2015. The box indicates the lower to the upper quartile. The horizontal line within the box represents the median. The whiskers indicate the lower and higher data points. The red crosses indicate outliers. The outliers were classified as two times the interquartile range from the median.

The North Sea in summer 2014 and 2015 showed concentrations of TEP_c in surface and bottom waters much higher (12.5 ± 5.1 μmol l^{-1} and 9.8 ± 4.7 μmol l^{-1}, respectively) compared to that of the Celtic Sea (3.3 ± 1.5 μmol l^{-1} and 5.2 ± 2.7 μmol l^{-1}, respectively) in spring and summer 2015. In addition, the North Sea was characterised by higher variability in TEP_c concentrations between the five different regions. This was attributed to environmental factors which controlled the TEP_c distribution on a regional scale in the two years of the survey (i.e. temperature, salinity, water circulation, river inputs) (section 5.8). Furthermore, seasonal stratification or mixing of the water column may be the major factor responsible in controlling the vertical and spatial distribution of TEP_c across the North Sea (section 5.8). Similarly, TEP_c in the Celtic Sea was associated with a salinity gradient from the coast to the shelf break (section 4.2.2). The annual cycle of TEP_c at SmartBuoy sites showed the highest TEP_c concentrations found during this research (e.g. 153 μmol l^{-1} of TEP_c at Warp in October 2015). TEP_c concentrations were high in winter in respect to that in summer, which may be explained by riverine inputs from the Thames and Scheldt/Rhine or resuspension and aggregation of TEP precursors (section 5.7.2).

In this study two different pathways have been hypothesized to be responsible for the production of TEP in shelf seas. In the first pathway TEP is produced during phytoplankton primary production. This was evident in coastal areas of the North Sea where phytoplankton blooms were observed, and in spring in the Celtic Sea where nutrients were not limiting to primary production. The highest TEP concentrations in the North Sea were seen in phytoplankton blooms (section 5.4.2 and 5.5.2) and in coastal areas (section 5.4.2 and 5.7.2). A statistically significant relationship is seen between chlorophyll and TEP concentrations over the North Sea which is dominated by the high TEP concentrations in productive areas (section 5.4.3 and 5.5.3), all of which supports the idea that primary productivity is related to TEP production. This has also been established in several studies where high TEP concentration has been associated with phytoplankton blooms (Passow and Alldredge, 1994; Kozlowski *et al.*, 1995; Passow *et al.*, 1995; Riebesell *et al.*, 1995; Mari and Kiørboe, 1996; Grossart *et al.*, 1997; Hong *et al.*, 1997; Alldredge *et al.*, 1998; Mari and Burd, 1998; Passow *et al.*, 2001). In the second pathway TEP production is linked to nutrient limitation. Nutrient limitation is another factor that may be responsible for the increase in TEP production via overflow production of carbon-rich TEP precursors, in the absence of nutrients required for the synthesis of compounds useful to the phytoplankton (e.g. Prowe *et al.*, 2009). It seems that when phytoplankton are nutrient limited there is a consequent increase in the release of

extracellular polysaccharides (i.e. TEP precursors) (Myklestad, 1995). High TEP concentrations in summer associated with low nutrients were observed in the northern stratified region of the North Sea and in summer in the Celtic Sea. In the Celtic Sea, TEP concentrations were higher in summer compared to spring, and incubation experiments indicated that nutrient stoichiometry and an imbalance between nutrients have a direct effect on the production of TEP, supporting the hypothesis that summer TEP production was controlled by the lack of nutrient availability (section 5.6.2)

The two proposed mechanisms for TEP production are opposing conditions, which may occur under different environmental conditions and involve different phytoplankton communities. For instance, coastal areas of the North Sea are areas of high primary production, characterised by terrestrial and riverine inputs of nutrients which may lead to the development of a specific phytoplankton community dominated by diatoms and *Phaeocystis pouchetii* (Reid *et al.*, 1990). On the contrary, the northern stratified region of the North Sea and Celtic Sea are seasonal stratified areas in summer where nutrient concentrations in surface waters may become limiting. This may promote the development of a specific summer phytoplankton community. For instance diatoms and coccolithophores are dominant in the Celtic Sea during late spring (Van Oostende *et al.*, 2012) and diatoms and flagellates are dominant in summer in the northern stratified region of the North Sea (Reid *et al.*, 1990). Due to the different environmental conditions and the different phytoplankton communities, TEP produced under each scenario may have a different composition, lability and stickiness. Nevertheless, it is not clear how nutrient stoichiometry affects TEP production (Gärdes *et al.*, 2012). In both scenarios it seems that nutrients plays a role in the production of TEP.

In both the North Sea and the Celtic Sea a negative relationship between TEP and nutrient concentrations was observed. This was also confirmed in the TEP incubation experiments carried out in the North Sea during the survey in summer 2015. In both the North Sea and the Celtic Sea TEP was correlated to chlorophyll *a* only in specific areas (Celtic Sea in the Station CC2; North Sea in the southern mixed region in the year 2014, transitional and northern stratified region in the year 2015). Therefore, phytoplankton biomass on its own cannot be used as a suitable indicator of TEP production, as it strongly depends on the physiological state of phytoplankton, as well as a range of physicochemical and biological variables (nutrient levels, phytoplankton community composition, phytoplankton growth phase and turbulence).

During the two years of the survey in the North Sea high TEP concentrations linked to phytoplankton blooms were observed. In particular, the phytoplankton bloom observed in the year 2014 was related to a bloom of the dinoflagellate *Karenia mikimotoi* (Elisa Capuzzo, personal communication) . This is supported by the literature where high TEP concentrations have been found during diatom blooms (Passow and Alldredge, 1994; Passow and Alldredge, 1995; Grossart *et al.*, 1997; Mari and Burd, 1998) as well as during blooms dominated by dinoflagellates (Alldredge *et al.*, 1998).

Hypothesis 2: *Transparent exopolymer particles aggregate into large particles that sink out, leading to export of carbon-rich POC. Aggregates containing TEP composition and size can substantially affect the quality, quantity, degradation and sinking of the exported carbon.*

TEP itself cannot sink because its density is less than that of seawater (from 700 to 840 kg m^{-3}) (Azetsu-Scott and Passow, 2004). It can act as a glue (Passow, 2002a) and promote the formation of fast sinking aggregates (Mari *et al.*, 2017). The buoyancy/sinking of aggregates containing TEP depends on their density, which depends on the ratio of TEP to other particles (of different density) in the aggregate (Engel and Schartau, 1999; Azetsu-Scott and Passow, 2004a; this study). Mari *et al.* (2017) suggested that an increase in the production of TEP might determine a decrease of the downward flux, or in the case of very high TEP production may lead to an upward flux that extends the residence time of aggregates containing TEP in surface waters (Azetsu-Scott and Passow, 2004a) and delays their sinking (Mari *et al.*, 2017). In this study the residence time of TEP was estimated with the use of a simple box model. The North Sea and Celtic Sea showed a residence time of TEP comparable to that reported in the literature (from 0.3 to 34 days; Wurl *et al.*, 2011). However, in the North Sea the residence time of TEP (2.7 ± 1 days) was about half of that estimated for the Celtic Sea (5.2 days), which indicates that in the North Sea TEP may be more quickly consumed and/or exported from the surface water to the bottom.

Given that, it is of primary importance to estimate the sinking rate aggregates and the effect of TEP on it. Few studies have attempted to quantify the effect of TEP on sinking rates, but it has been argued that high proportions of TEP in aggregates can lead to buoyant aggregates (Mari *et al.*, 2017). A modelling study estimated that small marine

aggregates with a size < 500 μm have a sinking velocity from 4 to 42 m d^{-1} (Kriest, 2002). Furthermore, another modelling study used a sinking rate of 10 m d^{-1} to model the dynamics of aggregates containing TEP (Oguz, 2017). This research attempted to estimate a likely sinking rate of aggregates containing TEP in the shelf seas. To this end independent approaches were used in the North Sea and Celtic Sea. The North Sea showed a similar sinking velocity between regions and years with an average of ~ 15 m d^{-1}. A comparable result found for the Celtic Sea, where the sinking velocity was on average of ~ 16 m d^{-1}. In spite of the high uncertainty in the calculation of the sinking rates of aggregates containing TEP, the independent approaches were in generally good agreement. This value of approximately 15 m d^{-1} may be considered representative of the sinking rate of aggregates containing TEP in shelf seas. However, it is inconsistent with the predictions of Mari *et al.* (2017), which estimated that summer aggregates are buoyant due to the high ratio of TEP (more of 5%) to other particles in the aggregates.

Hypothesis 3: *TEP production and associated carbon overconsumption occurs in summer when the phytoplankton community is nutrient limited. The effect increases the quantity of sinking carbon and therefore increases the efficiency of the continental shelf pump. By consequence, TEP should play a substantial role in controlling air-sea CO_2 flux in shelf seas.*

The new formulation developed to describe TEP dynamics in ERSEM was used in the Celtic Sea to investigate the fate of carbon exported due to TEP and the potential effect of TEP on the marine carbon cycle in terms of CO_2 uptake, carbon sequestration and C : N stoichiometry of the organic matter. In the Celtic Sea TEP increased the carbon and nutrient export from the water column to the sediments. This determined a consequent increase of the benthic respiration of ~30%. Increases in benthic respiration can be explained by observed decreases in DIC in surface waters, caused by the lesser primary production respired back to the water column. A reduction in surface DIC concentrations should lead to an increase of the CO_2 flux from the atmosphere into the sea. However, this effect may be partially balanced by the reduced GPP due to reduced nutrients in the model through greater export of fixed carbon and nutrients to the benthos. The TEP model in ERSEM does not produce realistic results and cannot be used in prognostic mode as it moves the model away from the state where it is optimized to agree with observations. As the TEP scheme has such a significant effect on primary production and free wintertime nutrient levels in the model, this indicates the potentially significant role that

TEP may play in the carbon cycle in temperate shelf. The increase of the benthic respiration suggested that TEP as a source of extra sinking organic carbon, may have a very important role in the biological shelf sea carbon pump. Without TEP the system would remineralise more material in the water column, resulting in higher nitrate concentrations and less drawdown of CO_2. A peak of TEP_c concentrations observed in surface waters with low NO_3 concentrations, supported the hypothesis of carbon overconsumption. TEP_c increased the export of carbon-rich POC with a higher C : N ratio. In the literature it has been reported that TEP has a C : N ratio exceeding 20, which is above the Redfield ratio (Engel and Passow, 2001; Mari *et al.*, 2001). Sinking POC in the BML showed a high C : N ratio, reaching a maximum of 30 indicating that TEP_c may have accounted for ~ 65% of the total exported POC. The export of high C : N material may be a key process in maintaining an effective carbon pump in shelf seas (Humphreys *et al.*, 2018) and this is a potential mechanism that has not previously been considered.

6.3 The role of other factors in controlling TEP dynamics

The modelling work presented in this thesis assumes that TEP is produced in surface waters and consequently exported. As with previous studies (Wurl *et al.*, 2011; Mari *et al.*, 2017) it was assumed here that production of TEP by phytoplankton, the composition and the density of aggregates containing TEP and bacterial degradation of TEP are the major factors that may control TEP dynamics. However, it is possible that other factors play a role in controlling TEP dynamics, in particular in the production, consumption and export of TEP. Those factors may be related to photodegradation of TEP in the Surface Microlayer (Mari *et al.*, 2017), specific phytoplankton community (e.g. differential production of TEP by different phytoplankton communities) (Passow and Alldredge, 1994; Passow and Alldredge, 1995; Grossart *et al.*, 1997; Alldredge *et al.*, 1998; Mari and Burd, 1998), production of TEP by bacteria (Schuster and Herndl, 1995; Stoderegger and Herndl, 1999; Passow, 2002b; Sugimoto *et al.*, 2007; Koch *et al.*, 2014), injection of air bubbles in surface waters due to wind speed (Wurl *et al.*, 2011; Mari *et al.*, 2017) and possible resuspension of TEP buried in sediments (this study).

For instance, the box model approach used in this study considers that all TEP produced in surface waters is eventually exported in form of aggregates containing TEP. However, another study has predicted that especially during periods of high TEP production the aggregates formed by TEP may be buoyant, extending their residence time in surface

waters (Mari *et al.*, 2017). An extension of the residence time of aggregates containing TEP in surface waters may reduce the amount of the TEP exported due to two processes that may occur in surface waters: the consumption of TEP by bacteria and the photodegradation of TEP by UV-B radiation in the Surface Microlayer. These processes were not considered in this study. This might in part explain the discrepancy found in this study between the observed primary production and the export rate of TEP predicted by the steady state box model applied to the Celtic Sea and North Sea datasets.

To account for the retention versus export of aggregates containing TEP the approach used in ERSEM and in the TEP aggregation model, assumes that the TEP produced in the surface waters aggregates with other particles, forming two different types of aggregates containing TEP: sinking aggregates and floating aggregates. Furthermore, the formation of aggregates containing TEP in ERSEM is supposed to be driven by the stickiness of TEP, which triggers the formation of aggregates containing TEP. However, other factors may need to be considered in the aggregation process of TEP such as the age of TEP, which has been reported to be associated with the stickiness of TEP, the particle size and the rate of collision between TEP and other particles (Mari *et al.*, 2017). For instance, old TEP is less sticky, this reduces the capability of TEP to aggregate solid particles and may have a negative effect on the formation of aggregates containing TEP. The rate of collision and the size of particles might be other key factors that drive the aggregation process of TEP (Mari *et al.*, 2017), which could be taken in to account in future modelling studies.

The specific phytoplankton community may be another key factor in controlling TEP dynamics due to the fact that in different periods of the year and in different locations the phytoplankton community is dominated by different phytoplankton groups (e.g. diatoms), which release different amounts of TEP. For instance, the dominance of a particular species in the phytoplankton community and the environmental conditions may play a key role in TEP production. In this research, the phytoplankton taxonomy was not investigated, however, a sample of seawater collected in the North Sea in 2014 by Cefas for phytoplankton taxonomy revealed high TEP concentrations associated with a phytoplankton bloom dominated by the dinoflagellate *Karenia mikimotoi*. Whilst there are a number of other factors requiring further study (e.g. production of TEP by bacteria, injection of air bubbles in surface waters due to wind speed and possible resuspension of

TEP buried in sediments), the factors considered in this study are likely to be the primary drivers of TEP dynamics.

6.4 Further research

To improve our understanding of the dynamics of TEP in shelf seas, future research is needed in the following areas:

Observations

Improvement of the method of TEP analysis is needed to obtain quantitative data, improve accuracy and make the analysis quicker, easier and more reliable. This could be in part achieved by using the TEP photographic method presented as part of this research. This new method does not improve data accuracy, however, it makes the analysis quicker and avoids the use of hazardous concentrated solution of sulfuric acid. Furthermore, a better way to convert TEP in TEP carbon content (TEP_c) is needed. Another challenge is to quantify the fraction of TEP_c in the pool of POC due to the evidence that TEP is not retained quantitatively on the standard GF/F filters used for POC determination (Passow and Alldredge, 1995). For instance, in this study the fraction of TEP_c in the pool of POC was estimated by subtracting the TEP_c concentration from the total POC concentration. The POC samples used in this research were collected as part of the Cefas POC sampling programme, therefore it was not possible to use a different filter from the standard GF/F glass fiber filter. Furthermore, it is not possible to use other filters (e.g. polycarbonate filter) than the standard GF/F glass fiber filter for POC determination due to the fact that the method involves the combustion of the filter at a high temperature. In order to get a valuable dataset it is also necessary to include TEP in routine monitoring programmes to obtain high-frequency data.

ERSEM

The next step in ERSEM would be to improve the processes used in the current TEP formulation. For instance, at present the aggregation process considers that floating aggregates once generated due to mixing and particle collision can further aggregate, forming higher density particles heavy enough to sink. This process is implicitly used by assuming that every day a fraction of the sinking aggregates becomes “heavy enough” to sink. In future research this will require the development of a specific process that links the floating and sinking aggregate pools. Another important step to improve the model

would be the introduction of other processes that control TEP dynamics, such as production of TEP by bacteria and the consumption of TEP due to zooplankton grazing. These two processes are not very well studied and documented. For instance, bacteria produce extracellular polymeric substances (EPS) (Decho, 1990), which might contribute to the total TEP production (Schuster and Herndl, 1995; Stoderegger and Herndl, 1999; Passow, 2002; Sugimoto *et al.*, 2007; Koch *et al.*, 2014). Another way that TEP can be removed from the surface waters is due to bacterial remineralization (a process already included in the model). Several studies have reported the capability of bacteria to colonise TEP (Alldredge *et al.*, 1993; Passow and Alldredge, 1994; Schuster and Herndl, 1995; Mari and Kiørboe, 1996) and a linear positive relationship between TEP and the alpha and beta glucosidase activity of bacteria has been observed (Smith *et al.*, 1995). However, the specific degradation rate of TEP is still unknown due to the practical difficulty of separating formation, degradation and the transformation of TEP by bacteria (Mari *et al.*, 2017). The only information available is from a study conducted on extracellular particulate carbohydrates (in part TEP) released by phytoplankton, which has shown a degradation rate due to bacterial remineralization of 0.53 d^{-1} that is much higher than that of POC (0.25 d^{-1}) (Harvey *et al.*, 1995; Mari *et al.*, 2017). Furthermore, zooplankton grazing on phytoplankton might indirectly affect TEP in the water column by removing its main producer (phytoplankton). ERSEM has a fixed sinking velocity for aggregates containing TEP. In the future ideally it would be better to have a variable sinking velocity calculated by the model as a function of the density of the aggregates and that of the seawater. To make predictions of TEP (e.g. concentrations, export and dynamics), it would be necessary to assess the skill of the TEP model against different TEP datasets. It is of primary importance to make predictions on TEP on a spatial scale and to cover a considerable portion of the sea, such as the North Sea. This could be achieved by taking this formulation to the next level with a 3D model to get a spatial distribution of TEP.

TEP in the aggregation model

A limitation in the TEP aggregation model was the uncertainty in the estimation of the composition of aggregates containing TEP, in particular the fraction of the minerals in the aggregates. In future research the collection of Total Suspended Solid (TSS) samples may provide a better estimation of the inorganic fraction of the aggregates containing TEP. This would substantially reduce the uncertainty in the model and would make this modelling approach a tool to predict the fate of TEP in the marine environment.

6.5 Conclusions

This research has addressed the role of TEP in carbon cycling by focusing on processes in surface waters and the potential export of aggregates containing TEP. The crucial role that TEP plays in the aggregation of particles is well known. However, there is a lack of information on the mechanisms of how TEP drives the aggregation process and affects the retention time in surface waters and sinking velocity of particles (Mari *et al.*, 2017). This study has demonstrated that TEP can play a potentially significant role in carbon cycling and export in shelf seas, where its concentration is high relative to the open ocean. In particular the main findings of this study are:

- The average concentration of TEP of ~ 10 μmol l^{-1} observed in both summers (2014 and 2015) in surface and bottom waters in the North Sea is consistent with the overconsumption of ~ 40 μmol kg^{-1} of DIC predicted for the North Sea in summer by Prowe *et al.* (2009). For instance, given a lifetime of TEP of a few days a continuous TEP production would be needed to maintain this concentration.
- Higher concentrations of TEP are associated with coastal areas where riverine inputs, nutrient inputs and phytoplankton blooms play a key role in the production of TEP.
- The linear positive relationship between TEP and chlorophyll *a* found in this study in specific locations indicates that this relationship strongly depends on multiple factors (e.g. physiological state of phytoplankton, physical, chemical and biological conditions).
- The ratio of TEP to other particles in aggregates may be a key factor in controlling the sinking or floating of aggregates containing TEP.
- Despite the uncertainties associated with the analysis, the results indicate that the sinking rate of aggregates containing TEP maybe in the order of 10 to 15 m d^{-1}.
- Nutrient stoichiometry and imbalance between nutrients have a direct effect on TEP production, although the mechanism is not clear. This is consistent with the idea of TEP production during phytoplankton blooms, under conditions of nutrient limitation and associated carbon overconsumption.

Furthermore, the simple modelling exercises used as part of this research illustrate that small changes in the production or degradation of TEP and its fraction in aggregates containing TEP would potentially affect the sinking of particles and therefore this would have an impact on benthic respiration, carbon export and nutrient balance in shelf seas. This is a potential key feature of shelf sea carbon cycling that has not previously been studied. However, the inherent uncertainties associated with TEP analysis, and the uncertainties in the results of model output are significant. Therefore, further study is essential to better understand the biogeochemical role of TEP in the marine carbon cycle. For instance, a more in-depth understanding of how environmental changes affect TEP production and its chemical composition is needed to improve modelling and understanding of carbon cycling in shelf seas. This information is critical to elucidating the role TEP in the shelf sea carbon cycle under future climate change scenarios.

References

Aldridge, J.N., Lessin, G., Amoudry, L.O., Hicks, N., Hull, T., Klar, J.K., Kitidis, V., McNeill, C.L., Ingels, J., Parker, E.R. and Silburn, B. (2017) Comparing benthic biogeochemistry at a sandy and a muddy site in the Celtic Sea using a model and observations. *Biogeochemistry* **135**: 155–182.

Alldredge, A.L. (1979) The chemical composition of macroscopic aggregates in two neretic seas. *Limnol Oceanogr* **24**: 855–866.

Alldredge, A.L., Passow, U., and Haddock, H.D. (1998) The characteristics and transparent exopolymer particle (TEP) content of marine snow formed from thecate dinoflagellates. *J Plankton Res* **20**: 393–406.

Alldredge, A.L., Passow, U., and Logan, B.E. (1993) The abundance and significance of a class of large, transparent organic particles in the ocean. *Deep Sea Res Part I Oceanogr Res Pap* **40**: 1131–1140.

Alonso-González, I.J., Arístegui, J., Lee, C., Sanchez-Vidal, A., Calafat, A., Fabrés, J., Sangrá, P., Masqué, P., Hernández-Guerra, A. and Benítez-Barrios, V. (2010) Role of slowly settling particles in the ocean carbon cycle. *Geophys Res Lett* **37**.

Aluwihare, L.I., Repeta, D.J., and Chen, R.F. (1997) A major biopolymeric component to dissolved organic carbon in surface sea water. *Nature* **387**: 166.

Alvarez-Fernandez, S., and Riegman, R. (2014) Chlorophyll in North Sea coastal and offshore waters does not reflect long term trends of phytoplankton biomass. *J sea Res* **91**: 35–44.

Anderson, L.A., and Sarmiento, J.L. (1994) Redfield ratios of remineralization determined by nutrient data analysis. *Global Biogeochem Cycles* **8**: 65–80.

Armstrong, R.A., Peterson, M.L., Lee, C., and Wakeham, S.G. (2009) Settling velocity spectra and the ballast ratio hypothesis. *Deep Sea Res Part II Top Stud Oceanogr* **56**: 1470–1478.

Arrigo, K.R. (2005) Marine microorganisms and global nutrient cycles. *Nature* **438**: 122.

Arrigo, K.R. (2007) Carbon cycle: marine manipulations. *Nature* **450**: 491.

Asper, V.L. (1987) Measuring the flux and sinking speed of marine snow aggregates. *Deep Sea Res Part A Oceanogr Res Pap* **34**: 1–17.

Azetsu-Scott, K., and Passow, U. (2004a) Ascending marine particles: Significance of transparent exopolymer particles (TEP) in the upper ocean. *Limnol Oceanogr* **49**: 741–748.

Banse, K. (1974) On the interpretation of data for the carbon to nitrogen ratio of phytoplankton1. *Limnol Oceanogr* **19**: 695–699.

Baretta, J.W., Ebenhöh, W., and Ruardij, P. (1995) The European regional seas ecosystem model, a complex marine ecosystem model. *Netherlands J Sea Res* **33**: 233–246.

Barrón, C., and Duarte, C.M. (2015) Dissolved organic carbon pools and export from the coastal ocean. *Global Biogeochem Cycles* **29**: 1725–1738.

Bauer, J.E., Cai, W.J., Raymond, P.A., Bianchi, T.S., Hopkinson, C.S., and Regnier, P.A.G. (2013) The changing carbon cycle of the coastal ocean. *Nature* **504**: 61.

Bauer, J.E., and Druffel, E.R.M. (1998) Ocean margins as a significant source of organic matter to the deep open ocean. *Nature* **392**: 482.

Bauer, J.E., Druffel, E.R.M., Wolgast, D.M., and Griffin, S. (2001) Sources and cycling of dissolved and particulate organic radiocarbon in the northwest Atlantic continental margin. *Global Biogeochem Cycles* **15**: 615–636.

Behrenfeld, M.J., O'Malley, R.T., Siegel, D.A., McClain, C.R., Sarmiento, J.L., Feldman, G.C., Milligan, A.J., Falkowski, P.G., Letelier, R.M. and Boss, E.S. (2006) Climate-driven trends in contemporary ocean productivity. *Nature* **444**: 752.

Belderson, R.H., and Stride, A.H. (1966) Tidal current fashioning of a basal bed. *Mar Geol* **4**: 237–257.

Biddanda, B.A., and Pomeroy, L.R. (1988) Microbial aggregation and degradation of phytoplankton-derived detritus in seawater. I. Microbial succession. *Mar Ecol Prog Ser* 79–88.

Biermann, A., Engel, A., and Riebesell, U. (2014) Changes in organic matter cycling in a plankton community exposed to warming under different light intensities. *J Plankton Res* **36**: 658–671.

Bijma, J., Pörtner, H.-O., Yesson, C., and Rogers, A.D. (2013) Climate change and the oceans–What does the future hold? *Mar Pollut Bull* **74**: 495–505.

Blackford, J.C., Allen, J.I., and Gilbert, F.J. (2004) Ecosystem dynamics at six contrasting sites: a generic modelling study. *J Mar Syst* **52**: 191–215.

Borges, A. V, Delille, B., and Frankignoulle, M. (2005) Budgeting sinks and sources of CO_2 in the coastal ocean: Diversity of ecosystems counts. *Geophys Res Lett* **32**.

Boyd, P.W., Jickells, T., Law, C.S., Blain, S., Boyle, E.A., Buesseler, K.O., Coale, K.H., Cullen, J.J., De Baar, H.J., Follows, M. and Harvey, M. (2007) Mesoscale iron enrichment experiments 1993-2005: synthesis and future directions. *Science* **315**: 612–617.

Boyd, P.W., and Trull, T.W. (2007) Understanding the export of biogenic particles in oceanic waters: Is there consensus? *Prog Oceanogr* **72**: 276–312.

Bozec, Y., Thomas, H., Elkalay, K., and Baar, H.J.W. de (2005) The continental shelf pump for CO_2 in the North Sea—evidence from summer observation. *Mar Chem* **93**: 131–147.

Brickman, D., and Loder, J.W. (1993) Energetics of the internal tide on northern Georges Bank. *J Phys Oceanogr* **23**: 409–424.

Brockmann, U.H., Laane, R., and Postma, J. (1990) Cycling of nutrient elements in the North Sea. *Netherlands J Sea Res* **26**: 239–264.

Brown, J. (1991) The final voyage of Rapaiti: A measure of sea-surface drift velocity in relation to the surface wind. *Mar Pollut Bull* **22**: 37–40.

Brown, J., Carrillo, L., Fernand, L., Horsburgh, K.J., Hill, A.E., Young, E.F., and Medler, K.J. (2003) Observations of the physical structure and seasonal jet-like circulation of the Celtic Sea and St. George's Channel of the Irish Sea. *Cont Shelf Res* **23**: 533–561.

Bruland, K.W., and Silver, M.W. (1981) Sinking rates of fecal pellets from gelatinous zooplankton (salps, pteropods, doliolids). *Mar Biol* **63**: 295–300.

Burchard, H., Bolding, K., and Villarreal, M.R. (1999) *GOTM, a general ocean turbulence model: theory, implementation and test cases*. Space Applications Institute.

Burd, A.B., and Jackson, G.A. (2009) Particle aggregation. *Ann Rev Mar Sci* **1**: 65–90.

Burnett, W.C., Bokuniewicz, H., Huettel, M., Moore, W.S., and Taniguchi, M. (2003) Groundwater and pore water inputs to the coastal zone. *Biogeochemistry* **66**: 3–33.

Butenschon, M., Clark, J.R., Aldridge, J.N., Allen, J.I., Artioli, Y., Blackford, J.C., Bruggeman, J., Cazenave, P., Ciavatta, S., Kay, S. and Lessin, G. (2016) ERSEM 15.06: a generic model for marine biogeochemistry and the ecosystem dynamics of the lower trophic levels. *Geosci Model Dev* **9**: 1293–1339.

Calbet, A. (2008) The trophic roles of microzooplankton in marine systems. *ICES J Mar Sci* **65**: 325–331.

Cauwet, G. (2002) DOM in the coastal zone. *Biogeochem Mar dissolved Org matter*.

Cefas (2018) Marine monitoring interactive map. Available at http://wavenet.cefas.co.uk/Smartbuoy/Map on 1st December 2018.

Chaichana, S. (2017) Dissolved organic carbon and nitrogen in coastal waters. Doctoral dissertation, Ph.D. Thesis, School of Environmental Sciences, University of East Anglia, United Kingdom.

Chen, C.T.A., and Borges, A.V. (2009) Reconciling opposing views on carbon cycling in the coastal ocean: Continental shelves as sinks and near-shore ecosystems as sources of atmospheric CO_2. *Deep Sea Res Part II Top Stud Oceanogr* **56**: 578–590.

Chen, G., Ziemba, L.D., Chu, D.A., Thornhill, K.L., Schuster, G.L., Winstead, E.L., Diskin, G.S., Ferrare, R.A., Burton, S.P., Ismail, S. and Kooi, S.A. (2011) Observations of Saharan dust microphysical and optical properties from the Eastern Atlantic during NAMMA airborne field campaign. *Atmos Chem Phys* **11**: 723–740.

Chin, W.C., Orellana, M. V, and Verdugo, P. (1998) Spontaneous assembly of marine dissolved organic matter into polymer gels. *Nature* **391**: 568.

Chou, C., Stetzer, O., Weingartner, E., Jurányi, Z., Kanji, Z.A., and Lohmann, U. (2011) Ice nuclei properties within a Saharan dust event at the Jungfraujoch in the Swiss Alps. *Atmos Chem Phys* **11**: 4725–4738.

Christina, L., and Passow, U. (2007) Factors influencing the sinking of POC and the efficiency of the biological carbon pump. *Deep Sea Res Part II Top Stud Oceanogr* **54**: 639–658.

Ciais, P., Sabine, C., Bala, G., Bopp, L., Brovkin, V., Canadell, J., Chhabra, A., DeFries, R., Galloway, J., Heimann, M. and Jones, C. (2013) Carbon and Other Biogeochemical Cycles. In Climate change 2013: the physical science basis. Contribution of Working Group I to the Fifth Assessment Report of the Intergovernmental Panel on Climate Change 465–570. Cambridge University Press.

Claquin, P., Probert, I., Lefebvre, S., and Veron, B. (2008) Effects of temperature on photosynthetic parameters and TEP production in eight species of marine microalgae. *Aquat Microb Ecol* **51**: 1–11.

Corzo, A., Morillo, J.A., and Rodríguez, S. (2000) Production of transparent exopolymer particles (TEP) in cultures of *Chaetoceros calcitrans* under nitrogen limitation. *Aquat Microb Ecol* **23**: 63–72.

Corzo, A., Rodríguez-Gálvez, S., Lubian, L., Sangrá, P., Martínez, A., and Morillo, J.A. (2005) Spatial distribution of transparent exopolymer particles in the Bransfield Strait, Antarctica. *J Plankton Res* **27**: 635–646.

Culver, M.E., and Smith, W.O. (1989) Effects of environmental variation on sinking rates of marine phytoplankton. *J Phycol* **25**: 262–270.

Dam, H.G., and Drapeau, D.T. (1995) Coagulation efficiency, organic-matter glues and the dynamics of particles during a phytoplankton bloom in a mesocosm study. *Deep Sea Res Part II Top Stud Oceanogr* **42**: 111–123.

Decho, A.W. (1990) Microbial exopolymer secretions in ocean environments: their role (s) in food webs and marine processes. *Ocean Mar Biol Annu Rev* **28**: 73–153.

Dickson, A.G., Sabine, C.L., and Christian, J.R. (2007) *Guide to best practices for ocean CO_2 measurements.* North Pacific Marine Science Organization.

Diesing, M., Kröger, S., Parker, R., Jenkins, C., Mason, C., and Weston, K. (2017) Predicting the standing stock of organic carbon in surface sediments of the North–West European continental shelf. *Biogeochemistry* **135**: 183–200.

Druffel, E.R.M., Williams, P.M., Bauer, J.E., and Ertel, J.R. (1992) Cycling of dissolved and particulate organic matter in the open ocean. *J Geophys Res Ocean* **97**: 15639–15659.

Duarte, C.M., and Cebrian, J. (1996) The fate of marine autotrophic production. *Limnol Oceanogr* **41**: 1758–1766.

Duarte, C.M., Middelburg, J.J., and Caraco, N. (2004) Major role of marine vegetation on the oceanic carbon cycle. *Biogeosciences Discuss* **1**: 659–679.

Ducklow, H.W., Steinberg, D.K., and Buesseler, K.O. (2001) Upper ocean carbon export and the biological pump. *Oceanogr DC OCEANOGRAPHY Soc* **14**: 50–58.

Ducrotoy, J.P., Elliott, M., and Jonge, V.N. de (2000) The North Sea. *Mar Pollut Bull* **41**: 5–23.

Dugdale, R.C., and Goering, J.J. (1967) Uptake of new and regenerated forms of nitrogen in primary productivity 1. *Limnol Oceanogr* **12**: 196–206.

Egge, J.K., Thingstad, T.F., Engel, A., Bellerby, R.G.J., and Riebesell, U. (2007) Primary production during nutrient-induced blooms at elevated CO_2 concentrations. *Biogeosciences Discuss* **4**: 4385–4410.

Ehrhardt, M.K., and Koeve, W. (1999) J. 1999. Determination of particulate organic carbon and nitrogen. *Methods seawater Anal 3rd ed Wiley-VCH* 437–444.

Eleveld, M.A., Pasterkamp, R., Woerd, H.J. van der, and Pietrzak, J.D. (2008) Remotely sensed seasonality in the spatial distribution of sea-surface suspended particulate matter in the southern North Sea. *Estuar Coast Shelf Sci* **80**: 103–113.

Elser, J.J., Dobberfuhl, D.R., MacKay, N.A., and Schampel, J.H. (1996) Organism size, life history, and N: P stoichiometry. *Bioscience* **46**: 674–684.

Elser, J.J., Fagan, W.F., Denno, R.F., Dobberfuhl, D.R., Folarin, A., Huberty, A., Interlandi, S., Kilham, S.S., McCauley, E., Schulz, K.L. and Siemann, E.H. (2000) Nutritional constraints in terrestrial and freshwater food webs. *Nature* **408**: 578.

Emeis, K.C., van Beusekom, J., Callies, U., Ebinghaus, R., Kannen, A., Kraus, G., Kröncke, I., Lenhart, H., Lorkowski, I., Matthias, V. and Möllmann, C. (2015) The North Sea—A shelf sea in the Anthropocene. *J Mar Syst* **141**: 18–33.

Engel, A. (2000a) The role of transparent exopolymer particles (TEP) in the increase in apparent particle stickiness (α) during the decline of a diatom bloom. *J Plankton Res* **22**: 485–497.

Engel, A. (2002) Direct relationship between CO_2 uptake and transparent exopolymer particles production in natural phytoplankton. .

Engel, A. (2004) Distribution of transparent exopolymer particles (TEP) in the northeast Atlantic Ocean and their potential significance for aggregation processes. *Deep Sea Res Part I Oceanogr Res Pap* **51**: 83–92.

Engel, A., Delille, B., Jacquet, S., Riebesell, U., Rochelle-Newall, E., Terbrüggen, A., and Zondervan, I. (2004) Transparent exopolymer particles and dissolved organic carbon production by *Emiliania huxleyi* exposed to different CO_2 concentrations: a mesocosm experiment. *Aquat Microb Ecol* **34**: 93–104.

Engel, A., Goldthwait, S., Passow, U., and Alldredge, A. (2002) Temporal decoupling of carbon and nitrogen dynamics in a mesocosm diatom bloom. *Limnol Oceanogr* **47**: 753–761.

Engel, A., Händel, N., Wohlers, J., Lunau, M., Grossart, H.P., Sommer, U., and Riebesell, U. (2010) Effects of sea surface warming on the production and composition of dissolved organic matter during phytoplankton blooms: results from a mesocosm study. *J Plankton Res* **33**: 357–372.

Engel, A., Koeve, W., and Zeitzschel, B. (1997) Verteilung Transparenter Exopolymer Partikel (TEP) im Nordostatlantik. Untersuchungen entlang eines 20 W Schnittes (Meteor 36/2). *Berichte Fachbereich Geowissenschaften Univ Bremen* **109**: 23.

Engel, A., and Passow, U. (2001) Carbon and nitrogen content of transparent exopolymer particles (TEP) in relation to their Alcian Blue adsorption. *Mar Ecol Prog Ser* **219**: 1–10.

Engel, A., Piontek, J., Grossart, H.-P., Riebesell, U.L.F., Schulz, K.G., and Sperling, M. (2014) Impact of CO_2 enrichment on organic matter dynamics during nutrient induced coastal phytoplankton blooms. *J Plankton Res* **36**: 641–657.

Engel, A., and Schartau, M. (1999) Influence of transparent exopolymer particles (TEP) on sinking velocity of *Nitzschia closterium* aggregates. *Mar Ecol Prog Ser* 69–76.

Engel, A., Thoms, S., Riebesell, U., Rochelle-Newall, E., and Zondervan, I. (2004) Polysaccharide aggregation as a potential sink of marine dissolved organic carbon. *Nature* **428**: 929.

Eppley, R.W., and Peterson, B.J. (1979) Particulate organic matter flux and planktonic new production in the deep ocean. *Nature* **282**: 677.

Fabricius, K.E., Wild, C., Wolanski, E., and Abele, D. (2003) Effects of transparent exopolymer particles and muddy terrigenous sediments on the survival of hard coral recruits. *Estuar Coast Shelf Sci* **57**: 613–621.

Fernand, L., Weston, K., Morris, T., Greenwood, N., Brown, J., and Jickells, T. (2013) The contribution of the deep chlorophyll maximum to primary production in a seasonally stratified shelf sea, the North Sea. *Biogeochemistry* **113**: 153–166.

Fernández, E., Cabal, J., Acuña, J., Bode, A., Botas, A., and García-Soto, C. (1993) Plankton distribution across a slope current-induced front in the southern Bay of Biscay. *J Plankton Res* **15**: 619–641.

Fujii, M., Murashige, S., Ohnishi, Y., Yuzawa, A., Miyasaka, H., Suzuki, Y., and Komiyama, H. (2002) Decomposition of phytoplankton in seawater. Part I: Kinetic analysis of the effect of organic matter concentration. *J Oceanogr* **58**: 438–443.

Fukao, T., Kimoto, K., and Kotani, Y. (2012) Effect of temperature on cell growth and production of transparent exopolymer particles by the diatom *Coscinodiscus granii* isolated from marine mucilage. *J Appl Phycol* **24**: 181–186.

Garcia, C.M., Prieto, L., Vargas, M., Echevarría, F., Garcia-Lafuente, J., Ruiz, J., and Rubin, J.P. (2002) Hydrodynamics and the spatial distribution of plankton and TEP in the Gulf of Cadiz (SW Iberian Peninsula). *J Plankton Res* **24**: 817–833.

Gärdes, A., Ramaye, Y., Grossart, H.-P., Passow, U., and Ullrich, M.S. (2012) Effects of Marinobacter adhaerens HP15 on polymer exudation by *Thalassiosira weissflogii* at different N: P ratios. *Mar Ecol Prog Ser* **461**: 1–14.

Gattuso, J.P., Frankignoulle, M., and Wollast, R. (1998) Carbon and carbonate metabolism in coastal aquatic ecosystems. *Annu Rev Ecol Syst* **29**: 405–434.

Geider, R.J., MacIntyre, H.L., and Kana, T.M. (1997) Dynamic model of phytoplankton growth and acclimation: responses of the balanced growth rate and the chlorophyll *a*: carbon ratio to light, nutrient-limitation and temperature. *Mar Ecol Prog Ser* **148**: 187–200.

Giering, S.L.C., Sanders, R., Martin, A.P., Henson, S.A., Riley, J.S., Marsay, C.M., and Johns, D.G. (2017) Particle flux in the oceans: Challenging the steady state assumption. *Global Biogeochem Cycles* **31**: 159–171.

Goodarz-Nia, I. (1977) Floc density, porosity and void ratio in colloidal systems and aerosols. *J Colloid Interface Sci* **62**: 131–141.

Greenwood, N., Parker, E.R., Fernand, L., Sivyer, D.B., Weston, K., Painting, S.J., Kröger, S., Forster, R.M., Lees, H.E., Mills, D.K. and Laane, R.W.P.M. (2010) Detection of low bottom water oxygen concentrations in the North Sea; implications for monitoring and assessment of ecosystem health. *Biogeosciences* **7**: 1357–1373.

Grossart, H., Simon, M., and Logan, B.E. (1997) Formation of macroscopic organic aggregates (lake snow) in a large lake: The significance of transparent exopolymer particles, plankton, and zooplankton. *Limnol Oceanogr* **42**: 1651–1659.

Gruber, N. (2015) Ocean biogeochemistry: Carbon at the coastal interface. *Nature* **517**: 148.

Guillard, R.R. (1975) Culture of phytoplankton for feeding marine invertebrates. In *Culture of marine invertebrate animals* 29–60. Springer, Boston, MA.

Haas, H. de, Boer, W., and Weering, T.C.E. van (1997) Recent sedimentation and organic carbon burial in a shelf sea: the North Sea. *Mar Geol* **144**: 131–146.

Haas, H. de, and Weering, T.C.E. van (1997) Recent sediment accumulation, organic carbon burial and transport in the northeastern North Sea. *Mar Geol* **136**: 173–187.

Haas, H. de, Weering, T.C.E. van, and Stigter, H. de (2002) Organic carbon in shelf seas: sinks or sources, processes and products. *Cont Shelf Res* **22**: 691–717.

Hamanaka, J., Tanoue, E., Hama, T., and Handa, N. (2002) Production and export of particulate fatty acids, carbohydrates and combined amino acids in the euphotic zone. *Mar Chem* **77**: 55–69.

Hansell, D.A. (2013) Recalcitrant dissolved organic carbon fractions.

Hansell, D.A., and Carlson, C.A. (2001) Marine dissolved organic matter and the carbon cycle. *Oceanography* **14**: 41–49.

Harvey, H.R., Tuttle, J.H., and Bell, J.T. (1995) Kinetics of phytoplankton decay during simulated sedimentation: changes in biochemical composition and microbial activity under oxic and anoxic conditions. *Geochim Cosmochim Acta* **59**: 3367–3377.

Heathershaw, A.D., and Codd, J.M. (1986) Depth-controlled changes in grain size and carbonate content on a shelf-edge sand bank. *Mar Geol* **72**: 211–224.

Heathershaw, A.D., New, A.L., and Edwards, P.D. (1987) Internal tides and sediment transport at the shelf break in the Celtic Sea. *Cont Shelf Res* **7**: 485–517.

Hedges, J.I., and Stern, J.H. (1984) Carbon and nitrogen determinations of carbonate-containing solids. *Limnol Oceanogr* **29**: 657–663.

Heinze, C., Maier-Reimer, E., and Winn, K. (1991) Glacial pCO_2 reduction by the world ocean: Experiments with the Hamburg carbon cycle model. *Paleoceanography* **6**: 395–430.

Heinze, C., Meyer, S., Goris, N., Anderson, L., Steinfeldt, R., Chang, N., Le Quere, C. and Bakker, D.C. (2015) The ocean carbon sink-impacts, vulnerabilities and challenges. *Earth Syst Dyn* **6**: 327–358.

Hickman, A.E., Moore, C.M., Sharples, J., Lucas, M.I., Tilstone, G.H., Krivtsov, V., and Holligan, P.M. (2012) Primary production and nitrate uptake within the seasonal thermocline of a stratified shelf sea. *Mar Ecol Prog Ser* **463**: 39–57.

Hill, P.S. (1992) Reconciling aggregation theory with observed vertical fluxes following phytoplankton blooms. *J Geophys Res Ocean* **97**: 2295–2308.

Holligan, P.M., Pingree, R.D., and Mardell, G.T. (1985) Oceanic solitons, nutrient pulses and phytoplankton growth. *Nature* **314**: 348.

Hong, Y., Smith, W.O., and White, A. (1997) Studies on transparent exopolymer particles (TEP) produced in the Ross Sea (Antarctica) and by *Phaeocystis antarctica* (Prymnesiophyceae). *J Phycol* **33**: 368–376.

Hood, R.R., Bates, N.R., Capone, D.G., and Olson, D.B. (2001) Modeling the effect of nitrogen fixation on carbon and nitrogen fluxes at BATS. *Deep Sea Res Part II Top Stud Oceanogr* **48**: 1609–1648.

Howarth, M.J. (2001) North sea circulation 1912–1921.

Humphreys, M.P., Achterberg, E.P., Hopkins, J.E., Chowdhury, M.Z., Griffiths, A.M., Hartman, S.E., Hull, T., Smilenova, A., Wihsgott, J.U., Woodward, E.M.S. and Moore, C.M. (2018) Mechanisms for a nutrient-conserving carbon pump in a seasonally stratified, temperate continental shelf sea. *Prog Oceanogr* .

Huthnance, J.M. (1995) Circulation, exchange and water masses at the ocean margin: the role of physical processes at the shelf edge. *Prog Oceanogr* **35**: 353–431.

Ierland, E.T. Van, and Peperzak, L. (1984) Separation of marine seston and density determination of marine diatoms by density gradient centrifugation. *J Plankton Res* **6**: 29–44.

Iversen, M.H., and Ploug, H. (2010) Ballast minerals and the sinking carbon flux in the ocean: Carbon-specific respiration rates and sinking velocity of marine snow aggregates. *Biogeosciences* **7**: 2613–2624.

Jackson, G.A. (1990) A model of the formation of marine algal flocs by physical coagulation processes. *Deep Sea Res Part A Oceanogr Res Pap* **37**: 1197–1211.

Jackson, G.A., and Burd, A.B. (1998) Aggregation in the marine environment. *Environ Sci Technol* **32**: 2805–2814.

Jennings, M.K., Passow, U., Wozniak, A.S., and Hansell, D.A. (2017) Distribution of transparent exopolymer particles (TEP) across an organic carbon gradient in the western North Atlantic Ocean. *Mar Chem* **190**: 1–12.

Jiao, N., Robinson, C., Azam, F., Thomas, H., Baltar, F., Dang, H., Hardman-Mountford, N.J., Johnson, M., Kirchman, D.L., Koch, B.P. and Legendre, L. (2014) Mechanisms of microbial carbon sequestration in the ocean–future research directions. *Biogeosciences* **11**: 5285–5306.

Johnson, M.T., Greenwood, N., Sivyer, D.B., Thomson, M., Reeve, a., Weston, K., and Jickells, T.D. (2013) Characterising the seasonal cycle of dissolved organic nitrogen using Cefas SmartBuoy high-resolution time-series samples from the southern North Sea. *Biogeochemistry* **113**: 23–36.

Joint, I.R., Owens, N.J.P., Pomroy, A.J., and Pomeroy, A.J. (1986) Seasonal production of photosynthetic picoplankton and nanoplankton in the Celtic Sea. *Mar Ecol Prog Ser* 251–258.

Kahl, L.A., Vardi, A., and Schofield, O. (2008) Effects of phytoplankton physiology on export flux. *Mar Ecol Prog Ser* **354**: 3–19.

Kähler, P., and Koeve, W. (2001) Marine dissolved organic matter: can its C : N ratio explain carbon overconsumption? *Deep Sea Res Part I Oceanogr Res Pap* **48**: 49–62.

Kajihara, M. (1971). Settling velocity and porosity of large suspended particles. *J Ocean Sot Jpn* **27**: 158–l62.

Kepkay, P.E., and Johnson, B.D. (1989) Coagulation on bubbles allows microbial respiration of oceanic dissolved organic carbon. *Nature* **338**: 63.

Kiørboe, T., Lundsgaard, C., Olesen, M., and Hansen, J.L.S. (1994) Aggregation and sedimentation processes during a spring phytoplankton bloom: A field experiment to test coagulation theory. *J Mar Res* **52**: 297–323.

Kiørboe, T., Tiselius, P., Mitchell-Innes, B., Hansen, J.L.S., Visser, A.W., and Mari, X. (1998) Intensive aggregate formation with low vertical flux during an upwelling-induced diatom bloom. *Limnol Oceanogr* **43**: 104–116.

Klaas, C., and Archer, D.E. (2002) Association of sinking organic matter with various types of mineral ballast in the deep sea: Implications for the rain ratio. *Global Biogeochem Cycles* **16**.

Knight, P.J., and Howarth, M.J. (1999) The flow through the North Channel of the Irish Sea. *Cont Shelf Res* **19**: 693–716.

Koch, B., Kattner, G., Witt, M., and Passow, U. (2014) Molecular insights into the microbial formation of marine dissolved organic matter: recalcitrant or labile? *Biogeosciences* **11**: 4173–4190.

Koeve, W. (2005) Magnitude of excess carbon sequestration into the deep ocean and the possible role of TEP. *Mar Ecol Prog Ser* **291**: 53–64.

Kondo, J. (1975) Air-sea bulk transfer coefficients in diabatic conditions. *Boundary-Layer Meteorol* **9**: 91–112.

Körtzinger, A., Koeve, W., Kähler, P., and Mintrop, L. (2001) C : N ratios in the mixed layer during the productive season in the northeast Atlantic Ocean. *Deep Sea Res Part I Oceanogr Res Pap* **48**: 661–688.

Kovac, N., Faganeli, J., Sket, B., and Bajt, O. (1998) Characterization of macroaggregates and photodegradation of their water soluble fraction. *Org Geochem* **29**: 1623–1634.

Kozlowski, W., Vernet, M., and Lamerdin, S.K. (1995) Predominance of cryptomonads and diatoms in Antarctic coastal waters. *Antarct J United States* **30**: 267–268.

Krembs, C. el, Eicken, H., Junge, K., and Deming, J.W. (2002) High concentrations of exopolymeric substances in Arctic winter sea ice: implications for the polar ocean carbon cycle and cryoprotection of diatoms. *Deep Sea Res Part I Oceanogr Res Pap* **49**: 2163–2181.

Kriest, I. (2002) Different parameterizations of marine snow in a 1D-model and their influence on representation of marine snow, nitrogen budget and sedimentation. *Deep Sea Res Part I Oceanogr Res Pap* **49**: 2133–2162.

Lande, R., and Wood, A.M. (1987) Suspension times of particles in the upper ocean. *Deep Sea Res Part A Oceanogr Res Pap* **34**: 61–72.

Lenhart, H., and Pohlmann, T. (1997) The ICES-boxes approach in relation to results of a North Sea circulation model. *Tellus A* **49**: 139–160.

Lenhart, H.J., Pätsch, J., Kühn, W., Moll, A., and Pohlmann, T. (2004) Investigation on the trophic state of the North Sea for three years (1994–1996) simulated with the ecosystem model ERSEM the role of a sharp NAOI decline. *Biogeosciences Discuss* 725–754.

Leppard, G.G., Massalski, A., and Lean, D.R.S. (1977) Electron-opaque microscopic fibrils in lakes: their demonstration, their biological derivation and their potential significance in the redistribution of cations. *Protoplasma* **92**: 289–309.

Liss, P.S., and Merlivat, L. (1986) Air-sea gas exchange rates: Introduction and synthesis. In *The role of air-sea exchange in geochemical cycling*. Springer, pp. 113–127.

Liu, K.K., Atkinson, L., Chen, C.T.A., Gao, S., Hall, J., Macdonald, R.W., McManus, L.T. and Quinones, R. (2000) Exploring continental margin carbon fluxes on a global scale. *Eos, Trans Am Geophys Union* **81**: 641–644.

Logan, B.E. (1986) Mass Transfer to Microorganisms in Aggregates and Biofilms. Doctoral dissertation, Ph.D. Thesis, Dept. of Civil Engineering, University of California, Berkeley.

Logan, B.E., and Hunt, J.R. (1987) Advantages to microbes of growth in permeable aggregates in marine systems. *Limnol Oceanogr* **32**: 1034–1048.

Logan, B.E., Passow, U., Alldredge, A.L., Grossartt, H.P., and Simont, M. (1995) Rapid formation and sedimentation of large aggregates is predictable from coagulation rates (half-lives) of transparent exopolymer particles (TEP). *Deep Sea Res Part II Top Stud Oceanogr* **42**: 203–214.

MacGilchrist, G.A., Shi, T., Tyrrell, T., Richier, S., Moore, C.M., Dumousseaud, C., and Achterberg, E.P. (2014) Effect of enhanced pCO_2 levels on the production of dissolved organic carbon and transparent exopolymer particles in short-term bioassay experiments. *Biogeosciences* **11**: 3695–3706.

MacIntyre, S., Alldredge, A.L., and Gotschalk, C.C. (1995) Accumulation of marines now at density discontinuities in the water column. *Limnol Oceanogr* **40**: 449–468.

Mackenzie, F.T., Lerman, A., and Andersson, A.J. (2004) Past and present of sediment and carbon biogeochemical cycling models. *Biogeosciences Discuss* **1**: 27–85.

Malpezzi, M.A., Sanford, L.P., and Crump, B.C. (2013) Abundance and distribution of transparent exopolymer particles in the estuarine turbidity maximum of Chesapeake Bay. *Mar Ecol Prog Ser* **486**: 23–35.

Mannino, A., Signorini, S.R., Novak, M.G., Wilkin, J., Friedrichs, M.A.M., and Najjar, R.G. (2016) Dissolved organic carbon fluxes in the Middle Atlantic Bight: An integrated approach based on satellite data and ocean model products. *J Geophys Res Biogeosciences* **121**: 312–336.

Mari, X. (1999) Carbon content and C : N ratio of transparent exopolymeric particles (TEP) produced by bubbling exudates of diatoms. *Mar Ecol Prog Ser* **183**: 59–71.

Mari, X., Beauvais, S., Lemée, R., and Pedrotti, M.L. (2001) Non-Redfield C : N ratio of transparent exopolymeric particles in the northwestern Mediterranean Sea. *Limnol Oceanogr* **46**: 1831–1836.

Mari, X., and Burd, A. (1998) Seasonal size spectra of transparent exopolymeric particles (TEP) in a coastal sea and comparison with those predicted using coagulation theory. *Mar Ecol Prog Ser* **163**: 63–76.

Mari, X., and Kiørboe, T. (1996) Abundance, size distribution and bacterial colonization of transparent exopolymeric particles (TEP) during spring in the Kattegat. *J Plankton Res* **18**: 969–986.

Mari, X., Passow, U., Migon, C., Burd, A.B., and Legendre, L. (2017) Transparent exopolymer particles: Effects on carbon cycling in the ocean. *Prog Oceanogr* **151**: 13–37.

Mari, X., Rassoulzadegan, F., Brussaard, C.P.D., and Wassmann, P. (2005) Dynamics of transparent exopolymeric particles (TEP) production by Phaeocystis globosa under N or P limitation: a controlling factor of the retention/export balance. *Harmful Algae* **4**: 895–914.

Mari, X., Rochelle-Newall, E., Torréton, J.-P., Pringault, O., Jouon, A., and Migon, C. (2007) Water residence time: a regulatory factor of the DOM to POM transfer efficiency. *Limnol Oceanogr* **52**: 808–819.

Mari, X., Torréton, J.-P., Trinh, C.B.T., Bouvier, T., Thuoc, C. Van, Lefebvre, J.-P., and Ouillon, S. (2012) Aggregation dynamics along a salinity gradient in the Bach Dang estuary, North Vietnam. *Estuar Coast Shelf Sci* **96**: 151–158.

McCave, I. (1975) Vertical flux of particles in the ocean. In *Deep Sea Research and Oceanographic Abstracts*. Elsevier 491–502.

McCave, I. (1971) Wave effectiveness at the sea bed and its relationship to bed-forms and deposition of mud. *J Sediment Res* **41** 89–96.

McDonnell, A.M.P., and Buesseler, K.O. (2010) Variability in the average sinking velocity of marine particles. *Limnol Oceanogr* **55**: 2085–2096.

Meng, S., Rzechowicz, M., Winters, H., Fane, A.G., and Liu, Y. (2013) Transparent exopolymer particles (TEP) and their potential effect on membrane biofouling. *Appl Microbiol Biotechnol* **97**: 5705–5710.

Miller, J.N., and Miller, J.C. (2010) *Statistics and chemometrics for analytical chemistry*. Sixth edit., Pearson Education.

Moll, A. (1998) Regional distribution of primary production in the North Sea simulated by a three-dimensional model. *J Mar Syst* **16**: 151–170.

Moore, C.M., Mills, M.M., Arrigo, K.R., Berman-Frank, I., Bopp, L., Boyd, P.W., Galbraith, E.D., Geider, R.J., Guieu, C., Jaccard, S.L. and Jickells, T.D. (2013) Processes and patterns of oceanic nutrient limitation. *Nat Geosci* **6**: 701.

Mopper, K., Ramana, K.S., and Drapeau, D.T. (1995) The role of surface-active carbohydrates in the flocculation of a diatom bloom in a mesocosm. *Deep Sea Res Part II Top Stud Oceanogr* **42**: 47–73.

Morán, X.A.G., Sebastián, M., Pedrís-Alií, C., and Estrada, M. (2006) Response of Southern Ocean phytoplankton and bacterioplankton production to short-term experimental warming. *Limnol Oceanogr* **51**: 1791–1800.

Mueller, J.A., Morand, J., and Boyle, W.C. (1967) Floc sizing techniques. *Appl Microbiol* **15**: 125–134.

Mueller, J.A., Voelkel, K.G., and Boyle, W.C. (1966) Nominal diameter of floc related to oxygen transfer. *J Sanit Eng Div* **92**: 9–20.

Müller-MNiklas, G., Stefan, S., Kaltenböok, E., and Herndl, G.J. (1994) Organic content and bacterial metabolism in amorphous aggregations of the northern Adriatic Sea. *Limnol Oceanogr* **39**: 58–68.

Myklestad, S., Haug, A., and Larsen, B. (1972) Production of carbohydrates by the marine diatom *Chaetoceros affinis* var. willei (Gran) Hustedt. II. Preliminary investigation of the extracellular polysaccharide. *J Exp Mar Bio Ecol* **9**: 137–144.

Myklestad, S.M. (1995) Release of extracellular products by phytoplankton with special emphasis on polysaccharides. *Sci Total Environ* **165**: 155–164.

Nagorsen, D.W., and Peterson, R.L. (1980) Mammal Collectors' Manual: A guide for collecting, documenting, and preparing mammal specimens for scientific research. *Life Sciences Miscellaneous Publications.*

Nasrabadi, T., Ruegner, H., Sirdari, Z.Z., Schwientek, M., and Grathwohl, P. (2016) Using total suspended solids (TSS) and turbidity as proxies for evaluation of metal transport in river water. *Appl Geochemistry* **68**: 1–9.

Newton, P.P., Lampitt, R.S., Jickells, T.D., King, P., and Boutle, C. (1994) Temporal and spatial variability of biogenic particles fluxes during the JGOFS northeast Atlantic process studies at 47 N, 20 W. *Deep Sea Res Part I Oceanogr Res Pap* **41**: 1617–1642.

Nightingale, P.D., Malin, G., Law, C.S., Watson, A.J., Liss, P.S., Liddicoat, M.I., Boutin, J. and Upstill-Goddard, R.C. (2000) *In situ* evaluation of air-sea gas exchange parameterizations using novel conservative and volatile tracers. *Global Biogeochem Cycles* **14**: 373–387.

Obernosterer, I., and Herndl, G.J. (1995) Phytoplankton extracellular release and bacterial growth: dependence on the inorganic N : P ratio. *Mar Ecol Prog Ser Oldend* **116**: 247–257.

Oguz, T. (2017b) Modeling aggregate dynamics of transparent exopolymer particles (TEP) and their interactions with a pelagic food web. *Mar Ecol Prog Ser* **582**: 15–31.

Oliver, M.J., Glenn, S., Kohut, J.T., Irwin, A.J., Schofield, O.M., Moline, M.A., and Bissett, W.P. (2004) Bioinformatic approaches for objective detection of water masses on continental shelves. *J Geophys Res Ocean* **109**.

Oostende, N. Van, Harlay, J., Vanelslander, B., Chou, L., Vyverman, W., and Sabbe, K. (2012) Phytoplankton community dynamics during late spring coccolithophore blooms at the continental margin of the Celtic Sea (North East Atlantic, 2006-2008). *Prog Oceanogr* **104**: 1–16.

Ortega-Retuerta, E., Duarte, C.M., and Reche, I. (2010) Significance of bacterial activity for the distribution and dynamics of transparent exopolymer particles in the Mediterranean Sea. *Microb Ecol* **59**: 808–818.

Ortega-Retuerta, E., Reche, I., Pulido-Villena, E., Agustí, S., and Duarte, C.M. (2009) Uncoupled distributions of transparent exopolymer particles (TEP) and dissolved carbohydrates in the Southern Ocean. *Mar Chem* **115**: 59–65.

Ortega-Retuerta, E., Sala, M.M., Borrull, E., Mestre, M., Aparicio, F.L., Gallisai, R., Antequera, C., Marrasé, C., Peters, F., Simó, R. and Gasol, J.M. (2017) Horizontal and Vertical Distributions of Transparent Exopolymer Particles (TEP) in the NW Mediterranean Sea are linked to chlorophyll *a* and O_2 variability. *Front Microbiol* **7**: 2159.

Pantin, H.M., and Evans, C.D.R. (1984) The Quaternary history of the central and southwestern Celtic Sea. *Mar Geol* **57**: 259–293.

Parker, B.C., and Diboll, A.G. (1966) Alcian stains for histochemical localization of acid and sulfated polysaccharides in algae. *Phycologia* **6**: 37–46.

Passow, U. (2000) Formation of transparent exopolymer particles, TEP, from dissolved precursor material. *Mar Ecol Prog Ser* 1–11.

Passow, U. (2002b) Production of transparent exopolymer particles (TEP) by phyto-and bacterioplankton. *Mar Ecol Prog Ser* **236**: 1–12.

Passow, U. (2002) Transparent exopolymer particles (TEP) in aquatic environments. *Prog Oceanogr* **55**: 287–333.

Passow, U., and Alldredge, A.L. (1994) Distribution, size and bacterial colonization of transparent exopolymer particles (TEP) in the ocean. *Mar Ecol Prog Ser* 185–198.

Passow, U., and Alldredge, A.L. (1995) A dye-binding assay for the spectrophotometric measurement of transparent exopolymer particles (TEP). *Limnol Oceanogr* **40**: 1326–1335.

Passow, U., and Alldredge, A.L. (1995) Aggregation of a diatom bloom in a mesocosm: The role of transparent exopolymer particles (TEP). *Deep Sea Res Part II Top Stud Oceanogr* **42**: 99–109.

Passow, U., Alldredge, A.L., and Logan, B.E. (1994) The role of particulate carbohydrate exudates in the flocculation of diatom blooms. *Deep Res Part I* **41**: 335–357.

Passow, U., Christina, L., Fairfield, C., and Schmidt, K. (2014) Aggregation as a function of and mineral particles. *Limnol Oceanogr* **59**: 532–547.

Passow, U., Kozlowski, W., and Vernet, M. (1995) Palmer LTER: temporal variability of transparent exopolymer particles in Arthur Harbor during the 1994–1995 growth season. *Antarct J United States* **30**: 265–266.

Passow, U., Shipe, R.F., Murray, A., Pak, D.K., Brzezinski, M.A., and Alldredge, A.L. (2001) The origin of transparent exopolymer particles (TEP) and their role in the sedimentation of particulate matter. *Cont Shelf Res* **21**: 327–346.

Pedrotti, M.L., Peters, F., Beauvais, S., Vidal, M., Egge, J., Jacobsen, A., and Marrasé, C. (2010) Effects of nutrients and turbulence on the production of transparent exopolymer particles: a mesocosm study. *Mar Ecol Prog Ser* **419**: 57–69.

Pingree, R.D. (1980) Physical oceanography of the Celtic Sea and English Channel. In *Elsevier Oceanography Series*. Elsevier 415–465.

Piontek, J., Händel, N., Langer, G., Wohlers, J., Riebesell, U., and Engel, A. (2009) Effects of rising temperature on the formation and microbial degradation of marine diatom aggregates. *Aquat Microb Ecol* **54**: 305–318.

Ploug, H., Grossart, H.-P., Azam, F., and Jørgensen, B.B. (1999) Photosynthesis, respiration, and carbon turnover in sinking marine snow from surface waters of Southern California Bight: implications for the carbon cycle in the ocean. *Mar Ecol Prog Ser* 1–11.

Ploug, H., Iversen, M.H., and Fischer, G. (2008) Ballast, sinking velocity, and apparent diffusivity within marine snow and zooplankton fecal pellets: Implications for substrate turnover by attached bacteria. *Limnol Oceanogr* **53**: 1878–1886.

Ploug, H., and Passow, U. (2007) Direct measurement of diffusivity within diatom aggregates containing transparent exopolymer particles. *Limnol Oceanogr* **52**: 1–6.

Polimene, L., Allen, J.I., and Zavatarelli, M. (2006) Model of interactions between dissolved organic carbon and bacteria in marine systems. *Aquat Microb Ecol* **43**: 127–138.

Polimene, L., Brunet, C., Butenschön, M., Martinez-Vicente, V., Widdicombe, C., Torres, R., and Allen, J.I. (2013) Modelling a light-driven phytoplankton succession. *J Plankton Res* **36**: 214–229.

Polimene, L., Mitra, A., Sailley, S.F., Ciavatta, S., Widdicombe, C.E., Atkinson, A., and Allen, J.I. (2015) Decrease in diatom palatability contributes to bloom formation in the Western English Channel. *Prog Oceanogr* **137**: 484–497.

Polimene, L., Pinardi, N., Zavatarelli, M., and Colella, S. (2006) The Adriatic Sea ecosystem seasonal cycle: Validation of a three-dimensional numerical model. *J Geophys Res Ocean* **111**.

Prieto, L., Navarro, G., Cozar, A., Echevarria, F., and Garcia, C.M. (2006) Distribution of TEP in the euphotic and upper mesopelagic zones of the southern Iberian coasts. *Deep Sea Res Part II Top Stud Oceanogr* **53**: 1314–1328.

Prowe, A.F., Thomas, H., Pätsch, J., Kühn, W., Bozec, Y., Schiettecatte, L.S., Borges, A.V. and de Baar, H.J. (2009) Mechanisms controlling the air–sea CO2 flux in the North Sea. *Cont Shelf Res* **29**: 1801–1808.

Puig, P., Palanques, A., Guillén, J., and Khatab, M. El (2004) Role of internal waves in the generation of nepheloid layers on the northwestern Alboran slope: implications for continental margin shaping. *J Geophys Res Ocean* **109**.

Quéré, C.L., Andrew, R.M., Canadell, J.G., Sitch, S., Korsbakken, J.I., Peters, G.P., Manning, A.C., Boden, T.A., Tans, P.P., Houghton, R.A. and Keeling, R.F. (2016) Global carbon budget 2016. *Earth Syst Sci Data* **8**: 605–649.

Quigg, A., Finkel, Z.V., Irwin, A.J., Rosenthal, Y., Ho, T.Y., Reinfelder, J.R., Schofield, O., Morel, F.M. and Falkowski, P.G. (2003) The evolutionary inheritance of elemental stoichiometry in marine phytoplankton. *Nature* **425**: 291.

Radić, T., Kraus, R., Fuks, D., Radić, J., and Pečar, O. (2005a) Transparent exopolymeric particles' distribution in the northern Adriatic and their relation to microphytoplankton biomass and composition. *Sci Total Environ* **353**: 151–161.

Ramaiah, N., and Furuya, K. (2002) Seasonal variations in phytoplankton composition and transparent exopolymer particles in a eutrophicated coastal environment. *Aquat Microb Ecol* **30**: 69–82.

Ramaiah, N., Yoshikawa, T., and Furuya, K. (2001) Temporal variations in transparent exopolymer particles (TEP) associated with a diatom spring bloom in a subarctic ria in Japan. *Mar Ecol Prog Ser* **212**: 79–88.

Ramus, J. (1977) Alcian blue: a quantitative aqueous assay for algal acid and sulfated polysaccharides. *J Phycol* **13**: 345–348.

Redfield, A.C. (1963) The influence of organisms on the composition of seawater. *sea* **2**: 26–77.

Rees, A.P., Joint, I., and Donald, K.M. (1999) Early spring bloom phytoplankton-nutrient dynamics at the Celtic Sea Shelf Edge. *Deep Sea Res Part I Oceanogr Res Pap* **46**: 483–510.

Reid, P.C., Lancelot, C., Gieskes, W.W.C., Hagmeier, E., and Weichart, G. (1990) Phytoplankton of the North Sea and its dynamics: a review. *Netherlands J Sea Res* **26**: 295–331.

Reigstad, M., and Wassmann, P. (2007) Does Phaeocystis spp. contribute significantly to vertical export of organic carbon? *Biogeochemistry* **83**: 217–234.

Reusch, T.B.H., and Boyd, P.W. (2013) Experimental evolution meets marine phytoplankton. *Evolution (N Y)* **67**: 1849–1859.

Riebesell, U. (1992) The formation of large marine snow and its sustained residence in surface waters. *Limnol Oceanogr* **37**: 63–76.

Riebesell, U., Reigstad, M., Wassmann, P., Noji, T., and Passow, U. (1995) On the trophic fate of *Phaeocystis pouchetii* (Hariot): VI. Significance of Phaeocystis-derived mucus for vertical flux. *Netherlands J Sea Res* **33**: 193–203.

Riebesell, U., Schulz, K.G., Bellerby, R.G.J., Botros, M., Fritsche, P., Meyerhöfer, M., *et al.* (2007) Enhanced biological carbon consumption in a high CO 2 ocean. *Nature* **450**: 545.

Riley, G.A. (1971) Particulate organic matter in sea water. In *Advances in marine biology*. Elsevier 1–118.

Rosati, A., and Miyakoda, K. (1988) A general circulation model for upper ocean simulation. *J Phys Oceanogr* **18**: 1601–1626.

Rost, B., Zondervan, I., and Wolf-Gladrow, D. (2008) Sensitivity of phytoplankton to future changes in ocean carbonate chemistry: current knowledge, contradictions and research directions. *Mar Ecol Prog Ser* **373**: 227–237.

Sabine, C.L., Feely, R.A., Gruber, N., Key, R.M., Lee, K., Bullister, J.L., Wanninkhof, R., Wong, C.S.L., Wallace, D.W., Tilbrook, B. and Millero, F.J. (2004) The oceanic sink for anthropogenic CO_2. *Science (80-)* **305**: 367–371.

Sailley, S.F., Polimene, L., Mitra, A., Atkinson, A., and Allen, J.I. (2015) Impact of zooplankton food selectivity on plankton dynamics and nutrient cycling. *J Plankton Res* **37**: 519–529.

Sambrotto, R.N., Savidge, G., Robinson, C., Boyd, P., Takahashi, T., Karl, D.M., Langdon, C., Chipman, D., Marra, J. and Codispoti, L. (1993) Elevated consumption of carbon relative to nitrogen in the surface ocean. *Nature* **363**: 248.

Sanders, R., Morris, P.J., Poulton, A.J., Stinchcombe, M.C., Charalampopoulou, A., Lucas, M.I., and Thomalla, S.J. (2010) Does a ballast effect occur in the surface ocean? *Geophys Res Lett* **37**.

Sardans, J., Rivas-Ubach, A., and Peñuelas, J. (2012) The C : N: P stoichiometry of organisms and ecosystems in a changing world: a review and perspectives. *Perspect Plant Ecol Evol Syst* **14**: 33–47.

Schartau, M., Engel, A., Schröter, J., Thoms, S., Völker, C., and Wolf-Gladrow, D. (2007) Modelling carbon overconsumption and the formation of extracellular particulate organic carbon. *Biogeosciences Discuss* **4**: 13–67.

Schuster, S., and Herndl, G.J. (1995) Formation and significance of transparent exopolymeric particles in the northern Adriatic Sea. *Mar Ecol Prog Ser* 227–236.

Seebah, S., Fairfield, C., Ullrich, M.S., and Passow, U. (2014a) Aggregation and sedimentation of Thalassiosira weissflogii (diatom) in a warmer and more acidified future ocean. *PLoS One* **9**: e112379.

Sharples, J., Moore, M.C., Rippeth, T.P., Holligan, P.M., Hydes, D.J., Fisher, N.R., and Simpson, J.H. (2001) Phytoplankton distribution and survival in the thermocline. *Limnol Oceanogr* **46**: 486–496.

Sieburth, J.M., Smetacek, V., and Lenz, J. (1978) Pelagic ecosystem structure: Heterotrophic compartments of the plankton and their relationship to plankton size fractions 1. *Limnol Oceanogr* **23**: 1256–1263.

Sigman, D.M., and Boyle, E.A. (2000) Glacial/interglacial variations in atmospheric carbon dioxide. *Nature* **407**: 859.

Simpson, J.H., and Bowers, D. (1981) Models of stratification and frontal movement in shelf seas. *Deep Sea Res Part A Oceanogr Res Pap* **28**: 727–738.

Simpson, J.H., and Hunter, J.R. (1974) Fronts in the Irish Sea. *Nature* **250**: 404.

Simpson, J.H., and McCandliss, R.R. (2013) "The Ekman Drain": a conduit to the deep ocean for shelf material. *Ocean Dyn* **63**: 1063–1072.

Smith, D.C., Steward, G.F., Long, R.A., and Azam, F. (1995) Bacterial mediation of carbon fluxes during a diatom bloom in a mesocosm. *Deep Sea Res Part II Top Stud Oceanogr* **42**: 75–97.

Smith, P.G., and Coackley, P. (1984) Diffusivity, tortuosity and pore structure of activated sludge. *Water Res* **18**: 117–122.

Smyth, T.J., Fishwick, J.R., Al-Moosawi, L., Cummings, D.G., Harris, C., Kitidis, V., Rees, A., Martinez-Vicente, V. and Woodward, E.M. (2009) A broad spatio-temporal view of the Western English Channel observatory. *J Plankton Res* **32**: 585–601.

Song, C., Ballantyne, F., and Smith, V.H. (2014) Enhanced dissolved organic carbon production in aquatic ecosystems in response to elevated atmospheric CO_2. *Biogeochemistry* **118**: 49–60.

Steinacher, M., Joos, F., Frölicher, T.L., Bopp, L., Cadule, P., Cocco, V., Doney, S.C., Gehlen, M., Lindsay, K., Moore, J.K. and Schneider, B. (2010) Projected 21st century decrease in marine productivity: a multi-model analysis. *Biogeosciences* **7**: 979–1005.

Sternberg, R.W., Berhane, I., and Ogston, A.S. (1999) Measurement of size and settling velocity of suspended aggregates on the northern California continental shelf. *Mar Geol* **154**: 43–53.

Sterner, R.W., and Hessen, D.O. (1994) Algal nutrient limitation and the nutrition of aquatic herbivores. *Annu Rev Ecol Syst* **25**: 1–29.

Stoderegger, K.E., and Herndl, G.J. (1999) Production of exopolymer particles by marine bacterioplankton under contrasting turbulence conditions. *Mar Ecol Prog Ser* **189**: 9–16.

Sugimoto, K., Fukuda, H., Baki, M.A., and Koike, I. (2007) Bacterial contributions to formation of transparent exopolymer particles (TEP) and seasonal trends in coastal waters of Sagami Bay, Japan. *Aquat Microb Ecol* **46**: 31–41.

Takahashi, T., Sutherland, S.C., Wanninkhof, R., Sweeney, C., Feely, R.A., Chipman, D.W., Hales, B., Friederich, G., Chavez, F., Sabine, C. and Watson, A. (2009) Climatological mean and decadal change in surface ocean pCO_2, and net sea–air CO_2 flux over the global oceans. *Deep Sea Res Part II Top Stud Oceanogr* **56**: 554–577.

Tambo, N., and Watanabe, Y. (1979) Physical characteristics of flocs—I. The floc density function and aluminium floc. *Water Res* **13**: 409–419.

Tariq, S. (2015) Development of an optical pH sensor for visualising the pH gradients in sea sediments. Doctoral dissertation, Ph.D. Thesis, School of Environmental Sciences, University of East Anglia, United Kingdom.

Taucher, J., Jones, J., James, A., Brzezinski, M.A., Carlson, C.A., Riebesell, U., and Passow, U. (2015) Combined effects of CO_2 and temperature on carbon uptake and partitioning by the marine diatoms *Thalassiosira weissflogii* and *Dactyliosolen fragilissimus*. *Limnol Oceanogr* **60**: 901–919.

Taucher, J., Schulz, K.G., Dittmar, T., Sommer, U., Oschlies, A., and Riebesell, U. (2012) Enhanced carbon overconsumption in response to increasing temperatures during a mesocosm experiment. *Biogeosciences (BG)* **9**: 3531–3545.

Ternon, E., Guieu, C., Loÿe-Pilot, M.D., Leblond, N., Bosc, E., Gasser, B., Miquel, J.C. and Martín, J. (2010) The impact of Saharan dust on the particulate export in the water column of the North Western Mediterranean Sea. *Biogeosciences* **7**: 809–826.

Thingstad, T.F., HagstrÖm, Å., and Rassoulzadegan, F. (1997) Accumulation of degradable DOC in surface waters: Is it caused by a malfunctioning microbial loop? *Limnol Oceanogr* **42**: 398–404.

Thomas, H., Bozec, Y., De Baar, H.J.W., Elkalay, K., Frankignoulle, M., Schiettecatte, L.S. and Borges, A.V. (2005) The carbon budget of the North Sea. *Biogeosciences* **1**: 367–392.

Thomas, H., Bozec, Y., Elkalay, K., and Baar, H.J.W. De (2004) Enhanced open ocean storage of CO_2 from shelf sea pumping. *Science (80-)* **304**: 1005–1008.

Thomas, H., Ittekkot, V., Osterroht, C., and Schneider, B. (1999) Preferential recycling of nutrients—the ocean's way to increase new production and to pass nutrient limitation? *Limnol Oceanogr* **44**: 1999–2004.

Thomsen, L., Aguzzi, J., Costa, C., Leo, F. De, Ogston, A., and Purser, A. (2017) The Oceanic Biological Pump: Rapid carbon transfer to depth at Continental Margins during Winter. *Sci Rep* **7**: 10763.

Thornton, D.C.O. (2009) Effect of low pH on carbohydrate production by a marine planktonic diatom (Chaetoceros muelleri). *Int J Ecol* **2009**.

Toggweiler, J.R. (1993) Carbon overconsumption. *Nature* **363**: 210.

Torres, R., Allen, J.I., and Figueiras, F.G. (2006) Sequential data assimilation in an upwelling influenced estuary. *J Mar Syst* **60**: 317–329.

Tsunogai, S., Watanabe, S., and Sato, T. (1999) Is there a "continental shelf pump" for the absorption of atmospheric CO_2? *Tellus B* **51**: 701–712.

Turner, J.T. (2002) Zooplankton fecal pellets, marine snow and sinking phytoplankton blooms. *Aquat Microb Ecol* **27**: 57–102.

Verdugo, P., Alldredge, A.L., Azam, F., Kirchman, D.L., Passow, U., and Santschi, P.H. (2004) The oceanic gel phase: a bridge in the DOM–POM continuum. *Mar Chem* **92**: 67–85.

Vlahos, P., Chen, R.F., and Repeta, D.J. (2002) Dissolved organic carbon in the Mid-Atlantic Bight. *Deep Sea Res Part II Top Stud Oceanogr* **49**: 4369–4385.

Waite, A.M., Olson, R.J., Dam, H.G., and Passow, U. (1995) Sugar-containing compounds on the cell surfaces of marine diatoms measured using concanavalin A and flow cytometry. *J Phycol* **31**: 925–933.

Wakelin, S.L., Holt, J.T., Blackford, J.C., Allen, J.I., Butenschön, M., and Artioli, Y. (2012) Modeling the carbon fluxes of the northwest European continental shelf: Validation and budgets. *J Geophys Res Ocean* **117**.

Walsh, J.J. (1991) Importance of continental margins in the marine biogeochemical cycling of carbon and nitrogen. *Nature* **350**: 53.

Ward, N.D., Bianchi, T.S., Medeiros, P.M., Seidel, M., Richey, J.E., Keil, R.G., and Sawakuchi, H.O. (2017) Where carbon goes when water flows: Carbon cycling across the aquatic continuum. *Front Mar Sci* **4**: 7.

Ward Jr, J.H. (1963) Hierarchical grouping to optimize an objective function. *J Am Stat Assoc* **58**: 236–244.

Wells, M.L., and Goldberg, E.D. (1993) Colloid aggregation in seawater. *Mar Chem* **41**: 353–358.

Weston, K., Fernand, L., Nicholls, J., Marca-Bell, A., Mills, D., Sivyer, D., and Trimmer, M. (2008) Sedimentary and water column processes in the Oyster Grounds: a potentially hypoxic region of the North Sea. *Mar Environ Res* **65**: 235–249.

Widdicombe, C.E., Eloire, D., Harbour, D., Harris, R.P., and Somerfield, P.J. (2010) Long-term phytoplankton community dynamics in the Western English Channel. *J Plankton Res* **32**: 643–655.

Wild, C. (2000) Effekte von Marine Snow—Sedimentation auf Steinkorallen (Hexacorallia, Scleractinia) des Great Barrier Reef. *Aust Dipl Univ Bremen, Biol Bremen* .

Willey, J.D., Kieber, R.J., Eyman, M.S., and Avery, G.B. (2000) Rainwater dissolved organic carbon: concentrations and global flux. *Global Biogeochem Cycles* **14**: 139–148.

Wohlers, J., Engel, A., Zöllner, E., Breithaupt, P., Jürgens, K., Hoppe, H.G., Sommer, U. and Riebesell, U. (2009) Changes in biogenic carbon flow in response to sea surface warming. *Proc Natl Acad Sci* **106**: 7067–7072.

Woodward, E.M.S., and Rees, A.P. (2001) Nutrient distributions in an anticyclonic eddy in the northeast Atlantic Ocean, with reference to nanomolar ammonium concentrations. *Deep Sea Res Part II Top Stud Oceanogr* **48**: 775–793.

Wurl, O. (2009) *Practical guidelines for the analysis of seawater*. CRC press.

Wurl, O., and Holmes, M. (2008) The gelatinous nature of the sea-surface microlayer. *Mar Chem* **110**: 89–97.

Wurl, O., Miller, L., and Vagle, S. (2011) Production and fate of transparent exopolymer particles in the ocean. *J Geophys Res Ocean* **116**: 1–16.

Wyatt, N.J., Kitidis, V., Woodward, E.M.S., Rees, A.P., Widdicombe, S., and Lohan, M. (2010) Effects of high CO_2 on the fixed nitrogen inventory of the Western English Channel. *J Plankton Res* **32**: 631–641.

Yamamuro, M., and Kayanne, H. (1995) Rapid direct determination of organic carbon and nitrogen in carbonate-bearing sediments with a Yanaco MT-5 CHN analyzer. *Limnol Oceanogr* **40**: 1001–1005.

Yano, T., Kodama, T., and Yamada, K. (1961) Fundamental studies on the aerobic fermentation: Part VIII. Oxygen transfer within a mold pellet. *Agric Biol Chem* **25**: 580–584.

Yool, A., and Fasham, M.J.R. (2001) An examination of the "continental shelf pump" in an open ocean general circulation model. *Global Biogeochem Cycles* **15**: 831–844.

Young, E.F., Brown, J., and Aldridge, J.N. (2001) Application of a large area curvilinear model to the study of the wind-forced dynamics of flows through the North Channel of the Irish Sea. *Cont Shelf Res* **21**: 1403–1434.

Zhou, J., Mopper, K., and Passow, U. (1998) The role of surface-active carbohydrates in the formation of transparent exopolymer particles by bubble adsorption of seawater. *Limnol Oceanogr* **43**: 1860–1871.

Zweifel, U.L., Norrman, B., and Hagstrom, A. (1993) Consumption of dissolved organic carbon by marine bacteria and demand for inorganic nutrients. *Mar Ecol Ser* **101**: 23.

Appendix 4

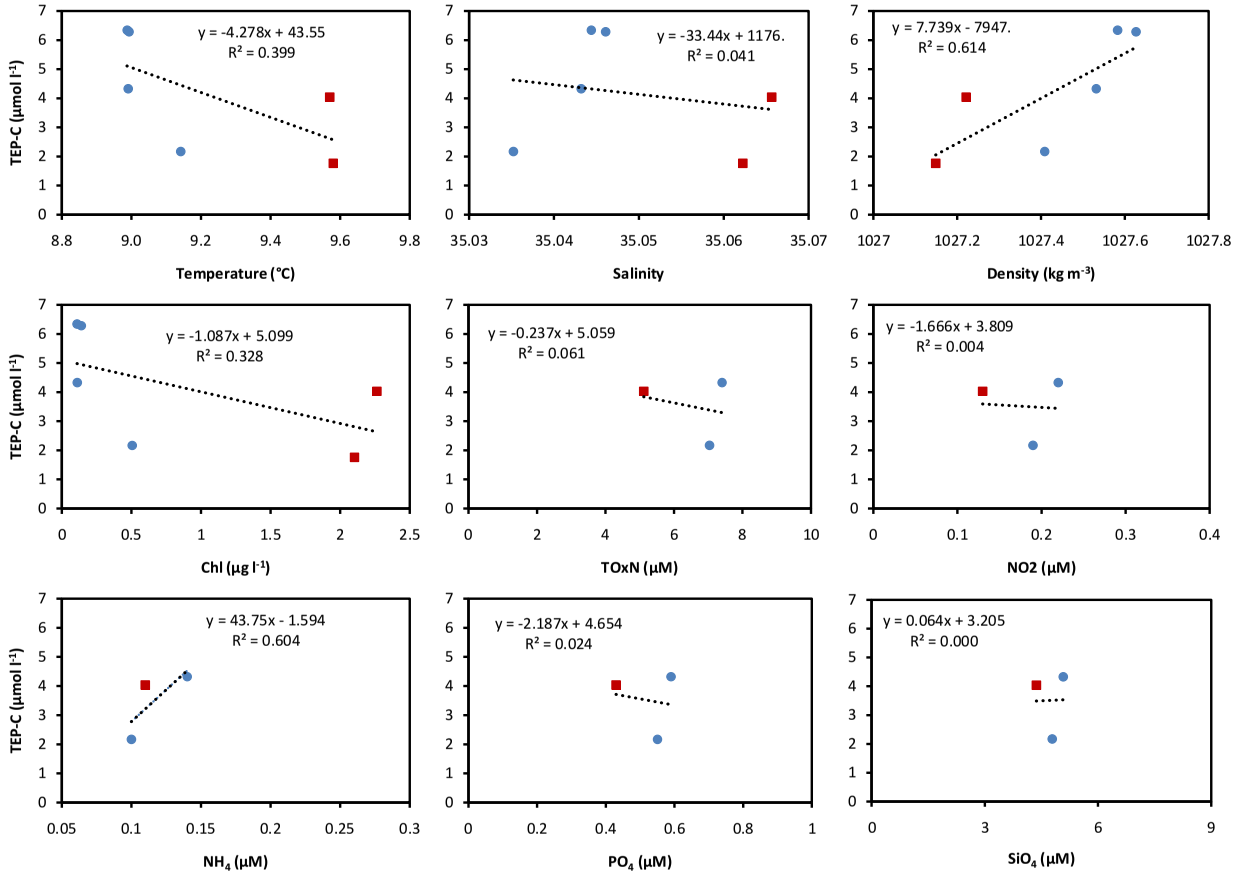

Figure 1a Relationship between TEP_c (µmol l^{-1}) and biological and physicochemical variables [temperature (°C), salinity, density (kg m^{-3}), chlorophyll *a* (µg l^{-1}), nitrate + nitrite (µM), nitrite (µM), ammonium (µM), phosphate (µM) and silicate (µM)] at Station Celtic Deep (A) in spring 2015 (whole water column ■ the red square indicates samples in the SML; ● the blue circle indicates samples in the BML).

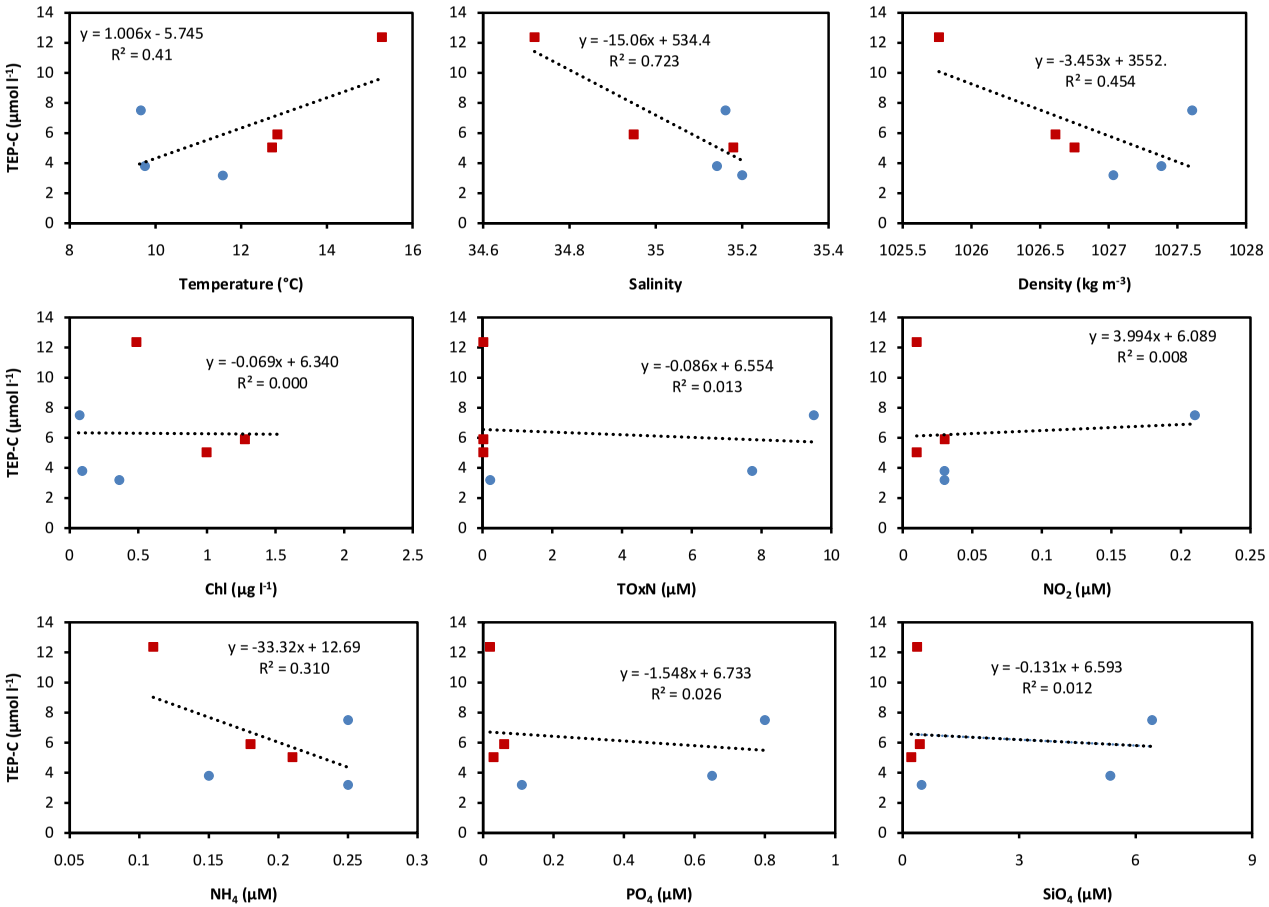

Figure 1b Relationship between TEP_c (µmol l^{-1}) and biological and physicochemical variables [temperature (°C), salinity, density (kg m-3), chlorophyll a (µg l^{-1}), nitrate + nitrite (µM), nitrite (µM), ammonium (µM), phosphate (µM) and silicate (µM)] at Station Celtic Deep (A) in summer 2015 (whole water column ■ the red square indicates samples in the SML; ● the blue circle indicates samples in the BML).

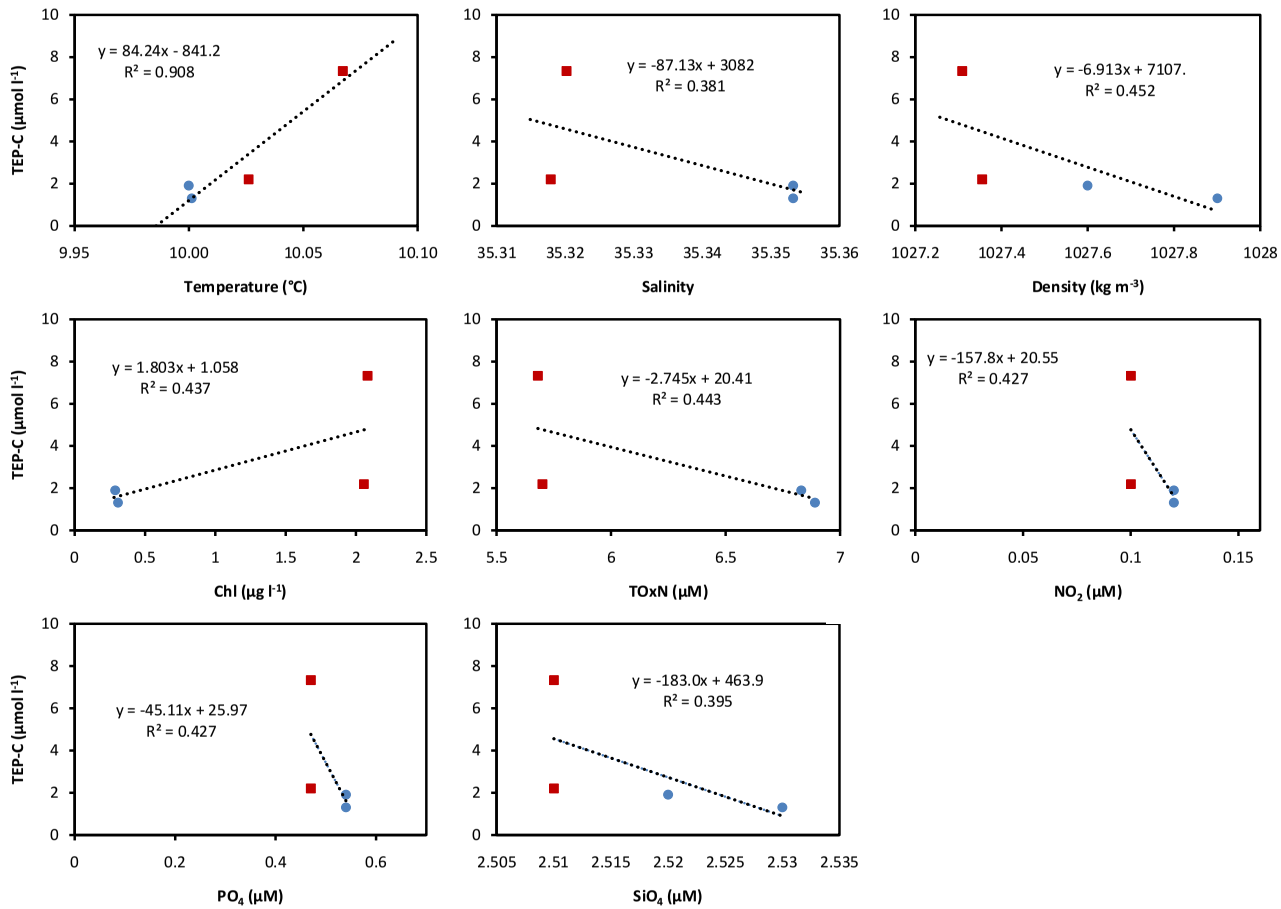

Figure 2a Relationship between TEP_c (µmol l^{-1}) and biological and physicochemical variables [temperature (°C), salinity, density (kg m^{-3}), chlorophyll *a* (µg l^{-1}), nitrate + nitrite (µM), nitrite (µM), ammonium (µM), phosphate (µM) and silicate (µM)] at Station Candy Floss (CCS) in spring 2015 (whole water column ■ the red square indicates samples in the SML; ● the blue circle indicates samples in the BML).

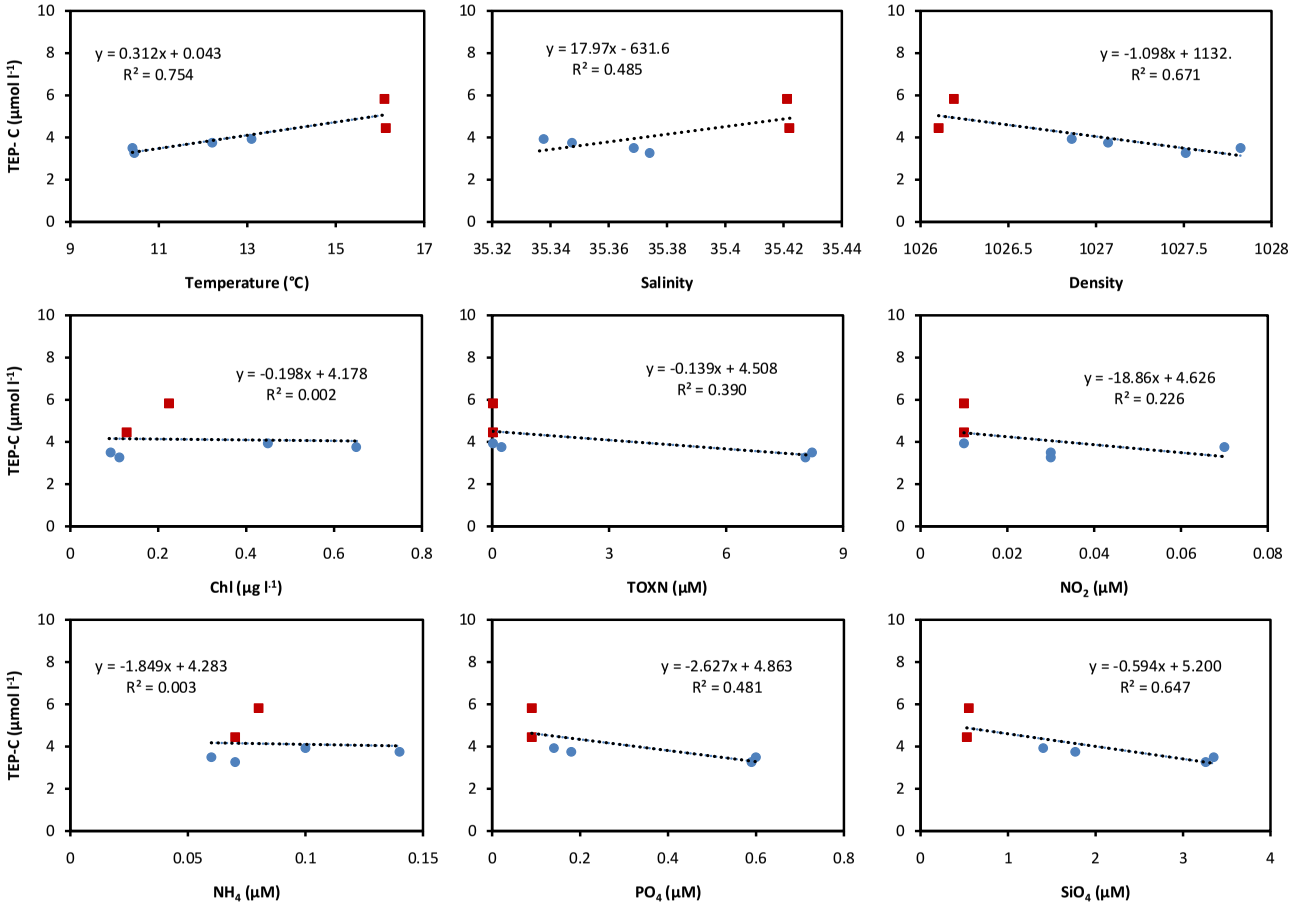

Figure 2b Relationship between TEP_c (µmol l^{-1}) and biological and physicochemical variables [temperature (°C), salinity, density (kg m^{-3}), chlorophyll *a* (µg l^{-1}), nitrate + nitrite (µM), nitrite (µM), ammonium (µM), phosphate (µM) and silicate (µM)] at Station Candy Floss (CCS) in summer 2015 (whole water column ■ the red square indicates samples in the SML; ● the blue circle indicates samples in the BML).

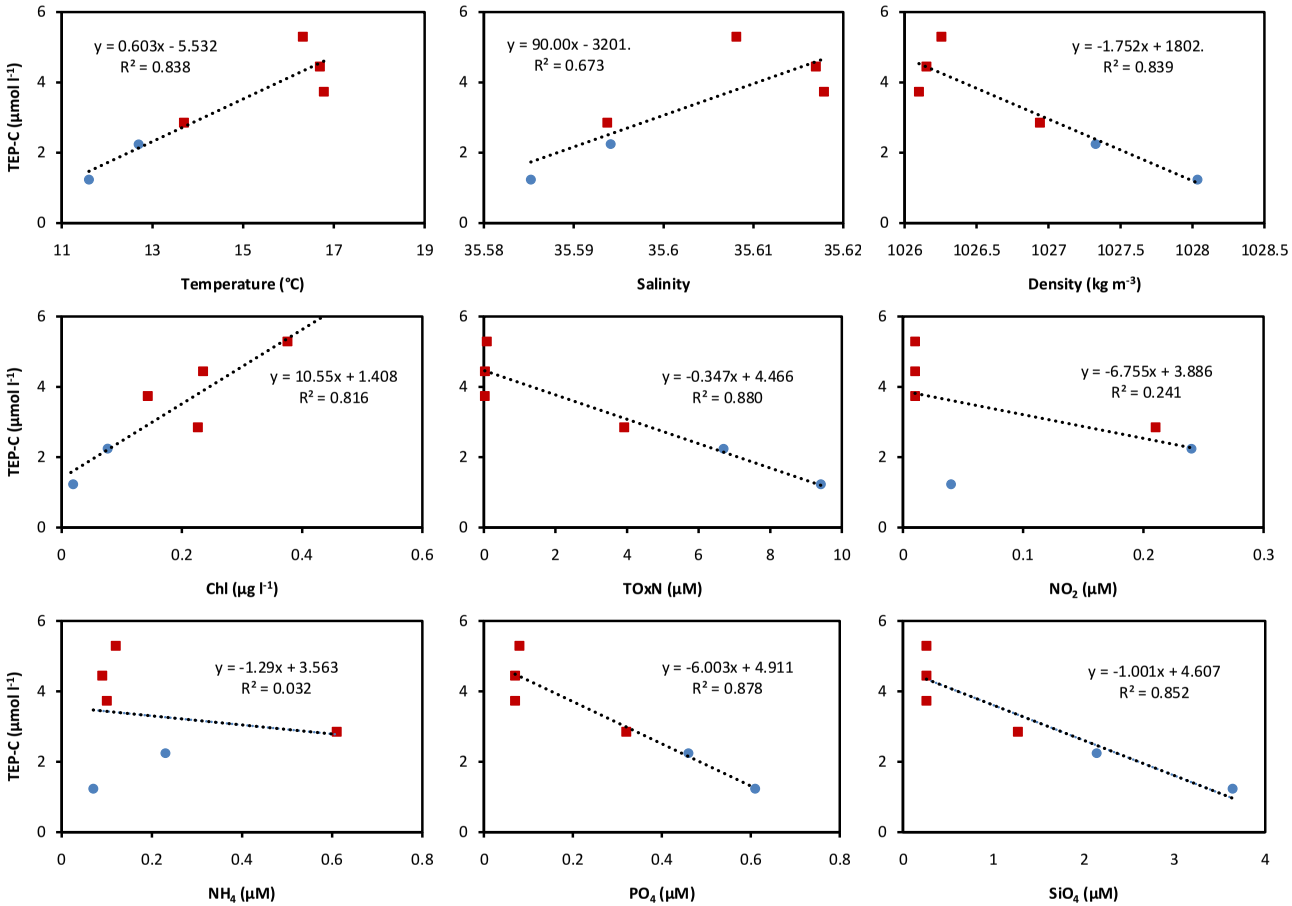

Figure 3 Relationship between TEP_c (µmol l^{-1}) and biological and physicochemical variables [temperature (°C), salinity, density (kg m^{-3}), chlorophyll *a* (µg l^{-1}), nitrate + nitrite (µM), nitrite (µM), ammonium (µM), phosphate (µM) and silicate (µM)] at Station Shelf Edge (CS2) in summer 2015 (whole water column ■ the red square indicates samples in the SML; ● the blue circle indicates samples in the BML).